# Functional involvement of voltage-gated Na$^+$ channels in regulation of membrane potential in MDA-MB-231 human breast cancer cells

**Ming Yang**

PhD

University of York

Biology

November 2015

# Abstract

Voltage-gated $Na^+$ channels (VGSCs) initiate and propagate action potentials in neurones. Functional VGSCs have been found in an increasing number of cancer cells and patient biopsies from different tissues. Blocking VGSCs using pharmacological agents or suppressing VGSC expression using RNA interference reduces cell metastatic behaviour, such as migration and invasion *in vitro* and metastasis *in vivo* in rodent models. In breast cancer, a high mRNA level of $Na_v1.5$, a VGSC isoform, correlates with metastasis and poor prognosis. However, the detailed mechanism(s) underlying VGSC-dependent metastatic cell behaviours is not fully understood.

Depolarised membrane potential ($V_m$) induces mitotic activity in neurones and causes tumourigenesis in *Xenopus laevis*. Given that VGSCs depolarise the $V_m$ upon action potential firing in neurones, using MDA-MB-231 human breast cancer cells where VGSCs are endogenously expressed, the present study hypothesised that VGSCs increase cell metastatic behaviours by depolarising the $V_m$.

This study found that VGSCs depolarise the $V_m$ of MDA-MB-231 cells by ~4 mV. Hyperpolarising the $V_m$ by blocking VGSCs with tetrodotoxin (TTX) or activating large conductance $Ca^{2+}$-activated $K^+$ channels using NS-1619 slowed cell migration to a similar extent. Rac1 is a small GTPase that potentiates cell migration via facilitating actin filament assembly. Both TTX and NS-1619 reduced the active Rac1 level at the leading edge of cells, suggesting that $V_m$ controls Rac1 activity/distribution and henceforth cell motility in MDA-MB-231 cells. However, MDA-MB-231 cell invasion was inhibited by TTX but not NS-1619, suggesting that $Na^+$, rather than $V_m$, may be the factor that underlies VGSC-dependent cell invasion. Finally, this study recorded $Na^+$ current carried by VGSCs in tumour cells in tissue slices from mice, suggesting that VGSCs are functional *in vivo*. In summary, the present study provides novel evidence elucidating mechanisms underlying VGSC-dependent metastatic cell behaviours. Future experiments should explore VGSC/$V_m$ as potential therapeutic targets in cancer treatment.

# Table of Contents

## Table of Figures

# Table of Tables

# Acknowledgements

My research in the past few years would not be possible without all the kind help and support from many people. Most of all, I would like to thank Dr Will Brackenbury for being a great mentor ever since I joined the lab in 2011. Will has helped me greatly in my development as a researcher, showing me how meticulously scientific research should be executed and managed. I would acknowledge Dr Chris Elliott and Dr Sangeeta Chawla in my thesis advisory panel for providing valuable guidance. I am also grateful for all the inspirational discussions with Dr Gareth Evans and Prof Miles Whittington.

Michaela Nelson has always been an indispensable member in the Brackenbury Lab by making the lab exemplarily organised, and our productive collaborations will always be remembered. I would like to thank Amy Thurber and Faheem Patel for being great colleagues in the group. I would also like to thank Dr Richard Kasprowicz and Dr Rakesh Suman for their help in the study, and Alan Haigh and Rita Pinto for all the trainings I received. I am also grateful for the friendship with Drs Matt Ainsworth, Anna Simon, Steve Hall, Mark Hunt and Nat Adams.

My deepest gratitude goes to my wonderful wife, who has been taking care of me over the past few years, patiently, gently and supportively. It is also the love and encouragement from my parents that take me through all these years. I am grateful to my grandfather, who is the first person that sparkled my passion in science and technology.

Finally, I would like to thank Ms Yun Hao and Mr Shiyuan Xiao, who led me into the wonderland of modern biological science in 2003.

## Declaration

I, Ming Yang, declare that this thesis is a presentation of original work and I am the sole author. This work has not previously been presented for an award at this, or any other, University. All sources are acknowledged as References. All experiments were performed by the author, with the exception of the ptychographic microscopy, which was performed by Dr Richard Kasprowicz and Dr Rakesh Suman as described in the Methods. Part of Chapter 1, and part of the results presented in Chapter 3 and Chapter 5 have been published in a number of journals. The publications of Ming Yang's are listed below:

Yang M, Kozminski DJ, Wold LA, Modak R, Calhoun JD, Isom LL & Brackenbury WJ (2012). Therapeutic potential for phenytoin: targeting Na(v)1.5 sodium channels to reduce migration and invasion in metastatic breast cancer. *Breast Cancer Res Treat* **134,** 603–615.

Yang M & Brackenbury WJ (2013). Membrane potential and cancer progression. *Front Physiol* **4,** 185.

Nelson M, Yang M, Dowle AA, Thomas JR & Brackenbury WJ (2015). The sodium channel-blocking antiepileptic drug phenytoin inhibits breast tumour growth and metastasis. *Mol Cancer* **14,** 13.

Nelson M, Yang M, Millican-Slater R & Brackenbury WJ (2015). Nav1.5 regulates breast tumor growth and metastatic dissemination in vivo. *Oncotarget* **6,** 32914–32929.

Mohammed F, Khajah M, Yang M, Brackenbury W & Luqmani Y (2016). Blockade of voltage-gated sodium channels inhibits invasion of endocrine-resistant breast cancer cells. *Int J Oncol,* **48,** 73-83.

# Chapter 1: General Introduction

## 1.1 The discovery of voltage-gated Na$^+$ channels

In 1952, during their research on the squid giant axon, Hodgkin and Huxley demonstrated that the electrical signals in nerve arise from the activation of a voltage-dependent Na$^+$ current ($I_{Na}$) at the axon membrane that transports $I_{Na}$ into the cell (Hodgkin & Huxley, 1952a, b, c, d). The fast inward $I_{Na}$ inactivates within 2 ms, and is replaced by a voltage-dependent, outward K$^+$ current ($I_K$) that brings the membrane to its electrically resting state (Hodgkin & Huxley, 1952a, b). $I_{Na}$ and $I_K$ result in the all-or-none nervous response called the action potential (Hodgkin, 1939; Hodgkin & Huxley, 1952d). Not only did their seminal work demonstrate the powerfulness of the voltage-clamp technique, which controls the voltage across the cell membrane and measures the membrane current (Hodgkin *et al.*, 1952), but it also established the foundation of research into electrical signals in modern physiology and neuroscience.

Together with the first successful intracellular recording of an action potential in the giant squid axon, Hodgkin, along with Cole & Curtis' work implied the existence of specialised machineries, later known as ion channels, at the cell membrane that permit the increased permeability of Na$^+$ and K$^+$ ions (Hodgkin, 1937; Cole & Curtis, 1939; Cole & Hodgkin, 1939). In the 1960s, researchers began to probe the structure of voltage-gated Na$^+$ channels (VGSCs) by identifying their binding sites with tetrodotoxin (TTX) and saxitoxin (STX) (Kao & Nishiyama, 1965; Camougis *et al.*, 1967; Hille, 1968), both selective VGSC blockers (Buchwald *et al.*, 1964). In the 1970s, solubilisation and purification of VGSCs labelled with TTX or STX was developed (Ritchie & Rogart, 1977a), which heralded the purification of the VGSC protein in 1980 from scorpion toxin-labelled N18 neuroblastoma cells (Beneski & Catterall, 1980). Along with a later study, which demonstrated a partial purification of a TTX-binding protein from electric eel electroplax (Agnew *et al.*, 1980), the purified 260 kDa neurotoxin-binding protein was

later known as the VGSC α subunit. Two smaller β subunits, namely β1 (36 kDa) and β2 (33 kDa), were discovered thereafter (Hartshorne *et al.*, 1982). In the 2000s, a splice variant of β1, β1B, was reported (Kazen-Gillespie *et al.*, 2000; Qin *et al.*, 2003), and β3 and β4 were also identified (Morgan *et al.*, 2000; Yu *et al.*, 2003). Recently, the crystal structures of bacterial VGSC proteins from *Arcobacter butzleri* at 2.7–3.2 Å resolution (Payandeh *et al.*, 2011; Payandeh *et al.*, 2012), *Alphaproteobacterium HIMB114* at 3.05 Å resolution (Zhang *et al.*, 2012) and *Magnetococcus sp. marinus* at 4.0 Å resolution (McCusker *et al.*, 2012) were solved.

In mammals, VGSCs are protein complexes that consist of one pore-forming α subunit covalently or non-covalently linked with one or more β subunits (Catterall, 2000; Isom, 2002; Brackenbury & Isom, 2011).

## 1.2 VGSC α subunits

To date, 10 VGSC α subunit proteins, $Na_v1.1$–$Na_v1.9$ and $Na_X$, have been identified in humans, and they are encoded by ten different genes (*SCN1A–SCN11A,* Table 1.1) (Goldin, 2001; Catterall, 2012). The α subunits have distinct expression profiles in human tissues and show different sensitivity to blockage by TTX (Table 1.1) (Offermanns & Rosenthal, 2008; Catterall, 2012).

### 1.2.1 The structure of VGSC α subunit

The VGSC α subunit is a transmembrane homotetramer. Each of the four domains (I–IV) has six transmembrane segments (S1–S6, Figure 1.1) (Noda *et al.*, 1984). The central pore-forming area consists of four S5–S6 segments and their re-entrant pore loops (Payandeh *et al.*, 2011), surrounded by the symmetrically distributed S1–S4 (Figure 1.1) (Payandeh *et al.*, 2011). The permeability of $Na^+$ through VGSCs is similar

Table 1.1. The expression of voltage-gated $Na^+$ channel α subunits in humans

| α subunit protein | Gene | Primary tissues | TTX sensitivity | Location in human chromosome | Typical channelopathies in humans | References |
|---|---|---|---|---|---|---|
| Na$_v$1.1 | SCN1A | CNS neurones | Sensitive | 2q24.3 | Epilepsy; GEFS+ | (Escayg et al., 2000; Spampanato et al., 2001) |
| Na$_v$1.2 | SCN2A | CNS neurones | Sensitive | 2q24.3 | Familial neonatal-infantile seizures | (Sugawara et al., 2001; Misra et al., 2008) |
| Na$_v$1.3 | SCN3A | CNS neurones | Sensitive | 2q24.3 | Epilepsy | (Holland et al., 2008) |
| Na$_v$1.4 | SCN4A | Skeletal muscle | Sensitive | 17q23.3 | Paramyotonia congenita; hypokalemic periodic paralysis | (Sokolov et al., 2007; Matthews et al., 2008) |
| Na$_v$1.5 | SCN5A | Heart and skeletal muscle | Resistant | 3p21-22 | Long QT syndrome; Brugada Syndrome; cardiac arrhythmia; sudden infant death syndrome; sudden cardiac death; atrial fibrillation; ventricular fibrillation | (Wang et al., 1995; Probst et al., 2003; Olson et al., 2005; Wilde & Brugada, 2011) |
| Na$_v$1.6 | SCN8A | CNS neurones | Sensitive | 12q13 | Familial ataxia | (Savio-Galimberti et al., 2012) |
| Na$_v$1.7 | SCN9A | PNS neurones | Sensitive | 2q24 | Congenital insensitivity to pain; paroxysmal extreme pain disorder; inherited erythromelalgia | (Cox et al., 2006; Dib-Hajj et al., 2009a; Dib-Hajj et al., 2009b) |
| Na$_v$1.8 | SCN10A | PNS (DRG) neurones | Resistant | 3p22.2 | Peripheral pain syndromes | (Liu & Wood, 2011; Schuelert & McDougall, 2012) |
| Na$_v$1.9 | SCN11A | PNS (DRG) neurones | Resistant | 3p22.2 | Neuropathy pain | (Dib-Hajj et al., 2015) |
| Na$_x$ | SCN6A, SCN7A | Uterus muscle, heart and hippocampus | Unknown | 2q24.3 | Temporal lobe epilepsy | (Gorter et al., 2010) |

CNS and PNS: central/peripheral nervous system; DRG: dorsal root ganglion; GEFS+: generalised epilepsy with febrile seizure plus; TTX: tetrodotoxin
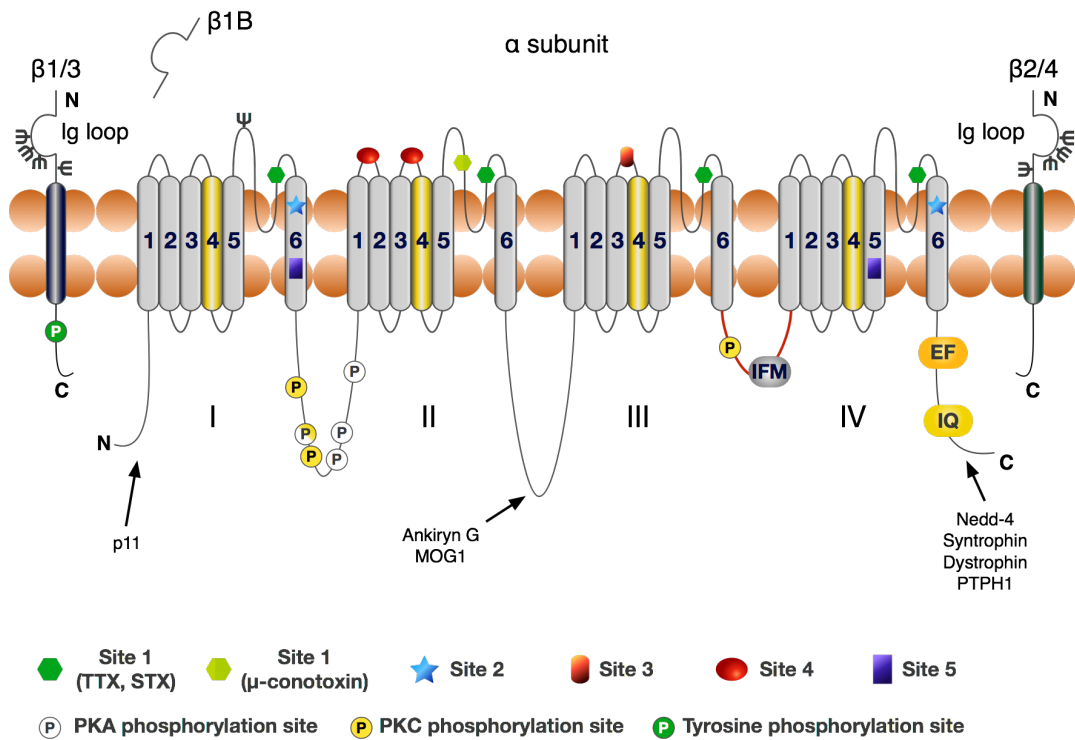
Figure 1.1. The structure of the voltage-gated Na⁺ channel (VGSC).

The VGSC α subunit contains four domains each with six transmembrane segments. Segment 4 (yellow) is the voltage sensor. The inactivation loop between domain III and IV is highlighted in red. The drug binding sites at the α subunit are shown (Cestele & Catterall, 2000). All VGSC β subunits contain an immunoglobulin (Ig) loop. β1–β4 are transmembrane proteins, whereas β1B is a secreted protein (Isom, 2002). There are various phosphorylation sites on both the α and β subunits. The binding sites for annexin II light chain (p11) (Okuse et al., 2002), ankiryn G (Lemaillet et al., 2003), multicopy suppressor of Gsp1 (MOG1) (Wu et al., 2008), Nedd-4 (van Bemmelen et al., 2004), syntrophin (Gee et al., 1998), dystrophin (Gee et al., 1998) and protein tyrosine phosphatase 1 (PTPH1) (Jespersen et al., 2006) are shown. EF: EF-hand motif. IFM: isoleucine-phenylalanine-methionine motif. IQ: isoleucine-glutamine domain. Ψ: glycosylation site.

to $Li^+$, but 12-fold greater than $K^+$ and many organic cations (Hille, 1971, 1972), and the selective $Na^+$ transportation is mediated by the ion selectivity filter formed by the side chains of four highly conserved glutamic acid residues on the S1–S2 loop (Heinemann *et al.*, 1992; Payandeh *et al.*, 2011). When $Na^+$ with planar waters of hydration approach the ion selectivity filter, the negatively charged glutamic acid residues interact with $Na^+$ and partially remove its water of hydration. $Na^+$ is hydrated while being transported through the pore and interacts with other bound water at the inner shell of the pore (Payandeh *et al.*, 2011). Interestingly, in spite of the high degree of structural similarity between VGSCs and voltage-gated $K^+$ channels (VGPCs), this mechanism is distinct from $K^+$ transportation through VGPCs, in which $K^+$ ions are deprived of water of hydration when passing through the channel (Zhou *et al.*, 2001).

## 1.2.2 Activation and inactivation of VGSC α subunits

The opening of VGSCs requires a small transmembrane capacitive current ("gating current") carried by "gating charges" (Hodgkin & Huxley, 1952d; Armstrong & Bezanilla, 1973; Hirschberg *et al.*, 1995). It is now known that the positively charged arginine residues at the VGSC S4 segment serve as the gating charges (Bezanilla, 2000; Catterall, 2000). When VGSCs are in their resting state, the gating charges are electrically neutralised by negatively charged residues in the S2 and S3 segments. Upon membrane potential ($V_m$) depolarisation (i.e. the transmembrane voltage becomes less negative, in contrast to $V_m$ hyperpolarisation where the voltage becomes more negative), the S4 segment moves towards the extracellular side by rotating, a conformation change that leads to the opening of the pore (Yang & Horn, 1995; Yang *et al.*, 1996; Bezanilla, 2000; Groome, 2014). This allows the fast influx of $Na^+$ within a few milliseconds upon channel activation, leading to a fast inward $I_{Na}$.

Following activation, VGSCs undergo fast inactivation, and thus the inward $I_{Na}$ is transient. Research using anti-peptide antibodies has demonstrated that the intracellular

loop between domain III and IV is the key element during fast inactivation (Vassilev *et al.*, 1988; Vassilev *et al.*, 1989). The detailed structure of the inactivation loop was later probed by nuclear magnetic resonance (NMR) (Rohl *et al.*, 1999). It is proposed that the loop contains an α-helix followed by a key hydrophobic sequence containing isoleucine-phenylalanine-methionine (the IFM motif, Figure 1.1, which can fold at a pair of glycine residues and plug to the inner mouth of the pore (West *et al.*, 1992; Kellenberger *et al.*, 1996; Kellenberger *et al.*, 1997a; Kellenberger *et al.*, 1997b; Rohl *et al.*, 1999). After fast channel inactivation, before the channel reaches full inactivation state, a small amount of $Na^+$ is still able to flow through the pore. This phenomenon results in a small $I_{Na}$, namely persistent $I_{Na}$, whose size comprises only a small percentage of the peak transient $I_{Na}$. However, persistent $I_{Na}$ does not fully inactivate and can last for hundreds of milliseconds (Stafstrom, 2011). In neurones, persistent $I_{Na}$ extends the duration of $V_m$ depolarisation and together with other types of $V_m$-depolarising currents, persistent $I_{Na}$ can mediate sustained neuronal excitability by lowering the threshold of action potential generation and therefore support repetitive firing (Stafstrom *et al.*, 1985; French *et al.*, 1990; Beck & Yaari, 2008).


### 1.2.3  Toxin-binding sites on VGSC α subunits

Many neurotoxins and synthetic compounds can bind to a number of sites on the VGSC α subunit and thus modify channel activity. So far, six neurotoxin binding sites have been identified (Table 1.2) and these have contributed greatly to the identification of VGSC structure-function relationships since the 1970s (Hille, 1975; Cestele & Catterall, 2000).

The binding site of TTX, STX and μ-conotoxin is called site 1 (Figure 1.1). These neurotoxins exhibit extracellular pore-blocking mechanism (Hille, 1968), because they bind to the re-entrant loop between S5 and S6 where the mouth of the pore is formed (Noda *et al.*, 1989; Terlau *et al.*, 1991). Upon binding to site 1, these toxins occlude

| Table 1.2. The neurotoxin binding sites on the voltage-gated Na$^+$ channel α subunit | | | |
|---|---|---|---|
| **Binding site** | **Locations** | **Neurotoxins** | **References** |
| Site 1 | Domain I, II, III and IV S5-S6 | TTX, STX, μ-conotoxin | (Noda *et al.*, 1989; Terlau *et al.*, 1991) |
| Site 2 | Domain I and IV S6 | Veratridine, batrachotoxin | (Ulbricht, 1969; Catterall, 1977; Ragsdale *et al.*, 1994, 1996) |
| Site 3 | Domain I and IV S3-S4 | α scorpion toxins, sea-anemone toxins | (Catterall & Beress, 1978; Rogers *et al.*, 1996) |
| Site 4 | Domain II S1-S2 and S3-S4 | β scorpion toxins | (Cestele *et al.*, 1998) |
| Site 5 | Domain I S6, domain IV S5 | Brevetoxins and ciguatoxins | (Benoit *et al.*, 1986; Lombet *et al.*, 1987; Trainer *et al.*, 1994) |
| Site 6 | Unknown | TxVIA | (Hasson *et al.*, 1993) |
| STX: saxitoxin; TTX: tetrodotoxin | | | |

extracellular $Na^+$ entry to the pore and therefore reduce $Na^+$ conductance (Narahashi *et al.*, 1964; Hille, 1968). It is suggested μ-conotoxin shares an overlapping but not identical binding region with TTX and STX. Additional extracellular residues at the S5–S6 segment in domain II are required for μ-conotoxin binding (Chahine *et al.*, 1998). VGSC isoforms show different binding affinity with neurotoxins that bind to site 1. For example, $Na_v1.1$–1.4, 1.6 and 1.7 can be blocked by TTX in the nanomolar range, whereas $Na_v1.5$, 1.8 and 1.9 are sensitive to TTX at micromolar concentrations (Table 1.1) (Goldin, 2001).

Neurotoxin binding site 2 is in the intramembrane region comprising S6 in both domain I and IV. Site 2-binding drugs such as veratridine and batrachotoxin have higher affinity for activated VGSCs and cause sustained channel activation, meanwhile shifting the voltage-dependence of activation to a more negative potential (Ulbricht, 1969; Albuquerque *et al.*, 1971). These effects are achieved by allosteric modulation of the channel, shifting the channel conformational equilibrium to the activated state (Catterall, 1977, 1980). It is proposed that the antiepileptic and anticonvulsant drug phenytoin also binds to this region (Ragsdale *et al.*, 1994, 1996).

α scorpion toxins and sea-anemone toxins (ATX) bind to an extracellular region between S3 and S4 in domain IV, and this site is known as neurotoxin binding site 3 (Catterall & Beress, 1978; Rogers *et al.*, 1996). Because the S4 segments are voltage sensors, it is proposed that α scorpion toxins and ATX inhibit conformational changes during the fast inactivation stage by restricting the movement of the S4 segment in domain IV (Rogers *et al.*, 1996), and therefore keeping VGSCs in their activated state.

β scorpion toxins act on the neurotoxin-binding site 4 in the S1–S2 and S3–S4 loops in domain II (Cestele *et al.*, 1998). By binding to the voltage sensor extracellular domain, β scorpion toxins restrict the movement of the S4 segment in domain II and stabilise the segment in its activated conformation, therefore causing a sustained

activation and a negative shift in the voltage-dependence of activation (Cestele *et al.*, 1998; Cestele & Catterall, 2000).

Similar to site 2, neurotoxin binding site 5 is also a transmembrane region at S6 in domain I plus S5 in domain IV, and its binding toxins include lipid-soluble brevetoxins and ciguatoxins (Benoit *et al.*, 1986; Lombet *et al.*, 1987; Trainer *et al.*, 1994). As with site 2-binding compounds, these toxins block the inactivation of the channel and result in a negative shift in the voltage-dependence of activation (Huang *et al.*, 1984; Benoit *et al.*, 1986).

The location of neurotoxin binding site 6 is as yet unknown. A site-6-binding toxin isolated from the venom of the cone snail *Conus textile*, TxVIA, increases action potential duration by inhibiting VGSC inactivation (Hasson *et al.*, 1993).

## 1.2.4  Localisation of VGSC α subunits in excitable cells

Different α subunit isoforms show significant diversity in tissue-specific expression (Table 1.1). In humans, $Na_v1.1$, $Na_v1.2$, $Na_v1.3$ and $Na_v1.6$ are widely expressed in the central nervous system (CNS) (Lu *et al.*, 1992; Malo *et al.*, 1994a; Malo *et al.*, 1994b; Plummer *et al.*, 1997), whereas the most abundant α subunits in dorsal root ganglion (DRG) neurones in the peripheral nervous system (PNS) are $Na_v1.7$, $Na_v1.8$ and $Na_v1.9$ (Klugbauer *et al.*, 1995; Rabert *et al.*, 1998; Dib-Hajj *et al.*, 1999a; Dib-Hajj *et al.*, 1999b; Jeong *et al.*, 2000). $Na_v1.4$ is mainly localised in skeletal muscle (George *et al.*, 1991; Wang *et al.*, 1992a), whereas $Na_v1.5$ is present mainly in the heart (Gellens *et al.*, 1992; George *et al.*, 1995). Finally, $Na_X$ has been found abundantly in uterus muscle, heart (George *et al.*, 1992) and hippocampus (Gorter *et al.*, 2010), where it may contribute to $Na^+$ sensing (Shimizu *et al.*, 2007).

VGSC α subunits also have dynamic expression profiles during development (Waxman, 2000). For example, in rats, the level of $Na_v1.3$ in the CNS peaks at birth and decreases during postnatal development (Beckh *et al.*, 1989; Felts *et al.*, 1997). In

adulthood, $Na_v1.1$, $Na_v1.2$ and $Na_v1.6$ become the major VGSCs in the CNS (Beckh *et al.*, 1989; Brysch *et al.*, 1991; Waxman *et al.*, 1994; Felts *et al.*, 1997; Schaller & Caldwell, 2000). During postnatal development, $Na_v1.2$ is replaced by $Na_v1.6$ following myelination and formation of nodes of Ranvier (Westenbroek *et al.*, 1989; Boiko *et al.*, 2001; Kaplan *et al.*, 2001). In addition, in rats, $Na_v1.5$ is expressed in neonatal but not adult skeletal muscle (Kallen *et al.*, 1990). Furthermore, genes encoding VGSC α subunits show alternative splicing during development (Copley, 2004; Diss *et al.*, 2004). For example, alternative splicing of two exons encoding the domain I segment 3 (DI:S3) region is responsible for expression of either "adult" and "neonatal" isoforms of $Na_v1.2$ (Sarao *et al.*, 1991), $Na_v1.3$ (Gustafson *et al.*, 1993; Lu & Brown, 1998), $Na_v1.5$ (Diss *et al.*, 2001), $Na_v1.6$ (Plummer *et al.*, 1997) and $Na_v1.7$ (Belcher *et al.*, 1995).

Immunocytochemistry and electron microscopy have demonstrated specific subcellular localisations of α subunit isoforms. At rat nodes of Ranvier, VGSCs are clustered at $> 10^3/\mu m^2$ (Quick & Waxman, 1977; Ritchie & Rogart, 1977a; Waxman, 2000). This is in sharp contrast to the density of VGSCs in the internodal axon membrane, which is $< 25/\mu m^2$ (Ritchie & Rogart, 1977b; Shrager, 1989). In rat hippocampal neurones, $Na_v1.1$ is highly expressed in the cell bodies, whereas $Na_v1.2$ is observed mainly in the axons (Gong *et al.*, 1999). In mouse cortical pyramidal neurones, a computation model estimated a high VGSC density that gives a conductance of ~2500 $pS/\mu m^2$, which is ~50 times of that in the proximal dendrites (Kole *et al.*, 2008).

## 1.2.5  Localisation and function of VGSC α subunits in non-excitable cells

The localisation of VGSCs is not restricted to the so-called "excitable cells" in the CNS/PNS, heart and skeletal muscle. Over the past four decades, VGSCs have also been found in "non-excitable" cells (Table 1.3) (Black & Waxman, 2013). The expression of VGSCs in these cells contributes to their cellular functionality: inhibiting VGSC α subunits with TTX reduces cell motility in dendritic cells (Kis-Toth *et al.*, 2011), microglia

| Table 1.3. The expression and function of voltage-gated Na$^+$ channel (VGSC) α subunits in non-excitable, non-cancerous cell types | | | |
|---|---|---|---|
| **Cell type** | **Type of VGSC α subunit or Na$^+$ current expressed** | **Effects upon VGSC blockade with TTX** | **References** |
| Astrocytes | Na$_v$1.2, 1.3, 1.5 and 1.6 | Reduced Na$^+$/K$^+$-ATPase activity and increased cell death | (Sontheimer et al., 1994) |
| Chrondrocytes | TTX-sensitive | Unknown | (Sugimoto et al., 1996) |
| Dendritic cells (CD1a$^+$) | Na$_v$1.7 | Inhibited cell migration; attenuated secretion; sensitised cells for activation | (Kis-Toth et al., 2011) |
| Endothelial cells | Na$_v$1.4, 1.5 and 1.6 | Increased shear-stress-induced ERK1/2 activation | (Traub et al., 1999) |
| Fibroblasts | Na$_v$1.2, 1.3, 1.5, 1.6 and 1.7 | Unknown | (Chatelier et al., 2012) |
| Keratinocytes | Na$_v$1.1, 1.6 and 1.8 | Inhibited ATP release | (Zhao et al., 2008) |
| Islet β-cells | Na$_v$1.2 and 1.3 | Reduced insulin release | (Donatsch et al., 1977; Pressel & Misler, 1991) |
| Macrophages | Na$_v$1.5 and 1.6 | Attenuated phagocytosis and invasion; reduced podosome formation | (Carrithers et al., 2007; Black et al., 2009; Carrithers et al., 2009) |
| Microglia | Na$_v$1.1, 1.5 and 1.6 | Reduced cell migration, phagocytosis and cytokine release | (Black et al., 2009) |
| Odontoblasts | Na$_v$1.2 | Reduced transmission of pain signals? | (Allard et al., 2006) |
| Oligodendrocyte precursor cells (NG2$^+$) | TTX-sensitive | Reduced ligand-induced migration | (Tong et al., 2009) |
| Osteoblasts | Na$_v$1.2 | Unknown | (Black et al., 1995) |
| Red blood cells | Na$_v$1.4 and 1.7 | Unknown | (Hoffman et al., 2004) |
| Retinal glial cells | Na$_v$1.6 | Reduced ligand-induced glutamate release | (Linnertz et al., 2011) |
| Schwann cells | Na$_v$1.2 and 1.3 | Unknown | (Oh et al., 1994) |
| T lymphocytes | Na$_v$1.5 | Inhibited cell migration; prevention of the positive selection of CD4$^+$ T cells | (Fraser et al., 2004; Lo et al., 2012) |
| Table is adapted from (Black & Waxman, 2013). | | | |

(Craner *et al.*, 2005; Black *et al.*, 2009; Pappalardo *et al.*, 2014a; Pappalardo *et al.*, 2014b) and NG2$^+$ oligodendrocyte precursor cells (Tong *et al.*, 2009). TTX also reduces the invasiveness of macrophages (Carrithers *et al.*, 2007; Carrithers *et al.*, 2009), T lymphocytes (Fraser *et al.*, 2004) and cancer cells (Section 1.4). $Na_v1.5$ contributes to CD4$^+$ CD8$^+$ double-positive selection of thymocytes by causing a sustained $Ca^{2+}$ influx (Lo *et al.*, 2012). In certain cell types, VGSCs also play a role in secretion: blocking $Na_v1.7$ with TTX in CD1a$^+$ dendritic cells reduces the release of tumour necrosis factor (TNF)-α and interleukin (IL)-10 from these cells (Kis-Toth *et al.*, 2011). Additionally, TTX reduces IL-1α, IL-1β and TNF-α release in microglia (Black *et al.*, 2009). In pancreatic islet β-cells, TTX attenuates insulin release (Donatsch *et al.*, 1977; Pressel & Misler, 1991). TTX-mediated blockage of $Na_v1.6$ in retinal glial cells reduces ligand-induced release of glutamate (Linnertz *et al.*, 2011). Moreover, TTX application inhibits subcutaneous ATP release in keratinocytes (Zhao *et al.*, 2008). Reduced levels of phagocytosis have been reported in TTX-treated macrophages and microglia (Carrithers *et al.*, 2007; Black *et al.*, 2009; Carrithers *et al.*, 2009). Furthermore, TTX reduces $Na^+/K^+$-ATPase activity and increases cell death in astrocytes (Sontheimer *et al.*, 1994). Finally, an increased activation of the shear-stress-induced extracellular signal-regulated kinase (ERK) 1/2 has been reported in TTX-treated endothelial cells (Traub *et al.*, 1999).

### 1.2.6 Regulation of VGSC α subunits

VGSC α subunits are subject to post-translational modifications. Soon after their purification, researchers found out that the VGSC α subunits can be phosphorylated by both cAMP-dependent protein kinase (PKA) (Costa *et al.*, 1982; Costa & Catterall, 1984a) and protein kinase C (PKC) (Costa & Catterall, 1984b). Protein sequencing of rat $Na_v1.2$ has demonstrated that PKA phosphorylates on four serine residues (S573, S610, S623 and S687) in the intracellular loop between domain I and II (Murphy *et al.*, 1993), whereas PKC phosphorylates on three serine residues (S554, S573 and S576) in the

same intracellular loop, and S1506 in the inactivation loop between domain III and IV (Figure 1.1) (Numann *et al.*, 1991; Schreibmayer *et al.*, 1991; West *et al.*, 1991). The dephosphorylation of VGSC α subunits in rat brain neurones is mediated by calcineurin, a $Ca^{2+}$-regulated phosphatase also known as phosphatase 2B, and phosphatase 1A or 2A (Murphy *et al.*, 1993; Chen *et al.*, 1995). Additionally, VGSCs in rat brain neurones are tyrosine phosphorylated and are modulated by association with the catalytic domain of receptor protein kinase tyrosine phosphatase β (RPTPβ) (Ratcliffe *et al.*, 2000).

The activation of PKA reduces $I_{Na}$ in $Na_v1.2$-expressing *Xenopus* oocytes and human embryonic kidney (HEK) 293 cells (Smith & Goldin, 1996; Cantrell *et al.*, 1997). Phosphorylation by PKC also reduces VGSC activity in Chinese hamster ovary (CHO) cells (Numann *et al.*, 1991) and *Xenopus* oocytes expressing $Na_v1.2$ (Dascal & Lotan, 1991; Schreibmayer *et al.*, 1991). Neither PKA nor PKC modulation changes the voltage-dependence of activation or kinetics in these cell models. The reduction of peak $I_{Na}$ caused by PKA phosphorylation is because VGSCs are shifted to a "null gating mode" in which the channels have lower probability of transiting to the open state upon $V_m$ depolarisation (Li *et al.*, 1992; Cantrell & Catterall, 2001). On the other hand, COS-7 cells that were transfected with mouse $Na_v1.8$ bearing mutated PKA phosphorylation sites at the domain I–II intracellular loop show a depolarised shift in the voltage-dependence of activation compared with those transfected with normal mouse $Na_v1.8$ (Fitzgerald *et al.*, 1999). In rat sensory neurones, activating PKA or PKC increases peak $I_{Na}$, and rather than modulating the channel directly, PKC enables subsequent PKA-mediated VGSC modulation (Gold *et al.*, 1998). Both the PKA- and PKC-mediated VGSC modulations show functional effects in the nervous system. For example, D1 G-protein-coupled dopamine receptors reduce peak $I_{Na}$ and therefore increase the threshold for action potential firing via PKA-dependent phosphorylation of VGSCs (Surmeier & Kitai, 1997). In rat pyramidal neurones, muscarinic receptor activation slows the inactivation of VGSCs via the PKC phosphorylation pathway and increases the

duration of action potentials, reducing the action potential firing frequency (Azouz *et al.*, 1994; Alroy *et al.*, 1999).

VGSC α subunits expressed in various mammalian cell models are also modulated by $Ca^{2+}$ (Young & Caldwell, 2005; Van Petegem *et al.*, 2012; Gabelli *et al.*, 2015). $Ca^{2+}$ directly regulates VGSCs by interacting with the EF-hand-like motifs in the C-terminus of the α subunit (Figure 1.1). The EF-hand-like motifs in different VGSC α subunit isoforms consist of overlapping, but not identical, residues: NMR data have demonstrated that $Na_v1.5$ residues 1788–1862 fold into the motifs (Chagot *et al.*, 2009), whereas in $Na_v1.2$ the responsible residues span from 1777 to 1882 (Miloushev *et al.*, 2009). In addition, $Ca^{2+}$ can indirectly modulate VGSCs by binding to calmodulin (CaM) (Deschenes *et al.*, 2002; Sarhan *et al.*, 2009; Sarhan *et al.*, 2012; Gabelli *et al.*, 2014; Gabelli *et al.*, 2015). CaM is a 17 kDa protein that can bind up to four $Ca^{2+}$ ions with its four EF-hand motifs (Chou *et al.*, 2001). CaM binds to VGSC α subunits at the isoleucine-glutamine (IQ) domains of the C-terminus (Herzog *et al.*, 2003; Biswas *et al.*, 2008; Sarhan *et al.*, 2012). Experiments using $Na_v1.5$ have shown that the increased intracellular $Ca^{2+}$ results in a ~10 mV depolarising shift in the steady-state inactivation relationship (Tan *et al.*, 2002; Wingo *et al.*, 2004; Biswas *et al.*, 2009).

The α subunits possess glycosylation sites located in the extracellular loop between S5 and S6 in domain I (Figure 1.1) (Bennett, 2002). In neuroblastoma cells in which endogenous VGSCs are expressed, inhibition of glycosylation reduced the number of α subunits at the cell surface (Waechter *et al.*, 1983). The removal of glycosylation in $Na_v1.4$ caused a depolarising shift in the voltage-dependence of activation and steady-state inactivation (Bennett *et al.*, 1997). However, for $Na_v1.5$, a depolarising shift was observed in activation and a hyperpolarising shift in inactivation (Zhang *et al.*, 2003), suggesting that glycosylation has different effects on individual VGSC types (Diss *et al.*, 2001).

In tsA-201 cells, co-expression of $Na_v1.2$ with $\beta\gamma$ subunits of G proteins ($G_{\beta\gamma}$) causes a hyperpolarising shift in the voltage-dependence of activation and steady-state inactivation (Ma *et al.*, 1997). $G_{\beta\gamma}$ also increases persistent $I_{Na}$, which therefore enhances neuronal excitability (Ma *et al.*, 1997). Furthermore, for $Na_v1.8$, annexin II light chain (p11) binds to the N-terminus of the channel and facilitates translocation to the plasma membrane (Okuse *et al.*, 2002). In rat $Na_v1.2$, a 9-amino acid motif at the intracellular loop between domain II and III (loop 2) is required for binding to ankyrin G (Lemaillet *et al.*, 2003), which is necessary for the retention of the neurofascin/$Na_v1.2$ loop 2 chimeric molecule at the axon initial segment (AIS) in cultured hippocampal neurones (Lemaillet *et al.*, 2003). Multicopy suppressor of *Gsp1* (MOG1) binds to the loop 2 of $Na_v1.5$ (Wu *et al.*, 2008). Overexpression of MOG1 increases the expression of $Na_v1.5$ at the cell surface of neonatal cardiomyocytes, which leads to increased $I_{Na}$ density (Wu *et al.*, 2008).

The C-terminus of $Na_v1.5$ also contains a binding site for Nedd4/Nedd4-like ubiquitin-protein ligases, where Nedd4-2-dependent $Na_v1.5$ ubiquitination in heart extracts and transfected HEK cells was observed (van Bemmelen *et al.*, 2004). Nedd4-2 does not alter the kinetics of $Na_v1.5$ in HEK cells but results in a reduced $Na_v1.5$ localisation at the cell membrane and therefore a decrease in $I_{Na}$ density (van Bemmelen *et al.*, 2004). The C-terminus of rat $Na_v1.4$ and brain VGSCs also contains the binding sites for syntrophin and dystrophin, which links VGSCs to the cytoskeleton and the extracellular matrix via dystrophin-associated protein complex (DAPC) (Gee *et al.*, 1998). Cardiomyocytes from dystrophin-deficient mice have reduced $I_{Na}$, suggesting the requirement of DAPC in maintaining the proper function of $Na_v1.5$ (Gavillet *et al.*, 2006). The interaction between $Na_v1.5$ and protein tyrosine phosphatase 1 (PTPH1) is also found at the C-terminus of the channel (Jespersen *et al.*, 2006). Co-expression of $Na_v1.5$ and PTPH1 in HEK293 cells showed a hyperpolarising shift in steady-state inactivation

(Jespersen *et al.*, 2006). Finally, the auxiliary VGSC β subunits also play an important role in modulating the activity of α subunits (Section 1.3.5).

### 1.2.7 VGSC α subunits and channelopathies

Mutations in VGSC α subunits lead to a number of diseases (channelopathies), in part due to alterations of the structure and/or the biophysical properties of the channel (Table 1.1) (Mantegazza *et al.*, 2010a; Mantegazza *et al.*, 2010b; Mantegazza & Catterall, 2012). To begin with, *SCN1A* missense mutations result in channel loss of function due to folding defects in the protein (Mantegazza *et al.*, 2010a). *SCN1A* mutations cause various types of epilepsy, including febrile epilepsy, Dravet syndrome and generalised epilepsy with febrile seizure plus (GEFS+) (Escayg *et al.*, 2000; Claes *et al.*, 2001; Spampanato *et al.*, 2001; Lossin *et al.*, 2002). In addition, a group of patients with benign familial neonatal-infantile seizures carry *SCN2A* mutations (Sugawara *et al.*, 2001; Misra *et al.*, 2008). An *SCN3A* mutation has also been described in a patient with cryptogenic paediatric partial epilepsy (Holland *et al.*, 2008). Frame-shift mutations in *SCN8A* have been identified in patients with familial ataxia (Trudeau *et al.*, 2006).

VGSC mutations are also linked to channelopathies in skeletal muscle. Four known missense mutations in exons 22 and 24 of *SCN4A* associate with paramyotonia congenita (Matthews *et al.*, 2008). Moreover, three mutations in the S4 segment have been shown to cause hypokalemic periodic paralysis (Sokolov *et al.*, 2007).

A group of mutations that cause cardiac channelopathies have also been identified in *SCN5A*. One of the most well-known cardiac disorders caused by mutations in *SCN5A* is long QT syndrome (Wang *et al.*, 1995), which is due to abnormal Na$_v$1.5 inactivation delaying the repolarisation stage during cardiac action potential firing. Long QT syndrome increases the risk for ventricular arrhythmias. It has also been reported that 20 % of patients with Brugada syndrome bear mutations in *SCN5A* (Probst *et al.*, 2003).

Other typical cardiac diseases that relate to mutations in *SCN5A* include sudden cardiac death, sudden infant death syndromes, cardiac arrhythmia (Wilde & Brugada, 2011) and atrial fibrillation (Olson *et al.*, 2005).

Na$_v$1.7 and Na$_v$1.8, expressed in the PNS, are involved in neuropathic pain syndromes, including spinal cord injury pain, phantom limb pain and painful diabetic neuropathy (Lampert *et al.*, 2010). Na$_v$1.7 plays a crucial role in mediating pain signals in the PNS. Mutations in *SCN9A* associate with congenital insensitivity to pain (Cox *et al.*, 2006), paroxysmal extreme pain disorder and inherited erythromelalgia (Dib-Hajj *et al.*, 2009a; Dib-Hajj *et al.*, 2009b). In addition, Na$_v$1.8 contributes to inflammatory pain and peripheral pain syndromes (Liu & Wood, 2011; Schuelert & McDougall, 2012). Na$_v$1.9 plays an important role in pain signalling (Dib-Hajj *et al.*, 2015). Gain-of-function mutations in *SCN11A* can cause familial episodic pain (Zhang *et al.*, 2013), painful peripheral neuropathy (Huang *et al.*, 2014) and loss of pain perception (Leipold *et al.*, 2013). Finally, mutations in *SCN7A*, which encodes Na$_X$ in human cerebellum, associate with temporal lobe epilepsy (Gorter *et al.*, 2010).

## 1.3   VGSC β subunits

Four β subunit genes that encode five β subunit proteins have been identified in humans (Table 1.4) (Brackenbury & Isom, 2011). *SCN1B* encodes β1 and its splice variant β1B, whereas *SCN2B*, *SCN3B* and *SCN4B* encode β2, β3 and β4, respectively.

## 1.3.1   Structure of VGSC β subunits

β1–β4 are transmembrane proteins, containing an extracellular N-terminus, single transmembrane segment and an intracellular C-terminus (Isom & Catterall, 1996). The alternative splice variant β1B is a soluble, secreted molecule without a transmembrane region (Figure 1.1) (Patino *et al.,* 2011). The β subunit extracellular immunoglobulin (Ig)

| Table 1.4. The expression of voltage-gated Na$^+$ channel β subunits in humans | | | | |
|---|---|---|---|---|
| **Gene** | **Protein** | **Primary tissues** | **Related neuronal disorders in humans** | **Reference** |
| *SCN1B* | β1 | CNS, PNS, skeletal muscle and heart | GEFS+; Dravet syndrome; Brugada syndrome; familiar atrial fibrillation; neuropathic pain | (Wallace *et al.*, 1998; Coward *et al.*, 2001; Wallace *et al.*, 2002; Scheffer *et al.*, 2007; Patino *et al.*, 2009; Ogiwara *et al.*, 2012) |
| *SCN1B* | β1B | CNS, PNS, skeletal muscle | Brugada syndrome; epilepsy | (Watanabe *et al.*, 2008; Hu *et al.*, 2012) |
| *SCN2B* | β2 | CNS, PNS skeletal muscle and heart | Neuropathic pain | (Coward *et al.*, 2001) |
| *SCN3B* | β3 | CNS, PNS and heart | Temporal lobe epilepsy | (van Gassen *et al.*, 2009) |
| *SCN4B* | β4 | CNS, PNS and heart | Huntington's disease? | (Oyama *et al.*, 2006) |
| CNS and PNS: central/peripheral nervous system; GEFS+: generalised epilepsy with febrile seizure plus. | | | | |

loop structure is unique among ion channel auxiliary subunits (Brackenbury & Isom, 2011). The intracellular domain of β1 and β2 interacts with ankyrin (Malhotra *et al.*, 2000), by which these β subunits anchor themselves to cytoskeleton (Malhotra *et al.*, 2002; Malhotra *et al.*, 2004).

Residues at both the N- and C-terminus of β1 and β3 non-covalently interact with the α subunit (Hartshorne *et al.*, 1982; Messner & Catterall, 1985; McCormick *et al.*, 1998; Meadows *et al.*, 2001; Spampanato *et al.*, 2004). However, both β2 and β4 covalently associate with α subunits via a single disulphide bond that is formed between the C26 residue at the extracellular region of either β subunit and one of multiple cysteine residues at the S5–S6 loop of the α subunit (Hartshorne *et al.*, 1982; Messner & Catterall, 1985; Yu *et al.*, 2003; Chen *et al.*, 2012).


## 1.3.2  Localisation of VGSC β subunits

The expression of β subunits has been reported in neurones in the CNS and PNS, as well as skeletal and cardiac muscle cells (Table 1.4) (Isom *et al.*, 1992; Isom *et al.*, 1995a; Morgan *et al.*, 2000; Yu *et al.*, 2003; Maier *et al.*, 2004; Lopez-Santiago *et al.*, 2007; Brackenbury *et al.*, 2010; Lopez-Santiago *et al.*, 2011; Kaufmann *et al.*, 2013). Similar to the α subunits, β subunits have also been identified in non-excitable cells, including rat astrocytes (Oh & Waxman, 1995), human glia (Aronica *et al.*, 2003) and endothelial cells (Andrikopoulos *et al.*, 2011b), as well as in cancer cells (Section 1.4.4). β subunit expression profiles depend on developmental stage. For example, in rat brain, the level of β1 and β2 increases during postnatal development and replaces β1B and β3, which peak at birth (Kazen-Gillespie *et al.*, 2000; Shah *et al.*, 2001). β1B is also the predominant splice variant during human foetal brain development (Patino *et al.*, 2011).

β subunits are localised to the AIS (Rasband, 2010; Buffington & Rasband, 2013) and nodes of Ranvier (Kaplan *et al.*, 2001; Chen *et al.*, 2004; Patino *et al.*, 2009;

Buffington & Rasband, 2013), agreeing with their roles in regulating the expression and gating of α subunits during action potential firing at these regions. Moreover, β1 localises to the growth cone in mouse cerebellar granule neurones (CGNs), where it contributes to the neurite outgrowth and pathfinding (Davis *et al.*, 2004; Brackenbury *et al.*, 2008; Brackenbury *et al.*, 2010).

### 1.3.3  VGSC β subunits are cell adhesion molecules

All VGSC β subunits are members of the Ig superfamily of cell adhesion molecules (CAMs) (Isom *et al.*, 1995a; Brackenbury & Isom, 2011). To date, both the homophilic interactions, by which the Ig domains from two identical β subunits interact, and the heterophilic interactions, by which the Ig domain of a β subunit interacts with other CAMs, have been reported (Malhotra *et al.*, 2000; McEwen & Isom, 2004).

β1-β1 homophilic interactions increase cell aggregation and ankyrin recruitment in *Drosophila* S2 cells (Malhotra *et al.*, 2000). Heterophilic adhesion partners of β1 include contactin (Kazarinova-Noyes *et al.*, 2001), neurofascin-155, neurofascin-186 (Ratcliffe *et al.*, 2001; McEwen *et al.*, 2004), N-cadherin (Malhotra *et al.*, 2000) and tenascin-R (Srinivasan *et al.*, 1998). Heterophilic interactions with β1 lead to various outcomes: β1-contactin (as well as β2-contactin) co-expression increases $Na_v1.2$ expression at the plasma membrane of CHL cells (Kazarinova-Noyes *et al.*, 2001). β1 (as well as β2)-bearing CHL cells are repelled from tenascin-R expressing extracellular matrix, indicating a role of β subunits in directing cell migration (Xiao *et al.*, 1999). β3 homophilic interactions have been reported in transfected HEK293 cells (Yereddi *et al.*, 2013) but not in transfected *Drosophila* S2 cells (McEwen *et al.*, 2009). It is proposed that, in contrast to β1, β3 has limited heterophilic interactions with other CAMs: for example, β3 does not associate with contactin (McEwen *et al.*, 2009). Finally, the homophilic interaction between β4-β4 has been identified in mouse striatum and striatonigral fibres (Miyazaki *et al.*, 2014).

β1-β1 homophilic interactions mediate neurite outgrowth in mouse CGNs (Davis *et al.*, 2004). Overexpression of β4 also induces neurite outgrowth in Neuro2a cells (Oyama *et al.*, 2006). Interestingly, co-culture of CGNs with β2-expressing fibroblast monolayers reduces the neurite length (Davis *et al.*, 2004), suggesting different β subunits have distinct roles in modulating neurite outgrowth in the CNS. β1-mediated neurite outgrowth requires the presence fyn kinase and contactin (Brackenbury *et al.*, 2008). In addition, $I_{Na}$ carried by $Na_v1.6$ is required for β1-mediated neurite outgrowth, and in turn, β1 expression enhances the size of the $I_{Na}$ (Brackenbury *et al.*, 2010). Therefore, there is reciprocal interaction between $Na_v1.6$ and β1 to regulate neurite outgrowth and excitability (Brackenbury *et al.*, 2010).

### 1.3.4 Regulation of VGSC β subunits

β subunits are subject to post-translational regulation. There is a tyrosine phosphorylation site at the intracellular domain of β1 (β1Y181) (Figure 1.1) (Malhotra *et al.*, 2002). The phosphorylation status of β1Y181 has been shown to affect the functional localisation of β1: in cardiomyocytes, tyrosine-phosphorylated β1 colocalises with $Na_v1.5$ at intercalated discs, whereas non-phosphorylated β1 is found at the T-tubules, colocalising with TTX-sensitive VGSCs (Malhotra *et al.*, 2004).

Three to four glycosylation sites are present at the Ig loop region of the β subunits (Messner & Catterall, 1985; Isom *et al.*, 1992). Sialylation, a common type of glycosylation in VGSCs induced by sialic acids, is necessary for the β1-dependent modulation of channel gating in CHO cells (Johnson *et al.*, 2004).

β1–β4 are all subject to proteolytic cleavage by α-, β- and γ-secretase (Kim *et al.*, 2005; Wong *et al.*, 2005). Both α- and β-secretase release the extracellular domain of β1–β4 from the full-length protein, whereas γ-secretase releases the intracellular domain into the cytoplasm (Wong *et al.*, 2005). Interestingly, the cleaved intracellular

domain of β2 traffics to the nucleus and increases $Na_v1.1$ mRNA and protein levels in cells from mouse cerebellum (Kim *et al.*, 2007).

### 1.3.5 β subunits modulate the activity of α subunits

The activity of VGSC α subunits is modulated by the auxiliary β subunits in the protein complex. In heterologous systems, co-expression of β1, β2 or β3 with rat $Na_v1.2$ in *Xenopus* oocytes accelerates channel inactivation and results in a shift of steady-state inactivation towards a more negative voltage (Isom *et al.*, 1992; Patton *et al.*, 1994; Isom *et al.*, 1995a; Isom *et al.*, 1995b; Morgan *et al.*, 2000). Co-expression of β1 or β2 with rat $Na_v1.6$ in *Xenopus* oocytes also accelerates channel inactivation and causes a hyperpolarising shift in the voltage-dependence of activation but shows no effect on the steady-state inactivation (Smith *et al.*, 1998a). Moreover, both β1 and β2 increase peak $I_{Na}$ density carried by $Na_v1.2$ in oocytes (Isom *et al.*, 1992; Isom *et al.*, 1995a). Finally, β4 has been shown to cause a negative shift in the voltage-dependence of $Na_v1.2$ or $Na_v1.4$ activation (Yu *et al.*, 2003) and in the steady-state inactivation of $Na_v1.5$ (Medeiros-Domingo *et al.*, 2007).

In Chinese hamster lung (CHL) cells, co-expressing β1 and $Na_v1.2$ gives similar results to *Xenopus* oocytes, including an increase in peak $I_{Na}$ density and a negative shift in the steady-state inactivation (Isom *et al.*, 1995b). Interestingly, β2 requires co-expression of β1 to exert its modulatory roles on $Na_v1.2$ in CHL cells (Kazarinova-Noyes *et al.*, 2001). In rat brain neurones, β2 increases membrane capacitance, likely due to its role in facilitating insertion of α subunits into the cell membrane (Schmidt *et al.*, 1985; Schmidt & Catterall, 1986; Isom *et al.*, 1995a). In HEK293 cells, co-expression of β1 or β3 increases the peak $I_{Na}$ carried by $Na_v1.7$, whereas β2 or β4 has no significant effect on the peak $I_{Na}$ (Laedermann *et al.*, 2013). β1 and β3 also cause a positive shift in steady-state inactivation (Laedermann *et al.*, 2013). When co-expressed with $Na_v1.3$ or

Na$_v$1.5, β3 negatively shifts the steady-state inactivation in CHO cells (Meadows *et al.*, 2002; Ko *et al.*, 2005).

The effect of β subunits on action potential firing and I$_{Na}$ has also been investigated *in vivo* using transgenic mice. Electrophysiological recordings from postnatal (10–18 days) *Scn1b* null mice show hyperexcitability in the CA3 region of the hippocampus (Brackenbury *et al.*, 2013). The hyperexcitability has also been reported in DRG neurones in the same animal model (Lopez-Santiago *et al.*, 2011). On the other hand, reduced I$_{Na}$ and impaired excitability have been observed in CGNs from *Scn1b*-null mice (Brackenbury *et al.*, 2010). Thus, β1 regulates neuronal excitability in a cell-type dependent manner.

*In vivo* evidence has also demonstrated that β1 regulates excitability in the heart. Increased transient and persistent I$_{Na}$ were recorded from ventricular cardiomyocytes of *Scn1b* null mice, leading to prolonged action potential repolarisation and QT interval (Lopez-Santiago *et al.*, 2007). Interestingly, ^{3}H-saxitoxin binding experiments show that the number of TTX-sensitive and TTX-resistant VGSCs increased in *Scn1b*-null ventricular myocytes (Lopez-Santiago *et al.*, 2007).

It is noteworthy that β1 also regulates the distribution and expression of the α subunits: compared to wildtype, CA3 hippocampal neurones in *Scn1b*-null mice have reduced Na$_v$1.1 but increased Na$_v$1.3 protein levels (Chen *et al.*, 2004), and a subpopulation of *Scn1b*-null CGNs show an increase in Na$_v$1.1 at the AIS (Brackenbury *et al.*, 2010). Localisation of Na$_v$1.6 at the AIS in a subpopulation of CGNs is also dependent on β1 (Brackenbury *et al.*, 2010). Additionally, *Scn2b*-null mice have reduced I$_{Na}$ at the nodes of Ranvier of mouse optic nerves (Chen *et al.*, 2002).


### 1.3.6  β subunits and neuronal disorders

Mutations in human β subunit genes associate with neuronal disorders (Table 1.4) (Savio-Galimberti *et al.*, 2012; Baroni & Moran, 2015). At least seven mutations in

*SCN1B* have been reported in GEFS+ patients (Wallace *et al.,* 1998; Wallace *et al.,* 2002). Six of these (C121W, R85C, R85H, I70_E74del, R125L and D25N) occur in the β1 Ig loop, suggesting the significance of the Ig structure in regulating excitability. Two β1 mutations, R125C and I106F, have been found in Dravet syndrome patients (Patino *et al.,* 2009; Ogiwara *et al.,* 2012). Brugada syndrome is associated with mutations including R214Q and E87Q in β1/β1B (Watanabe *et al.,* 2008; Hu *et al.,* 2012). R85H, another mutation in the Ig domain, and D153N mutation in the intracellular domain of β1 have been reported in patients with familial atrial fibrillation (Scheffer *et al.,* 2007). β1, as well as β2, has functional roles in conducting neuropathic pain (Coward *et al.,* 2001). Reduced β3 protein level can lead to temporal lobe epilepsy (van Gassen *et al.,* 2009). Finally, down-regulation of β4 may cause neurite degeneration in the striatum of Huntington's disease transgenic mice and patients with Huntington's disease (Oyama *et al.,* 2006).

## 1.4   The involvement of VGSCs in cancer progression

### 1.4.1   Breast cancer

Cancer is one of the leading causes of deaths. Globally, approximately 14 million new cancer cases and eight million cancer-related deaths were reported in 2012 (Torre *et al.,* 2015). 11 % of all cancer cases are breast cancer (BCa) (Maxmen, 2012). In women, BCa had the highest incidence (> 1.6 million) and was the leading cause of cancer-related deaths (> 0.5 million) worldwide in 2012, which accounted for 15 % of cancer-related deaths in females (Torre *et al.,* 2015). BCa is categorised into three groups according to the expression profiles of oestrogen receptor (ER), progesterone receptor (PR) and human epidermal growth factor receptor 2 (HER2). In the US, the "triple-negative (ER⁻/PR⁻/HER2⁻)" subtype has been found in 13 % of BCa patients. These patients have a significantly lower 5-year survival rate (Maxmen, 2012) and an

increased likelihood of distant recurrence within five years of diagnosis compared with those diagnosed with other types of BCa (Dent *et al.*, 2007). Until recently, adjuvant chemotherapy, which includes anthracyclines and/or taxanes (Joensuu & Gligorov, 2012; von Minckwitz & Martin, 2012), is the primary therapy for triple-negative BCa (Anders & Carey, 2008; Irvin & Carey, 2008), since this BCa subtype is resistant to HER2-targeted treatments using trastuzumab and hormonal therapies using tamoxifen and aromatase inhibitors (Cleator *et al.*, 2007). Triple-negative BCa shares many molecular features with cancers that carry *breast cancer 1* (*BRCA1*) mutations (Cleator *et al.*, 2007), including *p53* mutations (Crook *et al.*, 1997; Schlichtholz *et al.*, 1998), ER negativity (Lakhani *et al.*, 2005) and HER2 negativity (Lakhani *et al.*, 2002). Because BRCA1 plays a central role in repairing double-stranded DNA breaks by homologous recombination (Turner *et al.*, 2004), dysfunctional BRCA1 repairs damaged DNA with less accuracy that can lead to genome instability (Cleator *et al.*, 2007), one of the hallmarks of cancer (Hanahan & Weinberg, 2011). When the BRCA1 pathway is compromised, poly (ADP-ribose) polymerase (PARP)-dependent non-homologous recombination becomes the primary pathway during DNA repair (Javle & Curtin, 2011). A novel targeted therapy using PARP inhibitors was proposed for *BRCA1*-associated cancers, and the efficacy of PARP inhibitors in triple-negative BCa therapy has gained attention in the past few years (Do & Chen, 2013).

Cancer becomes difficult to cure when the cancer at the primary site (primary tumour) spreads to distant sites (metastasis). In BCa patients, the most common metastasis sites include lungs, bones, liver, pleura and adrenal glands, and metastases at multiple sites have been frequently found in patients (Weigelt *et al.*, 2005). Recent reports also showed increased incidence of brain metastasis arising from triple-negative BCa (Lin *et al.*, 2008; Niwinska *et al.*, 2010). Once BCa metastasises, the five-year survival rate is only 26 % (Lu *et al.*, 2009). Although adjuvant therapy, in which chemotherapy is often combined with other agents (e.g. tamoxifen and trastuzumab for

ER$^+$ and HER2$^+$ BCa patients, respectively), after primary BCa removal, has been used in treating BCa metastases, its side effects, such as premature menopause (Ganz, 2005), infertility (Ganz *et al.*, 2003) and sexual dysfunction (Howard-Anderson *et al.*, 2012), often lead to deteriorated quality of life in patients. Metastasis is regarded one of the hallmarks of cancer (Hanahan & Weinberg, 2011), and one of the key goals in clinical and basic cancer research is to effectively detect and reduce BCa metastasis and therefore improve the prognosis of BCa patients.

### 1.4.2  The metastatic cascade: involvement of migration and invasion

Metastasis is a complex sequence of events that includes cell detachment from the primary site, migration and invasion through the local tissue, penetration through the basement membrane into lymphatic and blood vessels (intravasation), travelling through the circulation, exiting the circulation (extravasation), settling at distant sites, and proliferation into new tumours (Figure 1.2) (Gupta & Massague, 2006).

An important event during malignant cancer cell migration and invasion in vivo is the way that the cells "sense" their surrounding environment and hence exert metastatic behaviours (Allinen *et al.*, 2004). Integrins, a family of cell adhesion receptors that bind to ligands in extracellular matrix (ECM), have a crucial role in interacting with the ECM and thus activating receptor tyrosine kinases (RTKs) and intracellular signals leading to cell migration and invasion (Giancotti & Ruoslahti, 1999; Hynes, 2002). Upon binding to the ECM, integrins recruit and partially activate focal adhesion kinase (FAK) (Oktay *et al.*, 1999), a molecule that is regarded as a central hub in cancer cell migration control (Sieg *et al.*, 2000; Schlaepfer & Mitra, 2004). Full phosphorylation of FAK is mediated by src kinase (Xing *et al.*, 1994), resulting in recruitment of a number of important effectors that promote cancer cell metastasis (Mitra & Schlaepfer, 2006), including the small GTPase Rac (Hsia *et al.*, 2003; Ishibe *et al.*, 2004), guanine nucleotide exchange factors
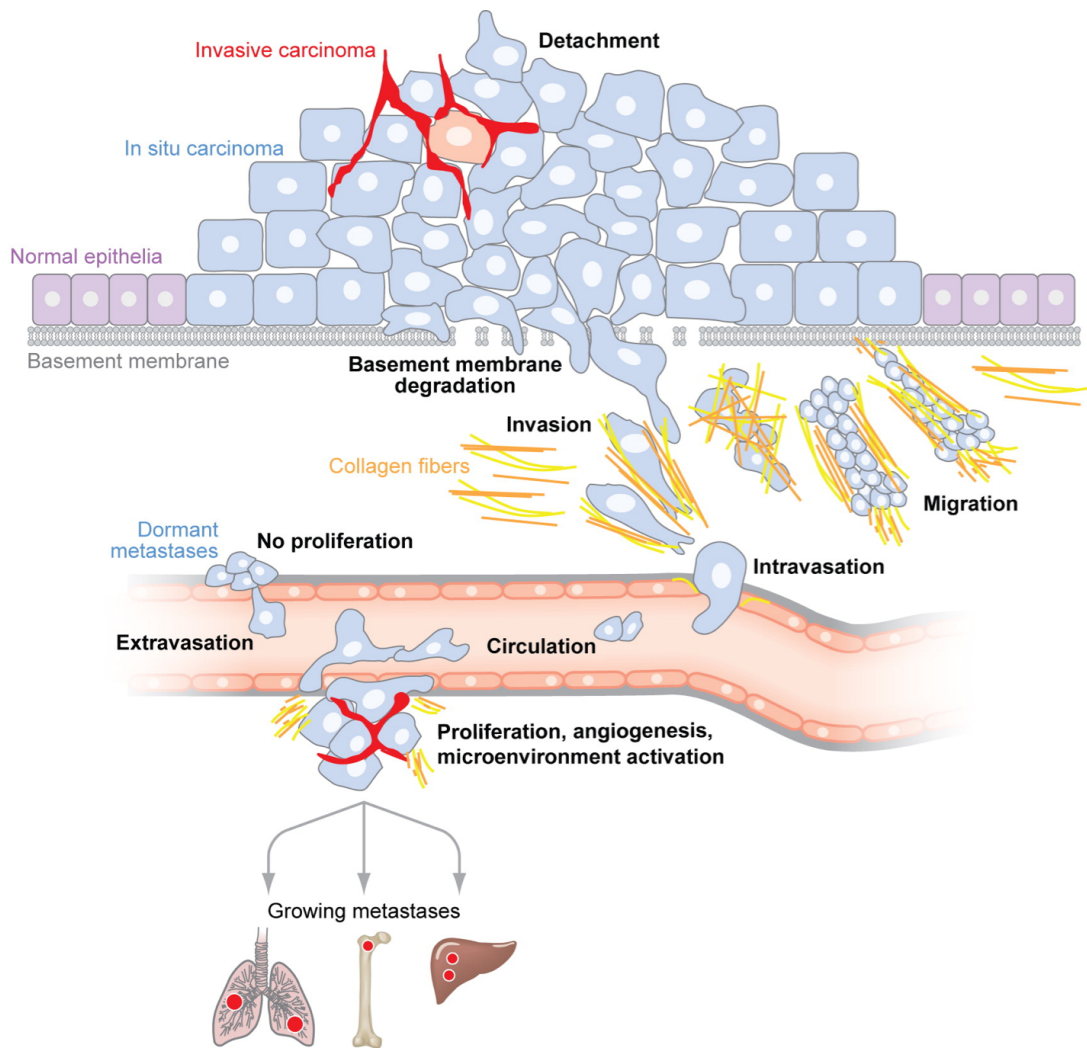
Figure 1.2. The metastatic cascade.

Metastasis involves several key steps, including (1) the detachment of cells from the primary site, (2) migration and invasion through the local tissue, (3) penetration through the basement membrane into lymphatic and blood vessels (intravasation), (4) travelling through the circulation, (5) exiting the circulation (extravasation), settling at distant sites, and (6) proliferation into new tumours. Figure is adapted from (Bacac & Stamenkovic, 2008).

(GEFs) (Zhai *et al.*, 2003), scaffold proteins GRB2 and ezrin (Schlaepfer *et al.*, 1994; Poullet *et al.*, 2001) and the proteolytic enzyme calpain (Carragher *et al.*, 2003; Chan *et al.*, 2010). A group of molecules from the small GTPase family are then activated by FAK, including Rho (Palazzo *et al.*, 2004), Rac and Cdc42 (Keely *et al.*, 1997). All of these proteins contribute to cell migration as well as invasion (Ridley *et al.*, 2003; Raftopoulou & Hall, 2004; Ridley, 2011). Rac and Cdc42 promote actin polymerisation by activating the Arp2/3 complex at the leading edge of the cell, leading to the formation of lamellipodia and filopodia, respectively (Nobes & Hall, 1995). On the other hand, Rho activation links to the ERK-Jun-amino-terminal kinase (JNK) pathway (Krueger *et al.*, 2001), which promotes cell migration by controlling myosin contraction (Kimura *et al.*, 1996) .

The invasion of cancer cells also involves the proteolytic cleavage of the ECM by matrix metalloproteinases (MMPs) (Egeblad & Werb, 2002; Bacac & Stamenkovic, 2008). A number of MMPs, including MMP-14, -15 and -16, are involved in the degradation of the basement membrane upon the first steps of invasion. MMP-14 has also been reported to regulate cancer cell morphology during invasion (Hotary *et al.*, 2003). CD44, a cell surface proteoglycan that promotes metastasis (McFarlane *et al.*, 2015), is also an interaction partner of MMP-14 (Kajita *et al.*, 2001; Mori *et al.*, 2002). Next, before invading through the basement membrane completely, MMPs indirectly promote local invasion, angiogenesis, and evasion of apoptosis by facilitating the maturation of growth factors including the epidermal growth factor (EGF) (Yu *et al.*, 2002), or by activating the tumour growth factor β (TGF-β) in a CD44-dependent pathway (Yu & Stamenkovic, 2000).

The cellular machineries and mechanisms involved in the metastatic cascade are highly complex and are often cell-type dependent. Although membrane proteins such as integrins and MMPs perform key roles in this process, interestingly, many types of ion channels and transporters at the plasma membrane are also involved and functionally

contribute to the metastasis. Thus, modulating ion channels and transporters in cancer has recently emerged as a potentially novel therapeutic modality. In addition to the reports showing the roles of $K^+$ channels (Huang & Jan, 2014; Pardo & Stuhmer, 2014), $Ca^{2+}$ channels (Prevarskaya *et al.*, 2007; Prevarskaya *et al.*, 2014), $Cl^-$ channels (Turner & Sontheimer, 2014) and ion transporters (Lastraioli *et al.*, 2015; Stock & Schwab, 2015) in promoting cancer cell metastatic behaviours, the therapeutic value of targeting VGSCs in cancer is becoming increasingly promising, given that VGSCs specifically promote cell metastatic behaviours, such as migration and invasion, *in vitro*, as well as tumour growth and metastasis *in vivo* (Besson *et al.*, 2015; Roger *et al.*, 2015).

### 1.4.3 α subunits in cancer

#### 1.4.3.1 Expression of α subunits in cancer

The first evidence of VGSC expression in cancer cells was reported in 1987 in theK562/ADM multidrug-resistant (MDR) human leukaemia cancer cell line (Yamashita *et al.*, 1987). Immediately following this study, another group found TTX-sensitive $I_{Na}$ in the human MDR T-cell leukaemia CCRF-CEM/VLB$_{100}$ cell line but not in the drug-sensitive CCRF-CEM cell line (Lee *et al.*, 1988). Both studies imply a relationship between $I_{Na}$/VGSC expression and malignancy. Since then, the VGSC mRNA and/or proteins have been found in increasing number of human cancer cell lines and patient tissue samples originating from various organs (Table 1.5).

In BCa cells, $I_{Na}$ carried by VGSCs was first identified in 2003 in the triple-negative, highly metastatic human MDA-MB-231 BCa cell line (Roger *et al.*, 2003). The $I_{Na}$ was absent in non-tumourigenic MCF-10A mammary epithelial cells and weakly metastatic MCF-7 and MDA-MB-468 BCa cells (Roger *et al.*, 2003; Fraser *et al.*, 2005). The mRNA expression level is > 100-fold higher in MDA-MB-231 cells compared with MCF-7 cells (Fraser *et al.*, 2005). Although $Na_v1.5$, $Na_v1.6$ and $Na_v1.7$ mRNA expression was found

Table 1.5. Expression of voltage-gated Na$^+$ channel α subunits in cancer

| Protein | Gene | Cancer type | References |
|---------|------|-------------|------------|
| Na$_v$1.1 | SCN1A | Ovarian | (Gao et al., 2010) |
| Na$_v$1.2 | SCN2A | Prostate, ovarian, cervical, mesothelioma | (Diss et al., 2001; Fulgenzi et al., 2006; Diaz et al., 2007; Gao et al., 2010) |
| Na$_v$1.3 | SCN3A | Prostate, ovarian, SCLC | (Diss et al., 2001; Onganer et al., 2005; Gao et al., 2010) |
| Na$_v$1.4 | SCN4A | Prostate, ovarian, cervical | (Diss et al., 1998; Diaz et al., 2007; Gao et al., 2010) |
| Na$_v$1.5 | SCN5A | Breast, colon, ovarian, lymphoma, neuroblastoma, NSCLC, SCLC | (Yamashita et al., 1987; Roger et al., 2003; Fraser et al., 2005; Onganer et al., 2005; Ou et al., 2005; Roger et al., 2007; Gao et al., 2010; House et al., 2010) |
| Na$_v$1.6 | SCN8A | Breast, cervical, ovarian, lymphoma, melanoma, mesothelioma, NSCLC, SCLC | (Diss et al., 2001; Fraser et al., 2005; Onganer et al., 2005; Fulgenzi et al., 2006; Diaz et al., 2007; Roger et al., 2007; Carrithers et al., 2009; Hernandez-Plata et al., 2012) |
| Na$_v$1.7 | SCN9A | Breast, prostate, cervical, ovarian, lymphoma, mesothelioma, NSCLC, SCLC | (Diss et al., 2001; Fraser et al., 2004; Fraser et al., 2005; Fulgenzi et al., 2006; Diaz et al., 2007; Roger et al., 2007; Gao et al., 2010) |
| Na$_v$1.8 | SCN10A | Prostate | (Suy et al., 2012) |
| Na$_v$1.9 | SCN11A | Lymphoma, SCLC | (Fraser et al., 2004; Onganer et al., 2005) |

NSCLC: non-small cell lung cancer; SCLC: small-cell lung cancer. Table is adapted from (Brackenbury, 2012).

in MDA-MB-231 cells, $Na_v1.5$ contributes to ~82 % of the total VGSC expression (Fraser *et al.*, 2005), and following studies using small-interfering RNA (siRNA) (Brackenbury *et al.*, 2007) and anti-peptide antibody (Chioni *et al.*, 2005) confirmed the $I_{Na}$ recorded in MDA-MB-231 cells is mainly carried by the neonatal splice variant of $Na_v1.5$. Neonatal $Na_v1.5$ protein is also found in human BCa tissues but not in normal breast, and increased neonatal $Na_v1.5$ mRNA expression associates with lymph node metastasis (Fraser *et al.*, 2005).

In prostate cancer (PCa) cell lines, $I_{Na}$ has been recorded from the highly metastatic rat Mat-LyLu but not weakly metastatic AT-2 cells (Grimes *et al.*, 1995). The $I_{Na}$ in Mat-LyLu cells is abolished by 100 nM TTX, suggesting presence of a TTX-sensitive VGSC isoform, later found to be neonatal $Na_v1.7$ (Diss *et al.*, 2001). TTX-sensitive $I_{Na}$, which is carried by $Na_v1.7$ (Diss *et al.*, 2001), was found in highly invasive human PC-3 cells, but was absent in the less invasive LNCaP cells (Laniado *et al.*, 1997). This is in agreement with VGSC mRNA expression levels in these cells: the $Na_v1.7$ mRNA level is ~$1 \times 10^6$-fold higher in Mat-LyLu cells than in AT-2 cells, and in PC-3 cells it is ~1100-fold higher compared to LNCaP cells (Diss *et al.*, 2001). The expression of α subunits in specimens from patients with benign prostatic hyperplasia or low-grade prostatic intraepithelial neoplasia is low compared to high-grade PCa, and the $Na_v1.7$ mRNA level is greater in high-grade PCa (Diss *et al.*, 2005; Diss *et al.*, 2008).

$I_{Na}$ carried by VGSCs has been reported in strongly metastatic H460, H23 and Calu-1 non-small-cell lung cancer (NSCLC) cell lines, but the current is absent in weakly invasive A549 and non-cancerous lung epithelial NL20 and BEAS-2B cells (Roger *et al.*, 2007; Campbell *et al.*, 2013). However, $Na_v1.6$ and $Na_v1.7$ mRNA are expressed in all of these cells (Roger *et al.*, 2007). In addition, TTX-sensitive current has also been recorded in human NCI-H128, NCI-H69 and NCI-H146 small-cell lung cancer cell lines (Pancrazio *et al.*, 1989). $Na_v1.3$, $Na_v1.5$ and $Na_v1.6$ mRNA was reported in H69, H209

and H510 small-cell lung cancer (SCLC) cells, and $Na_v1.9$ mRNA was also identified in H510 cells (Onganer *et al.*, 2005).

$Na_v1.5$ is functionally expressed in SW620, SW480 and HT29 human colon cancer cell lines (House *et al.*, 2010; Baptista-Hon *et al.*, 2014). $Na_v1.5$ expression is significantly higher in human colon cancer specimens than in normal colon tissues (House *et al.*, 2010). The $Na_v1.6$ mRNA expression level is significantly higher in colorectal carcinoma tissues compared to normal counterparts (Igci *et al.*, 2015). Moreover, TTX-sensitive $I_{Na}$ has been recorded in the primary cultures of human cervical cancer, where mRNA for $Na_v1.2$, $Na_v1.4$ and $Na_v1.7$ are found (Diaz *et al.*, 2007). Interestingly, analyses of RNA levels from biopsies showed that normal cervical cells express mRNA for $Na_v1.4$, whereas cervical cancer cells have up-regulated $Na_v1.2$, $Na_v1.6$ and $Na_v1.7$ mRNA (Diaz *et al.*, 2007). Agreeing with this, another study showed that $Na_v1.6$ and $Na_v1.7$ mRNA levels are higher in cervical cancer than in non-cancerous cervical biopsies (Hernandez-Plata *et al.*, 2012). The localisation of $Na_v1.6$ and $Na_v1.7$ is limited to the plasma membrane of cells from the intermediate and superficial zone of the cervical squamous epithelium in non-cancerous cervical biopsies, but VGSC expression is widely distributed in the plasma membrane, cytoplasm and nucleus region in most of the cells from cervical cancer biopsies (Hernandez-Plata *et al.*, 2012). $Na_v1.6$ contributes ~51 % of the total $I_{Na}$ in cervical cancer primary culture cells (Hernandez-Plata *et al.*, 2012). Additionally, real-time PCR (qPCR) analyses have shown increases in $Na_v1.2$, $Na_v1.4$, $Na_v1.5$ and $Na_v1.7$ mRNA expression in strongly metastatic ovarian cancer cells (Caov-3 and SKOV-3) in comparison to weakly metastatic Anglne ovarian cancer cells (Gao *et al.*, 2010). $Na_v1.5$ expression was only found in ovarian cancer with lymph node metastasis specimens (Gao *et al.*, 2010).

Finally, other cancerous tissue/cell lines in which VGSCs have been identified include human neoplastic mesothelial cells, where the TTX-sensitive $I_{Na}$ was reported (Fulgenzi *et al.*, 2006), and U251 human brain astrocytomas, where functional $Na_v1.5$

channels was reported (Xing *et al.,* 2014). Functional Na$_v$1.5 is present in NB-1 neuroblastoma cells (Ou *et al.,* 2005). THP-1 and HTB-66 melanoma cells express functional Na$_v$1.6 (Carrithers *et al.,* 2009). Na$_v$1.1, Na$_v$1.2, Na$_v$1.3, Na$_v$1.4, Na$_v$1.6 and Na$_X$ mRNA have also been identified in human glioma specimens, but further studies are needed in order to assess the VGSC protein level (Schrey *et al.*, 2002).

### 1.4.3.2 Functional roles of α subunits in cancer

VGSC activity potentiates a number of cell behaviours that contribute to metastasis *in vitro* including invasion, transwell migration, lateral motility, galvanotaxis, process extension, adhesion, plasma membrane endocytic activity, vesicular patterning, and gene expression (Table 1.6) (Brackenbury, 2012).

Blocking VGSCs using TTX (Fraser *et al.,* 2005; Brackenbury *et al.,* 2007), phenytoin (Yang *et al.,* 2012), ranolazine (Driffort *et al.,* 2014), or silencing Na$_v$1.5 with siRNA also reduces MDA-MB-231 cell invasion through Matrigel (Brackenbury *et al.,* 2007; Gillet *et al.,* 2009), whereas the cell *in vitro* proliferation is not affected. Similarly, TTX reduces Mat-LyLu and PC-3 PCa cell invasion but shows no effects on AT-2 and LNCaP cells where functional VGSCs are absent (Grimes *et al.,* 1995; Laniado *et al.,* 1997). Interestingly, overexpression of Na$_v$1.4 in LNCaP cells increases cell invasiveness, which can be reversed by TTX application, suggesting that VGSC expression is sufficient to promote invasion (Bennett *et al.,* 2004). Na$^+$ influx carried by VGSCs also increases H460, H23 and Calu-1 NSCLC cell invasion (Roger *et al.,* 2007). Moreover, TTX and siRNA targeting Na$_v$1.5 reduce the invasiveness of SW620, SW480 and HT29 human colon cancer cells, and blocking Na$_v$1.5 with ropivacaine in SW620 cells showed a similar effect (House *et al.,* 2010; Baptista-Hon *et al.,* 2014). Furthermore, in primary cervical cancer culture, TTX inhibits cell invasion but does not affect cell proliferation (Diaz *et al.,* 2007). Caov-3 and SKOV-3 ovarian cancer cells show reduced invasiveness, but not proliferation, after TTX treatment (Gao *et al.,* 2010).

In addition, TTX also suppresses the invasion of Jurkat lymphocytes (Fraser *et al.*, 2004), human neoplastic mesothelial cells (Fulgenzi *et al.*, 2006), and THP-1 and HTB-66 melanoma cells (Carrithers *et al.*, 2009). Finally, silencing neonatal Na$_v$1.5 with siRNA reduces U251 human brain astrocytoma cell invasion (Xing *et al.*, 2014).

Whether VGSCs control cell motility *in vitro* is under debate: TTX reduces the number of migrated MDA-MB-231 cells in some transwell migration studies (Fraser *et al.*, 2005; Isbilen *et al.*, 2006; Brackenbury *et al.*, 2007; Chioni *et al.*, 2010) but not others (Roger *et al.*, 2003). In addition, phenytoin reduces the lateral motility of MDA-MB-231 cells in wound healing assays (Yang *et al.*, 2012; Aktas *et al.*, 2015). TTX-treated Mat-LyLu cells show reduced transwell migration (Brackenbury *et al.*, 2007) and lateral motility (Fraser *et al.*, 2003). The transwell migration of PC-3M cells (Uysal-Onganer & Djamgoz, 2007) and the lateral motility of U251 cells (Xing *et al.*, 2014) are also reduced after TTX treatment. However, the transwell migration of H460, H23 and Calu-1 cells (Roger *et al.*, 2007), Caov-3 and SKOV-3 cells (Gao *et al.*, 2010), and primary cervical cancer culture cells is not affected by TTX (Diaz *et al.*, 2007). Therefore, whether or not VGSCs promote cancer cell migration is highly cell type-dependent. More experiments are needed in order to elucidate the role of VGSCs in controlling cancer cell migration.

Both Mat-LyLu and MDA-MB-231 cells are galvanotactic, meaning that they move directionally in response to an electric field. Mat-LyLu cells move towards the cathode (Djamgoz *et al.*, 2001), whereas MDA-MB-231 cells move towards the anode (Fraser *et al.*, 2005), following the application of an electric field of 3 V/cm. TTX application significantly reduces the galvanotaxis in both types of cells (Djamgoz *et al.*, 2001; Fraser *et al.*, 2005). On the other hand, veratridine enhances the galvanotactic movement of Mat-LyLu cells (Djamgoz *et al.*, 2001).

VGSCs change the morphology of Mat-LyLu cells by decreasing cell process length and increasing cell body diameter and process thickness (Fraser *et al.*, 1999). In

Table 1.6. Metastatic cell behaviours regulated by voltage-gated Na$^+$ channels

| Cellular activity | Cancer | VGSC subunit(s) implicated | References |
|---|---|---|---|
| Invasion | Breast, prostate, colon, cervical, NSCLC, lymphoma, melanoma | Na$_v$1.5, Na$_v$1.6, Na$_v$1.7, β2 | (Laniado et al., 1997; Smith et al., 1998b; Roger et al., 2003; Fraser et al., 2004; Fraser et al., 2005; Roger et al., 2007; Carrithers et al., 2009; Gao et al., 2010; House et al., 2010; Hernandez-Plata et al., 2012; Jansson et al., 2012) |
| Transwell migration | Breast, prostate | Na$_v$1.5, Na$_v$1.7 | (Fraser et al., 2005; Brackenbury & Djamgoz, 2006; Isbilen et al., 2006; Brackenbury et al., 2007; Uysal-Onganer & Djamgoz, 2007; Chioni et al., 2010) |
| Lateral motility | Breast, prostate, brain | Na$_v$1.5, Na$_v$1.7, β1, β2 | (Fraser et al., 2003; Yang et al., 2012; Xing et al., 2014) |
| Galvanotaxis | Breast, prostate | Na$_v$1.5, Na$_v$1.7 | (Djamgoz et al., 2001; Fraser et al., 2005; Chioni et al., 2009; Jansson et al., 2012) |
| Process extension | Breast, prostate | Na$_v$1.7, β1 | (Fraser et al., 1999; Chioni et al., 2009) |
| Adhesion | Breast, prostate | Na$_v$1.5, Na$_v$1.7, β1, β2 | (Palmer et al., 2008; Chioni et al., 2009; Jansson et al., 2012) |
| Endocytic activity at plasma membrane | Breast, prostate, SCLC | Na$_v$1.5, Na$_v$1.7 | (Mycielska et al., 2003; Fraser et al., 2005; Onganer et al., 2005) |
| Vesicular patterning | Breast, prostate | Na$_v$1.7 | (Krasowska et al., 2004, 2009) |
| Gene expression | Breast, prostate, colon | Na$_v$1.5, Na$_v$1.7, β1 | (Mycielska et al., 2005; Brackenbury et al., 2007; Chioni et al., 2009; House et al., 2010) |

NSCLC: non-small cell lung cancer; SCLC: small-cell lung cancer. Table is adapted from (Brackenbury, 2012).

MDA-MB-231 cells, inhibiting $Na_v1.5$ using small-hairpin RNA (shRNA) (Brisson *et al.*, 2013; Nelson *et al.*, 2015b) or ranolazine (Driffort *et al.*, 2014) causes less elongated cell morphology. Moreover, PC-3M and Mat-LyLu cells pre-treated with TTX show reduced adhesion to glass coverslips (Palmer *et al.*, 2008). Additionally, TTX reduces the endocytic/vesicular uptake of horseradish peroxidase in Mat-LyLu and MDA-MB-231 cells (Mycielska *et al.*, 2003; Krasowska *et al.*, 2004; Fraser *et al.*, 2005; Krasowska *et al.*, 2009), whereas opening VGSCs in MDA-MB-231 cells with aconitine has the opposite effect (Fraser *et al.*, 2005; Krasowska *et al.*, 2009). Aggregated vesicles are observed in Mat-LyLu and MDA-MB-231 cells following the uptake of horseradish peroxidase, which is attenuated by TTX treatment (Mycielska *et al.*, 2003; Krasowska *et al.*, 2004, 2009). Furthermore, interestingly, in NCL-H146 SCLC cells, VGSCs are involved in the initiation of action potential firing (Blandino *et al.*, 1995).

VGSC α subunits also regulate expression of invasion-related genes. In colon cancer, using HT29 cells, bioinformatic analyses revealed that $Na_v1.5$ mRNA may regulate the expression of genes that encode MMPs (e.g. *ADAM9*), members involved in $Ca^{2+}$ signalling (e.g. *CCR9*) and membrane remodelling (e.g. *CHMP4C*) (House *et al.*, 2010). A following study demonstrated that activating $Na_v1.5$ with veratridine increases invasion-related gene expression in SW620 cells, including *CD44*, *CLIC*, *WNT9A*, *ITGB*, *SEMA6A* and *VEGFC* (House *et al.*, 2015).

VGSCs potentiate cancer progression *in vivo*. Rats subcutaneously implanted with Mat-LyLu cells show significantly reduced tumour metastases and improved survival as a result of daily TTX injection into the tumour (Yildirim *et al.*, 2012). Daily injection with phenytoin significantly reduced tumour growth and metastasis to lungs, liver and spleen in mice bearing orthotopic tumour of MDA-MB-231 cells (Nelson *et al.*, 2015a). In addition, ranolazine treatment reduces metastasis to lungs after injection of MDA-MB-231 cells into the mouse tail vein (Driffort *et al.*, 2014). More recently, it has been shown that tumour growth and metastasis are significantly decreased in mice implanted with

MDA-MB-231 cells where $Na_v1.5$ expression is suppressed by shRNA, compared to those implanted with MDA-MB-231 cells infected with control scrambled shRNA (Nelson *et al.*, 2015b). Therefore, an increasing body of evidence shows the expression of VGSCs in cancer cells and cancer patient biopsies, and suggests a role in promoting metastatic behaviours, both *in vitro* and *in vivo*.

### 1.4.3.3 Mechanisms underlying α subunit-dependent cancer cell metastatic behaviours

Several models have been proposed in order to explain enhanced metastatic behaviours caused by VGSC α subunits, which include regulation of pH, gene expression and activity of protein kinases.

In MDA-MB-231 cells, $Na_v1.5$ has been shown to increase cell invasion by allosterically activating $Na^+$-$H^+$ exchanger type 1 (NHE1) at the plasma membrane. NHE1 regulates the intracellular pH and acidifies the immediate extracellular environment by extruding $H^+$, favouring the proteolytic activity of cathepsin B and S (Gillet *et al.*, 2009; Brisson *et al.*, 2011). $Na_v1.5$ co-immunoprecipitates with NHE1, and it is proposed that both the proteins form functional complexes located in caveolin-1-containing lipid rafts at invadopodia (Brisson *et al.*, 2011; Brisson *et al.*, 2013). Moreover, $Na_v1.5$ promotes src kinase activity and phosphorylation of cortactin and cofilin, which both lead to actin polymerisation (Brisson *et al.*, 2013). In addition, silencing $Na_v1.5$ expression by using shRNA reduces the protein level of the metastasis-promoting molecule CD44 in MDA-MB-231 cells (Nelson *et al.*, 2015b).

In SW620 colon cancer cells, veratridine increases the size of $I_{Na}$, cell invasiveness, and activates mitogen activated protein kinase (MAPK) signalling (House *et al.*, 2015). U0126, an inhibitor of MAPK/ERK kinase (MEK), abolishes the ERK phosphorylation caused by veratridine, suggesting VGSCs enhance SW620 cell invasion via the ERK signalling pathway. The process is mediated by PKA and the small GTPase

Rap1B, and ultimately leads to activation of various transcription factors (TFs) including ELK1, ETS-1 and c-Jun (House *et al.*, 2015). Interestingly, veratridine also increases the protein level of CD44, as in MDA-MB-231 cells (House *et al.*, 2015; Nelson *et al.*, 2015b), suggesting that the $Na_v$1.5-CD44 signalling axis may be universal in promoting metastasis in various types of cancer.

In H460 NSCLC cells, EGF increases cell invasion in a $Na_v$1.7-dependent manner (Campbell *et al.*, 2013). Application of the ERK inhibitor U0126 inhibits cell invasion and co-application of U0126 and TTX showed no additive effect, suggesting that $Na_v$1.7-dependent H460 cell invasion is via the ERK pathway (Campbell *et al.*, 2013). In summary, the proposed models suggest α subunits increase cancer cell invasion by several mechanisms. However, there may be further undiscovered mechanism(s), and future experiments are needed to clarify whether these mechanisms are widely applicable among all cancers.

### 1.4.3.4   Regulation of α subunit expression in cancer cells

The expression of α subunits in cancer cells is also subject to a variety of regulations. Autoregulation of VGSCs has been reported in PCa cells, where 48 h TTX pre-treatment reduces $Na_v$1.7 mRNA level in PC-3M cells (Mycielska *et al.*, 2005). In Mat-LyLu PCa cells, $I_{Na}$ activates PKA, which in turn potentiates $Na_v$1.7 mRNA expression and protein trafficking to the plasma membrane (Brackenbury & Djamgoz, 2006). Similarly, in MDA-MB-231 BCa cells, pre-treatment with the PKA activator forskolin for 24 h increases $Na_v$1.5 mRNA level as well as the protein level at the plasma membrane (Chioni *et al.*, 2010); on the other hand, pre-treatment with TTX reduces PKA phosphorylation and PKA-induced cell transwell migration (Chioni *et al.*, 2010).

Serum affects the size of $I_{Na}$ and the kinetics of the α subunits in Mat-LyLu cells (Ding & Djamgoz, 2004). Growth factors in serum have a number of effects on VGSCs: EGF increases $Na_v$1.7 mRNA level and protein expression in PC-3M cells, which then

potentiates cell migration, invasion and endocytosis (Uysal-Onganer & Djamgoz, 2007). In Mat-LyLu cells, EGF increases $I_{Na}$ density as well as cell transwell migration (Ding *et al.*, 2008). The mRNA level of $Na_v1.7$ is also up-regulated in H460 NSCLC cells after EGF treatment, along with increased cell invasion (Campbell *et al.*, 2013). Nerve growth factor (NGF) enhances $I_{Na}$ in Mat-LyLu cells (Brackenbury & Djamgoz, 2007); however, the NGF-induced increase in cell transwell migration is independent of VGSC activity (Brackenbury & Djamgoz, 2007). Additionally, the estrogen β-estradiol increases $I_{Na}$ in MDA-MB-231 cells, and the action is dependent on GPR30, a G-protein-coupled ER, and PKA (Fraser *et al.*, 2010). In summary, both the expression and function of α subunits in cancer cells are regulated by growth factors and hormones, and the autoregulation of α subunits also occurs.

### 1.4.4  β subunits in cancer

In addition to α subunits, VGSC β subunits have been identified in a number of cancer cells (Table 1.7) where they contribute to metastatic behaviour (Table 1.6). β1 has a relatively higher expression in MCF-7 cells than in MDA-MB-231 cells, and it facilitates MCF-7 cell adhesion to substrate but slows transwell migration (Chioni *et al.*, 2009). Overexpression of β1 in MDA-MB-231 cells increases MDA-MB-231 cell-cell adhesion and process outgrowth but reduces cell migration *in vitro* (Chioni *et al.*, 2009). Interestingly, silencing β1 using siRNA increases the $Na_v1.5$ mRNA and protein level in MCF-7 cells (Chioni *et al.*, 2009), whereas overexpressing β1 in MDA-MB-231 cells enhances $I_{Na}$ density (Chioni *et al.*, 2009). β1 mRNA and protein are present in patient BCa samples, and the β1 protein expression, determined by immunohistochemistry, is significantly higher in tumour tissue than normal breast tissue (Nelson *et al.*, 2014). Overexpression of β1 increases process outgrowth in MDA-MB-231 cells via homophilic

| Table 1.7. Voltage-gated Na$^+$ channels β subunit expression in cancer | | | |
|---|---|---|---|
| **Protein** | **Gene** | **Cancer type** | **References** |
| β1 | *SCN1B* | Breast, prostate, cervical, NSCLC | (Roger *et al.*, 2007; Diss *et al.*, 2008; Chioni *et al.*, 2009; Hernandez-Plata *et al.*, 2012; Nelson *et al.*, 2014) |
| β2 | *SCN2B* | Breast, prostate, cervical, NSCLC | (Roger *et al.*, 2007; Diss *et al.*, 2008; Chioni *et al.*, 2009; Hernandez-Plata *et al.*, 2012; Jansson *et al.*, 2012) |
| β3 | *SCN3B* | Prostate, NSCLC | (Roger *et al.*, 2007; Hernandez-Plata *et al.*, 2012) |
| β4 | *SCN4B* | Breast, prostate, cervical, NSCLC | (Roger *et al.*, 2007; Diss *et al.*, 2008; Chioni *et al.*, 2009; Hernandez-Plata *et al.*, 2012) |
| NSCLC: non-small cell lung cancer. Table is adapted from (Brackenbury, 2012). | | | |

adhesion, which is dependent on fyn kinase and $Na^+$ influx through α subunits (Nelson *et al.*, 2014), similar to its role in the CNS (Brackenbury *et al.,* 2008; Brackenbury *et al.*, 2010). Compared to control MDA-MB-231 cells, mice bearing β1-overexpressing MDA-MB-231 cells show increased tumour growth and vascularisation, together with increased metastasis to lungs and liver (Nelson *et al.*, 2014). Taken together, β1 expression enhances cell adhesion and process outgrowth but retards migration of BCa cells *in vitro*, where it also regulates the expression and activity of α subunits. *In vivo*, β1 potentiates BCa tumour growth and metastasis.

The total β subunit mRNA level in metastatic PC-3 and PC-3M cells is significantly higher than in weakly metastatic LNCaP cells, and β1 is again the predominant isoform (Diss *et al.*, 2008). However, the mRNA levels of β1–β4 are similar comparing PCa and non-PCa biopsies (Diss *et al.*, 2008), possibly because the processing of the tissue causes inaccuracy by including cells not only from PCa but also surrounding non-cancerous tissues, such as skeletal muscle, where β subunits are also expressed (Diss *et al.*, 2008). Additionally, β1–β4 mRNAs have been found in cervical cancer tissues. Compared to non-cancerous cervix tissues, β2, β3 and β4 mRNA levels are up-regulated in cervical cancer, whereas in primary culture, β2 and β4 mRNAs are hardly detected (Hernandez-Plata *et al.*, 2012). One possible explanation is that the roles of β subunits as cell adhesion molecules are different in biopsies and primary cultures (Hernandez-Plata *et al.*, 2012).

LNCaP cells overexpressing β2 display an elongated cell body with a reduced cell volume and increased migratory and invasive capacity, as well as a preferential binding to vitronectin compared to control LNCaP cells (Jansson *et al.*, 2012). In contrast to the role of β1 in the MDA-MB-231 BCa mouse model, subcutaneously implanted LNCaP-β2 cells show reduced tumour take and tumour volume *in vivo* (Jansson *et al.*, 2012). Thus, β1 and β2 may interact with different extracellular proteins in these different models and therefore exert distinct cellular behaviours.

*SCN3B* contains two response elements to p53 (Adachi *et al.*, 2004). *SCN3B* is up-regulated after DNA damage in a p53-dependent manner in mouse embryonic fibroblasts, and overexpression of p53 up-regulates the β3 mRNA level in HCT116, Saos2 and H1299 human cancer cell lines (Adachi *et al.*, 2004). Finally, although β1–β4 mRNA has been found in SCLC cell lines, their roles in regulating cell activity have not been studied (Roger *et al.*, 2007). In summary, VGSC β subunits are present in several cancer types, and they regulate key steps associated with metastasis.

### 1.4.5  Therapeutic value of VGSCs in BCa

Tumour microarray data have revealed that the $Na_v1.5$ mRNA level is significantly higher in BCa biopsies from patients than in normal breast samples, and is higher in BCa samples from patients who developed metastasis, recurrence, or who died in five years (Yang *et al.*, 2012), suggesting a relationship between $Na_v1.5$ expression and malignancy in patients. Recent *in vivo* data show that suppressing VGSC activity reduces tumour growth and metastasis in rodents (Yildirim *et al.*, 2012; Driffort *et al.*, 2014; Nelson *et al.*, 2015a; Nelson *et al.*, 2015b). Importantly, some of the studies adopted drugs inhibiting VGSCs that are approved by the US Food and Drug Administration (FDA) (Driffort *et al.,* 2014; Nelson *et al.*, 2015a), and repurposing these drugs may be a new strategy for cancer treatment. Riluzole, a compound that blocks VGSCs and the metabotropic glutamate receptor 1, reduces BCa growth in mice (Speyer *et al.*, 2012) and supresses metabolic activity in patients with melanoma (Yip *et al.*, 2009). A novel VGSC blocker, RS100642, reduces oxidative stress and improves animal survival in 7,12-dimethylbenz(a)anthracene (DMBA)-induced rat BCa model (Batcioglu *et al.*, 2012). Taken together, an increasing amount of evidence suggests that VGSC α subunits may be novel targets in cancer treatment.

## 1.5  Membrane potential as a functional signal in cancer progression

An important outcome of collective ion channel and transporter activity is the change in cellular $V_m$. $V_m$, defined as the voltage across the plasma membrane, arises due to the unequal distribution of various types of ions, including $Na^+$, $K^+$, $Cl^-$ and $Ca^{2+}$. As described by the Goldman-Hodgkin-Katz equation (Equation 1.1), the $V_m$ depends on the permeability (P) and both the intracellular and extracellular concentrations of major ions (Goldman, 1943; Hodgkin & Katz, 1949):

$$V_m = \frac{RT}{F} \ln \left( \frac{P_{Na^+}[Na^+]_o + P_{K^+}[K^+]_o + P_{Cl^-}[Cl^-]_i}{P_{Na^+}[Na^+]_i + P_{K^+}[K^+]_i + P_{Cl^-}[Cl^-]_o} \right) \qquad \text{(Equation 1.1)}$$

where R is the ideal gas constant, T temperature and F Faraday's constant. As described in Section 1.1, in excitable cells including neurones, skeletal muscle fibres and cardiomyocytes, action potentials initiate from the depolarisation of $V_m$.

Seminal work describing the functional roles of $V_m$ in non-excitable cells began in the late 1960s, pioneered by Clarence D. Cone Jr. While studying mitotic activities in sarcoma cells, he reported that $V_m$ undergoes hyperpolarisation before entering M phase (Cone, 1969), and that $V_m$ hyperpolarisation reversibly blocks DNA synthesis and mitosis (Cone, 1970). Cone and colleagues then demonstrated that $V_m$ depolarisation is able to initiate mitosis in CHO cells and mouse spleen lymphocytes (Cone & Tongier, 1971; Kiefer *et al.*, 1980), whereas hyperpolarised $V_m$ immediately precedes mitotic arrest (Cone & Tongier, 1973).

### 1.5.1  Depolarised $V_m$ correlates with tumourigenesis

As early as the 1970s, Clarence D. Cone Jr. postulated that the $V_m$ is correlated with the level of cell differentiation (Cone, 1971). A similar phenomenon was seen in earlier studies, which demonstrated significant $V_m$ depolarisation during malignant

transformation of normal cells (Tokuoka & Morioka, 1957; Johnstone, 1959). Indeed, recordings from rodent and human tissues revealed that proliferative cells, especially rapidly proliferating tumour cells, display relatively depolarised $V_m$, whereas non-proliferating, terminally differentiated somatic cells, such as muscle cells and neurones, are characterised by their hyperpolarised $V_m$ (Figure 1.3) (Binggeli & Weinstein, 1986; Blackiston *et al.*, 2009; Yang & Brackenbury, 2013).

Direct *in vitro* and *in vivo* comparisons of $V_m$ levels between normal and cancerous breast cells (Marino *et al.*, 1994), hepatocytes and hepatocellular carcinoma cells (Binggeli & Cameron, 1980; Stevenson *et al.*, 1989), normal and neoplastic adrenocortical tissues (Lymangrover *et al.*, 1975), normal embryonic fibroblasts and fibrosarcoma (Binggeli & Weinstein, 1985), benign and cancerous skin cells (Melczer & Kiss, 1957; Woodrough *et al.*, 1975), and between normal and cancerous ovarian tissue (Redmann *et al.*, 1972) show that cancer cells tend to be more depolarised than their normal counterparts. In a study where the $V_m$ of MCF-10A, MCF-7, MDA-MB-468 and MDA-MB-231 BCa cells was compared, $V_m$ was found to be more depolarised as the metastatic potential of the cell line increased: the $V_m$ of the strongly metastatic MDA-MB-231 cells is ~-19 mV, whereas the $V_m$ is ~-40 and ~-50 mV in MCF-7 and MCF-10A cells, respectively (Fraser *et al.*, 2005). In PCa, the $V_m$ of strongly metastatic PC-3 cells is ~5 mV more depolarised than the weakly metastatic LNCaP cells (Laniado *et al.*, 1997). These findings suggest a correlation between depolarised $V_m$ and cancer malignancy. Since $V_m$ is determined by the combined activities of ion channels/transporters at the cell membrane, it would be natural to consider $V_m$ merely as an epi-phenomenon resulting from changes in intracellular concentration of ions. However, over the past four decades, increasing evidence has shown that $V_m$ is a functional signal regulating a number of cell behaviours, including cell proliferation, migration and stem cell differentiation (Yang & Brackenbury, 2013).
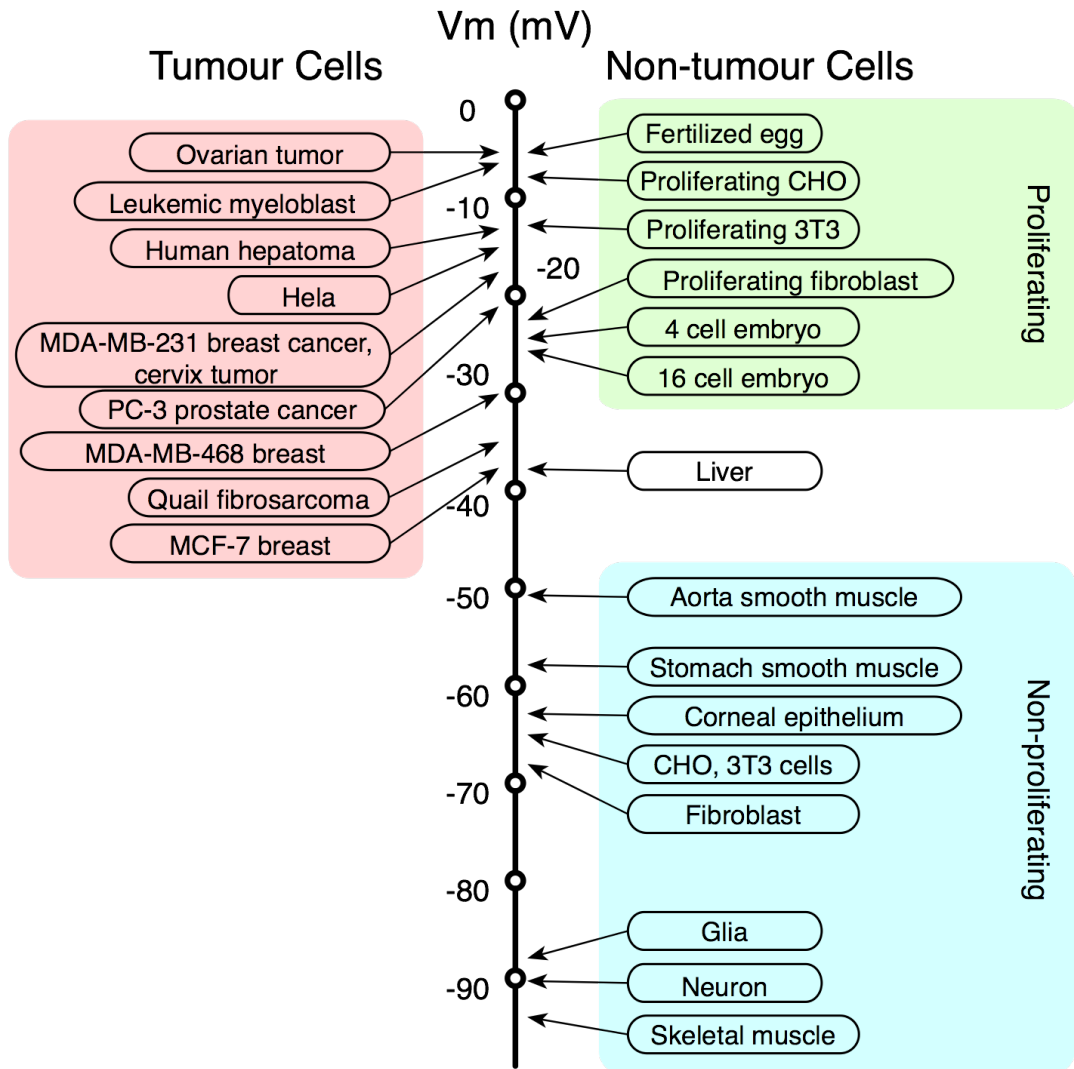
Figure 1.3. Membrane potential ($V_m$) scale.

Rapidly proliferating cancer cells possess relatively depolarised $V_m$ (red box), while the $V_m$ of quiescent cells is generally more hyperpolarised (cyan box). The $V_m$ of proliferative somatic cells is also depolarised. Figure is adapted from (Binggeli & Weinstein, 1986; Yang & Brackenbury, 2013).

### 1.5.2  $V_m$ and cell proliferation

Depolarisation can function as a signal initiating mitosis and DNA synthesis in both highly proliferative tumour and non-tumour cells (Orr *et al.*, 1972; Binggeli & Weinstein, 1986). Artificially altering the $V_m$ by modulating the extracellular ionic composition or applying the $Na^+/K^+$-ATPase inhibitor ouabain revealed interesting results: firstly, hyperpolarising the $V_m$ of CHO cells to -45 mV induces mitotic arrest, and cell division is fully blocked at -75 mV. The cell cycle is resumed by depolarising the $V_m$ to -10 mV (Cone, 1971). Secondly, quiescent ($G_0$) mature chick spinal cord neurones show mitotic activity after depolarisation (Cone & Cone, 1976). By contrast, hyperpolarised $V_m$ immediately precedes mitotic arrest (Cone & Tongier, 1973).

An additional layer of complexity in this model is that the $V_m$ fluctuates during cell cycle progression, and follows a multi-step and rhythmic pattern (Wonderlin & Strobl, 1996; Blackiston *et al.*, 2009) (Figure 1.4). $V_m$ hyperpolarisation at the $G_1/S$ checkpoint is generally required for S phase initiation. For example, depolarising the cell membrane halts $G_1/S$ progression in glia (Canady *et al.*, 1990), Schwann cells (Wilson & Chiu, 1993), lymphocytes (Price *et al.*, 1989; Freedman *et al.*, 1992; Wang *et al.*, 1992b), V79 Chinese hamster lung cells (Sachs *et al.*, 1974), C1300 mouse neuroblastoma cells (Boonstra *et al.*, 1981) and MCF-7 human BCa cells (Wonderlin *et al.*, 1995). The $V_m$ then remains relatively hyperpolarised through S phase in some cell types (Sachs *et al.*, 1974; Boonstra *et al.*, 1981; Strobl *et al.*, 1995; Wonderlin *et al.*, 1995), and more depolarised in others (Arcangeli *et al.*, 1995; MacFarlane & Sontheimer, 2000). Moreover, the $G_2/M$ transition exhibits a depolarised $V_m$ (Sachs *et al.*, 1974; Boonstra *et al.*, 1981; Blackiston *et al.*, 2009), although it is not yet clear whether or not this depolarisation is a prerequisite for $G_2/M$ progression. In rat cardiomyocytes, ouabain-induced depolarisation leads to an increased population in $G_2/M$ (and S) phase (Lan *et al.*, 2014). In D54-MG human glioma cells, the $V_m$ depolarisation at $G_2/M$ is likely
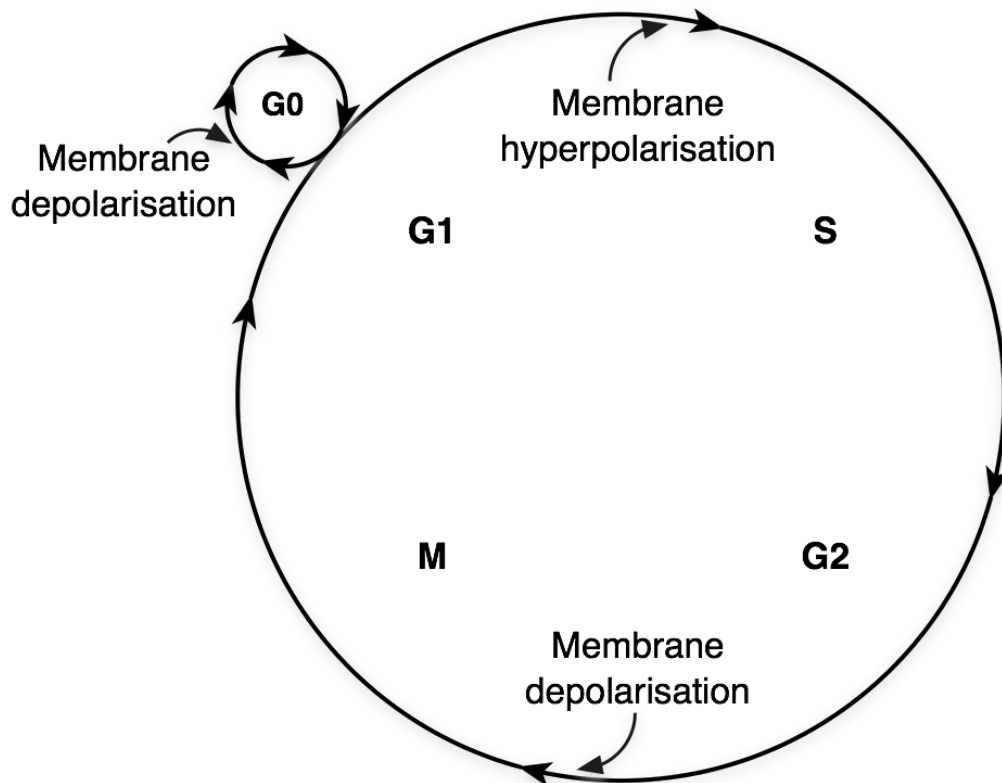
Figure 1.4. Membrane potential ($V_m$) and the progression of cell cycle.

$V_m$ undergoes hyperpolarisation at $G_1/S$ border, by virtue of $K^+$ efflux through various types of $K^+$ channels. Before cells enter M phase, increased $Cl^-$ efflux accompanies $V_m$ depolarisation. Quiescent cells at $G_0$ stage show mitotic activities after $V_m$ depolarisation. Figure is adapted from (Yang & Brackenbury, 2013).

mediated by $Cl^-$ efflux through the outward rectifying ClC3 channels (Habela *et al.*, 2008). In addition, exogenous ClC2 channels are highly expressed in M phase in NRK-49F rat kidney fibroblasts (Zheng *et al.*, 2002).

The fluctuation of $V_m$ levels across the cell cycle does not necessarily contradict the observation that depolarised $V_m$ could be a signature of cancer cells. The mean $V_m$ values in cancer cells are consistently depolarised relative to most normal somatic cell types (Figure 1.3). For example, MCF-7 cells arrested at $G_1$ phase have a $V_m$ of -9 mV and hyperpolarize to ~-30 mV in the S phase (Wonderlin *et al.*, 1995). Both these values are more depolarised than normal breast cells, e.g. the mean $V_m$ of unsynchronised MCF-10A cells is between -40 and -58 mV (Wonderlin *et al.*, 1995; Fraser *et al.*, 2005).

Evidence suggests that the fluctuation in $K^+$ conductance contributes significantly to changes in $V_m$ during the cell cycle. For example, in neuroblastoma and Ehrlich ascites cells, there is a transient decrease in $K^+$ efflux before entering the $G_2$ phase, and a relatively high level of $K^+$ efflux during the M phase (Mills & Tupper, 1976; Boonstra *et al.*, 1981). Given the diversity of $K^+$ channel types (Hille, 1992; Miller, 2000; Wang, 2004), their contributions to the $V_m$ and $V_m$-dependent cell cycle progression are probably context-dependent and highly complex. For example, inhibition of cell proliferation with $K^+$ channel inhibitors does not correlate with changes in the $V_m$ in rat C6 glioma cells (Rouzaire-Dubois *et al.*, 2000). In addition, the $V_m$ is likely to be determined by the collective activities of a variety of ions channels/transporters, which may exhibit reciprocal interactions and form a large and complex network responsible for $V_m$ regulation and its downstream effects.

### 1.5.3 Ion channel-dependent regulation of proliferation and $V_m$

Numerous studies have shown that pharmacological or genetic block of VGPCs reduces proliferation of cancer cells (Fraser *et al.*, 2000; Ouadid-Ahidouch *et al.*, 2000; Abdul & Hoosein, 2002; Chang *et al.*, 2003; Menendez *et al.*, 2010) (Figure 1.5).

Figure 1.5. Key ion channels that regulate membrane potential ($V_m$) and cell cycle progression in cancer.

Hyperpolarising channels would increase the driving force for $Ca^{2+}$ influx through voltage-independent channels, whereas inwardly rectifying $K^+$ channels (predominantly inward $I_K$, green) and chloride channels (outward $Cl^-$, green) would depolarise the $V_m$, thus enabling activation of voltage-dependent $Ca^{2+}$ influx. Time- and domain-dependent $Ca^{2+}$ signalling is then proposed to activate pathways that promote cell cycle progression and proliferation. $K_{Ca}$: $Ca^{2+}$-activated $K^+$ channel; EAG: ether à go-go channel; $K_V$: voltage-gated $K^+$ channel; $K_{ATP}$: ATP-sensitive $K^+$ channel; $K_{2P}$: two-pore domain $K^+$ channel; ERG: EAG-related gene $K^+$ channel; $K_{ir}$: classic inward-rectifier $K^+$ channel; ClC2/3: $Cl^-$ 2/3 channel. Figure is adapted from (Yang & Brackenbury, 2013).

Increasing evidence suggests that *Ether à go-go* (EAG) $K^+$ channels may serve as biomarkers for cancer (Ouadid-Ahidouch *et al.*, 2001; Farias *et al.*, 2004; Pardo *et al.*, 2005; Hemmerlein *et al.*, 2006; Ousingsawat *et al.*, 2007; Ortiz *et al.*, 2011; Rodriguez-Rasgado *et al.*, 2012). Inhibition of EAG channel expression reduces proliferation in several cancer cell lines, whereas implantation of CHO cells overexpressing EAG channels in mice induces tumours (Pardo *et al.*, 1999). In synchronised SH-SY5Y neuroblastoma cells, EAG current ($I_{EAG}$) is reduced to less than 5 % in $G_1$ phase, compared to unsynchronised controls, suggesting that the activity of EAG channels is cell-cycle dependent (Meyer & Heinemann, 1998). Indeed, in MCF-7 cells, inhibiting EAG channels with astemizole increases the proportion of cells in $G_1$ phase and reduces the proportion in S phase (Borowiec *et al.*, 2007). In contrast, activation of human EAG (hEAG) channels is responsible for hyperpolarisation at late $G_1$ before the cells enter the S phase (Ouadid-Ahidouch *et al.*, 2001). Interestingly, the hyperpolarisation is accompanied by increased $Ca^{2+}$-activated $K^+$ ($K_{Ca}$) channel currents (Ouadid-Ahidouch *et al.*, 2001), which might result from the elevated intracellular $Ca^{2+}$ due to the increased electrochemical gradient during the hyperpolarisation (Nilius & Wohlrab, 1992; Ouadid-Ahidouch & Ahidouch, 2008).

$K_{Ca}$ channels were thought to be one of the main controllers of the $V_m$ in Friend murine erythroleukemia cells (Arcangeli *et al.*, 1987). $K_{Ca}$ channels have been found in glioma (Liu *et al.*, 2002), PCa (Gessner *et al.*, 2005), BCa (Haren *et al.*, 2010) and the CD133$^+$ subpopulation of SH-SY5Y cells (Park *et al.*, 2010). Inhibiting $K_{Ca}$ channels with iberiotoxin (IbTx) arrests D54-MG glioma cells in S phase, and leads to apoptosis (Weaver *et al.*, 2004). Thus, the functional contribution of $K_{Ca}$ channels to cell cycle regulation appears to be distinct from VGPC channels. In addition, in MCF-7 cells, inhibition of ATP-sensitive $K^+$ ($K_{ATP}$) channels reversibly arrests cells in the $G_0/G_1$ phase (Woodfork *et al.*, 1995). The two-pore domain $K^+$ channel, TREK1, increases proliferation of PC-3 and LNCaP cells (Voloshyna *et al.,* 2008). In CHO cells,

overexpression of TREK1 increases the number of cells in S phase, and reduces the number of cells at $G_0/G_1$ phase (Voloshyna *et al.*, 2008).

Human EAG-related gene (HERG) $K^+$ channels are strongly inwardly rectifying and conduct $K^+$ influx when the voltage is more negative than the $K^+$ equilibrium potential (Trudeau *et al.*, 1995; Smith *et al.*, 1996). HERG current ($I_{HERG}$) is expressed at early developmental stages in the neural crest, central nervous system, dorsal root ganglion (DRG) and skeletal muscle, and is replaced by classic inward rectifier $K^+$ current ($I_{Kir}$) later in development (Arcangeli *et al.*, 1997; Crociani *et al.*, 2000). HERG channels are up-regulated in a number of cancers (Arcangeli, 2005). Moreover, $I_{HERG}$ increases tumour cell proliferation (Bianchi *et al.*, 1998; Wang *et al.*, 2002). The activity of $I_{HERG}$ itself is cell cycle dependent (Arcangeli *et al.*, 1995), suggesting a complex relationship between $I_{HERG}$, $V_m$ and proliferation. Additionally, inward rectifier $K^+$ ($K_{ir}$) channels have been reported in various cancer cell types, and are required for proliferation, including $K_{ir}2.2$ (Lee *et al.*, 2010), $K_{ir}3.1$ and $K_{ir}3.4$ (Plummer *et al.*, 2004; Takanami *et al.*, 2004; Plummer *et al.*, 2005; Wagner *et al.*, 2010). In contrast, overexpression of $K_{ir}4.1$ in glioma cells hyperpolarises the $V_m$ and increases the number of cells in quiescent $G_0/G_1$, reducing the proportion in $G_2/M$ phase (Higashimori & Sontheimer, 2007). Thus, different $K_{ir}$ channels may play opposing roles in regulation of $V_m$/proliferation, as a result of their heterogeneous voltage dependence.

The mechanisms underlying ion channel-dependent proliferation of cancer cells include direct interaction between ion channels and other pro-proliferative signalling pathways (Wang, 2004; Ouadid-Ahidouch & Ahidouch, 2008; Prevarskaya *et al.*, 2010). For example, co-expression of HERG and tumour necrosis factor receptor 1 (TNFR1) has been found at the cell membrane of SKBR3 BCa and SH-SY5Y neuroblastoma cells, and HERG appears to recruit TNFR1 to the membrane, therefore enhancing TNF-α-induced cancer cell proliferation (Wang *et al.*, 2002). Alternatively, ion channel-mediated $V_m$ hyperpolarisation would increase the electrochemical gradient for $Ca^{2+}$ and

therefore elevate the intracellular $Ca^{2+}$ concentration through voltage-independent $Ca^{2+}$ channels, such as transient receptor potential (TRP) channels (Nilius & Wohlrab, 1992; Wang, 2004; Ouadid-Ahidouch & Ahidouch, 2008). $Ca^{2+}$ signalling is functional across the whole cell cycle (Santella *et al.*, 2005). For example, $Ca^{2+}$ is required for $G_1$ progression and $G_1$/S transition (Hazelton *et al.*, 1979; Choi *et al.*, 2006). In turn, intracellular $Ca^{2+}$ and CaM can regulate $K_{Ca}$ and EAG channels (Khanna *et al.*, 1999; Ziechner *et al.*, 2006; Ouadid-Ahidouch & Ahidouch, 2008). Thus, there may be a reciprocal, autoregulatory relationship between ion channel activity, $V_m$, intracellular $Ca^{2+}$ signalling, and proliferation.

Changes in $V_m$ are likely to trigger intracellular signalling messengers such as $Ca^{2+}$ in order to drive sustained proliferation. $V_m$ is a double-edged sword when fulfilling its role in regulating intracellular $Ca^{2+}$: a depolarised $V_m$ activates voltage-gated $Ca^{2+}$ channels (VGCCs) that result in $Ca^{2+}$ influx (Borodinsky & Fiszman, 1998; Zhang *et al.*, 2008), whereas a hyperpolarised $V_m$ increases the transmembrane electrochemical gradient and therefore enhances the driving force for entry of $Ca^{2+}$ and other types of cations (Prevarskaya *et al.*, 2010; Schwab *et al.*, 2012; Yang & Brackenbury, 2013). Inhibition of $Ca^{2+}$ entry or CaM/CaM kinase (CaMK) shows cell cycle arrest at specific checkpoints. For example, depleting extracellular $Ca^{2+}$ results in human WI-38 fibroblasts accumulating at $G_1$ (Hazelton *et al.*, 1979); inhibition of CaMK arrests 3T3 cells at $G_1$ phase (Tombes *et al.*, 1995; Morris *et al.*, 1998). Moreover, TFs including the nuclear factor of activated T cells (NFAT), c-Myc, c-Jun and c-Fos are also $Ca^{2+}$-dependent (Prevarskaya *et al.*, 2014). Activation of these TFs then promotes cancer cell growth by inducing the expression of cyclins and cyclin-dependent kinases (CDKs) (Roderick & Cook, 2008). In summary, a multiplicity of ion channels (predominantly $K^+$-conducting) participates in $V_m$ regulation (both depolarisation and hyperpolarisation) in cancer cells. In turn, changes in $V_m$ promote transition through cell cycle checkpoints.

### 1.5.4 Role of $V_m$ in cancer cell migration

$V_m$ is regarded as an indirect factor that can affect cell migration, whose main regulatory role might be setting up the electrical driving force for $Ca^{2+}$ (Prevarskaya *et al.*, 2010; Schwab *et al.*, 2012). Intracellular $Ca^{2+}$ concentration ($[Ca^{2+}]_i$) displays a gradient in migrating cells, with the lowest concentration at the leading edge (Brundage *et al.*, 1991). "$Ca^{2+}$ flicker" describes a phenomenon whereby local $[Ca^{2+}]_i$ undergoes dynamic regulations during cell migration (Wei *et al.*, 2009; Wei *et al.*, 2012). In WI-38 fibroblasts, the membrane-stretch sensitive TRP melastatin channel TRPM7 collaborates with the store $Ca^{2+}$releasing inositol 1,4,5-trisphosphate (IP$_3$) receptor to induce stochastic $Ca^{2+}$ flicker activity at the leading edge of migrating cells. The transient increase in local $Ca^{2+}$ concentration steers directional turning. It is proposed that the $Ca^{2+}$ flickers facilitate local cytoskeletal rearrangement, force generation and integrin turnover (Wei *et al.*, 2009; Wei *et al.*, 2012). More, the retraction of the rear-end body is mediated by myosin contraction controlled by the phosphorylation of myosin regulatory light chain (MLC) through $Ca^{2+}$-dependent MLC kinase (MLCK) (Olson & Sahai, 2009). The $[Ca^{2+}]_i$ fluctuations play a role in regulating tractional forces (Lee *et al.*, 1999; Ridley *et al.*, 2003), direction sensing, and cytoskeleton reorganisation (Figure 1.6) (Pettit & Fay, 1998).

$V_m$ may also affect downstream intracellular signalling cascades that could contribute to cell migration in a $Ca^{2+}$-independent way. In kidney epithelial cells, $V_m$ depolarisation induces phosphorylation of MLC without inducing $Ca^{2+}$ signalling, but instead by activating the Rho-associated kinase (ROCK) pathway (Szaszi *et al.*, 2005). In addition, actin filaments undergo reorganisation following $V_m$ depolarisation in bovine eye endothelial and epithelial cells (Chifflet *et al.*, 2003; Chifflet *et al.*, 2004), suggesting a functional role for $V_m$ in cytoskeletal reorganisation, although it is not clear whether or not $Ca^{2+}$ signalling is involved.
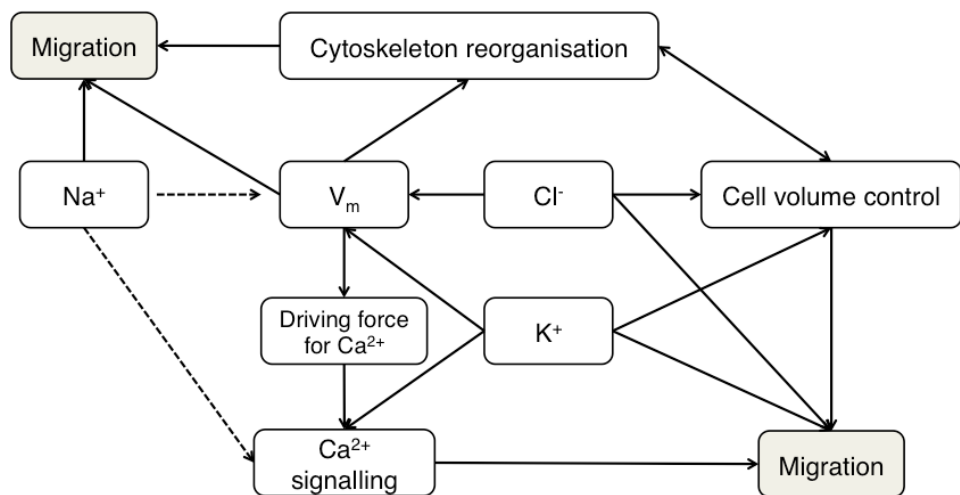
Figure 1.6. Relationships between $Na^+$, $K^+$, $Cl^-$ channels and membrane potential ($V_m$) in cancer cell migration.

$V_m$ provides the driving force for $Ca^{2+}$, and downstream $Ca^{2+}$ signalling leads to cell migration. $V_m$ also regulates cytoskeleton reorganisation. $Cl^-$ and $K^+$ channels both contribute to $V_m$ regulation and cell volume control. Inhibiting particular $Na^+$, $K^+$ and $Cl^-$ channels can reduce cancer cell migration. However, how $Na^+$ contributes to $V_m$ regulation and $Ca^{2+}$ signalling in cancer is less understood (dashed lines). Figure is adapted from (Yang & Brackenbury, 2013).

A number of $Na^+$, $K^+$ and $Cl^-$ channels, which may potentially contribute to the $V_m$, are directly implicated in cancer cell migration (Section 1.4.3.2). In several breast carcinoma/melanoma cell lines, $K_{Ca}2.3$, which is responsible for maintaining a hyperpolarised $V_m$, enhances migration, likely via promotion of intracellular $Ca^{2+}$ signalling (Potier *et al.*, 2006; Chantome *et al.*, 2009). In addition, $K_{Ca}3.1$ activity causes a local shrinkage at the rear of migrating MDCK-F cells, therefore supporting retraction at this pole during movement (Schwab *et al.*, 2006). In order to maintain electroneutrality, $K^+$ efflux must be accompanied by an anion, which is $Cl^-$ under most circumstances (Schwab *et al.*, 2007; Schwab *et al.*, 2012). In agreement with this, $Cl^-$ channels, which contribute to the depolarised $V_m$ in glioma cells, enhance migration and invasion by permitting the release of $K^+$, $Cl^-$ and water at the leading edge, resulting in shrinkage and facilitating movement into tortuous extracellular spaces (Soroceanu *et al.*, 1999; Sontheimer, 2008; Habela *et al.*, 2009; Schwab *et al.*, 2012). In summary, a direct role for $V_m$ in regulating cancer cell migration is much less clear than for proliferation. Additionally, it is noteworthy that the contribution of $Na^+$ channels to $V_m$, and whether $Na^+$ channel activity affects $Ca^{2+}$ signalling in cancer cells, are less studied (Figure 1.6).

## 1.5.5 $V_m$ and the differentiation of cancer stem cells

Stem cells and cancer cells share similar properties, such as the ability to differentiate and self-renew, increased membrane transporter activity and the ability to migrate and metastasise (Wicha *et al.*, 2006). The cancer stem cell (CSC) hypothesis contains two key concepts: (1) cancers arise from dysregulated transformation of normal tissue stem cells or progenitor cells, and (2) cellular components that display stem cell properties can lead to cancer progression (Wicha *et al.*, 2006). In contrast to normal, regulated asymmetric division of stem cells during tissue homeostasis, where a stem cell produces one copy of itself and one cell that later differentiates into a mature cell (Figure 1.7), the dysregulation of transformed CSCs during tumourigenesis involves "symmetric
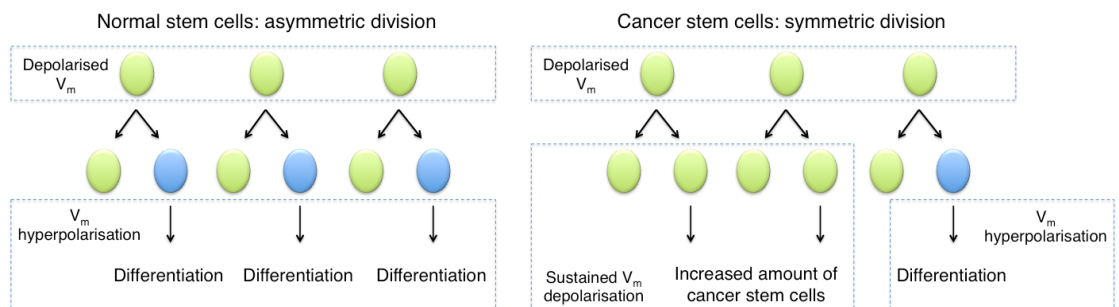
Figure 1.7. Membrane potential ($V_m$) in normal stem cell differentiation and hypothesised role for $V_m$ in cancer stem cells (CSCs).

Depolarised $V_m$ is needed during the maintenance of stem cells. Stem cell undergoes asymmetric division where it produces one copy of itself and one progeny that later differentiates into mature cells. The maturation requires $V_m$ hyperpolarisation (Sundelacruz *et al.*, 2008). However, CSCs frequently undergo symmetric division, in which one CSC divides into two identical CSC progenies (Wicha *et al.*, 2006). Sustained $V_m$ depolarisation may help to maintain the increasing CSCs in an undifferentiated state. Proliferation of CSCs may increase cancer malignancy. Figure is adapted from (Yang & Brackenbury, 2013).

division" in which each malignant CSC generates two identical daughter cells (giving rise to either proliferation or differentiation), which significantly expands the malignant CSC reservoir (Figure 1.7) (Liu *et al.*, 2005).

The involvement of $V_m$ in differentiation of normal stem cells has been previously reported. Studies in quail neural crest cells and a subpopulation of SH-SY5Y neuroblastoma cells have demonstrated that stem cells exhibit distinct bioelectrical profiles during development (Arcangeli *et al.*, 1997; Biagiotti *et al.*, 2006; Sundelacruz *et al.*, 2009). In particular, a hyperpolarised $V_m$ is required during stem cell maturation (Sundelacruz *et al.*, 2009). For example, $K_{ir}$-induced $V_m$ hyperpolarisation is required for human myoblast fusion (Liu *et al.*, 1998). In a genome-wide microarray analysis of depolarisation-regulated genes in postnatal mouse cerebellar granule neurones, among 87 depolarisation-responsive genes, 22 are developmentally up-regulated and 26 are developmentally down-regulated (Sato *et al.*, 2005). Remarkably, 18 of the 22 (82 %) developmentally up-regulated genes coincide with depolarisation down-regulated genes, and 20 of 26 (77 %) developmentally down-regulated genes coincide with depolarisation up-regulated genes (Sato *et al.*, 2005). $V_m$ hyperpolarisation is also a functional determinant of human mesenchymal stem cell (hMSC) differentiation. Pharmacologically induced $V_m$ depolarisation suppresses adipogenic and osteogenic differentiation of hMSCs (Sundelacruz *et al.*, 2008). In addition, depolarisation reduces the differentiation phenotype of hMSC-derived cells and enables plastic transdifferentiation (Sundelacruz *et al.*, 2013). Taken together, these data suggest that a depolarised $V_m$ may maintain cells in an undifferentiated stage at the gene expression level. Therefore, it is not unreasonable to postulate that depolarised $V_m$ may also contribute to maintaining a population of undifferentiated CSCs (Figure 1.7).

### 1.5.6  Depolarised $V_m$ regulates tumourigenesis and development *in vivo*

Studies published by Michael Levin's group have examined the functional roles of $V_m$ in development and tumourigenesis using *Xenopus laevis* and planarian flatworms. The researchers depolarised the $V_m$ of *Xenopus laevis* embryos by reducing the environmental $Cl^-$ concentration and concurrently activating the endogenous glycine receptor $Cl^-$ channels using ivermectin (Lobikin *et al.*, 2012). Using this method, the researchers found that during *Xenopus laevis* development, the depolarised melanocytes in the tadpole neural crest exhibit neoplastic phenotypes including over-proliferation, arborized cell morphology and increased local invasion.

One study demonstrated that these metastatic phenotypes are ion type and ion channel non-specific, because firstly, the phenotypes caused by depolarisation could be rescued by expressing hyperpolarising inward-rectifier $K^+$ channels, and secondly, the malignant phenotype could be induced or suppressed simply by adjusting extracellular $Cl^-$ concentration, as predicted by Goldman-Hodgkin-Katz equation (Lobikin *et al.*, 2012). Interestingly, overexpression of a human oncogene *Gli1* in *Xenopus laevis* embryos by microinjection induced tumour-like structures in developed tadpoles, and $Na^+$ imaging revealed that such structures are enriched for $Na^+$ (Lobikin *et al.*, 2012). SLC5A8, a sodium butyrate co-transporter, is shown to play a vital role in the $V_m$ signal transduction pathway: butyrate is suggested to act as a histone deacetylase inhibitor upon $V_m$ hyperpolarisation, and since acetylation of histones leads to arrest of cell proliferation, the over-proliferation of cells is reduced due to butyrate influx (Tseng & Levin, 2012; Chernet & Levin, 2013).

Studies also proposed that these effects are mediated by voltage control of serotonin release from melanocytes (Blackiston *et al.*, 2011; Chernet & Levin, 2013; Lobikin *et al.*, 2015): a depolarised $V_m$ increases serotonin export through the serotonin transporter (SERT) at plasma membrane, resulting in an increase in serotonin concentration in the extracellular microenvironment. Consequently, the serotonin

receptors, including 5HT-R2 and 5HT-R5, on nearby melanocytes and on pituitary melanotrope cells, are activated. The activation of 5HT receptors consequently stimulates adenylyl cyclase (AC), causing release of melanocyte-stimulating hormone; this increases the expression of *Sox10* and *Slug*, both TFs, across the animal body, which ultimately result in cell over-proliferation (Lobikin *et al.*, 2015).

During development of the *Xenopus laevis* embryo, a gradual $V_m$ hyperpolarisation is reported in the cells lining the neural tube at the start of neural fold formation and before the neural tube closure (Pai *et al.*, 2015). Hyperpolarising the embryo by expressing hyperpolarising ion channels reduces expression of brain TFs including *otx2*, *emx* and *bf1*. Unlike the model proposed in the melanocytes using the same animal model, here, both $Ca^{2+}$ flux and gap junction-mediated $V_m$ regulation, but not the serotonin signalling pathway, are involved in $V_m$-dependent brain development (Pai *et al.*, 2015).

In *Dugesia japonica* planaria, $V_m$ depolarisation plays a role during development and regeneration. Dissected planarian flatworm pharynx fragments (blastema) can regenerate and grow into a new flatworm. After dissection, it has been shown that $H^+$-$K^+$-ATPase activity depolarises the $V_m$ of the anterior blastema, and inhibition of the $H^+$-$K^+$-ATPase with SCH-28080 abolishes the depolarised $V_m$ and blocks anterior polarity and head regeneration (Beane *et al.*, 2011; Beane *et al.*, 2013). Interestingly, hyperpolarised blastemas become either tail- or headless, whereas ivermectin-induced $V_m$ depolarisation at the posterior of pharynx results in head formation (Beane *et al.*, 2011). It is suggested that depolarised $V_m$ increases $Ca^{2+}$ influx carried by VGCCs and therefore mediates regeneration (Beane *et al.*, 2011).

In summary, $V_m$ has been previously regarded simply as an outcome of the collective activity of ion channels/transporters at the cell membrane. However, more and more data suggest that $V_m$ is a functional signal in cell proliferation, migration and stem cell differentiation *in vitro* as well as tissue development and regeneration *in vivo*.

Cancer cells tend to possess a depolarised $V_m$, but the roles of $V_m$ in regulating cancer cell metastatic behaviours including migration and invasion are less studied. Similarly, it is unknown whether VGSCs are functionally involved in regulating the $V_m$ of BCa cells.

## 1.6 Hypothesis and aims

The overall hypothesis of the present study was that VGSCs in MDA-MB-231 cells increase cancer cell metastatic behaviours, including migration and invasion, via depolarising the $V_m$. The aims of this study were three-fold:

(1) To investigate the involvement of VGSCs in $V_m$ regulation in human MDA-MB-231 cells.

(2) To investigate whether $V_m$ contributes to VGSC-dependent cancer cell migration and invasion.

(3) To study the $V_m$ and $I_{Na}$ in primary tumours from mice xenografted with MDA-MB-231 cells.

The data presented in this thesis have resulted in several peer-reviewed publications, and a further manuscript in preparation, detailed in **Error! Reference source not found.**.

# Chapter 2: Materials and Methods

## 2.1 Cell culture

### 2.1.1 Cell lines

MDA-MB-231 human BCa cells were a gift from Prof Lori Isom (University of Michigan). MDA-MB-231 cells stably expressing enhanced green fluorescent protein (eGFP) and luciferase (Nelson *et al.*, 2014) were stably transduced with lentivirus for shRNAs targeting $Na_v1.5$ (hereafter called "$Na_v1.5$-shRNA" cells) or non-targeting control shRNA (hereafter called "shRNA control" cells) using MISSION pLKO.1-puro shRNA transduction particles (Sigma) (Nelson *et al.*, 2015b). Molecular identify of cells was confirmed by short tandem repeat analysis (Masters *et al.*, 2001). MCF-7 cells where the oestrogen receptor α was knocked-down using shRNA (namely pII cells) (Luqmani *et al.*, 2009) and control MCF-7 cells were a gift from Prof Yunus A. Luqmani (Kuwait University). Cells were confirmed to be mycoplasma-free (Section 2.1.5).

### 2.1.2 Maintenance and passage of cells

MDA-MB-231 cells were grown in Dulbecco's modified eagle medium (DMEM, Life Technologies) supplemented with 5 % foetal bovine serum (FBS, Life Technologies) and 4 mM L-glutamine (Life Technologies) at 37 °C, 5 % $CO_2$, 100 % relative humidity. For $Na_v1.5$-shRNA and shRNA control cells, G418 (4 μl/ml, Sigma), blasticidin (2 μl/ml, AppliChem) and puromycin (0.1 μl/ml, Sigma) were applied to the cell culture medium. Unless otherwise stated, cells were grown in T25 flasks (Corning) or 10 cm culture dishes (Corning). The cell culture medium was changed every 72 h for MDA-MB-231 cells, or 48 h for $Na_v1.5$-shRNA and shRNA control cells.

Cells were passaged when the density reached approximately 90 %. After aspirating the old medium, 1 ml trypsin-EDTA (0.05 %, Life Technologies) was applied to the cells, and the cells were transferred into cell incubator for 30 s before viewing at 10X under an inverted microscope. Cells were incubated for a further 15 s if they were not starting to lift from the culture surface. Before the cells started to lift off, trypsin-EDTA was removed from the culture dish or flask, and was replaced with 2 ml culture medium. Cells adherent to the surface were triturated gently using a P1000 pipette. Four to six drops of the cell suspension were transferred to a new culture dish or flask, and 10 ml culture medium was added. Cells were passaged no more than 10 times after thawing.

### 2.1.3  Cell counting

To count the cells, 20 µl of well-mixed cell suspension was placed in one chamber of an improved Neubauer haemocytometer and covered with a rectangular glass coverslip. Cells at each of the four corner squares were counted using a hand-held counter. The number of cells in the suspension was calculated using the following equation:

$$Cell\ number\ (per\ ml) = \frac{Total\ number\ of\ cells\ counted}{4} \times 10^4 \qquad \text{(Equation 2.1)}$$

### 2.1.4  Freezing and thawing cells

Cells were transferred to a 15 ml falcon tube after being removed from the surface of a ~90 % confluent culture dish or flask. Cells in the falcon tube were pelleted using a bench-top centrifuge at ~200 $g$ at room temperature. The supernatant was carefully removed using a P1000 pipette, and the pellet was resuspended in 1 ml

freezing medium, containing 70 % (v/v) DMEM, 20 % (v/v) FBS and 10 % (v/v) dimethyl sulfoxide (DMSO). Cells were then aliquoted into cryovials (200 µl/vial). The vials were placed upright in a polystyrene box and stored at -80 °C for one week before being transferred into a liquid nitrogen dewar for long-term storage.

To thaw the cells, culture medium (10 ml) was prepared in an empty flask. A cryovial containing frozen cells was taken from the liquid nitrogen dewar and thawed in a water bath at 37 °C for 30 s. The defrosted suspension was then gently transferred to the flask. After 24 h, the medium was changed.

### 2.1.5  Mycoplasma testing in cell cultures

Cells were confirmed to be free of mycoplasma contamination before use in experiments and were routinely tested at six-month intervals. Cells were plated on 13 mm uncoated glass coverslips in a 35 mm culture dish and cultured in culture medium for 48 h. The medium was then removed and cells were fixed with 1 ml methanol at room temperature for 5 min. Methanol was removed after cell fixation, 4',6-diamidino-2-phenylindole (DAPI) (1 ml) prepared at 0.5 µg/ml in methanol was added. Cells were incubated at room temperature for a further 10 min before washing once with methanol, followed by two additional washes using phosphate buffered saline (PBS, Life Technologies). Approximately 20 µl of Faramount mounting medium (Dako) was applied to a rectangular No. 1 glass microscope slide. The glass coverslip was then mounted onto the slide suing a pair of forceps, with the cell-growing surface facing the mounting medium. The slides were examined using an epi-fluorescence microscope (Section 2.9). Cells without mycoplasma contamination showed no DAPI staining in the cytoplasm, or adjacent to cells.

## 2.2 Pharmacology

Drugs used in the present study and the concentrations used are detailed in Table 2.1.

## 2.3 Tumour xenografts in mouse mammary fat pad

### 2.3.1 Ethics statement

Investigation has been conducted in accordance with the ethical standards according to the Declaration of Helsinki and according to national and international guidelines and has been approved by the University of York Ethical Review Process. The work presented in the current study was under authority of a Home Office-approved protocol (Project Licence number: 60/4277).

### 2.3.2 Animals

Female immunocompromised mice ($rag2^{-/-}$, $gc^{-/-}$) were obtained from the Yorkshire Cancer Research Unit at the University of York. Mice were maintained under specific pathogen free (SPF) conditions in individually ventilated cages. Each cage contained three to five mice with food and water provided *ad libitum*. Mice were weaned three weeks after birth, and were maintained for a further three weeks before surgery. In total, 50 mice from 13 cages were used in this study.

### 2.3.3 Tumour xenograft orthotopic implantation

The following work was done in a class II bio-safety cabinet, which was cleaned with 70 % ethanol before the procedure. Each mouse was weighed on a scale before being transferred to an anaesthesia chamber supplied with 2 % isoflurane for 2 min. Once unconscious, the animal was moved onto a sterile drape on a heat pad, with

| Table 2.1. Pharmacologial agents used in the study | | | |
|---|---|---|---|
| **Name** | **Manufacturer** | **Solvent and stock concentration** | **Working concentration** |
| Gramicidin | Sigma | Ethanol; 5 mM | 0.4 % v/v (20 µM) |
| IbTx | Alomone Labs | Water; 20 µM | 0.5 % v/v (100 nM) |
| Ionomycin | Cayman Chemical | Ethanol; 14.1 mM | 0.46 % v/v (10 µM) |
| Nifedipine | Alomone Labs | DMSO; 5 mM | 0.2 % v/v (10 µM) |
| NS-1619 | Alomone Labs | DMSO; 10 mM | 0.01 – 0.4 % v/v (1– 40 µM) |
| Nystatin | Serva | DMSO; 30 mg/ml | 0.4 % v/v (120 µg/ml) |
| Phenytoin | Sigma | 75 mM NaOH; 180 mM | 0.06 % v/v (100 µM) |
| TTX | Alomone Labs | Water; 1 mM | 3 % v/v (30 µM) |
| Veratridine | Alomone Labs | DMSO; 5 mM | 2 % v/v (20 µM) |
| IbTx: iberiotoxin; TTX: tetrodotoxin | | | |

constant isoflurane at 1.5 % supplied via a nose cone. Carprofen (100 µl) at 0.75 mg/ml was subcutaneously injected before an ear notch tag was applied. The mouse abdomen area was then gently shaved and cleaned with a piece of gauze sprayed with chlorhexidine (0.2 % w/v). A 2 mm-long incision was made at the centre of abdomen between the fourth inguinal mammary glands (Figure 2.1). The skin was separated from muscle and fat pad using forceps. Cells ($5 \times 10^5$) suspended in Matrigel/PBS were gently injected via a 1 ml insulin syringe. The wound was then closed using sutures. The mouse was transferred to a recovery cage, and the recovery from anaesthesia was monitored for 20 min. The animal was returned to its home cage after checking the wound.

### 2.3.4  Tumour size measurement using callipers

The health status and weights of the mice were checked the day after surgery. Animals were weighed every other day thereafter, until tumours developed (approximately seven days after surgery). When the tumour was observed in the mammary fat pad, the weight of the animal was measured daily, and the size of the tumour was monitored using callipers once a day. To determine the tumour volume, both the greatest longitudinal diameter (length) and the greatest transverse diameter (width) were measured using callipers, and the tumour volume was calculated as:

$$Tumour\ volume/weight\ (mm^3\ \text{or mg}) = 0.5 \times (length \times width^2)\ \text{(Equation 2.2)}$$

Mice were euthanised using a Schedule 1 method 20–37 days after surgery, or before the weight of the tumour reached 10 % of the animal's body weight, or if the weight loss approached 20 % of the body weight at the day of surgery (Workman *et al.*, 2010).
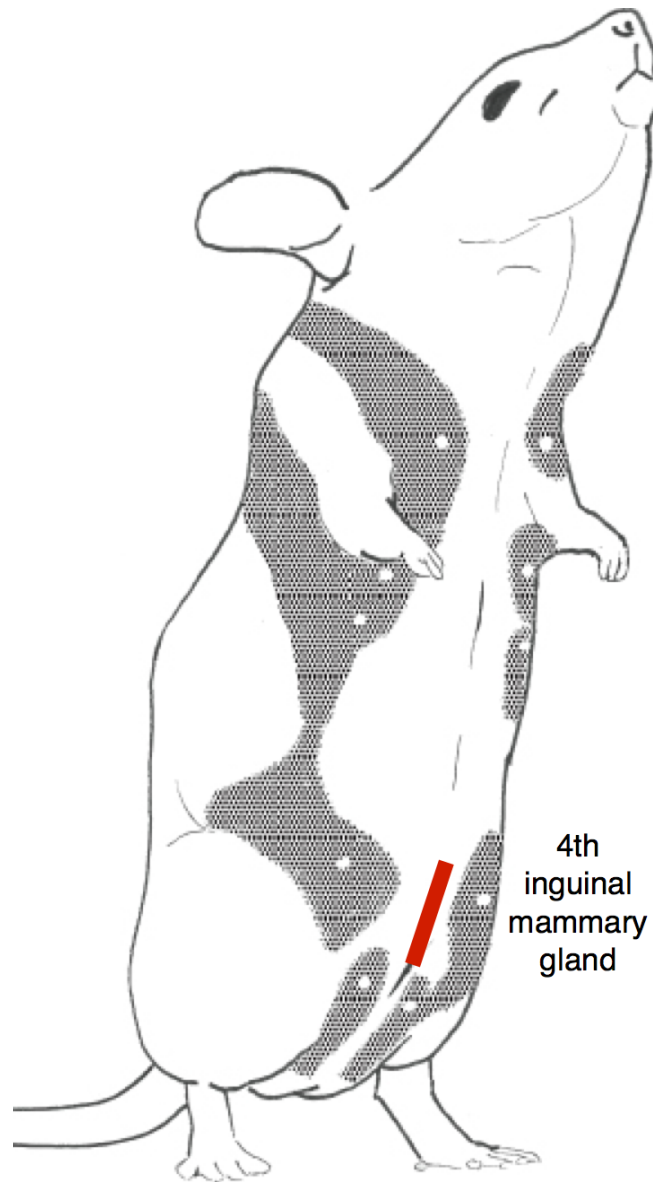
Figure 2.1. Location of mammary tissues in the female mouse.

In total, there are five pairs of mammary glands in the female mouse. The present study orthotopically implanted breast cancer cells in the fourth inguinal mammary gland. Red line indicates the incision site. Diagram is adapted from (Scudamore, 2014).

## 2.4 Electrophysiology

### 2.4.1 Cell preparation

Three days before recording, cells ($6 \times 10^4$) were plated on two uncoated glass coverslips in a 35 mm culture dish with 2 ml culture medium. Cells were incubated as in Section 2.1.2. The medium was changed 48 h after seeding the cells.

### 2.4.2 Solutions

Extracellular and intracellular recording solutions used in the present study and their components are in Table 2.2 and Table 2.3, respectively. In $Na^+$-free extracellular solutions, NaCl was replaced with equimolar choline chloride (ChoCl) or N-methyl-D-glucamine (NMDG). Extracellular solution with $Ba^{2+}$ was used to block $BK_{Ca}$ channels, and extracellular solution with $Cd^{2+}$ was used to block VGCCs (Hille, 2001).

For intracellular solutions, ethylene glycol tetraacetic acid (EGTA) was used to buffer $Ca^{2+}$. Free $Ca^{2+}$ concentration in the intracellular solution was calculated using the MaxChelator program (Stanford University). $Cs^+$ was used to inhibit VGPCs and $K_{ir}$ channels (Hille, 2001)

### 2.4.3 Equipment for voltage- and current-clamp recordings

Equipment for electrophysiology was set up as in Figure 2.2. A MultiClamp 700B amplifier (Molecular Devices) was used to record voltage-activated membrane current and voltage, and a Digidata 1440A data acquisition system (Molecular Devices) was used for analogue-digital signal conversion. A VC34 (Scientific Instruments) computer-controlled valve system and a Dymax 5 (Charles Austen Pumps) air pump were used to control solution flow. A current and voltage clamp headstage (Molecular Devices CV-

Table 2.2. Extracellular solutions used in this study

| Solution name and components (in mM) | NaCl | ChoCl | NMDG$^+$ | KCl | MgCl$_2$ | CaCl$_2$ | BaCl$_2$ | CdCl$_2$ | HEPES | Glucose | pH |
|---|---|---|---|---|---|---|---|---|---|---|---|
| Standard physiological saline solution (PSS) | 144 | - | - | 5.4 | 1 | 2.5 | - | - | 5 | 5.6 | 7.2, adjusted with NaOH |
| Extracellular solution with choline | - | 144 | - | 5.4 | 1 | 2.5 | - | - | 5 | 5.6 | 7.2, adjusted with KOH |
| Extracellular solution with NMDG | - | - | 144 | 5.4 | 1 | 2.5 | - | - | 5 | 5.6 | 7.2, adjusted with KOH |
| Extracellular solution with Ba$^{2+}$ | 144 | - | - | 2.5 | 1 | - | 4.5 | - | 5 | 4.5 | 7.2, adjusted with NaOH |
| Extracellular solution with Cd$^{2+}$ | 144 | - | - | 5.4 | 1 | 2.5 | - | 0.2 | 5 | 5.6 | 7.2, adjusted with NaOH |
| Extracellular solution with 10 mM Na$^+$ | 10 | - | - | 139.4 | 1 | 2.5 | - | - | 5 | 5.6 | 7.2, adjusted with KOH |
| Extracellular solution with 20 mM Na$^+$ | 20 | - | - | 129.4 | 1 | 2.5 | - | - | 5 | 5.6 | 7.2, adjusted with KOH |

ChoCl: choline chloride; HEPES: 4-(2-hydroxyethyl)-1-piperazineethanesulfonic acid; NMDG$^+$: N-methyl-D-glucamine

Table 2.3. Intracellular solutions used in this study

| Solution name and components (in mM) | NaCl | ChoCl | KCl | CsCl | MgCl$_2$ | CaCl$_2$ | EGTA | HEPES | Nystatin | pH |
|---|---|---|---|---|---|---|---|---|---|---|
| Standard intracellular solution | 5 | - | 145 | - | 2 | 1 | 11 | 10 | - | 7.4, adjusted with KOH |
| Cs$^+$-containing solution | 5 | - | - | 145 | 2 | 1 | 11 | 10 | - | 7.4, adjusted with CsOH |
| Perforated patch solution | - | 5 | 145 | - | 2 | - | 1 | 10 | 0.12 | 7.4, adjusted with KOH |
| Solution with 7.8 µM free Ca$^{2+}$ | 5 | - | 145 | - | 2 | 1 | 1 | 10 | - | 7.4, adjusted with KOH |
| Solution with 100 nM free Ca$^{2+}$ | 5 | - | 145 | - | 2 | 1 | 1.57 | 10 | - | 7.4, adjusted with KOH |

ChoCl: choline chloride; EGTA: ethylene glycol tetraacetic acid; HEPES: 4-(2-hydroxyethyl)-1-piperazineethanesulfonic acid
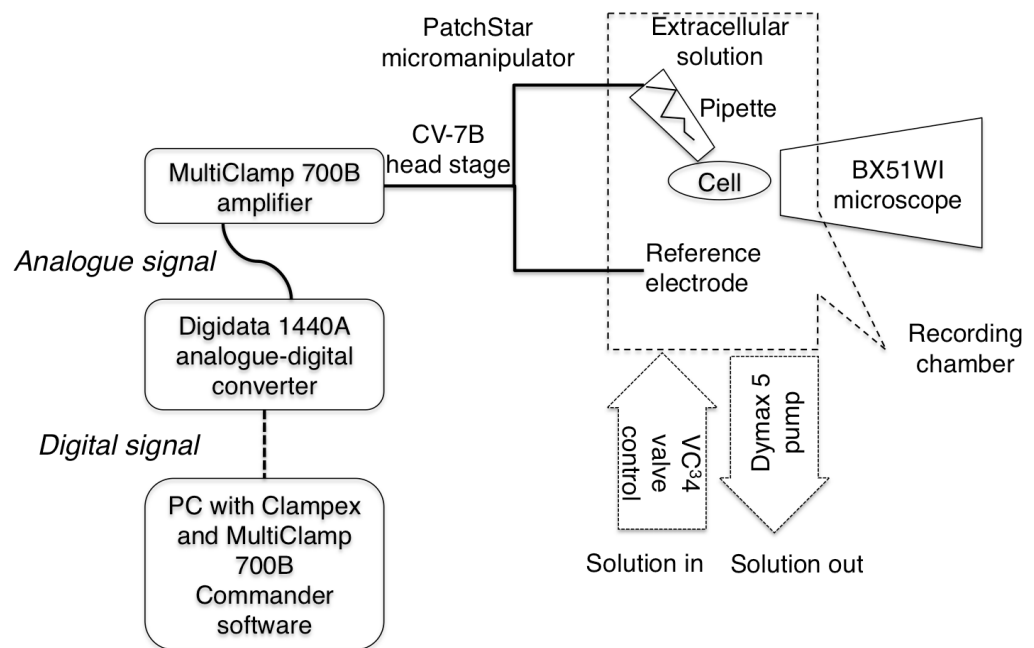
Figure 2.2. Electrophysiology equipment used in this study.

Perfusion of external solution was controlled by a VC34 valve control system and a Dymax 5 pump. Cells were immersed in extracellular solution and observed using an Olympus BX51WI microscope. Pipette movement was controlled by the PatchStar micromanipulator. The electrical signal was transmitted to the MultiClamp 700B amplifier through the CV-7B headstage. Analogue and digital signals were converted using the Digidata 1440A. User commands were sent to the amplifier using Clampex and the MultiClamp 700B Commander.

7B) was connected to a PatchStar micromanipulator (Scientifica) in order to control pipette movement. A silver wire was used as the recording electrode inside the pipette. Before installation onto the headstage the silver wire was chlorided by connecting to the positive pole of a 9 V cell, while the other end was soaked in 3 M KCl. It was re-chlorided at regular intervals.

Cells were observed using an Olympus BX51WI light microscope. A chamber (Warner Instruments RC-26GLP) fixed by a stage adaptor (Warner Instruments SA-OLY/2) was used to hold cells on coverslips under constant perfusion with extracellular physiological saline solution (PSS). The data acquired by the Digidata 1440A were saved to a PC running Clampex 10.4 and MultiClamp 700B Commander 2.1.0 software (Molecular Devices). User commands were sent to the MultiClamp 700B using this software.

### 2.4.4 Preparation of borosilicate pipettes

Both blunt ends of borosilicate glass capillaries (Harvard Apparatus GC150TF-7.5) were fire-polished in a Bunsen flame and then pulled into pipettes using a P-97 micropipette puller (Sutter Instrument). After pulling, pipette tips were fire-polished using a Narishige MF-830 microforge, in order to give resistances of 3.5–4.5 MΩ when filled with internal solution.

### 2.4.5 Recording current using whole-cell patch clamp from cultured cells

Current across the plasma membrane was recorded using the whole-cell patch clamp technique. A single target cell was located at 40X magnification. Approximately 10 μl intracellular solution was backfilled into glass pipette through a 0.45 μm filter and the pipette was installed onto the headstage. Approximately 2 ml of air was injected into the pipette using a syringe connecting to the headstage, providing positive

85

pressure. The pipette was firstly moved close to the bottom of the chamber under 10X magnification, and it was then moved to the target cell from above with 40X magnification. The pipette offset was compensated. When the pipette was slightly pressing the cell, giving a "dimple" on the cell membrane, positive pressure was released, and if a high resistance seal (gigaseal) did not start to form, 0.1–0.2 ml negative pressure was gently applied. When the seal resistance started to increase, holding voltage was set in Clampex (Table 2.4). When the seal resistance was stably at $\geq 1.1$ GΩ, approximately 0.3 ml suction was applied as negative pressure to break the cell membrane patch. Whole-cell capacitance, and fast and slow pipette capacitance values were displayed in the Multiclamp 700B Commander software panel, and were compensated. Typical series resistance was between 5–15 MΩ, and was compensated by 40–60 %.

Membrane currents were acquired and digitised at 50 kHz using a Digidata 1440A interface (Molecular Devices), low-pass filtered at 10 kHz and analysed using pCLAMP 10.4 software (Molecular Devices). Linear components of leak were subtracted using a P/6 protocol (Armstrong & Bezanilla, 1977).

### 2.4.6  Perforated patch clamp recordings

The perforated patch clamp technique was used to record the large-conductance $Ca^{2+}$-activated $K^+$ ($BK_{Ca}$) current in MDA-MB-231 cells (Akaike & Harata, 1994). A gigaseal was achieved as described above. However, instead of achieving whole-cell configuration by applying negative pressure, the target cell was continuously held between -25 and -60 mV, at whichever the seal was best maintained. In the "Membrane Test" window (2.5 mV test pulse sampling at 100 Hz), when the membrane capacitance transient current occurred (typically after 15–20 minutes), whole-cell capacitance was manually compensated. Typical series resistance ranged between 20

| Table 2.4. Holding potential applied to cells when forming a gigaseal | |
|---|---|
| **Seal resistance** | **Holding potential** |
| 20–30 MΩ | -25 mV |
| 30–100 MΩ | -50 mV |
| 100–300 MΩ | -65 mV |
| 300–500 MΩ | -70 mV |
| 500 MΩ–1.0 GΩ | -80 mV |

and 40 MΩ, and was compensated by 50–70 %.

### 2.4.7  Voltage-clamp protocols

The following protocols were used in the voltage-clamp experiments in this study. A 250 ms pre-pulse at -120 mV was applied to all of the protocols, unless otherwise stated:

(1)  Standard $I_{Na}$ stimulation protocol: cells were depolarised from -120 mV to -10 mV for 50 ms, repeated 10 times. The inter-pulse interval was 100 ms.

(2)  Standard $I_{Na}$ stimulation protocol with -80 mV pre-pulse: cells were depolarised from -80 mV to -10 mV for 50 ms, repeated 10 times. The inter-pulse interval was 100 ms.

(3)  Standard current-voltage protocol: cells were depolarised to voltages ranging from -80 mV to +30 mV for 60 ms in 5 mV increments. The inter-pulse interval was minimum.

(4)  $I_{Na}$ steady-state inactivation protocol: cells were depolarised to -10 mV for 60 ms following 250 ms conditioning pulses between -120 mV to -10 mV in 10 mV increments. The inter-pulse interval was 20 ms.

(5)  $BK_{Ca}$ current ($I_{BKCa}$)-voltage protocol in perforated patch configuration: cells were depolarised to voltages ranging from -60 mV to +90 mV for 300 ms in 10 mV increments. The inter-pulse interval was 50 ms.

### 2.4.8  $V_m$ measurement in I=0 mode

In the Multiclamp 700B, I=0 is a special mode of current clamp, where all input commands are disconnected. This mode reports the resting $V_m$ of the cells[1]. When the recording pipette was in contact with the extracellular PSS, the bridge balance and

---

[1] Multiclamp 700B Theory and Operation Rev. D, Axon Instruments, 2005.

pipette capacitance neutralisation were firstly adjusted in the current clamp mode. Gigaseal and whole-cell configuration were achieved in voltage clamp mode. Within 5 s of reaching whole-cell configuration, the steady-state $V_m$ of a cell was recorded in the I=0 mode.

To monitor the continuous $V_m$ change in individual cells in response to treatments, cells were held for 60 s in the standard PSS, 150 s in PSS plus treatment and a further 150 s for treatment washout. The mean $V_m$ over the last 5, 15, 30 and 60 s in each of the three stages was used to quantify the data. The flow rate was approximately 2 ml/min. The $V_m$ signal was sampled at 200 Hz, and low-pass filtered at 10 kHz. Liquid junction potentials were calculated using the integrated tool in Clampex 10.4 software and were compensated while analysing the data offline, using the following equation (Barry & Lynch, 1991):

$$Compensated\ V_m\ (mV) = Raw\ V_m - Liquid\ junction\ potential \quad \text{(Equation 2.3)}$$

### 2.4.9 Slice recording

Tumours were allowed to grow until diameter ≥ 6 mm before mice were euthanised by a Schedule 1 method. The tumour was then quickly dissected from the body and stored in ice-cold standard PSS for approximately 10 min. Fur and surrounding muscle tissues were removed from the tumour with a razor blade on ice. Tissue was kept moist by continually immersing with ice-cold PSS. The tumour tissue block was then fixed on the pedestal of vibratome (Campden Instruments) using cyanoacrylate glue and was horizontally supported by an ~8 mm × 8 mm 5 % agar block. The tissue was then covered with ice-cold PSS before slicing. A homemade holding chamber was made by putting 3–5 cell strainers (100 µm mesh, Corning) in a 10 cm cell culture dish, supplied with 20 ml standard PSS at room temperature. Slices

(250 µm) were cut and incubated in the cell strainers inside the holding chamber at room temperature for at least 20 minutes before recording.

A slice was transferred from the holding chamber to the recording chamber by using a homemade glass Pasteur pipette, and was held in place with an SHD-26GH/15 slice anchor (Warner Instruments). Areas without floating cells were firstly determined at 10X magnification, followed by targeting a healthy cell at 40X. The following criteria were applied when targeting a cell: the cell should be attached to the slice and should have a smooth plasma membrane, and for shRNA control cells, they should be eGFP-positive. The eGFP was excited by using a pE100 CoolLED at 470 nm and the fluorophore emission was gathered at $525 \pm 50$ nm. Once a cell was selected, its distance to the edge of the tumour slice was determined by using an eyepiece reticle. The slices were divided into three regions according to the distance from the edge: (1) periphery, which is $\leq 1$ mm from the edge; (2) intermediate region, which is $\geq 1$ mm but $\leq 1.5$ mm from the edge; and (3) centre, which is $\geq 1.5$ mm from the edge. $I_{Na}$ and $V_m$ were recorded as described in Section 2.4.5 and Section 2.4.8, respectively.

## 2.5 *In vitro* assays

### 2.5.1 MTT proliferation assay

MDA-MB-231 cell proliferation was measured using the thiazolyl blue tetrazolium bromide (MTT) assay (Grimes *et al.*, 1995). Stock MTT was dissolved in sterile PBS at 5 mg/ml. Cells ($3 \times 10^5$) were plated in each well of a 12-well plate supplemented with 1 ml culture medium. Three wells were prepared for each condition. After 24 h, the old medium was replaced with fresh culture medium containing appropriate treatments (Table 2.1). Cells were incubated overnight. The medium was aspirated the next day, replaced with MTT diluted at 1:5 in culture medium (final MTT concentration at 1 mg/ml). Cells were incubated in the dark for 4 h. MTT medium was then replaced with

1 ml DMSO to lyse the cells for 10 minutes, before 125 µl autoclaved glycine buffer (0.1 M glycine + 0.1 M NaCl, adjusted to pH at 10.5 with NaOH) was added. The 12-well plate was gently swirled and was incubated in the dark for a further 10 minutes. Aliquots (800 µl) were transferred to plastic cuvettes and absorbance at 570 nm was determined using a spectrophotometer. DMSO (1 ml) plus glycine buffer (125 µl) was used as blank during spectrophotometer calibration.

To convert the absorbance to cell number, another 12-well plate seeded with 1,000, 3,000, $1 \times 10^4$ and $3 \times 10^4$ cells (prepared in triplicate) was prepared along with the plate for experimental conditions. These cells were incubated for two hours before the medium was replaced with MTT. Cells were then lysed and the absorbance at 570 nm was taken as described above to generate a standard curve (Figure 4.12). The experiment was repeated three times on different days. For each technical repeat, three wells were prepared per condition.

## 2.5.2  Matrigel invasion assay

The invasion assay was carried out using 24-well BioCoat Matrigel Invasion Chambers (Corning). MDA-MB-231 cells ($2.5 \times 10^4$) were seeded in the upper compartment supplemented with 1 % FBS and appropriate treatments according to the manufacturer's instructions. The lower compartment contained 10 % FBS as a chemoattractant and appropriate treatments (Table 2.1). Cells were incubated at 37 °C for 24 h before the removal of non-invaded cells from the upper surface of chambers using cotton buds. Cells that invaded through the Matrigel and polyethylene terephthalate membrane were fixed using 4 % (w/v) paraformaldehyde in PBS for 10 min, and were washed three times with PBS, 5 min/time, before being stained with DAPI at 0.5 µg/ml in distilled water. The membrane was then carefully removed using a scalpel and mounted on a glass microscope slide in Faramount mounting medium

(Dako) and then sealed with 13 mm glass coverslip. DAPI-positive invaded cells on the membrane were counted using an epi-fluorescence microscope at 20X (Section 2.9). The experiment was repeated at least three times on different days. For each technical repeat, two wells were prepared per condition.

### 2.5.3  Wound healing assay

Cell migration was determined using wound healing assays (Fraser *et al.*, 2003). Ptychography was used to monitor cell movement (Marrison *et al.*, 2013). Cells (2 × $10^5$) were seeded on a glass bottomed 6-well plate and were allowed to grow for 48 h before a confluent cell monolayer was formed. A stainless steel spatula was used to make a straight wound through the cell monolayer (Figure 4.13a). Cells were then washed once with 37 °C DMEM to remove debris before appropriate treatments were applied (Table 2.1). Empirically, the doubling time of MDA-MB-231 cells cultured in our lab was 12-18 hours. To reduce the impact of cell proliferation on wound closure, given the accessibility of the image acquisition system, cells were allowed to migrate into the wound for 16 h.

Image acquisition by ptychography was done by Dr Richard Kasprowicz and Dr Rakesh Suman (PhaseFocus Ltd.). Images of the wounds were acquired using a Phasefocus VL-21 microscope over 16 h at 9 min intervals. Image sequences of the gap closure were analysed in a semi-automated fashion using TScratch software (Geback *et al.*, 2009), which calculated the percentage of cell-free space in each image. For each image sequence, the percentage of cell-free space was normalised relative to the initial free space measured in the first image. Half time ($t_{1/2}$) values for gap closure were obtained in order to quantify the differences in speed of gap closure between treatments. The $t_{1/2}$ of gap closure was obtained by averaging all time values associated with normalised gap closure values in the range of 45–55 %. Cell

proliferation during the wound healing assay was analysed by measuring the total cell volume of the whole field of view, over time using the Phasefocus Cell Analysis Toolbox image analysis package. To calculate proliferation, the cell volume data were normalised by expressing the cell volume as a ratio of the cell volume at 1.5 h. The experiment was repeated for three times on different days. For each technical repeat, two wells were prepared per condition.

## 2.6   Immunocytochemistry

MDA-MB-231 cells ($1.6 \times 10^5$) were cultured on glass coverslips in 4-well plates for 48 h in order to form a confluent cell monolayer. A wound was made on the monolayer (Section 2.5.3). Cells were then washed once with 37 °C DMEM to remove debris. Appropriate treatments was subsequently applied, and cells were to allowed to migrate into the wound for 3 h. Cells were fixed in 4 % (w/v) paraformaldehyde in PBS for 10 min, followed by three PBS washes (5 min/wash). The fixed cells were then treated with blocking buffer (1x PBS, 5 % v/v normal goat serum and 0.3% v/v Triton X-100) for 1 h. Cells were incubated with mouse anti-active Rac1 primary antibody (Neweast Biosciences) diluted to 1:500 in antibody dilution buffer (1% w/v bovine serum albumin and 0.3 % v/v Triton X-100 in PBS) at room temperature overnight. The solution was removed next day, and cells were washed three times with PBS before being incubated with Alexa 488-conjugated goat anti mouse IgG secondary antibody (1:500; Life Technologies) for 2 h at room temperature in the dark. Finally, after three washes with PBS, cells were then incubated with Alexa 633-conjugated phalloidin (1:50; Life Technologies) for 20 min at room temperature in the dark. Coverslips were then mounted on glass microscope slides in Prolong Gold with DAPI (Life Technologies). The slides were examined using a confocal microscope at 40X magnification (Section 2.10).

## 2.7   Ca$^{2+}$ imaging

Cells ($9 \times 10^4$) were cultured on coverslips for 48 h before incubating with 2.5 µM Fura-2-AM (PromoKine) plus 0.05 % (v/v) Pluronic F-127 (Invitrogen) in DMEM for 20 minutes at 37 °C in the dark. Cells were then washed twice in 37 °C DMEM with 5 % FBS, and were settled in dark at 37 °C for 20 min, and then at room temperature for a further 15 min before transferring onto a RC-20H closed bath imaging chamber (Warner Instruments) according to the manufacturer's instructions. Cells were perfused with appropriate solutions at room temperature. The imaging chamber with P-2H stage adapter was mounted on an epi-fluorescence microscope and observed at 20X. Extracellular solutions were applied using a two-channel gravity perfusion system with a peristaltic pump. The flow rate was approximately 500 µl/min. Cells were treated with a second solution for 6–12 min, 2 min after the experiment began, and were subsequently washed with standard PSS for 6 min, if applicable. At the end of the experiment, ionomycin (10 µM, Table 2.1) was added to the standard PSS as a positive control (Liu & Hermann, 1978).

## 2.8   Na$^+$ imaging

Cells ($6 \times 10^4$) were grown on glass coverslip for 24 h and were then labelled with 5 µM SBFI-AM (Sigma) and 0.1 % (v/v) Pluronic F-127 (Life Technologies) in DMEM with 0 % FBS at 37 °C in the dark for 1 h. Excess SBFI-AM was washed once with 37 °C DMEM supplemented with 5 % FBS. The coverslip was placed in a RC-20H closed bath imaging chamber (Warner Instruments) and was perfused with standard PSS with appropriate treatments at room temperature (Table 2.1). The chamber was mounted on an epi-fluorescece microscope with a P-2H stage adapter, and cells were observed at 40X. Extracellular solutions were applied using a two-channel gravity perfusion system

with a peristaltic pump. The flow rate was approximately 500 µl/min. Cells were treated with test solution for 12 min, 2 min after the experiment began. Cells were then treated with extracellular solution containing 10 mM $Na^+$ (Table 2.2). To calibrate the intracellular $Na^+$ concentration ($[Na^+]_i$), cells were subsequently perfused with extracellular solution with 10 and 20 mM $Na^+$ (Table 2.2) plus $Na^+$ ionophore gramicidin (20 µM, Table 2.1) at the end of experiment, 12 min each (Figure 5.1a). The experiment was repeated three or six times.

## 2.9  Epi-fluorescence microscopy

A Nikon Eclipse TE200 epi-fluorescence microscope was used for all epi-fluorescent imaging. SimplePCI 6.0 software was used to control the imaging system. Images were captured using a RoleraXR Fast1394 charge-coupled device (CCD) camera (QImaging). For mycoplasma test (Section 2.1.5) and Matrigel invasion assay (Section 2.5.2), DAPI was excited at 340 nm and the fluorescence signal was gathered at 512 nm. SBFI and Fura-2 were excited alternately at 340 and 380 nm, and fluorescence signal was collected at 512 nm. For $Ca^{2+}$ imaging, images were captured at 0.2 frames/s. The image plane was auto-focused every 40 frames. For $Na^+$ imaging, the image acquisition rate was 0.1 frames/s.

## 2.10  Confocal microscopy

Immunocytochemistry slides were examined using a Zeiss LSM 880 laser scanning confocal microscope with a 40X oil objective lens. ZEN 2012 software was used to control the microscope. The size of acquired images was 212.3 µm × 212.3 µm (1024 × 1024 pixels). The pinhole size was 1–1.05 airy unit. DAPI was excited at 405 nm, and the emission was collected at 410–500 nm. Alexa Fluor 488 was excited at 488 nm, and the emission at 500–580 nm was collected. Finally, Alexa Fluor 633 was

excited at 633 nm, and the fluorescence signal was collected at 638–747 nm. In each technical repeat, three or four images were taken on each coverslip, and two coverslips were examined in each experimental condition. Three technical repeats were performed.

## 2.11 Image analyses

Three analyses were performed to analyse different parameters in the immunocytochemistry study. Only cells at the edges of the wound were selected, and the image analyses were performed in a blinded fashion. Three technical repeats were performed.

Firstly, cell circularity was calculated using a free-hand tool in ImageJ software using the following equation (Brisson *et al.*, 2013):

$$Circularity = 4\pi \times \frac{Area}{Perimeter^2} \qquad \text{(Equation 2.4)}$$

For each technical repeat, 20–25 cells per condition were analysed blinded to treatment.

Secondly, cells were categorised into two groups: with and without obvious lamellipodia. For each technical repeat, 40–50 cells per condition were analysed blinded to treatment.

Thirdly, the signal intensity of F-actin and active Rac1 at lamellipodia was analysed as described in (Dang *et al.*, 2013), with the following modifications: ImageJ with the Radial Profile Extended plugin (Philippe Carl, CNRS, France) was used in the analysis. In the plugin, the starting radius was set to 0.28 µm, radius increment = 0.28 µm, ending radius = 5.6 µm and total integrated angle = 90 °, resulting 20 arcs in total (Figure 4.17b). Both F-actin and active Rac-1 signal density on each of the arcs were

obtained and were normalised relative to those at the innermost arc. For each technical repeat, 20–30 cells were analysed blinded to treatment in each condition.

For $Ca^{2+}$ and $Na^+$ imaging, image files (in stacked TIFF format) generated from the time-lapse experiments were opened in ImageJ software. 20–70 (in $Ca^{2+}$ imaging) or 7–20 ($Na^+$ imaging) randomly selected adhesive single cells in the field of view were selected as regions of interest (ROI). The images were split according to the excitation wavelength. The fluorescence intensities of all the cell of interest over time at the two wavelengths were gathered by using the stack measurement function of the ROI manager plugin in the ImageJ software. The ratio of fluorescence intensity at 340 and 380 nm (340/380 ratio) was calculated for each cell in Microsoft Excel.

In $Na^+$ imaging, the $[Na^+]_i$ equalled to the extracellular $Na^+$ concentration ($[Na^+]_o$) after gramicidin treatment (Roger *et al.*, 2007). A linear relationship between $[Na^+]_i$ and fluorescence intensity was obtained for a given individual cell by correlating its mean 340/380 ratio over the last 1 min of 10 and 20 mM $Na^+$ treatment with $[Na^+]_i$ = 10 and 20 mM, respectively (Figure 5.1c). Using the linear relationship, the 340/380 ratio of the same cell in other experimental conditions was therefore converted to $[Na^+]_i$. Unless otherwise stated, $[Na^+]_i$ of 7–20 cells in each technical repeat was calculated individually and then averaged.

## 2.12 Curve fitting

All curve fitting analyses were done using the Graphpad Prism 6.0 software. The conductance-voltage relationships were calculated using the following equation (Ding & Djamgoz, 2004):

$$G = \frac{I}{V - V_{rev}}$$ (Equation 2.5)

where G is the conductance, I the current amplitude, V the command voltage, and $V_{rev}$ the reversal potential calculated using the Nernst equation:

$$V_{rev} = \frac{RT}{zF} \ln \frac{Cation\ concentration\ outside\ the\ cell}{Cation\ concentration\ inside\ the\ cell}$$

(Equation 2.6)

where R is the universal gas constant, T the absolute temperature, z valence of ion, F the Faraday constant. In the present study, the $V_{rev}$ for $Na^+$ was +86.3 mV when using the standard PSS and the standard intracellular solution.

The steady-state inactivation (availability) and conductance-voltage relationship were fitted by the Boltzmann equation:

$$X = \frac{1}{1+e^{(V_{\frac{1}{2}}-V)/k}}$$

(Equation 2.7)

where X is the fitted parameter (availability or conductance), $V_{1/2}$ the voltage at which half-maximal conductance or availability occurs, k the slope factor and V the command voltage.

The current-voltage relationship of $I_{BKCa}$ was fitted to a single exponential equation (Sanguinetti & Jurkiewicz, 1990):

$$Y = Y_0 \times e^{kx}$$

(Equation 2.8)

where $Y_0$ is the Y value when x is at 0, and k the rate constant.

Finally, the drug dose-response curve was fitted to a sigmoidal logistic equation (Roger et al., 2003):

$$Percentage\ of\ block = \frac{100}{1+(\frac{IC_{50}}{drug\ concentration})^n} \qquad \text{(Equation 2.9)}$$

where $IC_{50}$ is the concentration of drug at which half of its maximal effect occurs; and n the slope giving the Hill coefficient.

## 2.13 Statistics

Data are presented as mean ± SEM. Graphpad Prism 6.0 software was used to perform all statistical analyses. Paired or unpaired Student's two-tailed t-test was used to compare two samples. Multiple comparisons were made using ANOVA followed by Tukey *post-hoc* tests. Fisher's exact test was used to examine the distribution of samples within a population. To analyse tables with more than two rows or columns, Bonferroni correction was applied for multiple comparisons (MacDonald & Gardner, 2000). Results were considered significant at $P < 0.05$.

# Chapter 3: Na$^+$- and VGSC-dependent V$_m$ regulation in MDA-MB-231 cells

## 3.1 Introduction

VGSCs are protein complexes that comprise one pore-forming α subunit and one or more auxiliary β subunits (Catterall, 2012). In excitable cells, such as neurones, cardiomyocytes and skeletal muscle cells, VGSCs depolarise the V$_m$ to initiate action potential firing (Hille, 2001). Functional α subunits have been identified in an increasing number of cancer cells and patient tissue samples from various tissue origins, including breast, prostate, colon, cervix, lungs and brain. VGSCs potentiate metastatic cell behaviours such as invasion and migration *in vitro* (Brackenbury, 2012; Roger *et al.*, 2015), and their activity/expression increases tumour growth (Nelson *et al.*, 2015a) and metastasis (Yildirim *et al.*, 2012; Driffort *et al.*, 2014; Nelson *et al.*, 2015a; Nelson *et al.*, 2015b) in rodent models. In BCa patient tissue samples, the mRNA level of Na$_v$1.5 correlates with lymph node metastasis (Fraser *et al.*, 2005) and poor prognosis (Yang *et al.*, 2012), suggesting that targeting VGSCs may have therapeutic value in cancer treatment.

β subunits are also present in cancer cells originating from breast, prostate, cervix and lung (Roger *et al.*, 2007; Diss *et al.*, 2008; Chioni *et al.*, 2009; Hernandez-Plata *et al.*, 2012; Jansson *et al.*, 2012). β subunits regulate metastasis-related cell activity *in vitro*. For example, β1 overexpression increases invasion and process outgrowth in MDA-MB-231 cells (Nelson *et al.*, 2014) and reduces migration in wound healing asays (Chioni *et al.*, 2009). MDA-MB-231 cells overexpressing β1 show increased primary tumour growth, vascularisation and metastasis to lungs and liver in mice (Nelson *et al.*, 2014).

Several models have been proposed to explain the mechanisms underlying VGSC α subunit-dependent cancer cell invasion and migration. Firstly, in MDA-MB-231 cells, $Na^+$ influx carried by $Na_v1.5$ allosterically regulates NHE1, which increases the efflux of $H^+$ through plasma membrane and causes an acidic extracellular environment that favours the proteolytic activity of cysteine cathepsin B and S (Gillet *et al.*, 2009; Brisson *et al.*, 2011), and ultimately enhances cell invasion. $Na_v1.5$ activity also increases src kinase activity and phosphorylation of the actin-nucleation-promoting factor cortactin, which can lead to invadopodia formation (Brisson *et al.*, 2013). Additionally, reduced $Na_v1.5$ expression decreases the protein level of the metastasis-promoting molecule CD44 (Nelson *et al.*, 2015b). Moreover, in SW620 colon cancer cells, increased $Na^+$ influx carried by $Na_v1.5$ causes sustained activation of MAPK and increases the expression of invasion-related genes including *CD44*, *CLIC*, *WNT9A*, *ITGB*, *SEMA6A* and *VEGFC* (House *et al.*, 2015). In H460 NSCLC cells, $Na_v1.7$-dependent cell invasion is mediated via the ERK pathway (Campbell *et al.*, 2013).

Activity of ion channels can regulate the $V_m$ of cells. Cancer cells usually possess a more depolarised $V_m$ than their normal counterparts (Binggeli & Weinstein, 1986; Yang & Brackenbury, 2013). In PCa cells, the $V_m$ of strongly metastatic PC-3 cells is ~5 mV more depolarised than the weakly metastatic LNCaP cells (Laniado *et al.*, 1997), and in BCa cells, depolarised $V_m$ associates with increased cancer cell metastatic potential: compared to non-metastatic, VGSC-negative MCF-7 cells (~-40 mV), strongly metastatic VGSC-expressing MDA-MB-231 cells have a more depolarised $V_m$ (~-20 mV) (Fraser *et al.*, 2005). However, whether the depolarised $V_m$ is caused by $Na^+$ influx via VGSCs is not known.

Importantly, $V_m$ is now regarded more than an epi-phenomenon in non-excitable cells: a large amount of data has shown that $V_m$ regulates cell cycle progression in normal (Blackiston *et al.*, 2009) and cancer cells (Yang & Brackenbury, 2013). A depolarised $V_m$ can cause reorganisation of actin filament network in bovine eye

endothelial and epithelial cells (Chifflet $et$ $al.$, 2003; Chifflet $et$ $al.$, 2004; Chifflet $et$ $al.$, 2005). In kidney epithelial cells, $V_m$ depolarisation induces phosphorylation of MLC by activating the ROCK pathway (Szaszi $et$ $al.$, 2005). Furthermore, $in$ $vivo$ evidence shows that depolarised $V_m$ leads to tumourigenesis in $Xenopus$ $laevis$ (Blackiston $et$ $al.$, 2011; Lobikin $et$ $al.$, 2012; Lobikin $et$ $al.$, 2015). Taken together, $V_m$ has been suggested as an instructive signal in cancer progression, but whether or not VGSCs increase cancer cells metastatic behaviours by depolarising the $V_m$ is not known.

The relationship between tumour ER status and prognosis in BCa patients has been long established. In general, compared to $ER^+$ tumours, BCa patients bearing $ER^-$ tumours have higher risk of mortality (Parl $et$ $al.$, 1984; Aaltomaa $et$ $al.$, 1991b, a; Crowe $et$ $al.$, 1991; Dunnwald $et$ $al.$, 2007). ER status associates with distinct gene expression pattern in BCa patients (Perou $et$ $al.$, 2000; Gruvberger $et$ $al.$, 2001; Sorlie $et$ $al.$, 2001; van 't Veer $et$ $al.$, 2002), and is known as the most important discriminator of gene expression profiles (Sotiriou $et$ $al.$, 2003). Compared to $ER^-$ MDA-MB-231 cells, $ER^+$ MCF-7 cells show weaker metastatic potential (Thompson $et$ $al.$, 1992; Roger $et$ $al.$, 2003; Fraser $et$ $al.$, 2005). Indeed, C4 and C4-12, two MCF-7 cell sublines where ER expression is lost, show abolished oestrogen-mediated, insulin-like growth factor-I receptor-dependent cell growth (Oesterreich $et$ $al.$, 2001). Despite all the evidence showing the high malignancy of $ER^-$ cells and the roles of VGSCs in promoting cell metastatic behaviours, it was not until 2010 that researchers investigated the interplay between oestrogen signalling and VGSCs in cancer: GPR30 (a G-protein-coupled oestrogen receptor) is identified in MDA-MB-231 cells, and external application of β-oestradiol (E2) or G-1, a GPR30 agonist, increases $I_{Na}$ in a PKA-dependent manner (Fraser $et$ $al.$, 2010). Additionally, acute application of E2 increased MDA-MB-231 cell adhesion, which is abrogated by co-application with TTX, suggesting the importance of VGSCs in mediating oestrogen signalling (Fraser $et$ $al.$,

2010). However, whether ERα regulates functional VGSC expression has not been studied.

### 3.1.1 Hypotheses and aims

The main hypothesis underlying this Chapter was that VGSCs depolarise the resting $V_m$ of MDA-MB-231 cells. A second hypothesis was that ER knockdown in MCF-7 cells may lead to functional VGSC expression.

The specific aims were:

(1) To investigate whether or not extracellular $Na^+$ regulates the $V_m$ in MDA-MB-231 cells.

(2) To study the involvement of VGSCs in regulating the $V_m$ in MDA-MB-231 cells.

(3) To record membrane current in MCF-7 and pII (a derivative MCF-7 cell line where ERα expression was stably down-regulated) cells.

### 3.2 Results

### 3.2.1 $Na^+$ conductance depolarises the $V_m$ of MDA-MB-231 cells

The effect of extracellular $Na^+$ on the $V_m$ of MDA-MB-231 cells was investigated using whole-cell patch clamp recording in I=0 mode (Section 2.4.8). Standard intracellular solution was used in all experiments recording the cell $V_m$ (Table 2.3).

Firstly, whether or not $Na^+$ conductance through plasma membrane regulates the $V_m$ was studied. In these experiments, NaCl in the standard extracellular PSS was replaced with equimolar ChoCl or NMDG (Table 2.2). The $V_m$ of MDA-MB-231 cells was continuously measured over a 6 min experiment that comprised three steps: (1) cells were initially perfused with the standard PSS for 60 s, followed by (2) $Na^+$-free

PSS treatment for 150 s, and (3) a final washout with the standard PSS for a further 150 s (Figure 3.1a).

Replacement of extracellular NaCl with ChoCl reversibly hyperpolarised the $V_m$ of MDA-MB-231 cells (Figure 3.1a). In order to quantify the data, the mean $V_m$ over the ast 5 s, 15 s, 30 s and 60 s of each of the three experimental steps was analysed, with the liquid junction potentials compensated (3 mV in standard PSS and 5.3 mV in ChoCl, Section 2.4.8) (Figure 3.1b, Table 3.1). Comparisons of the mean $V_m$ over the last 5 s of the three steps showed that the $V_m$ of MDA-MB-231 cells significantly hyperpolarised from -10.4 ± 1.0 mV to -20.4 ± 2.0 mV after ChoCl treatment (P < 0.001; ANOVA with Tukey *post-hoc* test; n = 10). By washing out ChoCl with standard PSS, the $V_m$ recovered to -12.9 ± 2.3 mV (P < 0.001 compared with ChoCl; P = 0.22 compared with standard PSS; ANOVA with Tukey *post-hoc* test; n = 10). Statistical analyses comparing the $V_m$ across other measurement intervals (15 s, 30 s and 60 s) are in Figure 3.1b and Table 3.1.

Next, NMDG was used as an alternative extracellular NaCl substitute to confirm the results. Similar to ChoCl, NMDG reversibly hyperpolarised the $V_m$ of MDA-MB-231 cells (Figure 3.2a). Taking the mean $V_m$ over the last 5 s of the three experimental steps as an example, with the liquid junction potentials compensated (3 mV in standard PSS and 7.7 mV in NMDG), NMDG significantly hyperpolarised the $V_m$ from -10.3 ± 2.0 mV to -24.8 ± 2.4 mV (P < 0.001; ANOVA with Tukey *post-hoc* test; n = 7), and the $V_m$ subsequently recovered to -13.2 ± 2.7 mV after NMDG washout (P < 0.001 compared with NMDG; P = 0.15 compared with standard PSS; ANOVA with Tukey *post-hoc* test; n = 7). Statistical analyses of the $V_m$ using other measurement intervals are shown in Figure 3.2b and Table 3.2. In summary, these two experiments demonstrated that extracellular $Na^+$ depolarises the $V_m$ of MDA-MB-231 cells by 10–15 mV, suggesting the dependence of $V_m$ on inward $Na^+$ conductance.
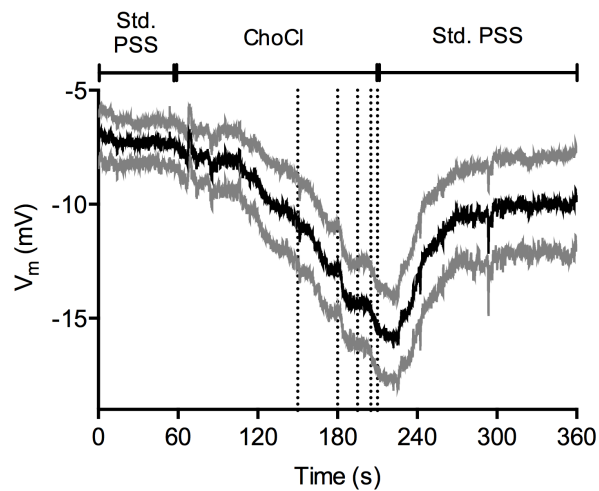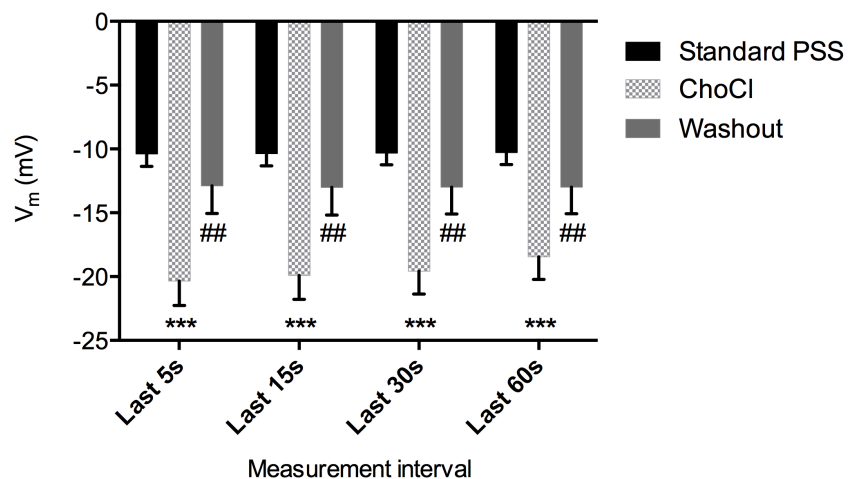
Figure 3.1. Replacement of extracellular NaCl with choline chloride (ChoCl) hyperpolarises the membrane potential ($V_m$) of MDA-MB-231 cells.

(**a**) MDA-MB-231 cells were perfused with standard physiological saline solution (PSS) for 60 s followed by $Na^+$-free ChoCl solution for 150 s, which was subsequently washed out using standard PSS for a further 150 s. Black and grey traces show mean ± SEM (n = 10). Dotted vertical lines take the ChoCl treatment period as an example to indicate various measurement intervals (last 5 s, 15 s, 30 s and 60 s) in each of the three steps. Liquid junction potentials (3 mV in standard PSS and 5.3 mV in ChoCl) are not compensated. (**b**) The mean $V_m$ was compared over the indicated measurement intervals. Liquid junction potentials (3 mV in standard PSS and 5.3 mV in ChoCl) are compensated. (***) P < 0.001 compared with standard PSS; (##) P < 0.01 compared with ChoCl solution; ANOVA with Tukey *post-hoc* test (n = 10). Data are mean ± SEM.

| Table 3.1. Mean membrane potential ($V_m$) of MDA-MB-231 cells after choline chloride (ChoCl) treatment and washout. | | | |
|---|---|---|---|
| **Measurement interval** | **$V_m$ in standard PSS (mV)** | **$V_m$ in ChoCl (mV)** | **$V_m$ in washout (mV)** |
| Last 5 s | -10.4 ± 1.0 | -20.4 ± 2.0 *** | -12.9 ± 2.3 ## |
| Last 15 s | -10.4 ± 1.0 | -19.9 ± 2.0 *** | -13.0 ± 2.3 ## |
| Last 30 s | -10.3 ± 1.0 | -19.6 ± 1.9 *** | -13.0 ± 2.2 ## |
| Last 60 s | -10.3 ± 1.0 | -18.5 ± 1.9 *** | -13.0 ± 2.2 ## |
| Liquid junction potentials (3 mV in standard PSS and 5.3 mV in ChoCl) were compensated offline. PSS: physiological saline solution. (***) $P < 0.001$ compared with $V_m$ in standard PSS; (##) $P < 0.01$ compared with $V_m$ in ChoCl; ANOVA with Tukey post-hoc test (n = 10). Data are mean ± SEM. | | | |

**a**
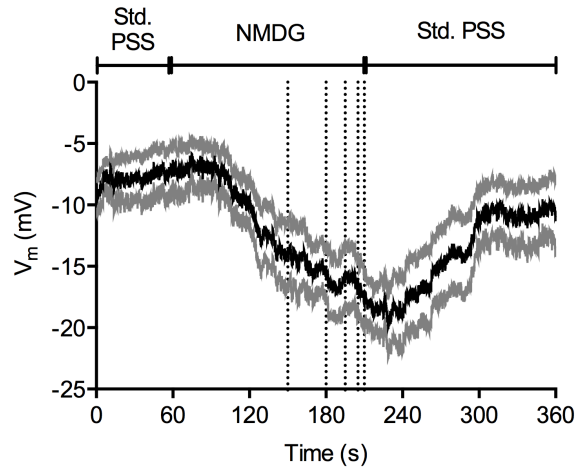
**b**
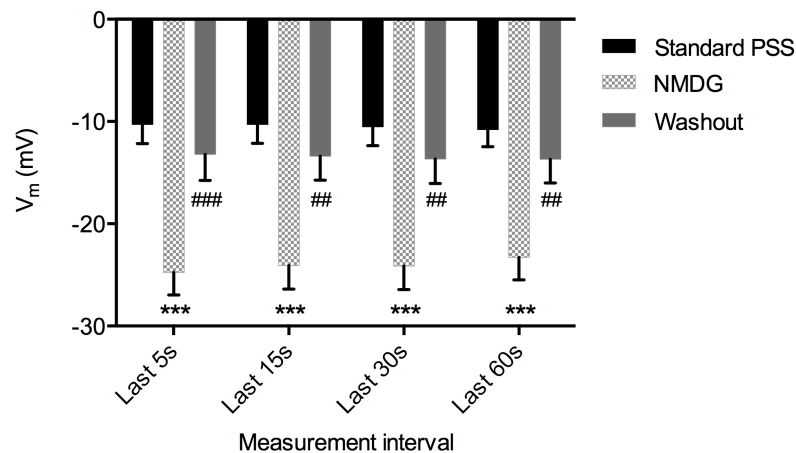
Figure 3.2. Replacement of extracellular NaCl with N-methyl-D-glucamine (NMDG) hyperpolarises the membrane potential ($V_m$) of MDA-MB-231 cells.

(**a**) MDA-MB-231 cells were perfused with standard physiological saline solution (PSS) for 60 s followed by $Na^+$-free NMDG solution for 150 s, which was subsequently washed out using standard PSS for a further 150 s. Black and grey traces show mean ± SEM (n = 7). Dotted vertical lines take the NMDG treatment period as an example to indicate various measurement intervals (last 5 s, 15 s, 30 s and 60 s) in each of the three steps. Liquid junction potentials (3 mV in standard PSS and 7.7 mV in NMDG) are not compensated. (**b**) The mean $V_m$ was compared over the indicated measurement intervals. Liquid junction potentials (3 mV in standard PSS and 7.7 mV in NMDG) are compensated. (***) P < 0.001 compared with standard PSS; (##) P < 0.01 compared with NMDG solution; ANOVA with Tukey *post-hoc* test (n = 7). Data are mean ± SEM.

| Table 3.2. Mean membrane potential ($V_m$) of MDA-MB-231 cells after N-methyl-D-glucamine (NMDG) treatment and washout. | | | |
|---|---|---|---|
| Measurement interval | $V_m$ in standard PSS (mV) | $V_m$ in NMDG (mV) | $V_m$ in washout (mV) |
| Last 5 s | -10.3 ± 2.0 | -24.8 ± 2.4 *** | -13.2 ± 2.7 ### |
| Last 15 s | -10.3 ± 2.0 | -24.1 ± 2.5 *** | -13.4 ± 2.5 ## |
| Last 30 s | -10.5 ± 2.0 | -24.1 ± 2.5 *** | -13.7 ± 2.6 ## |
| Last 60 s | -10.8 ± 1.8 | -23.3 ± 2.4 *** | -13.7 ± 2.5 ## |
| Liquid junction potentials (3 mV in standard PSS and 7.7 mV in NMDG) were compensated offline. PSS: physiological saline solution. (***) $P < 0.001$ compared with $V_m$ in standard PSS; (##) $P < 0.01$ compared with $V_m$ in NMDG; ANOVA with Tukey *post-hoc* test (n = 7). Data are mean ± SEM. | | | |

### 3.2.2 VGSC window current in MDA-MB-231 cells

In neurones, in spite of its small amplitude compared to the transient $I_{Na}$, persistent $I_{Na}$ has an important role in shaping the action potential firing pattern, especially in the subthreshold voltage range (Stafstrom, 2011). Therefore, this study hypothesised that VGSCs may carry persistent $I_{Na}$, which would depolarise the steady-state $V_m$ in MDA-MB-231 cells. Indeed, eliciting $I_{Na}$ in MDA-MB-231 cells using the standard $I_{Na}$ stimulation protocol (Section 2.4.7) showed both transient and persistent $I_{Na}$ (measured as mean current between 45 ms and 50 ms following depolarisation) (Figure 3.3a and b). Voltage-dependent activation (Figure 3.3c) and the steady-state inactivation (Figure 3.3d) of VGSCs were investigated. Normalised conductance ($G/G_{Max}$) was calculated from the current data and plotted as a function of voltage (Section 2.12) (Figure 3.3e; n = 14). Normalised current ($I/I_{Max}$) was plotted as a function of the pre-pulse voltage (Figure 3.3e; n = 9). Both $G/G_{Max}$ and $I/I_{Max}$ curves were fitted with Boltzmann functions (Section 2.12). Overlapping the $G/G_{Max}$ and $I/I_{Max}$ curves revealed a window $I_{Na}$ between -50 mV and -10 mV (Figure 3.3e, dotted box; Figure 3.3f, shadowed area). At the typical resting $V_m$ of ~-10 mV (Table 3.1 and Table 3.2), 1.0 ± 0.4 % of the VGSCs in MDA-MB-231 cells are available to carry persistent $I_{Na}$ and thus may regulate the $V_m$ (Figure 3.3f).
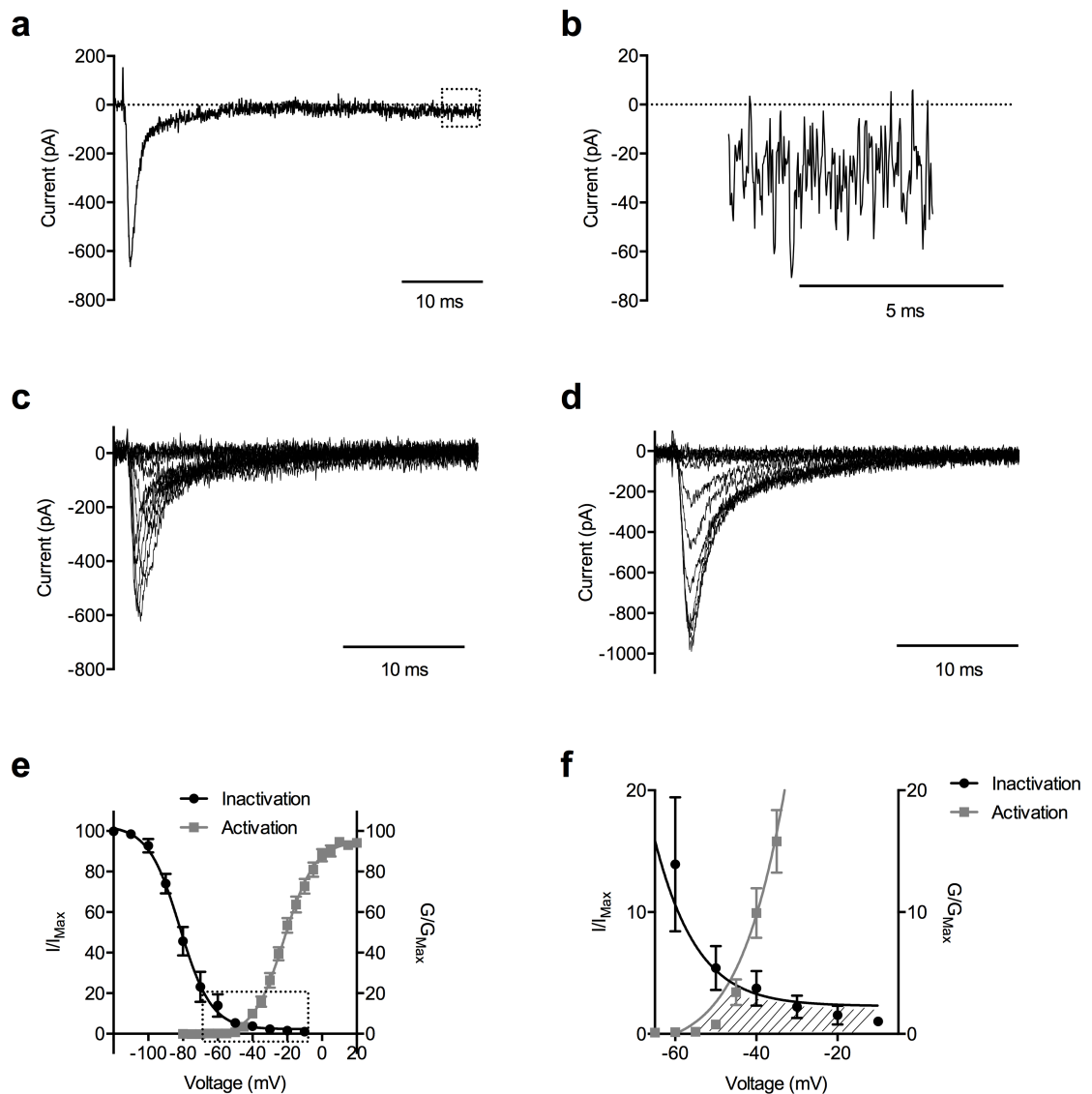
Figure 3.3. The window Na$^+$ current (I$_{Na}$) in MDA-MB-231 cells.

(**a**) Typical whole-cell recording of I$_{Na}$ in MDA-MB-231 cell. Dotted box shows the persistent I$_{Na}$. (**b**) The persistent I$_{Na}$ in (a). Cells were depolarised to -10 mV for 50 ms following a 250 ms pre-pulse at -120 mV. Persistent I$_{Na}$ was measured as mean current between 45 ms and 50 ms following depolarisation. (**c**) Typical whole-cell recording from MDA-MB-231 cell by depolarising the cells to voltages in the range -80 to +30 mV (60 ms) in 5 mV increments following a 250 ms pre-pulse at -120 mV. Every other I$_{Na}$ trace is shown for clarity. (**d**) Steady-state inactivation of whole-cell I$_{Na}$. I$_{Na}$ was elicited by -10 mV pulse (60 ms) following 250 ms conditioning voltage pre-pulses between -120 mV and -10 mV in 10 mV increments. (**e** and **f**) Activation and steady-state inactivation of I$_{Na}$ recorded from MDA-MB-231 cells. Normalised conductance (G/G$_{Max}$) was calculated from the current data and plotted as a function of voltage (n = 14). Normalised current (I/I$_{Max}$) was plotted as a function of the pre-pulse voltage (n = 9). Data are fitted with Boltzmann functions. The area inside the dotted box of (e) is presented in (f). Shadowed area in (f) indicates the window I$_{Na}$. Data are mean ± SEM.

### 3.2.3 TTX reduces $I_{Na}$ and hyperpolarises the $V_m$ of MDA-MB-231 cells

The predominant VGSC isoform expressed in MDA-MB-231 cells is $Na_v1.5$ (Fraser *et al.*, 2005), which is a TTX-resistant VGSC subtype that can only be blocked by TTX in the micromolar range (Goldin, 2001). To confirm the channel blocking effect of TTX, $I_{Na}$ was firstly recorded in the standard PSS using the $Cs^+$-containing intracellular solution. Perfusion with 30 µM TTX for 2 min significantly reduced transient (Figure 3.4a) as well as persistent $I_{Na}$ (Figure 3.4b). Transient $I_{Na}$ was reduced to 12.2 ± 0.8 % after TTX treatment (Figure 3.4c; $P < 0.001$; ANOVA with Tukey *post-hoc* test; n = 7), and when TTX was subsequently washed out using standard PSS for 2 min, transient $I_{Na}$ recovered to 106.4 ± 6.7 % (Figure 3.4c; $P < 0.001$ compared with TTX; $P = 0.49$ compared with standard PSS; ANOVA with Tukey *post-hoc* test; n = 7). As for persistent $I_{Na}$, TTX reduced the current to 26.7 ± 5.9 % of control (Figure 3.4d; $P < 0.05$; ANOVA with Tukey *post hoc* test; n = 4), and following washout persistent $I_{Na}$ recovered to 103.5 ± 31.2 % (Figure 3.4d; $P < 0.05$ compared with TTX; $P = 0.99$ compared with control; ANOVA with Tukey *post hoc* test; n = 4). The data suggest that TTX at 30 µM potently blocks transient and persistent $I_{Na}$ in MDA-MB-231 cells.

Next, the study examined whether VGSCs regulate the $V_m$ of MDA-MB-231 cells using TTX. Since TTX inhibited $Na^+$ influx through VGSCs, the reduction in $[Na^+]_i$ should cause a hyperpolarised $V_m$. To test this, cells were consecutively perfused with standard PSS for 60 s, followed by 30 µM TTX for 150 s, and finally washout with standard PSS for a further 150 s). TTX, but not the vehicle (148 µM citrate at pH = 4.8), significantly hyperpolarised the $V_m$ of MDA-MB-231 cells (Figure 3.5a and b). The mean $V_m$ over the last 5 s, 15 s, 30 s and 60 s of each of the three experimental steps after TTX and vehicle treatment was analysed with the liquid junction potentials (3 mV) compensated (Figure 3.5c and d; Table 3.3 and Table 3.4).
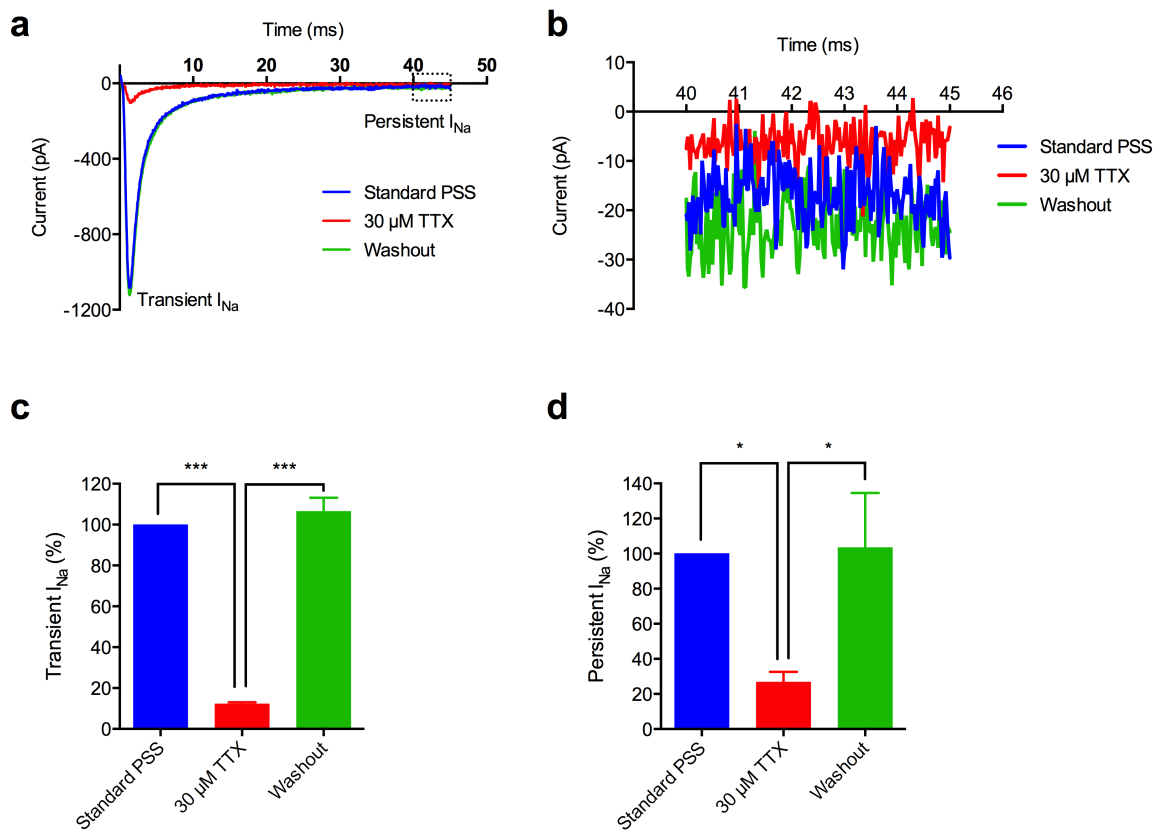
Figure 3.4. Tetrodotoxin (TTX) reduces transient and persistent $Na^+$ current ($I_{Na}$) in MDA-MB-231 cells.

(**a**) Representative $I_{Na}$ recorded from MDA-MB-231 cells in standard physiological saline solution (PSS) (blue), 30 µM TTX (red) and after washout (green). Transient $I_{Na}$ is labelled, and the dotted box shows the persistent $I_{Na}$. (**b**) Enlargement of the dotted box in (a), showing the persistent $I_{Na}$. $I_{Na}$ was elicited by depolarising the cell to -10 mV following a 250 ms pre-pulse at -120 mV. Persistent $I_{Na}$ between 45–50 ms after depolarisation was adopted in data analyses. (**c**) Normalised transient $I_{Na}$ after 30 µM TTX treatment and subsequent washout. (\*\*\*) $P < 0.001$; ANOVA with Tukey *post-hoc* test (n = 7). (**d**) Normalised persistent $I_{Na}$ after 30 µM TTX treatment and the subsequent washout (\*) $P < 0.05$; ANOVA with Tukey *post-hoc* test (n = 4). Data are mean ± SEM.
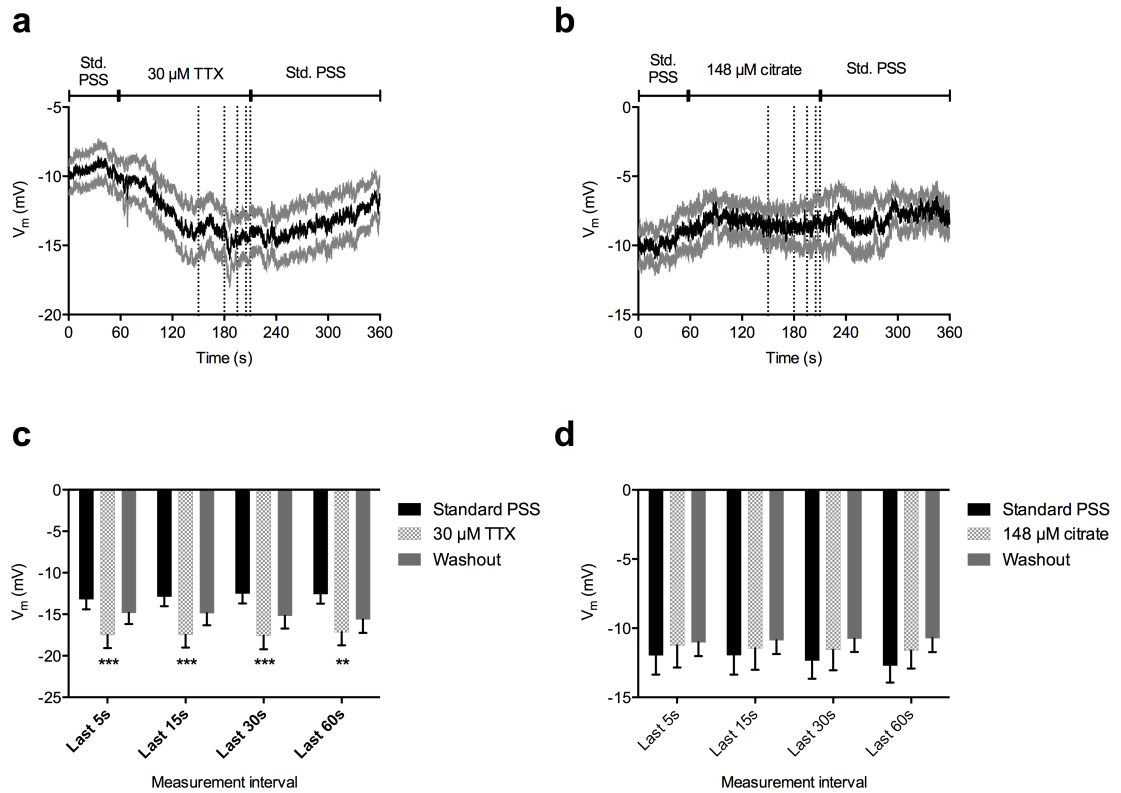
Figure 3.5. Tetrodotoxin (TTX) hyperpolarises the membrane potential ($V_m$) of MDA-MB-231 cells.

MDA-MB-231 cells were treated with standard physiological saline solution (PSS) for 60 s before being perfused with (**a**) 30 µM TTX or (**b**) vehicle, 148 µM citrate at pH = 4.8, for 150 s. TTX and citrate buffer were subsequently washed out with standard PSS for a further 150 s. Black trace shows the mean $V_m$ of n = 17 (a) or n = 13 (b), and the grey traces show the SEM. Dotted vertical lines indicate the various measurement intervals (last 5 s, 15 s, 30 s and 60 s). Liquid junction potentials (3 mV) are not compensated. The mean $V_m$ over indicated measurement intervals after (**c**) TTX or (**d**) citrate buffer treatment. Liquid junction potentials (3 mV) are compensated. (**) $P < 0.01$ and (***) $P < 0.001$ compared to PSS; ANOVA with Tukey *post-hoc* test [n = 17 in (c) and n = 13 in (d)]. Data are mean ± SEM.

| Table 3.3. Mean membrane potential ($V_m$) of MDA-MB-231 cells after tetrodotoxin (TTX, 30 µM) treatment and washout. | | | |
|---|---|---|---|
| **Measurement interval** | **$V_m$ in standard PSS (mV)** | **$V_m$ in 30 µM TTX (mV)** | **$V_m$ in washout (mV)** |
| Last 5 s | -13.2 ± 1.3 | -17.5 ± 1.6 *** | -14.8 ± 1.4 |
| Last 15 s | -12.9 ± 1.2 | -17.5 ± 1.6 *** | -14.9 ± 1.5 |
| Last 30 s | -12.5 ± 1.2 | -17.6 ± 1.7 *** | -15.2 ± 1.6 |
| Last 60 s | -12.2 ± 1.2 | -16.8 ± 1.5 ** | -15.3 ± 1.6 |
| Liquid junction potentials (3 mV) were compensated offline. PSS: physiological saline solution. (**) $P < 0.01$; (***) $P < 0.001$ compared with $V_m$ in standard PSS; ANOVA with Tukey *post-hoc* test (n = 17). Data are mean ± SEM. | | | |

| Table 3.4. Mean membrane potential ($V_m$) of MDA-MB-231 cells after citrate (148 µM; pH = 4.8) treatment and washout. | | | |
|---|---|---|---|
| **Measurement interval** | **$V_m$ in standard PSS (mV)** | **$V_m$ in 148 µM citrate (mV)** | **$V_m$ in washout (mV)** |
| Last 5 s | -12.0 ± 1.5 | -11.2 ±1.7 (n.s.) | -11.0 ± 1.0 |
| Last 15 s | -12.0 ± 1.5 | -11.5 ± 1.6 (n.s.) | -10.9 ± 1.0 |
| Last 30 s | -12.3 ± 1.4 | -11.6 ± 1.5 (n.s.) | -10.8 ± 1.0 |
| Last 60 s | -12.7 ± 1.3 | -11.6 ± 1.4 (n.s.) | -10.7 ± 1.0 |
| Liquid junction potentials (3 mV) were compensated offline. PSS: physiological saline solution. n.s. not significant compared with $V_m$ in standard PSS; ANOVA with Tukey *post-hoc* test (n = 13). Data are mean ± SEM. | | | |

At the last 5 s of each of the three steps, 30 µM TTX significantly hyperpolarised the $V_m$ of MDA-MB-231 cells from -13.2 ± 1.3 mV to -17.5 ± 1.6 mV (P < 0.001; ANOVA with Tukey *post-hoc* test; n = 17). The $V_m$ partially recovered to -14.8 ± 1.4 mV after drug washout, such that it was not significantly different compared to the $V_m$ recorded in standard PSS (P = 0.37; ANOVA with Tukey *post-hoc* test; n = 17) or in TTX (P = 0.07; ANOVA with Tukey *post-hoc* test; n = 17). Statistical analyses of the $V_m$ using other measurement intervals are in Figure 3.5c and Table 3.3.

Importantly, applying the same experimental procedure, citrate (148 µM, pH = 4.8), vehicle for 30 µM TTX, did not change the $V_m$ significantly (Figure 3.5d; Table 3.4). Taking the last 5 s of each of the three experimental steps as example, the mean $V_m$ in standard PSS and citrate was -12.0 ± 1.5 mV and -11.2 ± 1.7 mV, respectively (P = 0.93; ANOVA with Tukey *post hoc* test; n = 13). After washout, the $V_m$ was -11.0 ± 1.0 mV (P = 0.99; ANOVA with Tukey *post hoc* test; n = 13). Statistical analyses of the $V_m$ using other measurement intervals are in Figure 3.5d and Table 3.4, showing that citrate did not alter the $V_m$. In summary, the data showed that blocking VGSCs using TTX hyperpolarised the $V_m$ by approximately 4.3 mV.

### 3.2.4 Phenytoin reduces $I_{Na}$ and hyperpolarises the $V_m$ of MDA-MB-231 cells

Phenytoin is a class 1b VGSC-blocking antiarrhythmic agent. During action potential firing, phenytoin decreases the phase 0 (depolarisation) slope, reduces the action potential duration, and increases effective refractory period (Vaughan Williams, 1975). Phenytoin causes tonic and use-dependent inhibition on $I_{Na}$ in MDA-MB-231 cells (Yang *et al.*, 2012). The tonic block is more potent at more depolarised holding voltages (Ragsdale *et al.*, 1991). Previously, phenytoin at 50 µM was shown to inhibit transient $I_{Na}$ by 43 % and persistent $I_{Na}$ by 42 % when MDA-MB-231 cells were

depolarised to -10 mV from -120 mV. The tonic block following depolarisation to -10 mV from -80 mV was stronger, as the transient and persistent $I_{Na}$ was inhibited by 80 % and 49 % (Yang *et al.*, 2012). In the present study, 100 µM phenytoin was used in order to obtain greater inhibition of transient and persistent $I_{Na}$. The $I_{Na}$ was recorded in standard PSS using $Cs^+$-containing intracellular solution. When the holding potential was -120 mV, perfusion with phenytoin (100 µM) for 2 min inhibited both transient $I_{Na}$ (Figure 3.6a) and persistent $I_{Na}$ (Figure 3.6b): after incubation with phenytoin for 2 min, transient $I_{Na}$ was reduced to 51.9 ± 3.2 %, compared to standard PSS (Figure 3.6c; P < 0.001; ANOVA with Tukey *post hoc* test; n = 9). Washout (2 min) partially recovered the transient $I_{Na}$ to 72.6 ± 4.0 % of control (Figure 3.6a and c; P < 0.001; ANOVA with Tukey *post hoc* test; n = 9). Similarly, phenytoin (100 µM) significantly reduced the persistent $I_{Na}$ to 63.2 ± 10.8 %, compared to standard PSS (Figure 3.6b and d; P < 0.01; ANOVA with Tukey *post hoc* test; n = 4). Washout recovered the persistent $I_{Na}$ to 102.6 ± 1.3 % compared to standard PSS (Figure 3.6b and d; P < 0.01 compared with phenytoin; P = 0.96 compared with standard PSS; ANOVA with Tukey *post hoc* test; n = 9).

Phenytoin showed stronger inhibition when the holding potential was at -80 mV (Figure 3.7a and b). The transient $I_{Na}$ was reduced to 11.9 ± 3.8 % of standard PSS (Figure 3.7c; P < 0.001; ANOVA with Tukey *post hoc* test; n = 4). The transient $I_{Na}$ was partially recovered to 54.8 ± 7.5 % (Figure 3.7c; P < 0.001 compared with standard PSS and phenytoin; ANOVA with Tukey *post hoc* test; n = 4). Similarly, phenytoin reduced the persistent $I_{Na}$ to 5.3 ± 8.2 %, compared to standard PSS (Figure 3.7d; P < 0.001; ANOVA with Tukey *post hoc* test; n = 3), and the persistent $I_{Na}$ only recovered to 54.0 ± 12.2 % (Figure 3.7d; P < 0.05 compared with standard PSS and phenytoin; ANOVA with Tukey *post hoc* test; n = 3). In summary, phenytoin at 100 µM showed stronger tonic block of both transient and persistent $I_{Na}$ at a more depolarised holding potential.
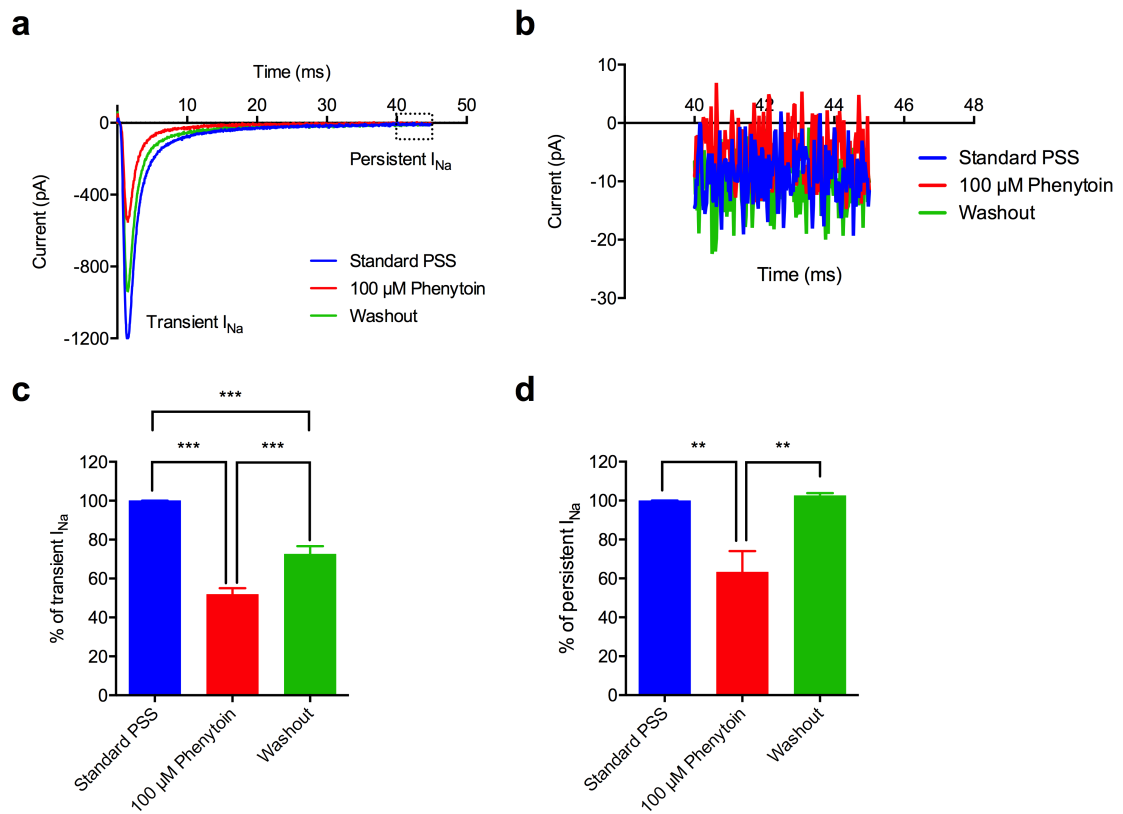
Figure 3.6. Phenytoin inhibits Na$^+$ current ($I_{Na}$) in MDA-MB-231 cells at holding potential = -120 mV.

(**a**) Representative $I_{Na}$ recorded from MDA-MB-231 cells in standard physiological saline solution (PSS) (blue), 100 µM phenytoin (red) and after washout (green). Transient $I_{Na}$ is labelled, and the dotted box shows the persistent $I_{Na}$. (**b**) Enlargement of the dotted box in (a), showing the persistent $I_{Na}$. $I_{Na}$ was elicited by depolarising the cell to -10 mV following a 250 ms pre-pulse at -120 mV. Persistent $I_{Na}$ between 45–50 ms after depolarisation was adopted in data analyses. (**c**) Normalised transient $I_{Na}$ after 100 µM phentoin treatment and subsequent washout. (**) $P < 0.01$; ANOVA with Tukey *post-hoc* test (n = 9). (**d**) Normalised persistent $I_{Na}$ after 100 µM phenytoin treatment and the subsequent washout (**) $P < 0.001$; ANOVA with Tukey *post-hoc* test (n = 4). Data are mean ± SEM.
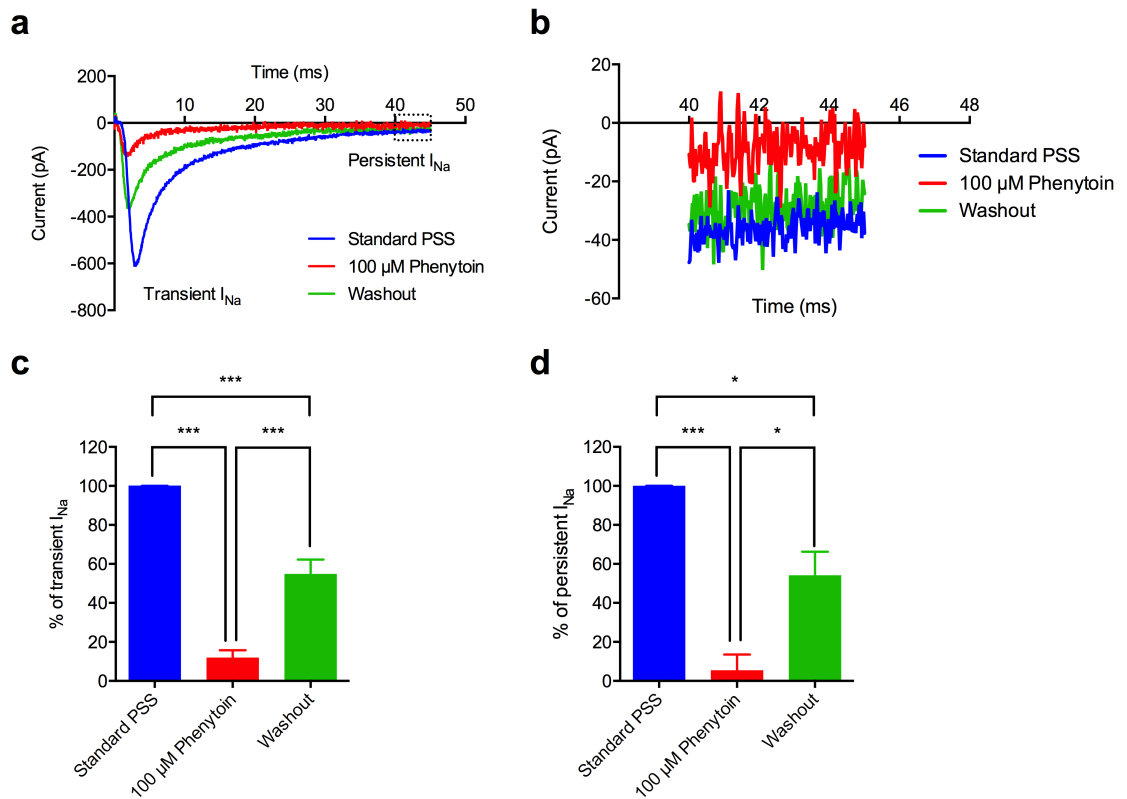
Figure 3.7. Phenytoin inhibits Na$^+$ current ($I_{Na}$) in MDA-MB-231 cells at holding potential = -80 mV.

(**a**) Representative $I_{Na}$ recorded from MDA-MB-231 cells in standard physiological saline solution (PSS) (blue), 100 µM phenytoin (red) and after washout (green). Transient $I_{Na}$ is labelled, and the dotted box shows the persistent $I_{Na}$. (**b**) Enlargement of the dotted box in (a), showing the persistent $I_{Na}$. $I_{Na}$ was elicited by depolarising the cell to -10 mV following a 250 ms pre-pulse at -80 mV. Persistent $I_{Na}$ between 45–50 ms after depolarisation was adopted in data analyses. (**c**) Normalised transient $I_{Na}$ after 100 µM phentoin treatment and subsequent washout. (***) P < 0.001; ANOVA with Tukey *post-hoc* test (n = 4). (**d**) Normalised persistent $I_{Na}$ after 100 µM phenytoin treatment and the subsequent washout (***) P < 0.001; (*) P < 0.05; ANOVA with Tukey *post-hoc* test (n = 3). Data are mean ± SEM.

Next, the effect of 100 µM phenytoin on steady-state $V_m$ of MDA-MB-231 cells was investigated. Cells were initially perfused with standard PSS for 60 s, followed by phenytoin/vehicle for 150 s, and then a washout step with standard PSS for a further 150 s. Phenytoin, but not the vehicle (75 µM NaOH), significantly hyperpolarised the $V_m$ (Figure 3.8a and b). At the last 5 s of each of the three experimental steps, the $V_m$ of MDA-MB-231 cells hyperpolarised from -12.6 ± 1.5 mV to -15.7 ± 1.7 mV after phenytoin treatment (Figure 3.8c; Table 3.5; P < 0.001; ANOVA with Tukey *post hoc* test; n = 12), however, the $V_m$ only partially recovered to -14.6 ± 1.9 mV following washout (Figure 3.8c; Table 3.5; P = 0.59; n = 12). Similarly, the $V_m$ was significantly hyperpolarised in the last 15 s, 30 s and 60 s following phenytoin treatment (Figure 3.8c; Table 3.5; n = 12). In contrast, NaOH (75 µM), the vehicle for 100 µM phenytoin, did not significantly change the $V_m$ (Figure 3.8d), as the mean $V_m$ was -10.8 ± 1.5 mV, -11.0 ± 1.3 mV, and -10.1 ± 2 mV in standard PSS, NaOH and washout, respectively, in the last 5 s of each step (Figure 3.8d; Table 3.6; P = 0.98 comparing NaOH and standard PSS; n = 9). Similarly, the $V_m$ was not significantly changed using other measurement intervals (Figure 3.8d; Table 3.6; n = 9). In summary, like TTX, phenytoin showed similar $V_m$-hyperpolarising effect on MDA-MB-231 cells by blocking VGSCs.
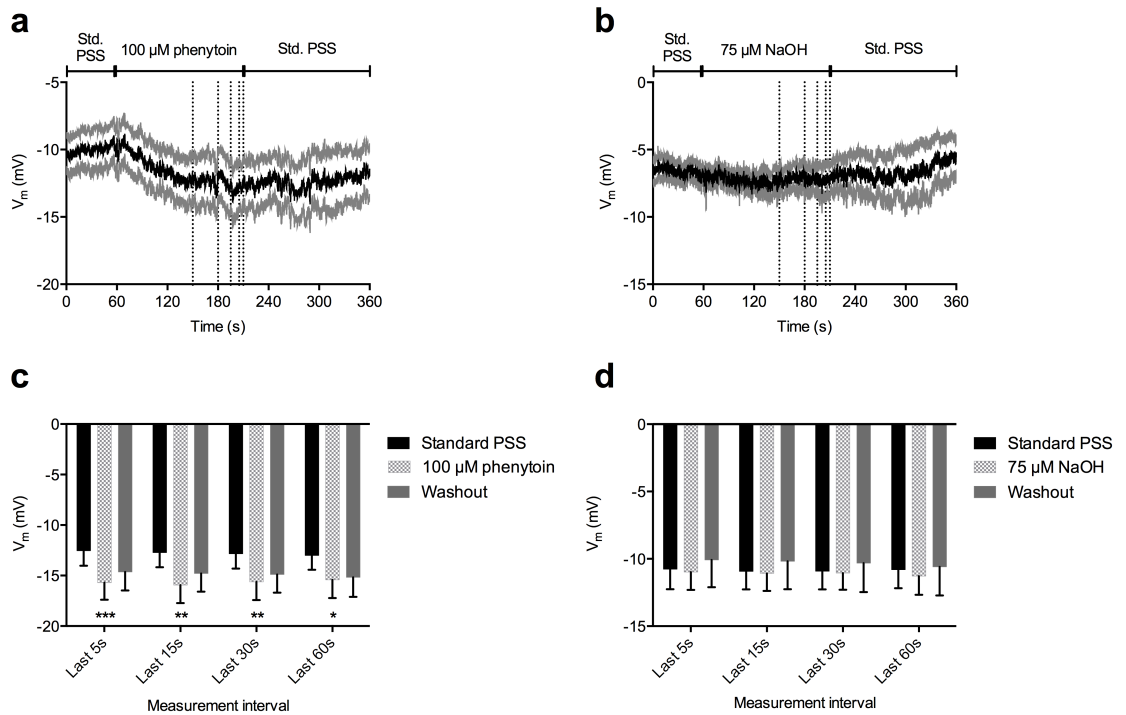
Figure 3.8. Phenytoin hyperpolarises the membrane potential ($V_m$) of MDA-MB-231 cells.

MDA-MB-231 cells were treated with standard physiological saline solution (PSS) for 60 s before being perfused with (**a**) 100 µM phenytoin or (**b**) vehicle, 75 µM NaOH, for 150 s. Phenytoin and NaOH were subsequently washed out with standard PSS for a further 150 s. Black trace shows the mean $V_m$ of n = 12 (a) or n = 9 (b), and the grey traces show the SEM. Dotted vertical lines indicate the various measurement intervals (last 5 s, 15 s, 30 s and 60 s). Liquid junction potentials (3 mV) are not compensated. The mean $V_m$ over indicated measurement intervals after (**c**) phenytoin or (**d**) NaOH treatment. Liquid junction potentials (3 mV) are compensated. (*) $P < 0.05$; (**) $P < 0.01$ and (***) $P < 0.001$ compared to standard PSS; ANOVA with Tukey *post-hoc* test [n = 12 in (c) and n = 9 in (d)]. Data are mean ± SEM.

| Table 3.5. Mean membrane potential ($V_m$) of MDA-MB-231 cells after phenytoin (100 µM) treatment and washout. | | | |
|---|---|---|---|
| **Measurement interval** | **$V_m$ in standard PSS (mV)** | **$V_m$ in 100 µM phenytoin (mV)** | **$V_m$ in washout (mV)** |
| Last 5 s | -12.6 ± 1.5 | -15.7 ± 1.7 *** | -14.6 ± 1.9 |
| Last 15 s | -12.7 ± 1.5 | -15.9 ± 1.9 ** | -14.8 ± 1.9 |
| Last 30 s | -12.9 ± 1.5 | -15.6 ± 1.9 ** | -14.9 ± 1.9 |
| Last 60 s | -13.0 ± 1.5 | -15.4 ± 1.9 * | -15.2 ± 2.0 |
| Liquid junction potentials (3 mV) were compensated offline. PSS: physiological saline solution. (*) $P < 0.05$; (**) $P < 0.01$; (***) $P < 0.001$ compared with $V_m$ in standard PSS; ANOVA with Tukey *post-hoc* test (n = 12). Data are mean ± SEM. | | | |

| Table 3.6. Mean membrane potential ($V_m$) of MDA-MB-231 cells after NaOH (75 µM) treatment and washout. | | | |
|---|---|---|---|
| **Measurement interval** | **$V_m$ in standard PSS (mV)** | **$V_m$ in 75 µM NaOH (mV)** | **$V_m$ in washout (mV)** |
| Last 5 s | -10.8 ± 1.5 | -11.0 ± 1.3 (n.s.) | -10.1 ± 2.0 |
| Last 15 s | -10.9 ± 1.3 | -11.1 ± 1.3 (n.s.) | -10.2 ± 2.1 |
| Last 30 s | -10.9 ± 1.3 | -11.1 ± 1.2 (n.s.) | -10.3 ± 2.1 |
| Last 60 s | -10.9 ± 1.3 | -11.1 ± 1.2 (n.s.) | -10.3 ± 2.1 |
| Liquid junction potentials (3 mV) were compensated offline. PSS: physiological saline solution. n.s. not significant compared with $V_m$ in standard PSS; ANOVA with Tukey *post-hoc* test (n = 9). Data are mean ± SEM. | | | |

### 3.2.5 Veratridine increases the persistent $I_{Na}$ and depolarises the $V_m$ in MDA-MB-231 cells

Blocking VGSCs using TTX and phenytoin hyperpolarised the $V_m$. To further investigate the role of VGSC in the $V_m$ regulation in MDA-MB-231 cells, the present study hypothesised that activating VGSCs would cause a $V_m$ depolarisation. Veratridine is an alkaloid that binds to the toxin binding site 2, and it increases persistent $I_{Na}$ by increasing the channel opening probability but decreases transient $I_{Na}$ by decreasing single channel conductance (Ulbricht, 1998; Wang & Wang, 2003). In the following experiment, veratridine at 100 µM was adopted as a VGSC opener (House *et al.*, 2015).

Firstly, the effects of veratridine on $I_{Na}$ were tested using the whole-cell patch clamp technique in voltage-clamp mode using the standard current-voltage protocol (Section 2.4.7). $I_{Na}$ was firstly recorded in standard PSS before cells were perfused with 100 µM veratridine for 2 min, followed by a 2 min washout. Veratridine increased persistent $I_{Na}$ of MDA-MB-231 cells, and the persistent $I_{Na}$ increased further even after washout (Figure 3.9a and b). The current-voltage relationships of both transient and persistent $I_{Na}$ are shown in (Figure 3.9c and d), where the $I_{Na}$ was normalised to whole-cell capacitance: veratridine and the following washout did not significantly alter the transient current-voltage relationship (Figure 3.9c; ANOVA with Tukey *post hoc* test; n = 6). The peak transient $I_{Na}$ was slightly reduced, albeit not significantly, from -12.1 ± 2.2 pA/pF to -9.3 ± 1.2 pA/pF after veratridine treatment (Figure 3.9d; P = 0.10 compared to standard PSS; ANOVA with Tukey *post hoc* test; n = 6), and was -9.8 ± 1.5 pA/pF after washout.

The persistent $I_{Na}$ density, measured 45–50 ms after depolarisation, increased upon depolarisation to voltages in the range of -25 mV to -10 mV (Figure 3.9e; P < 0.05; ANOVA with Tukey *post hoc* test; n = 6), and the persistent $I_{Na}$ density increased
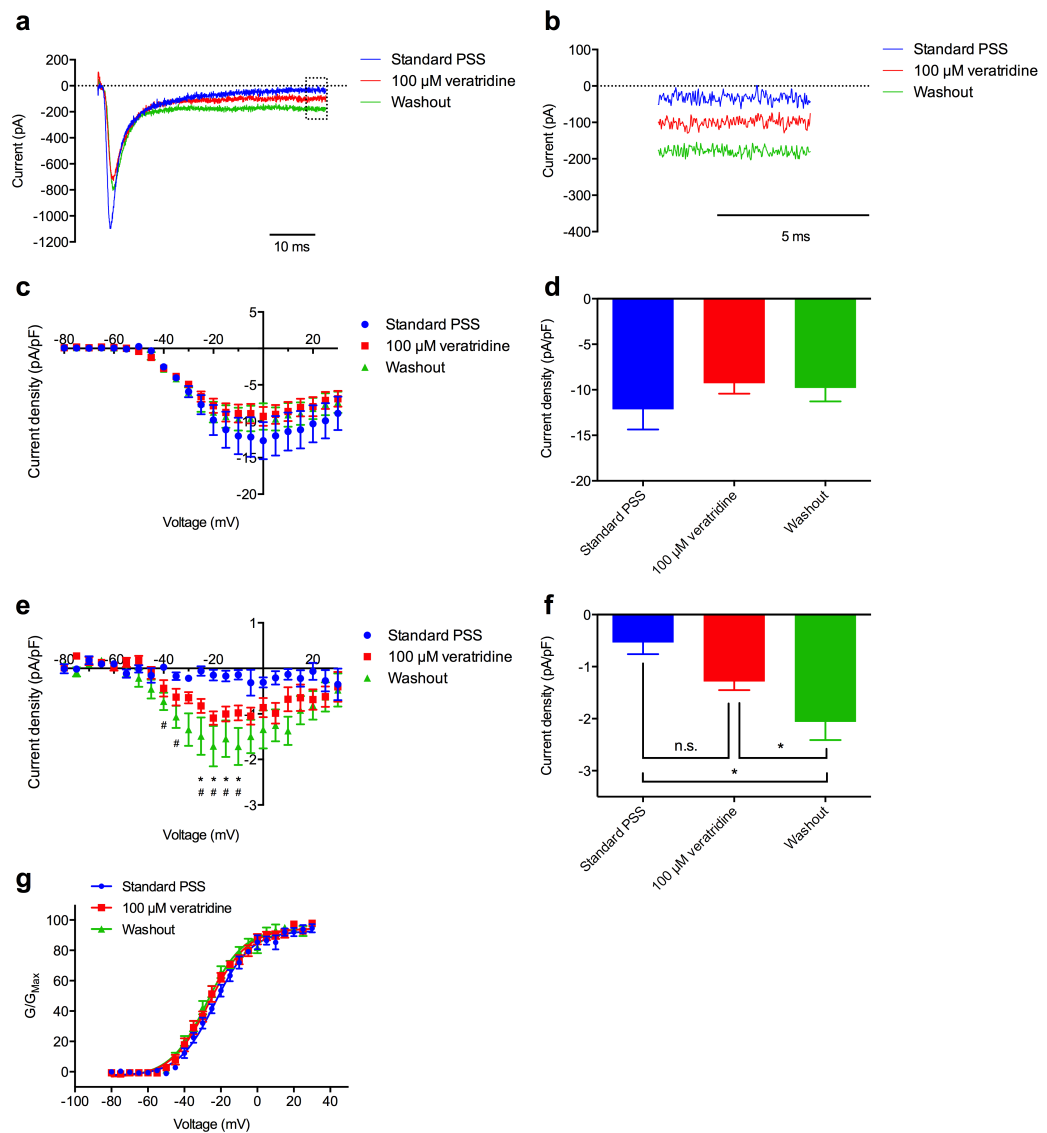
Figure 3.9. Veratridine increases the persistent Na$^+$ current (I$_{Na}$) in MDA-MB-231 cells.

Representative transient (**a**) and persistent (**b**) I$_{Na}$ in an MDA-MB-231 cell in standard PSS, followed by 2 min veratridine (100 µM) treatment and 2 min washout. Cell was depolarised to 0 mV for 60 ms from a 250 ms pre-pulse at -120 mV. Dotted box in (a) represents the persistent I$_{Na}$ that is shown in (b). Persistent I$_{Na}$ between 45–50 ms after depolarisation was adopted in data analyses. (**c**) The current-voltage relationship of transient I$_{Na}$ and (**d**) the peak transient I$_{Na}$ density after veratridine treatment and washout (n = 6). (**e**) The current-voltage relationship of persistent I$_{Na}$. (*) P < 0.05 comparing standard PSS and veratridine; (#) P < 0.05 comparing standard PSS and washout. (**f**) The mean persistent I$_{Na}$ density after veratridine treatment and washout. (*) P < 0.05; n.s. not significant; ANOVA with Tukey *post hoc* test (n = 6). (**g**) The normalised conductance of I$_{Na}$ in all experimental conditions (n = 6), fitted with Boltzmann equations. Cells were depolarised to voltages between -80 mV to +30 mV in 5 mV increments following a 250 ms pre-pulse at -120 mV. Data are mean ± SEM.

further after washout (Figure 3.9e; P < 0.05; ANOVA with Tukey *post hoc* test; n = 6). The maximal persistent $I_{Na}$ was increased from -0.5 ± 0.2 pA/pF in standard PSS to -1.3 ± 0.2 pA/pF in veratridine (Figure 3.9f; P = 0.06; ANOVA with Tukey *post hoc* test; n = 6). Following washout the maximal persistent $I_{Na}$ increased further to -2.1 ± 0.4 pA/pF, which was significantly different compared with standard PSS (Figure 3.9f; P < 0.05; ANOVA with Tukey *post hoc* test; n = 6) as well as the veratridine treatment (Figure 3.9f; P < 0.05; ANOVA with Tukey *post hoc* test; n = 6).

Veratridine at 100 µM did not change the voltage-dependence of activation (Figure 3.9g). $I_{Na}$ characteristics including $V_{1/2}$, k, activation voltage ($V_a$), voltage at current peak ($V_p$) and time to peak ($T_p$) were constant after veratridine treatment and following washout (Table 3.7). Because (1) veratridine increased the persistent $I_{Na}$ in a non-reversible manner, and (2) 4 min after veratridine treatment (including washout) the persistent $I_{Na}$ was significantly increased at voltages between -25 mV and -10 mV, the effect of veratridine on MDA-MB-231 cell $V_m$ was assessed by measuring the steady-state $V_m$ after incubating cells with 100 µM veratridine for 6 min, instead of performing a time-course $V_m$ measurement as done in previous sections. Veratridine depolarised the $V_m$ from -16.4 ± 1.4 mV to -12.6 ± 1.4 mV (Figure 3.10; P < 0.05; t-test; n = 14 in each condition). Together with the data presented in Section 3.2.3 and Section 3.2.4, modulation of VGSCs by using pharmacological agents has revealed a functional role for VGSCs in regulating the $V_m$ of MDA-MB-231 cells.

| Table 3.7. Characteristics of Na$^+$ current after veratridine (100 µM) treatment and washout. | | | | |
|---|---|---|---|---|
| **Parameters and conditions** | **Standard PSS** | **Veratridine (100 µM)** | **Washout** | **P** |
| $V_{1/2}$ (mV) | -23.0 ± 1.8 | -26.6 ± 1.8 | -27.89 ± 1.5 | 0.07 |
| k (mV) | 10.1 ± 0.8 | 10.1 ± 0.5 | 10.2 ± 0.5 | 0.98 |
| $V_a$ (mV) | -39.2 ± 0.8 | -42.5 ± 2.1 | -42.5 ± 1.1 | 0.23 |
| $V_p$ (mV) | -1.7 ± 1.1 | -1.7 ± 1.1 | -5.0 ± 2.2 | 0.23 |
| $T_p$ (ms) | 2.7 ± 0.5 | 2.1 ± 0.6 | 2.1 ± 0.4 | 0.40 |
| $V_{1/2}$: the voltage at which half-maximal conductance or availability occurs; k: slope factor; $V_a$: activation voltage; $V_p$: voltage at current peak; $T_p$: time to peak. ANOVA with Tukey *post hoc* test (n = 6). Data are mean ± SEM. | | | | |
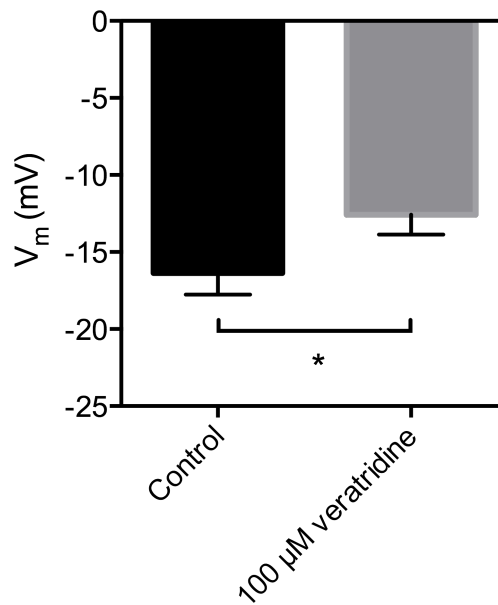
Figure 3.10. Veratridine depolarises the $V_m$ of MDA-MB-231 cells.

Cells were pre-treated with DMSO (2 % v/v) or 100 µM veratridine in the standard PSS for 6 min before their steady-state $V_m$ was recorded. (*) $P < 0.05$; t-test (n = 14 in each condition). Data are mean ± SEM.

### 3.2.6 Suppressing Na$_v$1.5 expression using shRNA hyperpolarises the V$_m$ of MDA-MB-231 cells

In addition to inhibiting VGSC activity using pharmacological agents, Na$_v$1.5, the main VGSC isoform in MDA-MB-231 cells (Fraser *et al.*, 2005), was stably down-regulated by lentiviral shRNA in order to specifically examine how Na$_v$1.5 regulates cell metastatic behaviours compared to cells transduced with non-targeting control shRNA. Genetically suppressing Na$_v$1.5 expression also has advantages such as the avoidance of non-target effects associated with certain pharmacological agents, e.g. phenytoin also inhibits HERG channels at high concentration (IC$_{50}$ ≥ 300 µM) (Danielsson *et al.*, 2003). Stable knockdown with shRNA also enables the study of long-term effects of Na$_v$1.5 on cell behaviour.

I$_{Na}$ from cells that were stably transduced with two different sets of shRNA ("Na$_v$1.5-shRNA 1" and "Na$_v$1.5-shRNA 2" cells) or with non-targeting control shRNA ("shRNA control" cells) were tested in the study Figure 3.11. Both Na$_v$1.5 mRNA and protein levels were reduced in Na$_v$1.5-shRNA 1 and 2 cells (Nelson *et al.*, 2015b). Using the standard current-voltage protocol (Section 2.4.7) whole-cell I$_{Na}$ recording showed that both Na$_v$1.5-shRNA 1 (Figure 3.11a) and Na$_v$1.5-shRNA 2 (Figure 3.11b) cells had smaller I$_{Na}$ compared to shRNA control cells (Figure 3.11c), which is also displayed in the current-voltage relationship (Figure 3.11d). The peak I$_{Na}$ density of shRNA control, Na$_v$1.5-shRNA 1 and Na$_v$1.5-shRNA 2 cells was -14.9 ± 2.1 pA/pF, -0.1 ± 0.1 pA/pF and -7.9 ± 2.2 pA/pF, respectively (Figure 3.11e). Since Na$_v$1.5-shRNA 1 cells showed the greatest I$_{Na}$ reduction than cells bearing Na$_v$1.5-shRNA 2 (Figure 3.11d and e; P < 0.05; ANOVA with Tukey *post hoc* test; n = 8), the steady-state V$_m$ of Na$_v$1.5-shRNA 1 cells (hereafter referred to as Na$_v$1.5-shRNA cells) was recorded and compared with shRNA control cells (Figure 3.12). Down-regulation of Na$_v$1.5
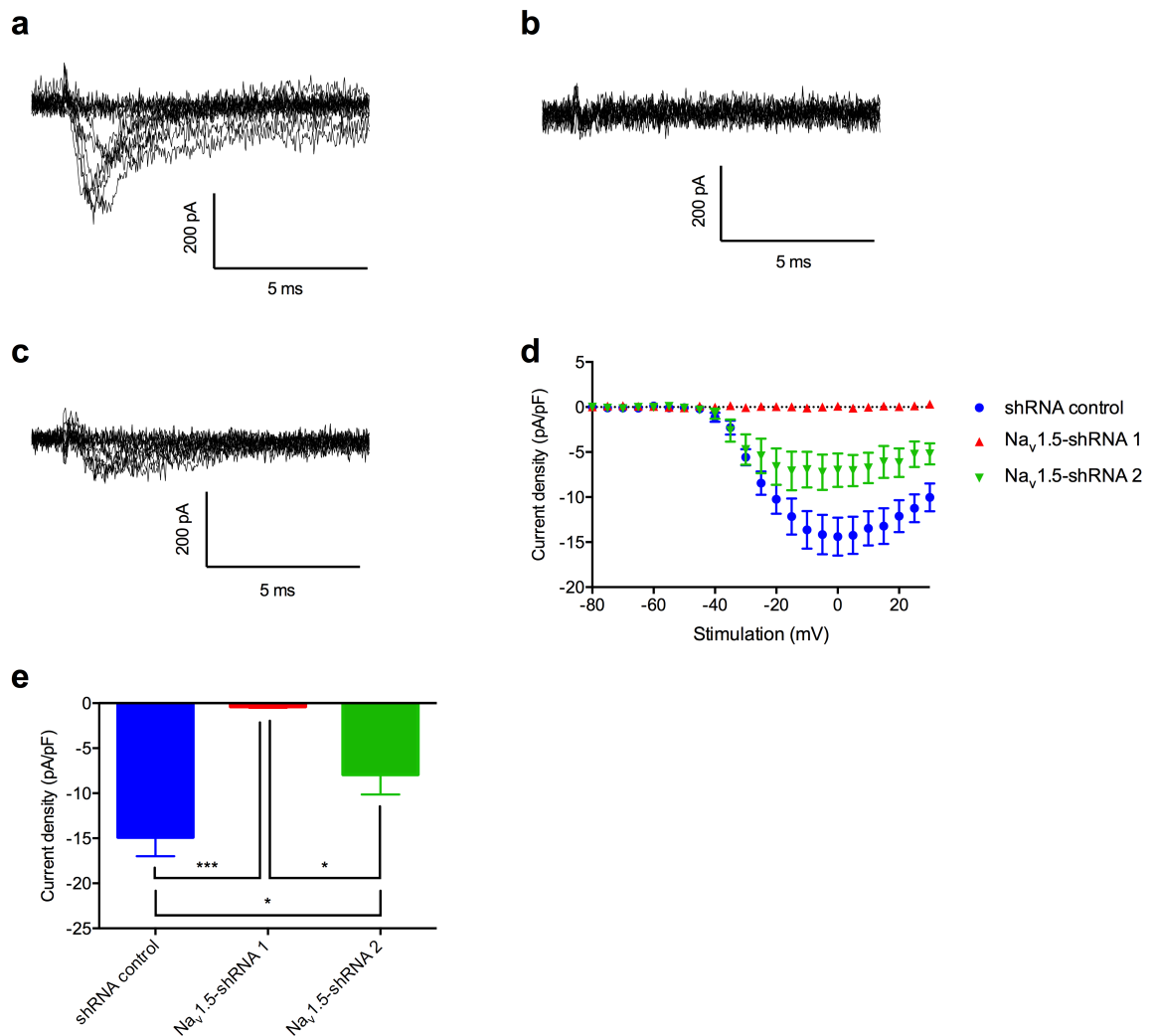
Figure 3.11. Down-regulating Na$_v$1.5 using small-hairpin RNA (shRNA) reduced the Na$^+$ current (I$_{Na}$) in MDA-MB-231 cells.

Representative I$_{Na}$ traces in (**a**) non-targeting shRNA-expressing (shRNA control) cells, (**b**) Na$_v$1.5-shRNA 1 cells and (**c**) Na$_v$1.5-shRNA 2 cells. I$_{Na}$ was elicited after depolarisation to voltages ranging from -80 mV to +30 mV in 5 mV increments following a 250 ms pre-pulse at -120 mV. Every other I$_{Na}$ trace is shown for clarity. (**d**) Current-voltage relationship of the transient I$_{Na}$ recorded from shRNA control and Na$_v$1.5-shRNA 1 and 2 cells. (**e**) Peak transient I$_{Na}$ density of shRNA control and Na$_v$1.5-shRNA 1 and 2 cells. (*) P < 0.05; (***) P < 0.001; ANOVA with Tukey *post hoc* test (n = 8 in each condition). Data are mean ± SEM.
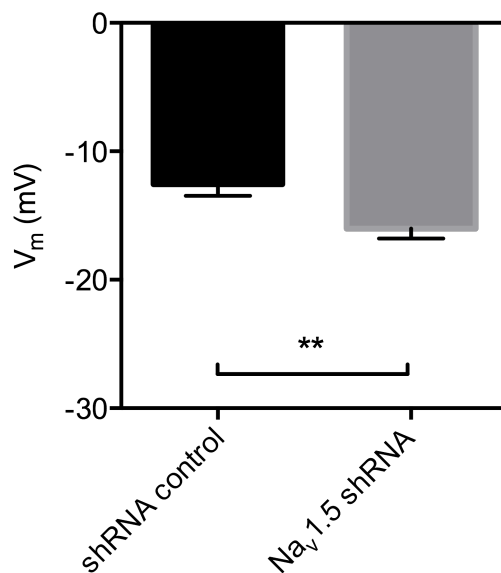
Figure 3.12. Na$_v$1.5 causes a steady-state membrane potential (V$_m$) depolarisation in MDA-MB-231 cells.

Comparison of the V$_m$ recorded in cells bearing control non-targeting shRNA (shRNA control cells) and in cells where Na$_v$1.5 expression was down-regulated with lentiviral shRNA (Na$_v$1.5-shRNA cells). (**): $P < 0.01$; t-test (n = 16 in each condition). Data are mean ± SEM.

significantly hyperpolarised the $V_m$ from -12.6 ± 0.9 mV to -16.0 ± 0.8 mV (Figure 3.12; $P < 0.01$; t-test; n = 16 in each condition). Taken together, data presented in this Chapter so far suggest that VGSCs depolarise the steady-state $V_m$ of MDA-MB-231 cells by 3.2–4.3 mV.

### 3.2.7 Voltage-dependent $I_{Na}$ recorded in ERα⁻ MCF-7 cells

pII is an MCF-7 derivative cell line where ERα was stably knocked down by using shRNA (Luqmani *et al.*, 2009). To test the hypothesis that down-regulation of ER in BCa cells may increase malignancy by inducing VGSC expression, the membrane currents of pII and parental control MCF-7 cells was also investigated in the present study.

The standard intracellular solution (Cs⁺-free) was used while recording the whole-cell current. In the control MCF-7 cells, both inward and outward current were absent in eight cells recorded after depolarisation from -120 mV (250 ms) to voltages ranging between -60 mV and +80 mV for 60 ms (Figure 3.13a). Interestingly, however, two out of five pII cells recorded showed fast voltage-dependent inward current together with voltage-dependent persistent outward current (Figure 3.13b). Additionally, two cells exhibited only persistent outward current. The current-voltage relationships of the inward and outward current are shown in Figure 3.13c (n = 2) and Figure 3.13d (n = 4), respectively. Alongside with these findings, our collaborators confirmed the expression of $Na_v1.5$ mRNA and protein in pII cells (Mohammed *et al.*, 2015). Therefore, it is likely that the fast inward current is $I_{Na}$ carried by $Na_v1.5$. In summary, a voltage-dependent inward $I_{Na}$, was seen in a proportion of ERα-knockdown pII cells but not in parental MCF-7 cells. Further experiments should examine the TTX sensitivity of the inward current and the type of persistent outward current.
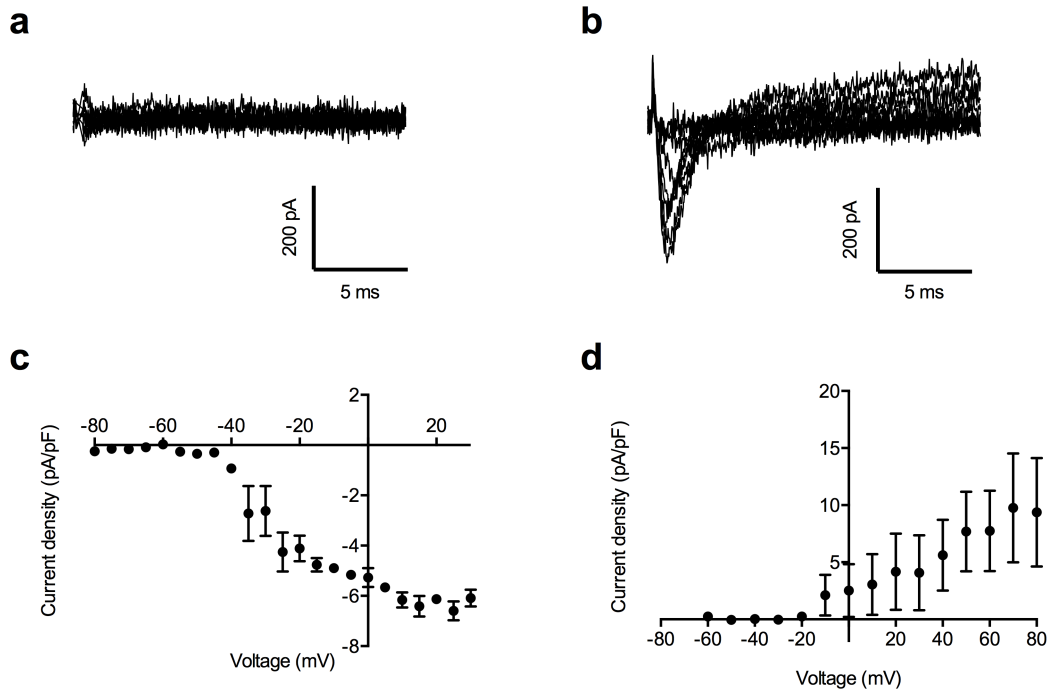
Figure 3.13. Membrane current recorded from pII and parental MCF-7 cells.

Representative whole-cell current recorded from (**a**) control MCF-7 cells (n = 8) and (**b**) pII cells where ERα expression was down-regulated using shRNA. The current-voltage relationship of (**c**) inward (n = 2) and (**d**) outward (n = 4) current recorded from pII cells. Cells were depolarised to voltages between -60 mV and +80 mV in 10 mV increments following a 250 ms pre-pulse at -120 mV. Every other $I_{Na}$ trace is shown for clarity. In (d), the mean current between 45 ms and 50 ms after the test-pulse was analysed. Data are mean ± SEM.

## 3.3 Discussion

In the standard PSS, the $V_m$ of MDA-MB-231 cells is approximately -10 mV. The value significantly deviates from the equilibrium potential of $K^+$ and $Cl^-$ (-82 mV and 0.06 mV, respectively, under the experimental condition in this study), while the $Na^+$ equilibrium potential is +86.3 mV. $Na^+$ conductance therefore may act as an important determinant of the depolarised $V_m$ of MDA-MB-231 cells. Indeed, data in this Chapter show that depletion of extracellular $Na^+$ hyperpolarises the $V_m$ of MDA-MB-231 cells by 10–14 mV. Using pharmacological agents or shRNA, data in this Chapter also show that VGSCs cause a steady-state $V_m$ depolarisation of 3.2–4.3 mV in MDA-MB-231 cells.

Specifically suppressing $Na_v1.5$ expression using shRNA abolishes the $I_{Na}$ in MDA-MB-231 cells, supporting the previous study showing that $Na_v1.5$ is the predominant VGSC isoform in MDA-MB-231 cells (Brackenbury *et al.*, 2007). Considering that TTX (30 µM), phenytoin (100 µM) and $Na_v1.5$-shRNA hyperpolarised the $V_m$ to a similar extent, TTX- and phenytoin-induced $V_m$ hyperpolarisation is likely caused by blockade of $Na_v1.5$ in MDA-MB-231 cells. In addition, $Na_v1.5$-dependent $V_m$ depolarisation may be independent of other $V_m$ regulation pathway, since the hyperpolarised $V_m$ in $Na_v1.5$-shRNA cells has not been compensated for over time in culture.

In H460 NSCLC cells, blocking $Na_v1.7$ with TTX (0.5 µM) hyperpolarises the $V_m$ by 10 mV (Campbell *et al.*, 2013), which is a greater effect than blocking $Na_v1.5$ in MDA-MB-231 cells. One possible explanation is that H460 cells have a more hyperpolarised $V_m$ (-27 mV), and at this voltage, the window $I_{Na}$ is stronger in H460 cells compared with that in MDA-MB-231 cells (Campbell *et al.*, 2013). In addition, the present study has recorded the continuous $V_m$ from individual cells that were perfused with phenytoin or TTX, which can reveal the immediate effect of the drugs on $V_m$ and diminish cell-to-cell differences that would occur from recording independent cells from

two conditions, as in (Campbell *et al.*, 2013). Another study reported that the $V_m$ of other VGSC-expressing NSCLC cells does not significantly differ from those where VGSCs are absent (Roger *et al.*, 2007). Comparisons between a number of cell lines with distinct $I_{Na}$ and $I_K$ current profiles, as in (Roger *et al.*, 2007), cannot determine whether or not VGSCs regulate cell $V_m$. On the other hand, continuous pharmacological experiments on single cells as in the present study, clearly shows that VGSCs regulate the $V_m$ in MDA-MB-231 cells.

The mean $V_m$ did not fully recover after eliminating TTX or phenytoin from the recording chamber (Sections 3.2.3 and 3.2.4). Since phenytoin binds to the toxin binding site 2, which is at the intracellular side (Lipkind & Fozzard, 2010), it may require much longer time in the washout step before the drug dissociates from the VGSC complex. Additionally, when MDA-MB-231 cells are at their typical $V_m$ (~-10 mV), VGSCs are mostly in the inactivated state that has higher affinity for phenytoin (Ragsdale *et al.*, 1991; Kuo & Bean, 1994), making drug dissociation by washout more difficult. However, TTX can be washed out relatively easily since it binds to toxin binding site 1 at the extracellular loop (Noda *et al.*, 1989; Terlau *et al.*, 1991), confirmed by the voltage-clamp study (Figure 3.4). Considering that TTX does not show state-dependent binding (Narahashi *et al.*, 1964), one possible explanation is that other ion channels and transporters are activated when the $V_m$ is hyperpolarised by blocking VGSCs, and therefore it may take longer for cells to recover their original $V_m$ after washout. Indeed, the $V_m$ slowly but constantly depolarises during washout. Further work is required to test these possibilities.

Veratridine is a VGSC agonist that has been shown to increase persistent $I_{Na}$ whilst decreasing transient $I_{Na}$ (Ulbricht, 1969). In the present study, voltage-clamp experiments using veratridine (100 µM) showed a similar result (Figure 3.9). Moreover, the persistent $I_{Na}$ increased further after veratridine washout. Possible reasons are: (1) veratridine is a membrane-soluble protein which tightly binds to the neurotoxin-binding

site 2 (Ulbricht, 1998; Cestele & Catterall, 2000), and (2) veratridine binds preferentially to open channels (Barnes & Hille, 1988; Ulbricht, 1998). Consequently, the effect of veratridine became stronger because of repeated channel openings during the recording protocols. The persistent $I_{Na}$ after depolarisation to voltages from -25 mV to -10 mV significantly increased following veratridine application (Figure 3.9), and this agrees well with the findings that veratridine depolarised the $V_m$ by 3.8 mV (Figure 3.10), because the $V_m$ of MDA-MB-231 cells lies within this voltage range. A similar result has been reported in H460 cells, where the $V_m$ depolarised by 4 mV after treatment with 50 μM veratridine (Campbell *et al.*, 2013).

Several questions are raised by these results. The VGSC-dependent $V_m$ regulation only contributes to 30–40 % of the extracellular $Na^+$-dependent $V_m$ depolarisation in MDA-MB-231 cells, suggesting that there are other $Na^+$-permeable pathways at the cells plasma membrane that can depolarise the $V_m$, such as epithelial $Na^+$ channels (ENaC), NHE1, $Na^+$-$Ca^{2+}$ exchanger (NCX) and $Na^+$ transporters including the $Na^+$-$K^+$-$2Cl^-$ co-transporter. Further experiments should address their roles in $V_m$ regulation in MDA-MB-231 cells. Additionally, compared to MCF-7 cells, which have a $V_m$ of -40 mV (Fraser *et al.*, 2005), results in this Chapter show that the depolarised $V_m$ of MDA-MB-231 cells is only partly due to $Na^+$ influx. Therefore, the absence of $V_m$-hyperpolarising ion channels/transporters and/or the presence of other $V_m$-depolarising ion channels/transporters may also contribute to the depolarised $V_m$ of MDA-MB-231 cells.

In pII cells, a MCF-7 cell derivative where ERα is stably knocked down, a voltage-dependent fast inward current was recorded, which was absent in control MCF-7 cells. Further study suggested that the current is probably $I_{Na}$ carried by $Na_v1.5$. TTX, phenytoin and siRNA targeting $Na_v1.5$ significantly reduced EGF-induced invasion in pII cells (Mohammed *et al.,* 2015). Although microarray data show that $Na_v1.5$ mRNA level does not correlate with ER status in BCa patient samples (Yang *et al.*, 2012), ER

down-regulation may still increase functional channel expression and/or channel trafficking to the plasma membrane of BCa cells. Further study should focus on determining the electrophysiological characteristics of the $I_{Na}$-like current recorded in pII cells and investigate how ER down-regulation induced the functional current.

## 3.4 Conclusion

This Chapter demonstrated that replacement of the extracellular NaCl with ChoCl and NMDG hyperpolarised the $V_m$ of MDA-MB-231 cells by approximately 10 and 14 mV, respectively. In addition, inhibiting VGSC activity using TTX, phenytoin and $Na_v1.5$-targeting shRNA showed that VGSCs depolarise the steady-state $V_m$ of MDA-MB-231 cells by 3.2–4.3 mV. On the other hand, increasing the persistent $I_{Na}$ using veratridine depolarised the $V_m$ by 3.8 mV. Thus, $Na^+$ conductance across the plasma membrane regulates the $V_m$, partly contributed by VGSCs (Figure 3.14). Whether the depolarised $V_m$ has functional roles in promoting MDA-MB-231 cells metastatic behaviours will be investigated in the following Chapter.
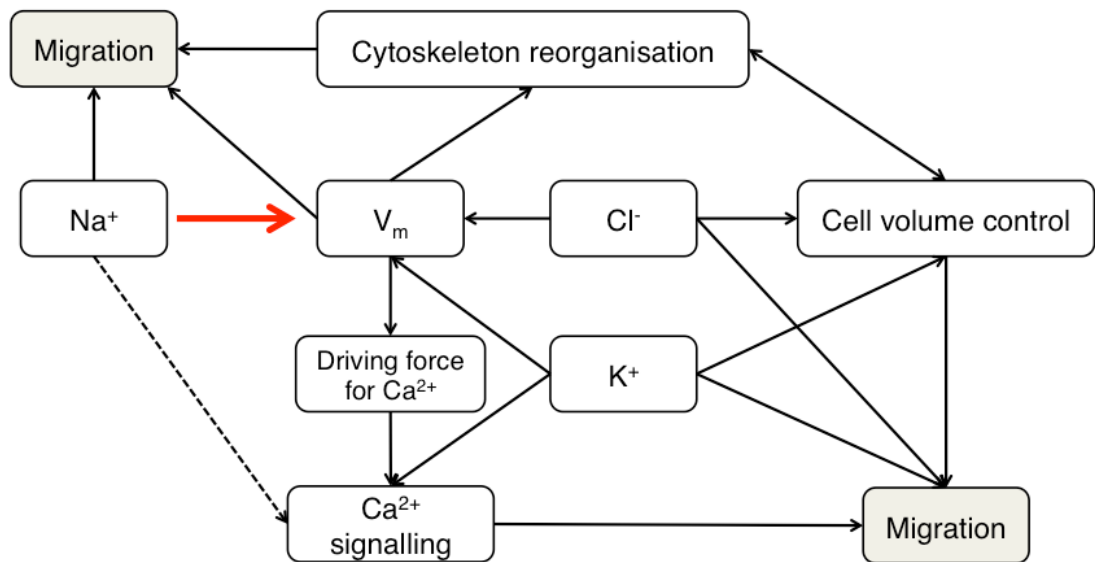
Figure 3.14. Na$^+$ conductance contributes to membrane potential (V$_m$) regulation in cancer cells.

An update to Figure 1.6 with the findings in this Chapter showing the involvement of Na$^+$ in V$_m$ regulation (red line). The relationship between Na$^+$ and Ca$^{2+}$ signalling has not been studied (dashed line). Figure is adapted from (Yang & Brackenbury, 2013).

# Chapter 4: Functional role of the depolarised $V_m$ caused by VGSCs in MDA-MB-231 cells *in vitro*

## 4.1 Introduction

Over the past few decades, functional VGSCs have been identified in an increasing number of cancer cell lines where they promote metastatic cell behaviours including cell migration and invasion (Brackenbury, 2012; Roger *et al.*, 2015). For BCa, recent *in vivo* experiments showed that inhibiting VGSC α subunits with phenytoin decreases BCa cell growth and metastasis (Nelson *et al.*, 2015a), and that ranolazine-treated mice had reduced BCa cell colonisation to the lungs (Driffort *et al.*, 2014). However, the detailed mechanism(s) by which VGSCs increase cancer cell metastatic behaviours is not fully understood. It is proposed that in MDA-MB-231 cells, $Na_v1.5$ increases $H^+$ efflux through NHE1, resulting in a lower extracellular pH that promotes proteolytic activity of cysteine cathepsin B and S, thus increasing cell invasion (Gillet *et al.*, 2009; Brisson *et al.*, 2011). A following study demonstrated that inhibiting $Na_v1.5$ with TTX decreased src kinase activity and phosphorylation of the actin nucleation promoting factor cortactin (Brisson *et al.*, 2013). In MDA-MB-231 cells where $Na_v1.5$ is down-regulated by using shRNA, the protein level of the metastasis-promoting molecule CD44 is also reduced (Nelson *et al.*, 2015b). Furthermore, in SW620 human colon cancer cells, VGSC activity leads to persistent MAPK activation in a Rap1-dependent manner, with the downstream effect of activating expression of invasion-related genes including CD44 (House *et al.*, 2015). Finally, β1–β1 homophilic adhesion increases MDA-MB-231 cell process outgrowth in a fyn kinase-dependent pathway, where $Na^+$ influx is also required (Nelson *et al.*, 2014). However, other undiscovered mechanisms may also underlie VGSC-dependent metastatic cell behaviours. For

example, in a wound healing assay, rat cortical astrocytes show elevated $[Ca^{2+}]_i$ upon wound scratching, which is attenuated by blocking NCX or VGSCs using KB-R7943 or TTX, respectively (Pappalardo *et al.*, 2014b). The inhibitory effects on $[Ca^{2+}]_i$ caused by these two compounds are similar, and therefore it is proposed that $Na^+$ influx through VGSCs regulates $[Ca^{2+}]_i$ through NCX (Pappalardo *et al.*, 2014b). $Na^+$ influx through VGSCs increases $[Ca^{2+}]_i$ in THP-1 macrophages via NCX on the mitochondrial membrane (Carrithers *et al.*, 2009). In human umbilical vein endothelial cells, $Na^+$ carried by VGSCs increases $Ca^{2+}$ influx through NCX, which is necessary in vascular endothelial growth factor (VEGF)-induced ERK1/2 activation (Andrikopoulos *et al.*, 2011a; Andrikopoulos *et al.*, 2011b).

Cancer cells possess a depolarised $V_m$ compared to their counterparts from normal tissues (Binggeli & Weinstein, 1986; Yang & Brackenbury, 2013). A depolarised $V_m$ is not merely an epi-phenomenon that is the outcome of the collective activity of many ion channels and transporters at the plasma membrane: apart from its involvement in promoting cell cycle progression and maintaining stem cells in an undifferentiated state (Sundelacruz *et al.*, 2009; Yang & Brackenbury, 2013), depolarised $V_m$ is also able to promote cytoskeleton reorganisation (Chifflet *et al.*, 2003; Chifflet *et al.*, 2004). In a wound healing assay using bovine corneal endothelial cells, $V_m$ depolarisation occurs in cells at the edge of the wound and extends inwards, and the depolarised $V_m$ causes actin network reorganisation during wound healing (Chifflet *et al.*, 2005). The $V_m$ depolarisation is caused by increased $Na^+$ permeability via ENaC, but the resulting cytoskeleton reorganisation is $Na^+$-independent (Chifflet *et al.*, 2005).

Cell migration comprises several key steps, including extension of the lamellipodium, formation of new adhesion sites at the front, cell body contraction and detachment of adhesions at the rear (Raftopoulou & Hall, 2004). Members of the Rho small GTPase family, including Rho, Rac and Cdc42, have pivotal roles in cell

migration. These GTPases switch between a GTP-bound active form and a GDP-bound inactive form. GEFs activate small GTPases by increasing the release of GDP and binding of GTP. Upon activation, the most well established function of these small GTPases is their contribution to cell migration and morphogenesis by regulating the actin and microtubule cytoskeleton (Hall, 1998). However, Rho, Rac and Cdc42 have distinct effects on the actin cytoskeleton: in 3T3 fibroblasts, activation of Rho results in the formation of stress fibres at the rear of the cell, Cdc42 causes the formation of filopodia, and Rac leads to the formation of lamellipodia (Nobes & Hall, 1995). During lamellipodia formation, Rac initiates actin polymerisation through the Arp2/3 complex mediated by the nucleation-promoting Wiskott-Aldrich syndrome protein-family verprolin-homologous proteins (WAVE) (Jaffe & Hall, 2005). The instructive role of Rac1, a member of the Rac family, during lamellipodium formation has been confirmed by an optogenetic study: activation of a photoactivatable Rac1 is sufficient to induce lamellipodium extension, cell motility and control the directionality of cell movement (Wu *et al.*, 2009). In addition to their roles in controlling the cytoskeleton, Rac GTPases are capable of activating JNKs, leading to alterations in gene expression (Coso *et al.*, 1995). Rac also participates in regulation of the mitogen-activated protein (MAP) signalling pathway: mixed lineage kinase 3 (MLK3), a MAP kinase kinase kinase, is a direct binding target of Rac (Brancho *et al.*, 2005). In COS-7 cells, a MLK3 dominant negative mutant abolished JNK activation by Rac (Teramoto *et al.*, 1996).

$V_m$ can be a functional signal in regulating small GTPases. The activation of Ras and Rap1, a small GTPase that is required in NGF-induced ERK activation (York *et al.*, 1998), caused by $V_m$ depolarisation has been reported in mouse cortical neurones (Baldassa *et al.*, 2003). In PC12 cells, the depolarised $V_m$ increases the active Ras level in a PKA-dependent manner (Obara *et al.*, 2007). More recently, a study has demonstrated that in baby hamster kidney cells, $V_m$ depolarisation enhances phosphatidylserine and nanoclustering of K-Ras, a Ras mutant and one of the most

141

frequently activated oncogenes (Kranenburg, 2005), and K-Ras-dependent MAPK signalling (Zhou *et al.*, 2015). Therefore, $V_m$ may regulate metastatic cell behaviours through small GTPases.

In humans, $BK_{Ca}$ channels are encoded by *KCNMA1* and may associate with auxiliary β subunits (β1–β4) (Salkoff *et al.*, 2006). The $BK_{Ca}$ channel protein has seven transmembrane domains, an extracellular N-terminus, and an intracellular C-terminus (Meera *et al.*, 1997; Yuan *et al.*, 2010), where three $Ca^{2+}$ binding sites are located (Schreiber & Salkoff, 1997; Xia *et al.*, 2002). The channel monomer comprises one voltage-sensing module and one $Ca^{2+}$-sensing module that are both important in channel opening (Barrett *et al.*, 1982; Latorre & Brauchi, 2006). However, evidence suggests that the activation of $BK_{Ca}$ channels is primarily caused by $V_m$ depolarisation whereas $Ca^{2+}$ functions as an amplifier (Meera *et al.*, 1996; Stefani *et al.*, 1997). In *Xenopus* oocytes, when $[Ca^{2+}]_i$ is ≤ 100 nM, $BK_{Ca}$ channels become purely voltage-gated and independent of $Ca^{2+}$, with an activation $V_{1/2} \geq 220$ mV (Meera *et al.*, 1996). In a physiological range of $V_m$, $BK_{Ca}$ channels function in $Ca^{2+}$-dependent mode, where $V_{1/2}$ values linearly increase with cytosolic free $[Ca^{2+}]$ (Cui *et al.*, 1997).

VGSCs depolarise the $V_m$ of MDA-MB-231 cells by approximately 4 mV (Section 3.2.6). Considering that MDA-MB-231 cells have a $V_m$ at ~-10 mV (Section 3.2.1), inhibition of VGSCs accounts for a ~40 % increase in the transmembrane voltage. Given that VGSCs regulate $V_m$ in MDA-MB-231 cells and that $V_m$ is functionally instructive in regulating metastatic cell behaviours in other cell models, it is possible that VGSCs may regulate metastatic cell behaviours via modulation of the $V_m$. To specifically study the role of $V_m$ without altering the $Na^+$ conductance through VGSCs, it is possible to modulate the $V_m$ of MDA-MB-231 cells through activating endogenously expressed $BK_{Ca}$ channels (Khaitan *et al.*, 2009; Ma *et al.*, 2012).

### 4.1.1 Hypothesis and aims

The hypothesis of the Chapter was that depolarised $V_m$ is an instructive signal in promoting MDA-MB-231 cell metastatic behaviours including proliferation, migration and invasion. The specific aims were:

(1) To investigate whether or not $V_m$ can alter $[Ca^{2+}]_i$ in MDA-MB-231 cells.

(2) To hyperpolarise the $V_m$ to a similar extent to 30 μM TTX by activating $BK_{Ca}$ channels.

(3) To study the effect of $V_m$ hyperpolarisation on MDA-MB-231 cell migration and invasion.

(4) To investigate the active Rac1 distribution in MDA-MB-231 cell lamellipodia after $V_m$ hyperpolarisation.


## 4.2 Results

### 4.2.1 Monitoring $[Ca^{2+}]_i$ in MDA-MB-231 cells using Fura-2

Using MDA-MB-231 cells, Fura-2 was chosen as the intracellular $Ca^{2+}$ fluorescent indicator for the following reasons: firstly, Fura-2 has the lowest dissociation constant ($K_d$) among all the Fura-2/Indo-1 derivatives at 0.14 μM, which is close to the $[Ca^{2+}]_i$ of MDA-MB-231 cells reported previously [97 ± 2 nM in (Winnicka *et al.*, 2008), and 142 ± 39 nM in (Sareen *et al.*, 2007)]. Since the sensitivity of a $Ca^{2+}$ fluorescent indicator is most reliable in a $[Ca^{2+}]_i$ range below or close to the $K_d$ (Takahashi *et al.*, 1999), Fura-2 should be the most suitable intracellular $Ca^{2+}$ indicator to use in MDA-MB-231 cells. Secondly, Fura-2 is a ratiometric fluorescent indicator that allows for better quantitative measurement of $[Ca^{2+}]_i$ measurement compared to single wavelength indicators (Bootman *et al.*, 2013).

To begin with, a control experiment using standard PSS was carried out in order to monitor the $[Ca^{2+}]_i$ of MDA-MB-231 cells, reported as 340/380 ratio (Section 2.7).

Fura-2 labelled MDA-MB-231 cells were observed under a Nikon Eclipse TE200 epi-fluorescence microscope (Section 2.9) and perfused with standard PSS at room temperature for 14 min. Cells were excited alternately at 340 nm and 380 nm, and fluorescence emission at 512 nm was collected using a RoleraXR Fast 1394 CCD camera (Section 2.9). Over the standard PSS treatment period, the majority of the cells did not show obvious $[Ca^{2+}]_i$ oscillations (Figure 4.1a and b; n = 55 from one of three repeats), whereas some cells (n = 5 out of 55) showed a slow increase and subsequent decrease in $[Ca^{2+}]_i$ ("$Ca^{2+}$ spike"; Figure 4.1c, arrow head). At the end of the experiment, ionomycin (10 µM), a positive control (Liu & Hermann, 1978), increased the $[Ca^{2+}]_i$ in all the cells. The 340/380 ratios of the individual cells were averaged in Figure 4.1e and f (n = 55).

## 4.2.2 Extracellular $Na^+$ depletion does not significantly alter $[Ca^{2+}]_i$ in MDA-MB-231 cells

Replacing extracellular $Na^+$ with ChoCl caused a $V_m$ hyperpolarisation of 10 mV (Section 3.2.1). This hyperpolarisation might increase the driving force of $Ca^{2+}$ entry via $Ca^{2+}$-permeable channels (Prevarskaya *et al.*, 2014), and hence increase the $[Ca^{2+}]_i$ in MDA-MB-231 cells. To test this, Fura-2 labelled cells were perfused with ChoCl solution for 6 min following 2 min in standard PSS. ChoCl did not change the $[Ca^{2+}]_i$ in MDA-MB-231 cells (data from one of three technical repeats are shown in Figure 4.2a–d; n = 70), nor did the following washout (Figure 4.2a–d). The mean 340/380 ratios of cells were 1.0 ± 0.1, 1.0 ± 0.1, and 1.0 ± 0.1 over the last 30 s of standard PSS, ChoCl and washout, respectively, showing no statistical difference (Figure 4.2e; P = 0.23; ANOVA with Tukey *post hoc* test; n = 3). Therefore, $V_m$ hyperpolarisation by removal of extracellular $Na^+$ does not cause a significant change in the $[Ca^{2+}]_i$ in MDA-MB-231
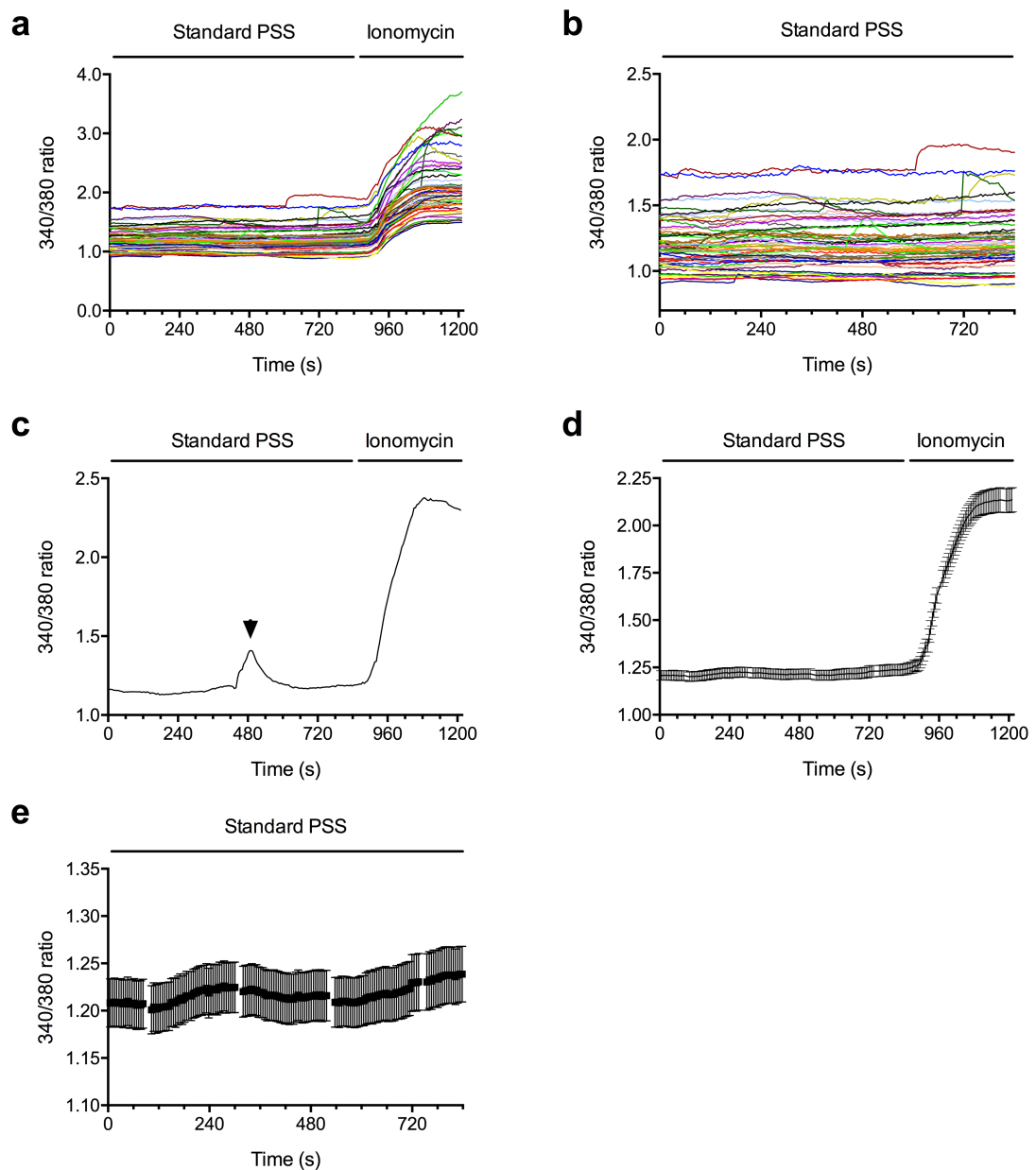
Figure 4.1. Intracellular $Ca^{2+}$ concentration ($[Ca^{2+}]_i$) of MDA-MB-231 cells in standard physiological saline solution (PSS).

(**a**) The $[Ca^{2+}]_i$ of individual cells, presented as the ratio of fluorescence signals subsequently collected at excitation wavelengths 340 nm and 380 nm (340/380 ratio), during standard PSS treatment for 14 min, before ionomycin (10 µM) as the positive control was applied. The 340/380 ratios of cells during standard PSS treatment are also shown in (**b**). (**c**) A representative cell exhibiting a $Ca^{2+}$ spike. (**d**) and (**e**) show the averaged trace of (a) and (b), respectively (n = 55 from one of three repeats). Data are mean ± SEM in (d) and (e).
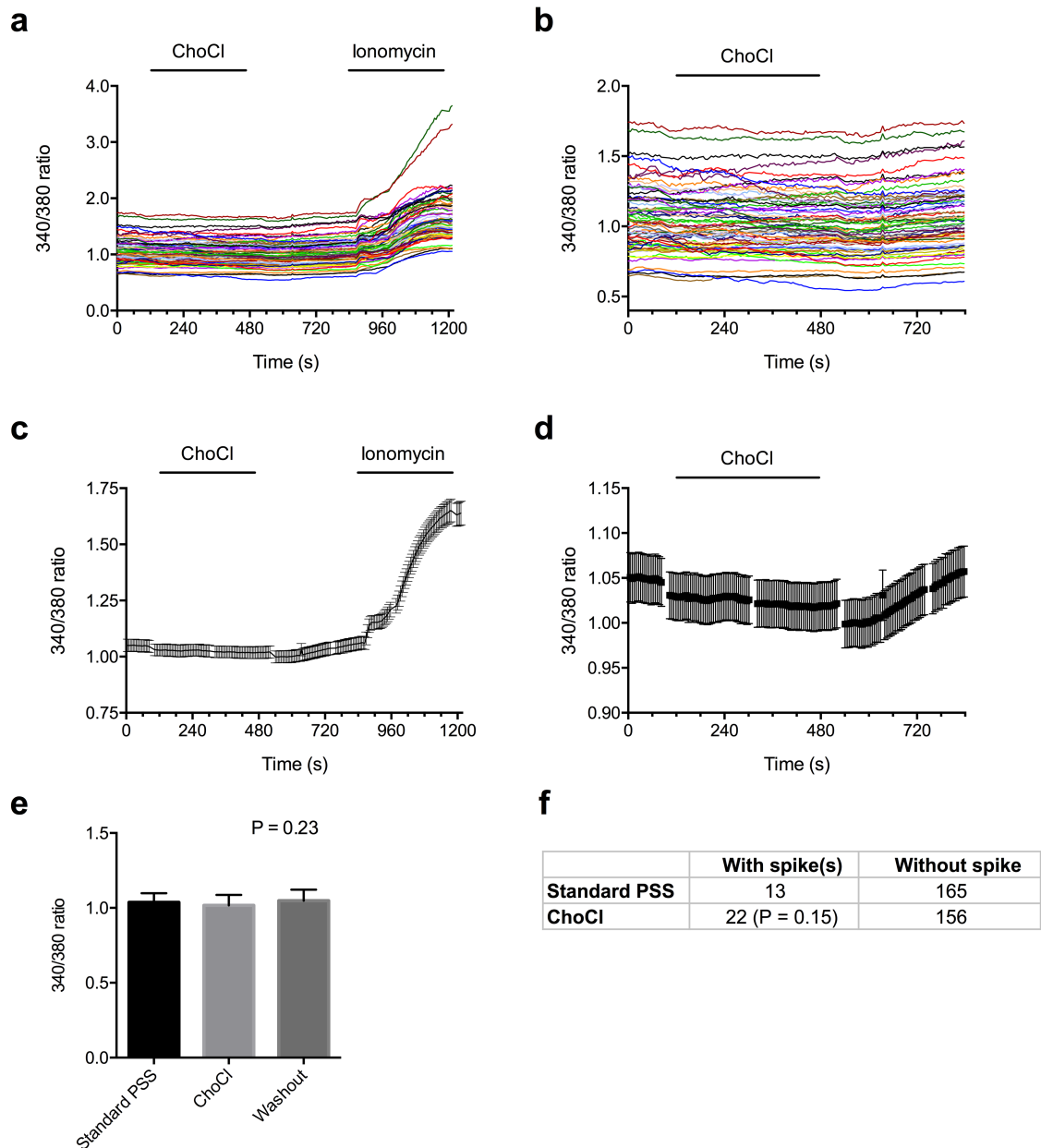
Figure 4.2. Intracellular $Ca^{2+}$ concentration ($[Ca^{2+}]_i$) of MDA-MB-231 cells after choline chloride (ChoCl) treatment.

(**a**) The $[Ca^{2+}]_i$ of individual cells, presented as the ratio of fluorescence signals subsequently collected at excitation wavelength = 340 nm and 380 nm (340/380 ratio), in standard physiological saline solution (PSS) for 2 min, followed by 6 min ChoCl treatment and a further 6 min washout, before ionomycin (10 μM) as the positive control was applied. The 340/380 ratios of cells before ionomycin treatment are also shown in (**b**). (**c**) and (**d**) show the averaged trace of (a) and (b), respectively (n = 70 from one of three repeats). (**e**) The mean 340/380 ratio over the last 30 s of standard PSS, ChoCl treatment and washout. (**f**) The number of cells that exhibit $Ca^{2+}$ spikes in standard PSS and ChoCl. ANOVA with Tukey *post hoc* test in (e) (n = 3). Fisher's exact test in (f) (178 cells from three repeats). Data are mean ± SEM in (c), (d) and (e).

cells. Additionally, the number of cells that exhibited $Ca^{2+}$ spikes during ChoCl treatment did not significantly differ compared to that in the standard PSS (Figure 4.2f; P = 0.15; Fisher's exact test; 178 cells from three repeats).

### 4.2.3 TTX application does not change the $[Ca^{2+}]_i$ in MDA-MB-231 cells

Since depletion of extracellular $Na^+$ does not change $[Ca^{2+}]_i$, blocking VGSCs with TTX should not bring significant change to the $[Ca^{2+}]_i$. Indeed, application of 30 μM TTX showed no significant change in the $[Ca^{2+}]_i$ on individual MDA-MB-231 cells, nor did the following washout (data from one of three technical repeats are shown in Figure 4.3a–d; n = 55). The mean 340/380 ratios over the last 30 s of standard PSS, TTX treatment and washout were 1.0 ± 0.0, 1.0 ± 0.1 and 1.1 ± 0.1, respectively (Figure 4.3e; P = 0.24; ANOVA with Tukey *post hoc* test; n = 3). Compared to standard PSS, TTX at 30 μM did not significantly change the number of cells that showed $Ca^{2+}$ spikes (Figure 4.3f; P = 0.15; Fisher's exact test; 185 cells from three repeats).

In a following experiment, MDA-MB-231 cells were pre-treated with 30 μM TTX for 48 h before the drug was washed out 2 min after starting image acquisition. This was to investigate whether or not $[Ca^{2+}]_i$ changes when the VGSC-mediated $Na^+$ influx is resumed after inhibition for 48 h. Representative 340/380 ratios of cells from one of three technical repeats are shown in Figure 4.4a–d. $[Ca^{2+}]_i$ of MDA-MB-231 cells did not significantly change after TTX washout: the mean 340/380 ratio over the last 30 s of TTX treatment and washout was 1.1 ± 0.1 and 1.1 ± 0.1, respectively (Figure 4.4e; P = 0.40; t-test; n = 3). Washing out TTX using standard PSS did not significantly alter the number of cells that exhibited $Ca^{2+}$ spikes (Figure 4.4f; P = 0.55; Fisher's exact test; 100 cells from three repeats). In summary, these data demonstrate that in MDA-MB-231 cells, replacing extracellular $Na^+$ with choline does not significantly change the $[Ca^{2+}]_i$. Acutely blocking VGSCs with TTX, or release of the cells from 48 h TTX
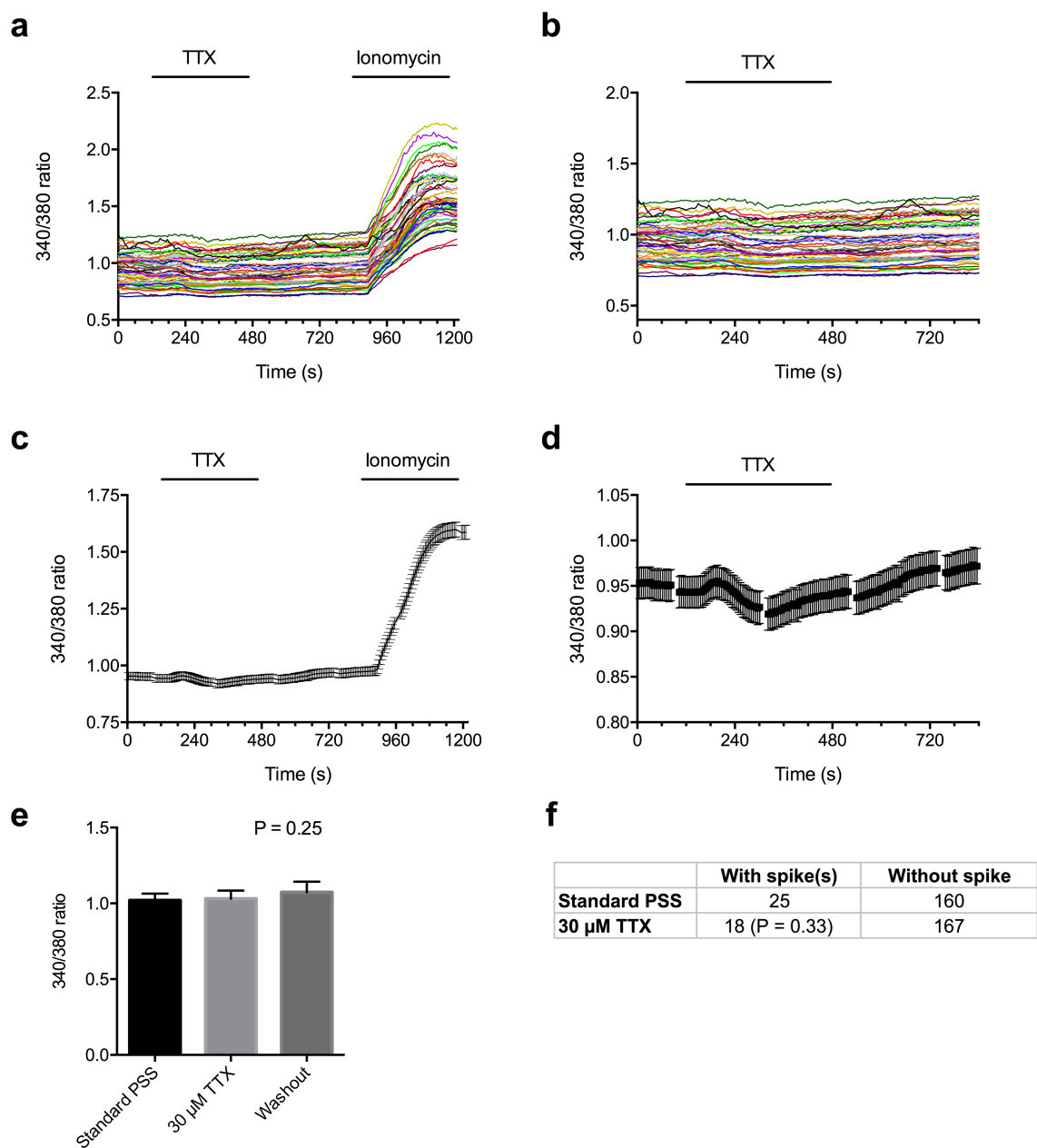
Figure 4.3. Intracellular $Ca^{2+}$ concentration ($[Ca^{2+}]_i$) of MDA-MB-231 cells after acute tetrodotoxin (TTX) treatment.

(**a**) The $[Ca^{2+}]_i$ of individual cells, presented as the ratio of fluorescence signals subsequently collected at excitation wavelength = 340 nm and 380 nm (340/380 ratio), in standard physiological saline solution (PSS) for 2 min, followed by 6 min TTX (30 µM) treatment and a further 6 min washout, before ionomycin (10 µM) as the positive control was applied. The 340/380 ratios of cells before ionomycin treatment are also shown in (**b**). (**c**) and (**d**) show the averaged trace of (a) and (b), respectively (n = 55 from one of three repeats). (**e**) The mean 340/380 ratio over the last 30 s of standard PSS, TTX treatment and washout. (**f**) The number of cells that exhibit $Ca^{2+}$ spikes in standard PSS and TTX. ANOVA with Tukey *post hoc* test in (e) (n = 3). Fisher's exact test in (f) (185 cells from three repeats). Data are mean ± SEM in (c), (d) and (e).
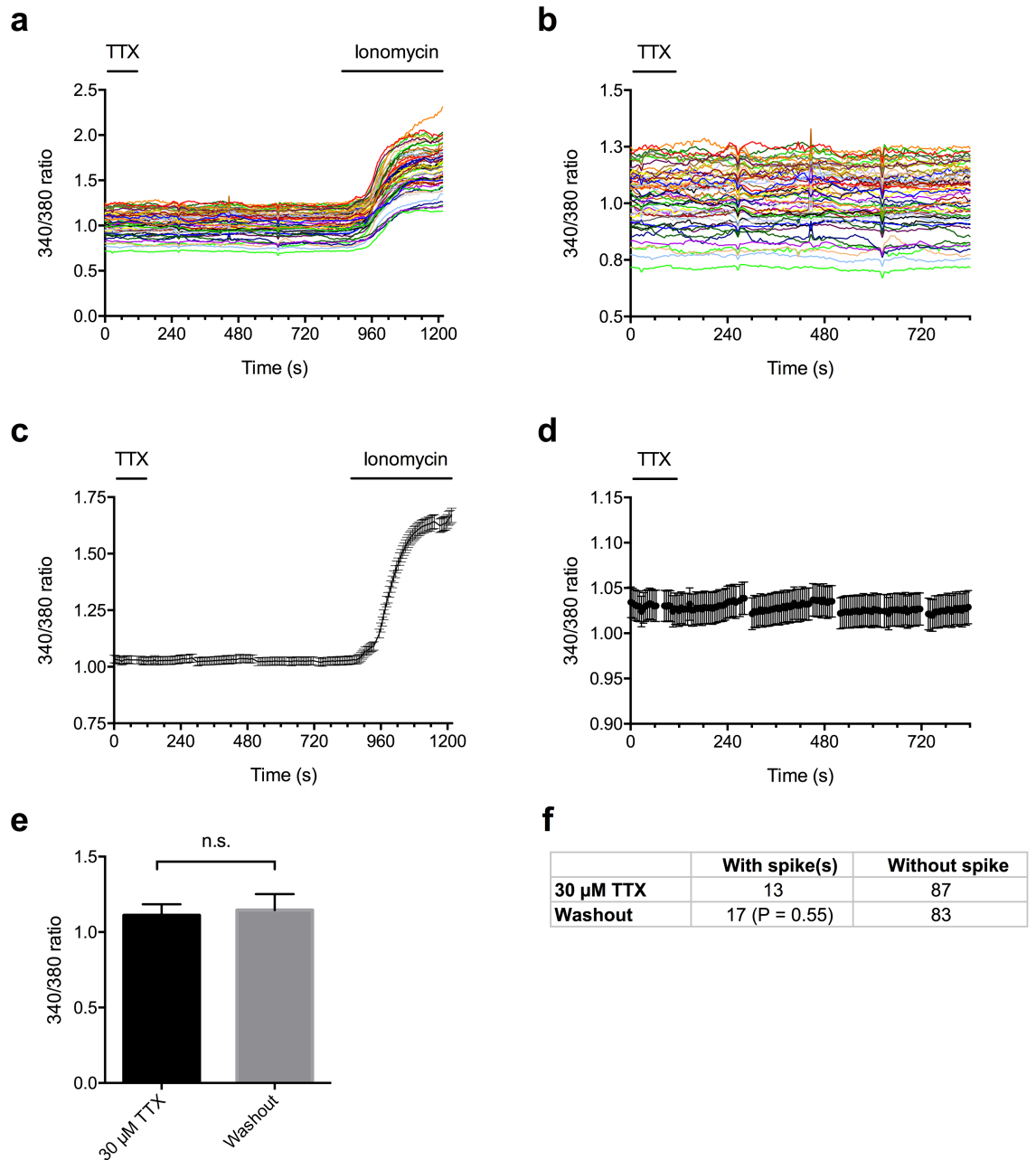
Figure 4.4. Intracellular Ca$^{2+}$ concentration ([Ca$^{2+}$]$_i$) of MDA-MB-231 cells released from 48 h tetrodotoxin (TTX) treatment.

(**a**) The [Ca$^{2+}$]$_i$ of individual cells, presented as the ratio of fluorescence signals subsequently collected at excitation wavelength = 340 nm and 380 nm (340/380 ratio). Cells were pre-incubated with TTX (30 μM) for 48 h. TTX was washed out 2 min after image acquisition started for 12 min, before ionomycin (10 μM) as the positive control was applied. The 340/380 ratios of cells before ionomycin treatment are also shown in (**b**). (**c**) and (**d**) show the averaged trace of (a) and (b), respectively (n = 55 from one of three repeats). (**e**) The mean 340/380 ratio over the last 30 s of TTX treatment and washout. (**f**) The number of cells that exhibit Ca$^{2+}$ spikes in TTX and following washout. n.s.: not significant. t-test in (e) (n = 3). Fisher's exact test in (f) (100 cells from three repeats). Data are mean ± SEM in (c), (d) and (e).

treatment did not change the $[Ca^{2+}]_i$. Therefore, $V_m$ hyperpolarisation and/or VGSCs may not regulate $[Ca^{2+}]_i$ in MDA-MB-231 cells.

### 4.2.4  Recording endogenous $I_{BKCa}$ in MDA-MB-231 cells

#### 4.2.4.1  Whole-cell patch clamp recording

In kidney tubular cells, $V_m$ depolarisation induces MLC phosphorylation via the ROCK pathway in a $Ca^{2+}$-independent manner (Szaszi *et al.*, 2005). In the next part of the study, in order to hyperpolarise the $V_m$ of MDA-MB-231 cells without blocking VGSCs, endogenously expressed $BK_{Ca}$ channels were modulated (Roger *et al.*, 2004; Khaitan *et al.*, 2009). The typical $V_m$ of MDA-MB-231 cells (~-10 mV) is more positive than the $V_{rev}$ of $K^+$ (-82 mV). Consequently, upon activation, $BK_{Ca}$ channels should carry outward $I_{BKCa}$ and therefore hyperpolarise the $V_m$.

Firstly, membrane current was recorded from MDA-MB-231 cells using the whole-cell patch clamp technique by depolarising the $V_m$ from -120 mV to +80 mV using $Cs^+$-free intracellular solution where the free $[Ca^{2+}]$ was buffered at 5.7 nM (Section 2.4.2). However, the outward $I_{BKCa}$ was not observed (Figure 4.5a). Since the activation of $BK_{Ca}$ channels requires both $Ca^{2+}$ and $V_m$ depolarisation (Barrett *et al.*, 1982), the free $[Ca^{2+}]$ in the intracellular solution was increased to 100 nM, which is close to the concentration measured in MDA-MB-231 cells previously (Sareen *et al.*, 2007; Winnicka *et al.*, 2008). At this concentration, persistent outward current was seen in one out of five MDA-MB-231 cells (Figure 4.5b).

Next, the free $[Ca^{2+}]$ in the intracellular solution was increased further to 7.8 µM. Interestingly, in whole-cell patch clamp mode, in addition to the transient $I_{Na}$ and the persistent outward current observed in Figure 4.5b, non-inactivating inward current was also recorded when depolarising the $V_m$ to ≥ +30 mV (Figure 4.6a). The mean current amplitude between 100 ms and 150 ms after depolarisation was then analysed

**a**



100 pA

10 ms

**b**



200 pA

10 ms
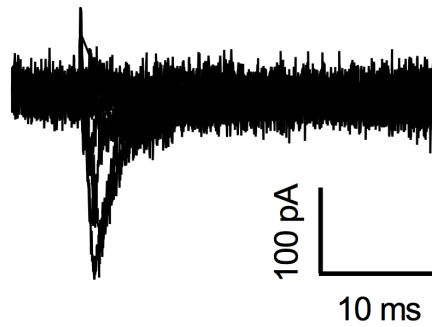
Figure 4.5. Recording the current of large-conductance $Ca^{2+}$ activated $K^+$ ($BK_{Ca}$) channels in MDA-MB-231 cells using whole-cell patch clamp technique.

Representative current traces from MDA-MB-231 cells with free $[Ca^{2+}]$ buffered at (**a**) 5.7 nM and (**b**) 100 nM in the intracellular (pipette) solution. At free $[Ca^{2+}]$ = 100 nM, one out of five cells showed persistent outward current. Cells were held at -120 mV for 250 ms before depolarising to voltages ranging from -60 mV to +80 mV for 100 ms in 10 mV increments. Every other current trace is shown for clarity.

**a**
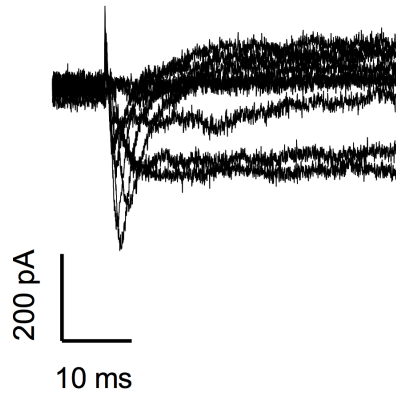


**b**
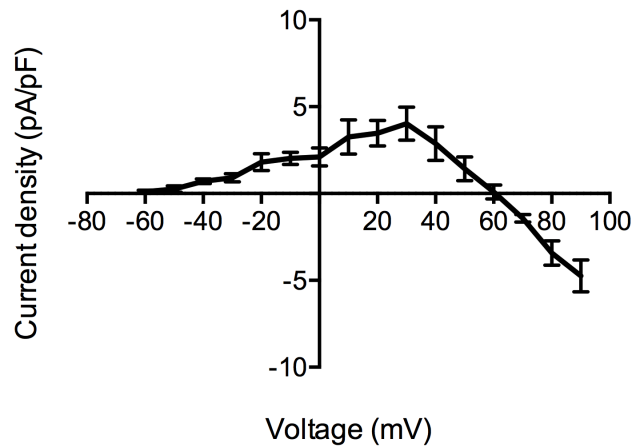


Figure 4.6. A persistent inward current recorded in MDA-MB-231 cells.

(**a**) The representative current trace and (**b**) the current-voltage relationship recorded from MDA-MB-231 cells in whole-cell patch clamp mode where the free [$Ca^{2+}$] in the intracellular (pipette) solution was buffered at 7.8 μM. Cells were depolarised to voltages from -60 mV to +90 mV for 300 ms in 10 mV increments following a 250 ms pre-pulse at -120 mV. Every other current trace is shown for clarity. Panel (b) shows the mean current over 50 ms, 100 ms after the depolarisation takes place (n = 3). Data are mean ± SEM.

because (1) the transient $I_{Na}$ was inactivated within 10 ms after depolarisation, and (2) 50 ms after depolarisation, the size of the persistent $I_{Na}$ is small (Section 3.2.3), and therefore $I_{Na}$ at 100 ms after depolarisation would not contaminate measurement of other currents. As shown in the current-voltage relationship (Figure 4.6b; n = 3), the outward current density gradually increases from -60 mV. The membrane current peaks at +30 mV with the value of 4.0 ± 1.0 pA/pF (n = 3), and the inward current becomes the dominant type of current after this voltage, indicated by the decrease of membrane current density. The size of the slow inward current increases linearly as the depolarisation becomes more positive. At +90 mV, where the recording protocol terminates, the mean current density is -4.7 ± 1.0 pA/pF (n = 3).

This persistent inward current has not been previously reported in MDA-MB-231 cells. The characteristic slow inactivation and voltage-dependent activation are similar to those of L-type VGCCs (Hille, 2001). In order to investigate whether or not the current is $Ca^{2+}$ carried by VGCCs, extracellular $Ca^{2+}$ was replaced with $Ba^{2+}$. $Ba^{2+}$ blocks $BK_{Ca}$ channels but can be a charge carrier through VGCCs (Armstrong & Matteson, 1985; Neyton & Miller, 1988; Hainsworth *et al.*, 2006). None of the three tested cells treated with $Ba^{2+}$-containing PSS showed persistent inward current at depolarised voltages (Figure 4.7a; n = 3). The current density at +90 mV was 1.5 ± 0.9 pA/pF (n = 3), significantly different to that recorded using $Ba^{2+}$-free extracellular saline solution, which was -4.7 ± 0.9 pA/pF (Figure 4.6; P < 0.01; t-test; n = 3). There was also a reduction, although not statistically significant, of the peak outward current density compared with the cells in the standard extracellular PSS [1.8 ± 1.0 pA/pF at +80 mV in the $Ba^{2+}$-containing extracellular saline solution (Figure 4.7b) vs. 4.0 ± 1.0 pA/pF at +30 mV in the standard PSS (Figure 4.6b). P = 0.17; t-test; n = 3 in both conditions]. In addition, extracellular co-application of 20 µM nifedipine and 200 µM $Cd^{2+}$, which both block L-type VGCCs (Rosenberg *et al.*, 1988; Furukawa *et al.*, 1999),
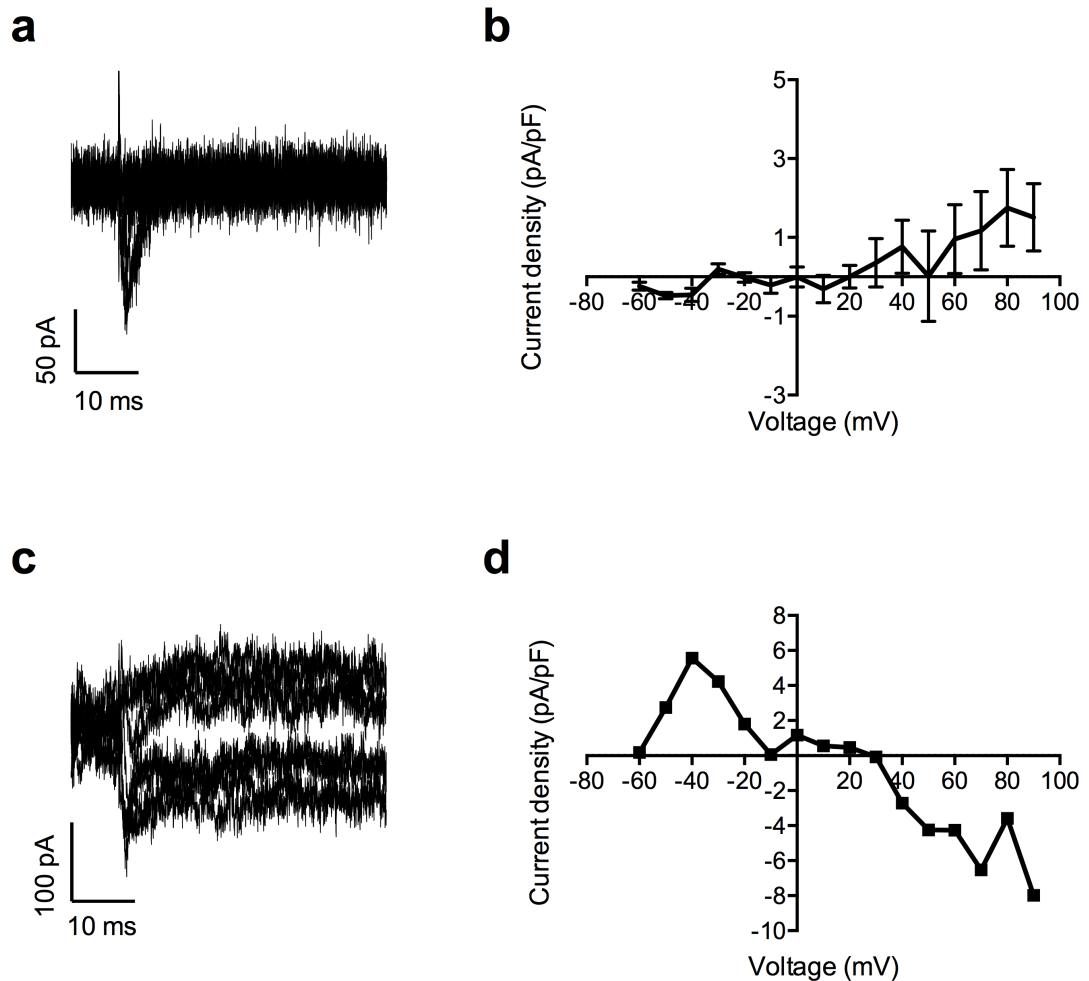
Figure 4.7. The effects of Ba$^{2+}$, and co-application of nifedipine and Cd$^{2+}$ on the membrane current.

(**a**) The representative current trace, and (**b**) the current-voltage relationship of the membrane current recorded from MDA-MB-231 cells treated with extracellular Ba$^{2+}$ in whole-cell patch clamp mode where the free [Ca$^{2+}$] in the intracellular (pipette) solution was buffered at 12.2 μM (n = 3). (**c**, **d**) Without Ba$^{2+}$, 200 μM Cd$^{2+}$ was added to the PSS. Nifedipine (20 μM) was also applied extracellularly. The recorded membrane current from a single cell is shown in (c) and the current-voltage-relationship in (d) (n = 1). Cells were depolarised to voltages from -60 mV to +90 mV for 300 ms in 10 mV increments following a 250 ms pre-pulse at -120 mV. Every other current trace is shown for clarity. Panel (b) and (d) show the mean current over 50 ms, starting from 100 ms after the depolarisation. Data are mean ± SEM in (b) and mean only in (d).

did not inhibit the persistent inward current (Figure 4.7c and d; n = 1). Taken together, these data suggest that VGCCs do not carry the persistent inward current.

Because $[Ca^{2+}]_i$ at micromolar range is much higher than in physiological conditions and the principle goal of the current experiment was to record $I_{BKCa}$, the nature of this persistent inward current was not investigated further.

### 4.2.4.2   Perforated patch clamp recording

As an ionophore, nystatin selectively induces a conductance for monovalent ions but no permeability for divalent ions such as $Ca^{2+}$ (Cass & Dalmark, 1973). Therefore, in order to leave the $[Ca^{2+}]_i$ of MDA-MB-231 cells at its physiological level, perforated patch clamp using nystatin (120 µM) was adopted to isolate the outward $I_{BKCa}$ in MDA-MB-231 cells. Both $I_{Na}$ and persistent outward current were observed in all three cells tested (Figure 4.8).

In order to further characterise the persistent outward current, in the next experiment, NS-1619, a BK$_{Ca}$ channel activator (Macmillan *et al.*, 1995), and IbTx, a BK$_{Ca}$ channel blocker (Calderone, 2002), were applied to MDA-MB-231 cells and membrane current was recorded in perforated patch clamp mode. Compared to control (Figure 4.9a), application of 1 µM NS-1619 increased the amplitude of the persistent outward current (Figure 4.9b). Co-application of 1 µM NS-1619 and 100 nM IbTx inhibited the outward current (Figure 4.9c). The current-voltage relationships of the membrane current under three conditions are fitted into exponential equations (Section 2.12), as shown in Figure 4.9d. In summary, the outward persistent current recorded in MDA-MB-231 cells using perforated patch clamp recording is $I_{BKCa}$.
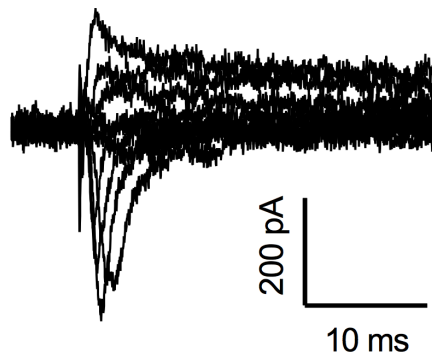
**200 pA**

**10 ms**
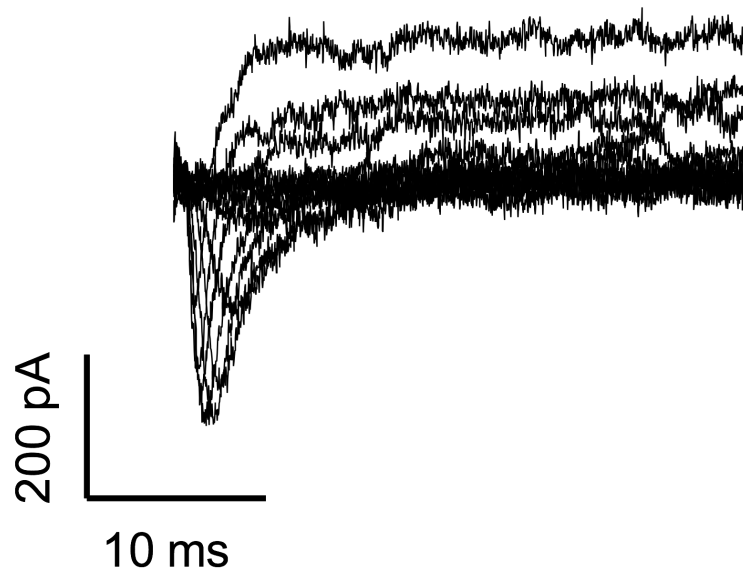
Figure 4.8. Recording the current of large-conductance $Ca^{2+}$ activated $K^+$ ($BK_{Ca}$) channels in MDA-MB-231 cells using perforated patch clamp technique.

Nystatin (120 µM) was used in perforated patch clamp recordings. Three out of three cells tested showed both inward $Na^+$ current and persistent outward current. Cells were held at -120 mV for 250 ms before depolarising to voltages ranging from -60 mV to +80 mV for 100 ms in 10 mV increments. Every other current trace is shown for clarity.
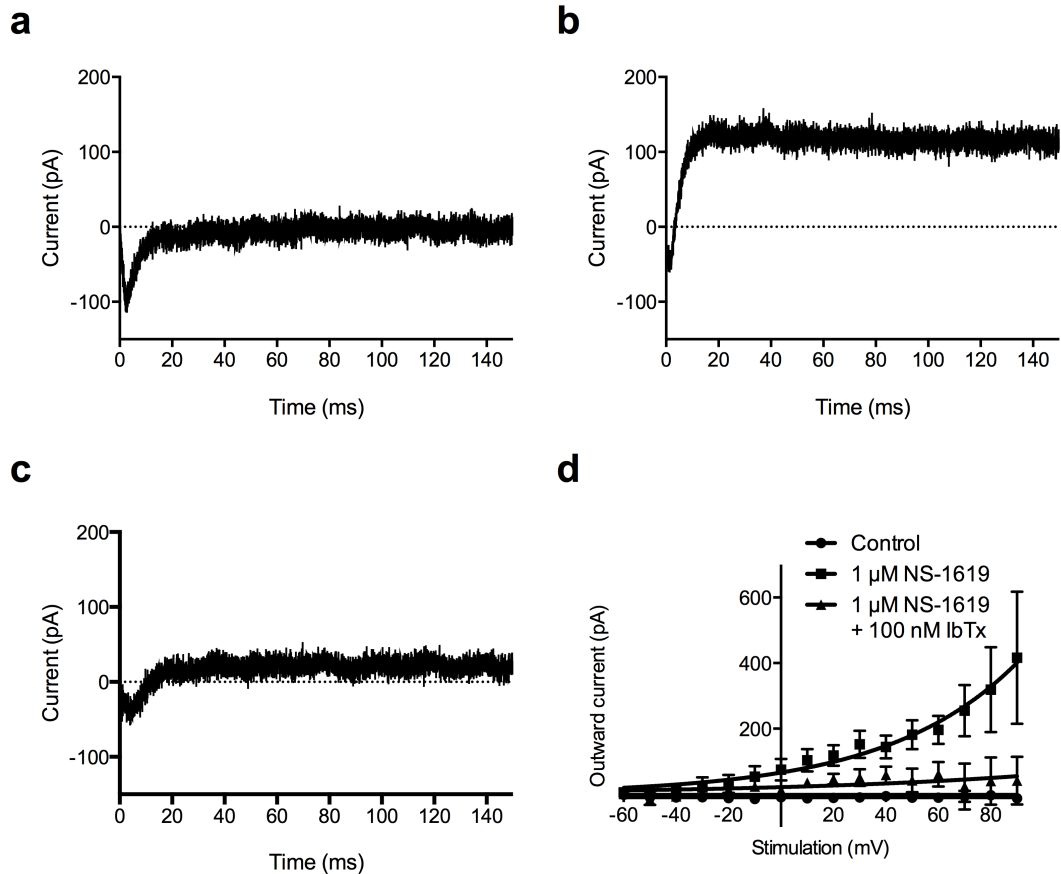
Figure 4.9. The NS-1619- and iberiotoxin (IbTx)-sensitive large-conductance $Ca^{2+}$-activated $K^+$ ($BK_{Ca}$) current in MDA-MB-231 cells.

Perforated patch clamp recordings showing membrane current, elicited by +80 mV depolarisation following a 250 ms pre-pulse at -120 mV, in (**a**) control, (**b**) following 1 µM NS-1619 treatment, and (**c**) after further co-application of 1 µM NS-1619 and 100 nM IbTx. (**d**) Current-voltage relationship of the $BK_{Ca}$ current. Data are fitted to single exponential equations. $BK_{Ca}$ current was activated from a -120 mV (250 ms) pre-pulse to voltages between -60 mV and +90 mV for 300 ms in 10 mV increments (n = 5). Panel (d) analysed the mean current over 50 ms, starting from 100 ms after the depolarisation. Data are mean ± SEM.

### 4.2.5  Hyperpolarising the $V_m$ of MDA-MB-231 cells using NS-1619

When the resting $V_m$ is more positive than the $V_{rev}$ for $K^+$, NS-1619 increases $K^+$ efflux through $BK_{Ca}$ channels, thus hyperpolarising the $V_m$ (Prior *et al.*, 1998). Next, using whole-cell patch clamp, the effect of NS-1619 on $V_m$ of MDA-MB-231 cells was investigated. Using intracellular solution containing 100 nM $[Ca^{2+}]$ (Table 2.3), cells were incubated with NS-1619 for 6 min before the recording. NS-1619 at 1 μM, 5 μM, 10 μM and 40 μM hyperpolarised the steady-state $V_m$ of MDA-MB-231 cells to -15.0 ± 0.6 mV (n = 12), -25.2 ± 1.13 mV (n = 6), -31.7 ± 3.2 mV (n = 10) and -51.8 ± 3.3 mV (n = 9), respectively, in a dose-dependent manner (Figure 4.10a). Compared with the $V_m$ in the standard PSS, which is -10.6 ± 1.3 mV (n = 12), 1 μM NS-1619 significantly hyperpolarised the $V_m$ by 4.4 mV to -15.0 ± 0.6 mV (Figure 4.10b; P < 0.01; t-test; n = 12), similar to the hyperpolarisation caused by 30 μM TTX (Section 3.2.3).

Finally, the $V_m$ recorded using the standard intracellular solution (free $[Ca^{2+}]$ = 5.7 nM, Table 2.3) is -10.3 ± 1.0 mV (n = 10), which does not significantly differ from that recorded using the intracellular solution with 100 nM free $[Ca^{2+}]$, which is -10.6 ± 1.2 mV (Figure 4.11; P = 0.82; t-test; n = 12), suggesting that at the physiological $[Ca^{2+}]_i$ of 100 nM (Sareen *et al.*, 2007; Winnicka *et al.*, 2008), $BK_{Ca}$ channels have negligible contribution to regulating the $V_m$ in MDA-MB-231 cells in the absence of NS-1619.

### 4.2.6  NS-1619 does not affect MDA-MB-231 cell proliferation

The dynamic change of $V_m$ has instructive roles in promoting cell cycle progression: $V_m$ undergoes hyperpolarisation at $G_1$/S border and depolarisation at $G_2$/M (Blackiston *et al.*, 2009; Yang & Brackenbury, 2013). Blocking VGSCs using TTX or phenytoin hyperpolarises the $V_m$ in MDA-MB-231 cells (Section 3.2.3 and Section 3.2.4). However, previously published studies show that these inhibitors do not affect
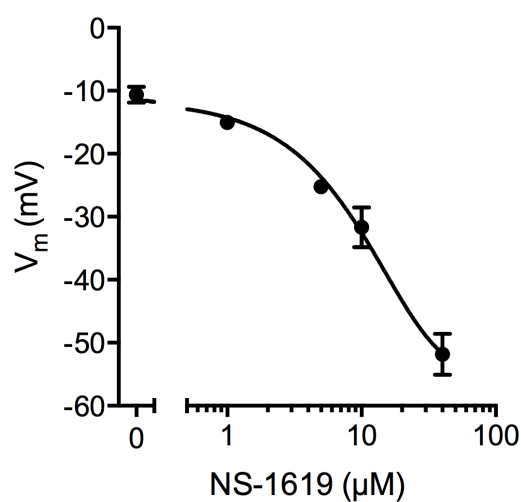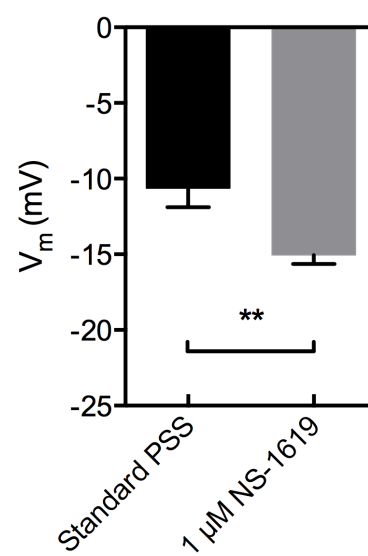
Figure 4.10. NS-1619 hyperpolarises the membrane potential ($V_m$) of MDA-MB-231 cells.

(**a**) The dose-response curve of 1, 5, 10 and 40 µM NS-1619 on the steady-state $V_m$ of MDA-MB-231 cells (n ≥ 6). The data are fitted to a sigmoidal logistic equation. (**b**) Effect of 1 µM NS-1619 on the steady-state $V_m$ of MDA-MB-231 cells. Cells were incubated with the drug for 2 min before their $V_m$ was recorded using whole-cell patch clamp. (**) $P < 0.01$; t-test (n = 12 in each condition). Data are mean ± SEM. Liquid junction potential (3 mV) is compensated.
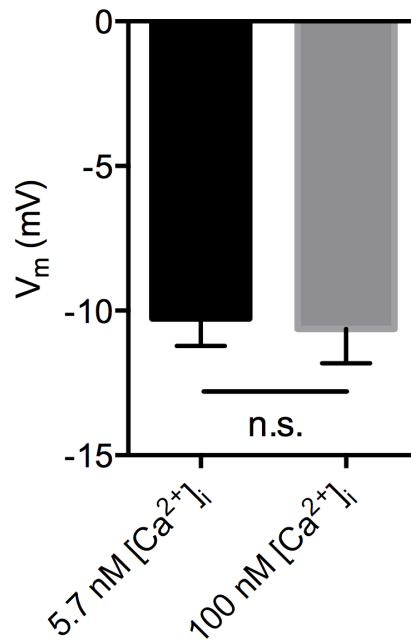
Figure 4.11. Membrane potential ($V_m$) recorded in whole-cell patch mode with different free [$Ca^{2+}$] in the recording pipette.

The $V_m$ recorded using intracellular (pipette) solution with free [$Ca^{2+}$] buffered at 5.7 nM and 100 nM using EGTA in whole-cell patch clamp mode. Liquid junction potential is compensated. n.s. not significant; t-test (n = 10 and 12 in 5.7 nM and 100 nM [$Ca^{2+}$], respectively). Data are mean ± SEM.

the proliferation of MDA-MB-231 cells *in vitro* (Roger *et al.*, 2003; Fraser *et al.*, 2005; Yang *et al.*, 2012). Here, NS-1619 was applied at two concentrations and its hyperpolarising effects on MDA-MB-231 cell proliferation was measured using the MTT assay (Section 2.5.1). Figure 4.12a shows a typical linear standard curve generated for one of the three technical repeats, relating the absorbance of MTT at 570 nm to cell number, with $R^2 = 0.98$. The cell numbers after 24 h incubation with 1 µM or 40 µM NS-1619 were $(7.2 \pm 0.6) \times 10^4$ and $(7.1 \pm 0.6) \times 10^4$, respectively, which is not significantly different from that of control at $(7.2 \pm 0.6) \times 10^4$ (Figure 4.12b; P = 1.00 and 0.94 comparing control with 1 µM and 40 µM NS-1619, respectively; ANOVA with Tukey *post hoc* test; n = 9). In summary, these data suggest that hyperpolarising the $V_m$ using NS-1619 does not affect MDA-MB-231 cell proliferation.

### 4.2.7  NS-1619 reduces MDA-MB-231 cell migration

Since blockade of VGSCs reduces MDA-MB-231 cell motility (Fraser *et al.*, 2003; Yang *et al.*, 2012), the effect of hyperpolarising the $V_m$ with NS-1619 or TTX on migration was examined using ptychrography technique. MDA-MB-231 cells were grown into confluent monolayers before a wound was made. Cells were then washed once with 37 °C DMEM with 0 % FBS to remove cell debris before TTX (30 µM) or NS-1619 (1 µM) was applied. The cells were then allowed to migrate into wounds for 16 h, at 37 °C, 5 % $CO_2$ under a Phasefocus VL-21 microscope. Figure 4.13a shows representative wounds under all conditions at the beginning and end of the experiment.

Because cells undergo volume increase during mitosis, the cell volume measured using ptychography is a direct indicator of cell proliferation (Marrison *et al.*, 2013). Neither 30 µM TTX nor 1 µM NS-1619 significantly altered the rate of cell volume increase (Figure 4.13b; n = 3). The cell volume gradient was $(2.8 \pm 0.1) \times 10^4$ µm$^3$/h in control, $(2.0 \pm 0.1) \times 10^4$ µm$^3$/h and $(2.2 \pm 0.3) \times 10^4$ µm$^3$/h after 30 µM TTX and 1 µM
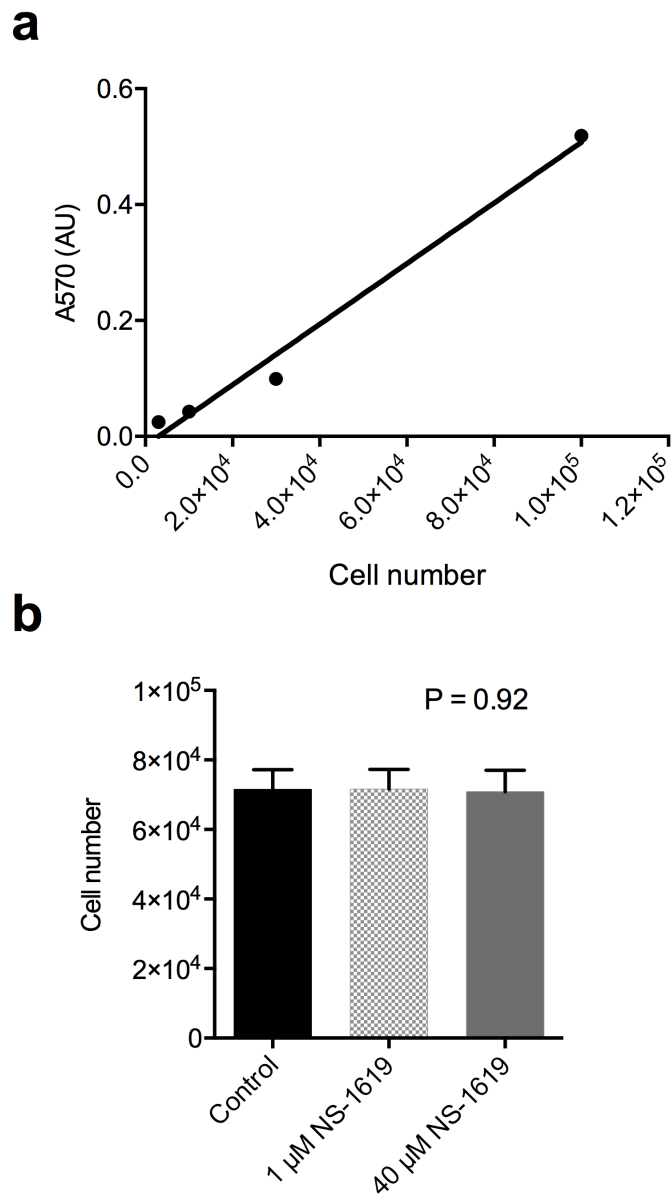
Figure 4.12. NS-1619 does not affect MDA-MB-231 cell proliferation.

MDA-MB-231 cell proliferation was determined by using 3-(4,5-dimethylthiazol-2-yl)-2,5-diphenyltetrazolium bromide (MTT) assay. (**a**) Representative linear standard curve relating the absorbance of MTT at 570 nm (A570) with cell number. (**b**) The number of cells after 24 h treatment with 1 µM or 40 µM NS-1619. ANOVA with Tukey *post hoc* test (n = 9). Data are mean ± SEM.
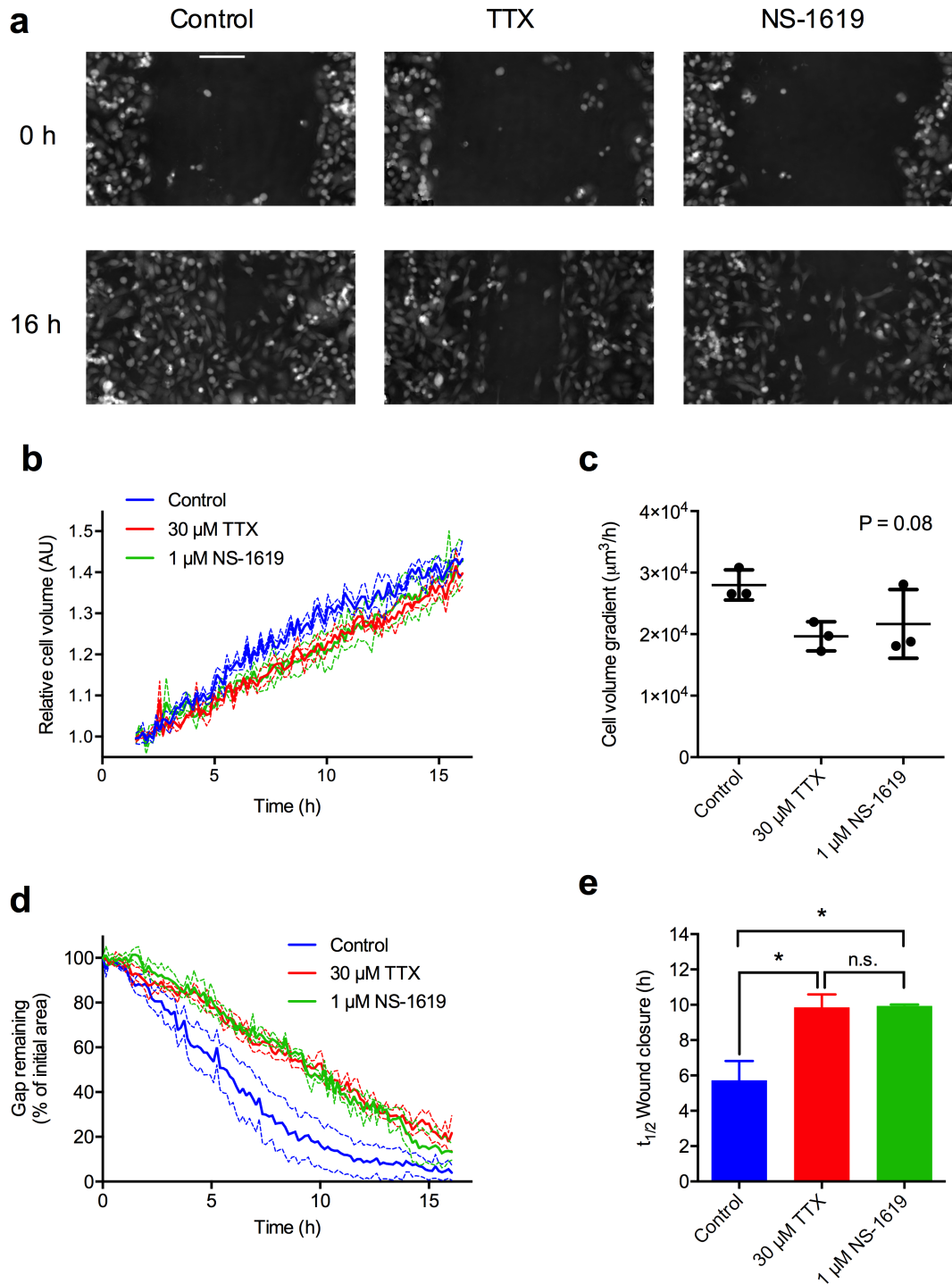
Figure 4.13. NS-1619 and tetrodotoxin reduce MDA-MB-231 cell lateral migration.

(**a**) Representative wounds at the beginning (0 h) and the end (16 h) of wound healing assay with TTX (30 µM) or NS-1619 (1 µM) treatment. (**b**) Cell proliferation, indicated by the normalised cell volume during wound healing assays. Dashed lines show mean ± SEM. (**c**) Cell volume gradient, an index of cell growth rate, during the wound healing assays. (**d**) Normalised wound area ("gap") in the wound healing assays. Dashed lines show mean ± SEM. (**e**) $t_{1/2}$ of wound closure in (d). Scale bar = 100 µm. (*) $P < 0.05$; n.s. not significant; ANOVA with Tukey *post hoc* test (n = 3). Data are mean ± SEM.

NS-1619 treatment, respectively (Figure 4.13b; P = 0.10 and 0.16 comparing TTX and NS-1619 with control, respectively; P = 0.54 comparing with TTX and NS-1619; ANOVA with Tukey *post hoc* test; n = 3).

While the cells migrated into the wound, the remaining wound area (gap remaining) was measured over 16 h (Figure 4.13d). The $t_{1/2}$ of wound closure increased from 5.7 ± 1.1 h in control to 9.8 ± 0.7 h in 30 µM TTX and 9.9 ± 0.1 h in 1 µM NS-1619 (Figure 4.13e; P < 0.05 comparing TTX or NS-1619 with control; P = 1.00 comparing 30 µM TTX with 1 µM NS-1619; ANOVA with Tukey *post hoc* test; n = 3). Thus, by hyperpolarising the $V_m$ to a comparable voltage, TTX and NS-1619 increased the $t_{1/2}$ of wound closure to a similar extent, suggesting that VGSCs may increase MDA-MB-231 cell motility by depolarising the $V_m$.

### 4.2.8  NS-1619 does not affect MDA-MB-231 cell invasion

Blocking VGSCs with TTX reduces MDA-MB-231 cell Matrigel invasion (Fraser *et al.*, 2005; Brackenbury *et al.*, 2007). Next, the functional role of $V_m$ in mediating invasion was investigated. MDA-MB-231 cells were grown on Matrigel-coated invasion chambers with TTX or NS-1619 for 24 h before the invaded cells were fixed using paraformaldehyde and stained with DAPI. The number of DAPI-positive cells was counted under an epi-fluorescence microscope. TTX at 30 µM significantly reduced the number of invaded cells to 58.3 ± 6.5 % of control (Figure 4.14a; P < 0.01 compared with control, ANOVA with Tukey *post hoc* test; n = 7), whereas NS-1619 at 1 µM did not significantly alter the number of invaded cells (Figure 4.14a; P = 0.98 compared with control and P < 0.05 compared with TTX; ANOVA with Tukey *post hoc* test; n = 7). Moreover, using 40 µM NS-1619 to hyperpolarise the $V_m$ of MDA-MB-231 cells further to -51.8 ± 3.3 mV (Figure 4.10a) did not significantly change the number of invaded cells compared with control (Figure 4.14b; 114.3 ± 24.5 % of control; P = 0.58; ANOVA
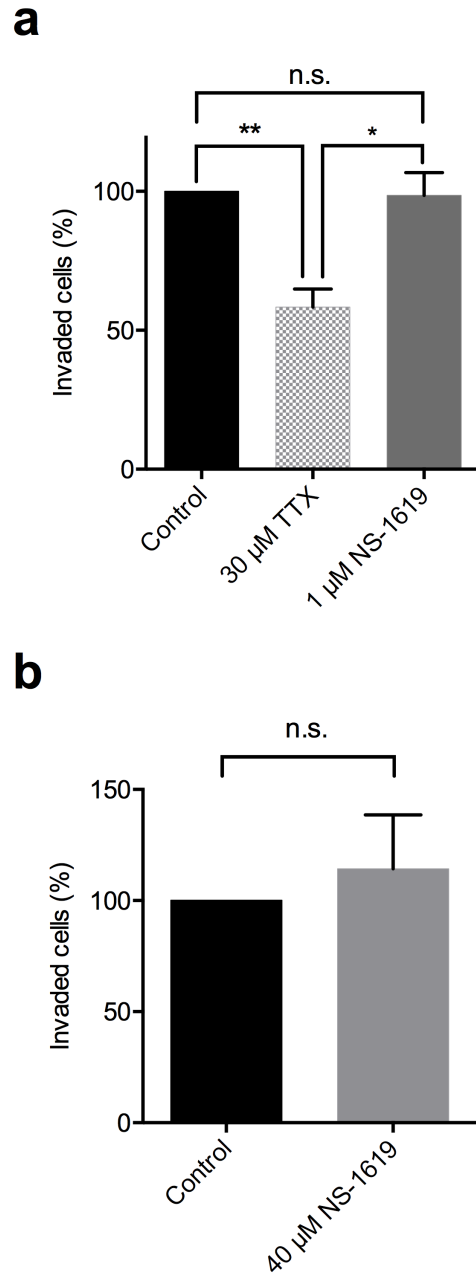
Figure 4.14. NS-1619 does not alter MDA-MB-231 invasion *in vitro*.

(**a**) Invaded cells (normalised to control) after 24 h treatment with 30 µM TTX or 1 µM NS-1619 were measured using the Matrigel invasion assay. (*) P < 0.05; (**) P < 0.01, respectively; ANOVA with Tukey *post hoc* test (n = 7). (**b**) Invaded cells after 40 µM NS-1619 treatment for 24 h. n.s. not significant; t-test (n = 6). Data are mean ± SEM.

with Tukey *post hoc* test; n = 6), suggesting that $V_m$ may not be a factor regulating MDA-MB-231 cell invasion *in vitro*.

### 4.2.9 TTX and NS-1619 alter MDA-MB-231 cell morphology

In MDA-MB-231 cells, $Na_v1.5$ modulates cytoskeletal components and promotes an elongated cell morphology (Brisson *et al.*, 2013; Nelson *et al.*, 2015b). Additionally, blocking VGSCs with ranolazine increases the circularity of MDA-MB-231 cells (Driffort *et al.*, 2014), whereas TTX application reduces process length on Mat-LyLu cells (Fraser *et al.*, 1999). To test whether $Na_v1.5$-mediated morphology regulation is dependent on $V_m$, a wound was made on confluent MDA-MB-231 cell monolayer followed by a wash with 37 °C DMEM with 0 % FBS to remove cell debris before TTX (30 μM) or NS-1619 (1 μM) was applied. Cells were then allowed to migrate into the wound for 3 h before being fixed with paraformaldehyde. F-actin and nucleus were labelled with Alexa 633-conjugated phalloidin and DAPI, respectively. Cells were then examined using a Zeiss LSM 880 laser scanning confocal microscope. The boundaries of single cells (20–25 cells per condition in each of three technical repeats) at both ends of the wound were determined using the free-hand line tool in ImageJ software (Figure 4.15a), and circularity was calculated using the same software according to Equation 2.4. TTX (30 μM) significantly increased the circularity from 0.54 ± 0.17 in control to 0.64 ± 0.15 (Figure 4.15a and b; $P < 0.001$; ANOVA with Tukey *post hoc* test; n = 61 in control and n = 62 in TTX). Similarly, NS-1619 (1 μM) increased the circularity to 0.61 ± 0.15 ($P < 0.05$ compared with control; ANOVA with Tukey *post hoc* test; n = 61 in control and n = 67 in NS-1619). Interestingly, there was no statistically significant difference in circularity between TTX and NS-1619 treatment ($P = 0.56$; ANOVA with Tukey *post hoc* test; n = 62 in TTX and n = 67 in NS-1619), suggesting both the drugs reduced the elongated morphology of MDA-MB-231 cells to a similar degree.

**a**

Control        TTX        NS-1619

Actin

DAPI

Circularity = 0.32    Circularity = 0.55    Circularity = 0.65

**b**
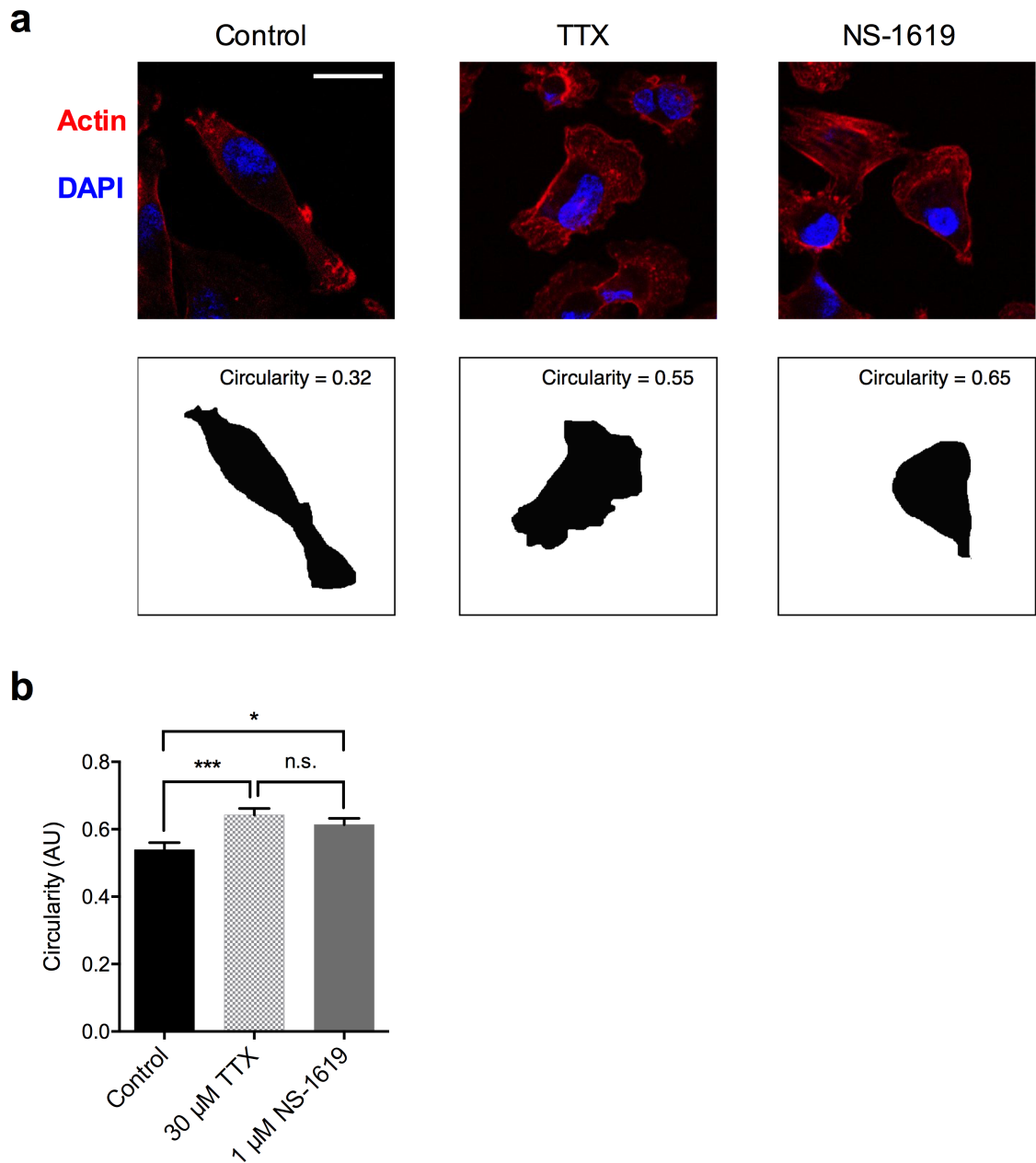
Figure 4.15. Tetrodotoxin (TTX) and NS-1619 increase MDA-MB-231 cell circularity.
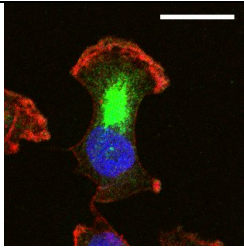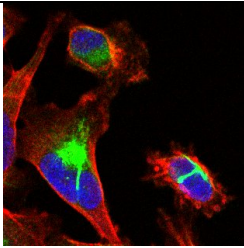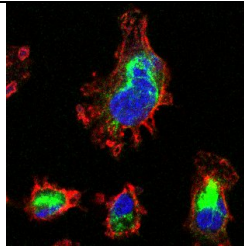
(**a**) Representative cell morphology after TTX (30 μM) and NS-1619 (1 μM) treatment for 3 h. Cells were stained with Alexa 633-conjugated phalloidin (red) and DAPI (blue). Lower row shows the boundaries of cells of interest in the upper row, by which the circularity of cells was calculated. (**b**) Circularity of MDA-MB-231 cells after TTX and NS-1619 treatment. (*)$P < 0.05$; (***) $P < 0.001$; n.s. not significant; ANOVA with Tukey *post hoc* test (n = 61, 62 and 67 in control, TTX and NS-1619, respectively). Data are mean ± SEM. Scale bar = 20 μm.

### 4.2.10 TTX and NS-1619 reduce the proportion of MDA-MB-231 cells bearing lamellipodia

The protrusion of lamellipodia initiates cell migration (Small *et al.*, 2002). Given that both TTX and NS-1619 reduce MDA-MB-231 cell migration and induce a round morphology, these compounds may reduce the formation of lamellipodia in MDA-MB-231 cells. The proportion of cells with a lamellipodium after TTX (30 µM) and NS-1619 (1 µM) treatment was analysed using the images acquired in Section 4.2.9. The proportion of cells with lamellipodium was compared pairwise using Fisher's exact tests among control, TTX and NS-1619 treatments, resulting in three comparisons. Bonferroni correction was applied for multiple comparisons: with three pairwise comparisons, the P value must be less than $0.05 \div 3 = 0.016$ to be significant at the P < 0.05 level (MacDonald & Gardner, 2000). The pairwise P value between control and TTX was 0.0002, suggesting the distribution of samples was significantly different between the two conditions, i.e. TTX reduced the proportion of MDA-MB-231 cells bearing a lamellipodium (Table 4.1). The P value comparing NS-1619 and control was < 0.0001, suggesting that NS-1619 also reduced the proportion of cells with lamellipodium (Table 4.1). However, the proportion of cells bearing a lamellipodium did not differ between TTX and NS-1619 (P = 0.84). In summary, both TTX (30 µM) and NS-1619 (1 µM) significantly reduced the proportion of cells bearing a lamellipodium to a similar degree, consistent with these compounds inhibiting migration.

### 4.2.11 TTX and NS-1619 reduce the active Rac1 level at the leading edge of MDA-MB-231 cells

The small GTPase Rac1 is one of the key molecules required for the formation of lamellipodia, by promoting the assembly of actin filaments (Ridley, 2015). Activating Rac1 is sufficient to induce cell migration (Wu *et al.*, 2009; Montell *et al.*, 2012). Since

| | Control | 30 µM TTX | 1 µM NS-1619 |
|---|---|---|---|
| | **Control** | **30 µM TTX** | **1 µM NS-1619** |
| **Representative cells** |  |  |  |
| **Cells with lamellipodium** | 109 | 72 * | 66 * |
| **Cells without lamellipodium** | 41 | 69 * | 73 * |
| **Total # of cells** | 150 | 141 | 139 |

Table 4.1. The proportion of MDA-MB-231 cells bearing a lamellipodium after tetrodotoxin (TTX) and NS-1619 treatment.

(*) adjusted $P < 0.05$ compared with control. Fisher's exact test with Bonferroni corrections for multiple comparisons. Three technical repeats were preformed. Red: F-actin; green: active Rac1; blue: DAPI. Scale bar = 20 µm.

hyperpolarising $V_m$ using TTX (30 µM) and NS-1619 (1 µM) retarded MDA-MB-231 cell migration (Section 4.2.7) and reduced the proportion of cells with a lamellipodium (Section 4.2.10), it is possible that $V_m$ may regulate Rac1 activity, actin filament assembly and thus cell migration. To test this, MDA-MB-231 cells were fixed during a wound healing assay using paraformaldehyde as described in Section 4.2.9, and were labelled with an anti-active Rac1 antibody. Cells were then labelled with Alexa 488-conjugated secondary antibody and Alexa 633-conjugated phalloidin, and nuclei were labelled with DAPI. Samples were examined using a Zeiss LSM 880 confocal microscope. The active Rac1 fluorescence intensity was strong at the leading edge of cells in control, but was weaker in TTX (30 µM)- or NS-1619 (1 µM)-treated MDA-MB-231 cells (Figure 4.16, arrows).

In order to quantify the data, a 90 ° quadrant mask with a radius of 5.6 µm encompassing the lamellipodium/cell leading edge was applied to cells that were migrating into the wound (Figure 4.17a). Inside the mask, the signal density of F-actin and active Rac1 across a series of arcs with various radii was gathered and normalised to that of the innermost arc (Figure 4.17b). Treatment with TTX (30 µM) or NS-1619 (1 µM) reduced the F-actin signal density in outer arcs within the lamellipodia (Figure 4.15a, Figure 4.17c, Table 4.1). The active Rac1 signal density at the leading edge of lamellipodia was also significantly reduced (Figure 4.15a, Figure 4.17d, Table 4.1). For example, the active Rac1 signal in the arc with radius of 4.76 µm was 129.4 ± 4.6 % in control, 113.9 ± 4.2 % in TTX ($P < 0.05$ compared with control; ANOVA with Tukey *post hoc* test; n = 67 in control and n = 66 in TTX) and 107.9 ± 3.5 % in NS-1619 ($P < 0.001$ compared with control; $P = 0.56$ compared with 30 µM TTX; ANOVA with Tukey *post hoc* test; n = 71). Therefore, in MDA-MB-231 cells, decreased active Rac1 levels at the leading edge caused by $V_m$ hyperpolarisation may reduce lamellipodia formation, induce round morphology and reduce motility, by inhibiting F-actin.
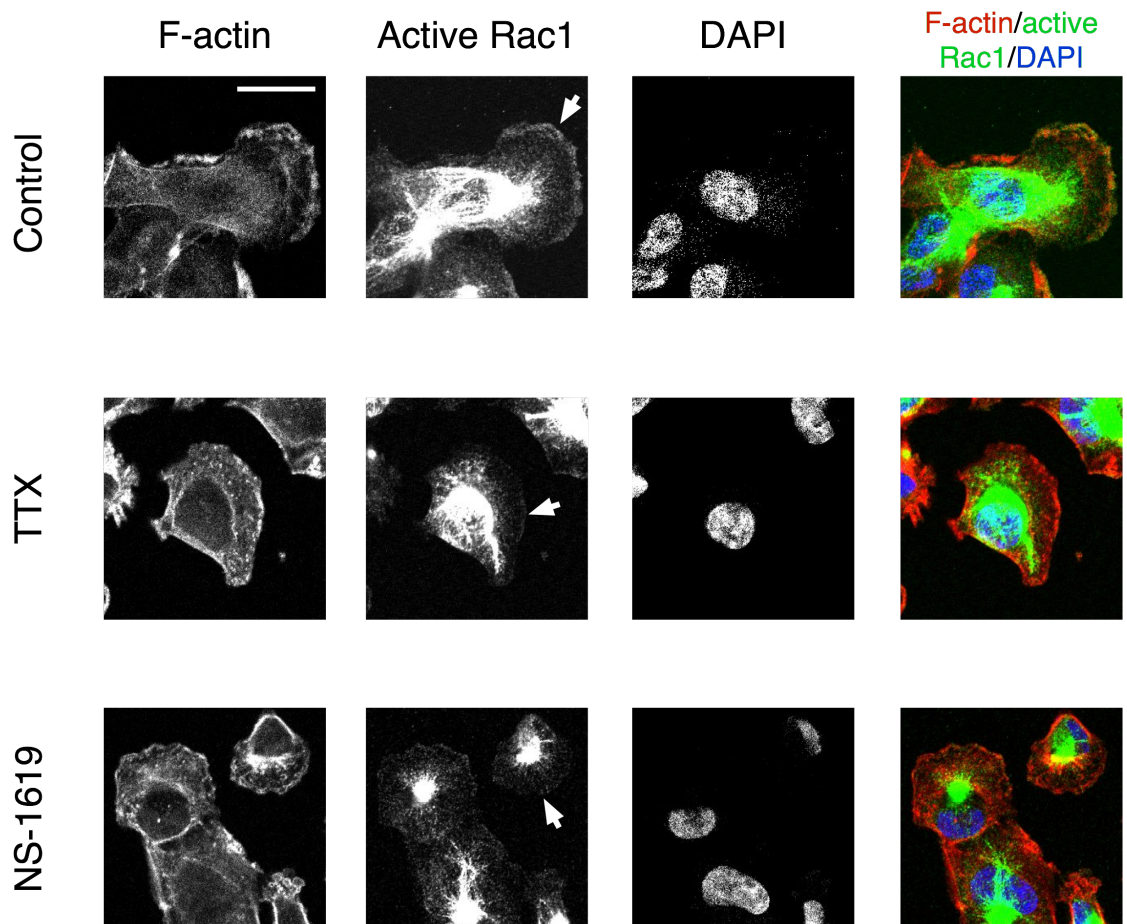
Figure 4.16. The expression of F-actin and active Rac1 in MDA-MB-231 cells after tetrodotoxin (TTX) and NS-1619 treatment.

In a wound healing assay, MDA-MB-231 cells were allowed to migrate into the wound for 3 h in the presence/absence of TTX (30 µM) or NS-1619 (1 µM). Cells were then fixed with paraformaldehyde and labelled with mouse anti-active Rac1 antibody, followed by Alexa 488 conjugated goat anti mouse IgG secondary antibody. F-actin was labelled with Alexa 633-conjugated phalloidin. Cells were then mounted on microscope slides with DAPI and were examined using a Zeiss LSM 880 laser scanning confocal microscope. White arrows highlight active Rac1 staining at cell leading edge. Scale bar = 20 µm.
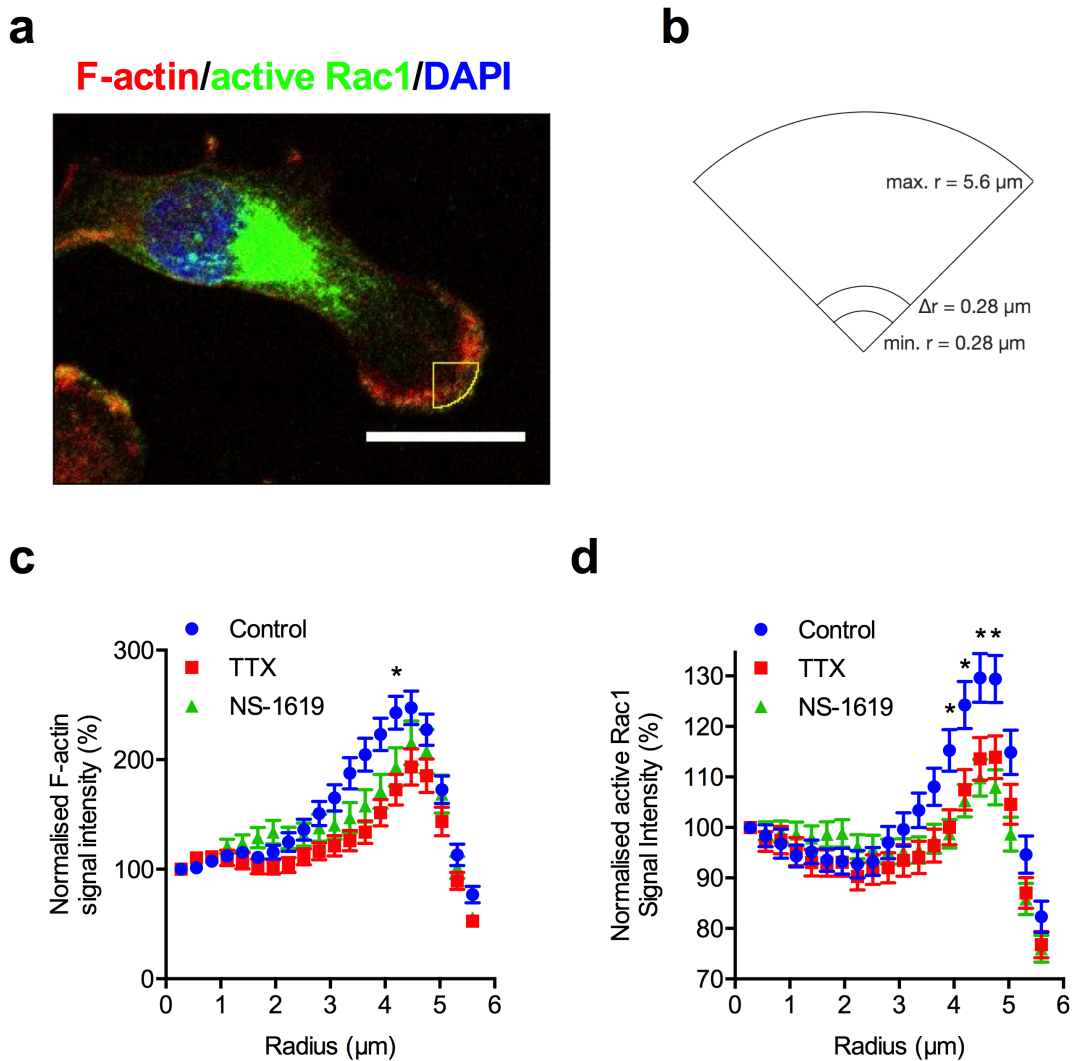
Figure 4.17. F-actin and active Rac1 signal intensity in the lamellipodium of MDA-MB-231 cells.

(**a**) Representative cell (in control condition) showing the quadrant mask as the region of interest for analysing F-actin and active Rac1 signal intensity at lamellipodia. (**b**) The signal density was measured across 20 arcs with various radii, in 0.28 μm increments, within the quadrant. (**c**) Normalised F-actin and (**d**) active Rac1 signal density across the arcs indicated in (b). (*) $P < 0.05$ comparing control and TTX (30 μM), and comparing control and NS-1619 (1 μM); ANOVA with Tukey *post hoc* test (n = 61, 62 and 67 in control, TTX and NS-1619, respectively). Data are mean ± SEM. Scale bar = 20 μm.

Taken together, data in this Chapter suggest that $V_m$ hyperpolarisation does not significantly alter the $[Ca^{2+}]_i$ in MDA-MB-231 cells. Activating $BK_{Ca}$ channels with NS-1619 mimicked TTX-induced $V_m$ hyperpolarisation. Comparisons between cells treated with TTX and NS-1619 demonstrated that VGSC-induced $V_m$ hyperpolarisation inhibits MDA-MB-231 cell motility, causes round cell morphology; reduces the proportion of cells with a lamellipodium, and decreases the level of active Rac1 at cell leading edge. In contrast, VGSCs appear to promote invasion independent of the $V_m$.

## 4.3   Discussion

### 4.3.1   $V_m$ hyperpolarisation does not change $[Ca^{2+}]_i$ in MDA-MB-231 cells

Since $V_m$ changes have been shown to regulate $[Ca^{2+}]_i$ via $Ca^{2+}$-permeable channels (Schwab *et al.*, 2012), in the present study, it was hypothesised that $V_m$ hyperpolarisation might change $[Ca^{2+}]_i$ in MDA-MB-231 cells. However, replacing extracellular NaCl with ChoCl to hyperpolarise the $V_m$, or blocking VGSCs using TTX did not cause significant changes to the $[Ca^{2+}]_i$, nor the number of cells that exhibit $Ca^{2+}$ spikes. Interestingly, unpublished data from Dr Scott Fraser (Imperial College London) presented at the 2015 Ion Channels, Transporters and Cancer meeting reported that at room temperature, MDA-MB-231 cells in ATP- and serum-free saline solution show spontaneous $Ca^{2+}$ spikes, measured using Fluo-4 as the $Ca^{2+}$ fluorescence indicator, and TTX reduced the occurrence and the magnitude of these $Ca^{2+}$ spikes (Fraser *et al.*, 2015). Furthermore, high KCl application at the end of the experiment caused a large increase in $[Ca^{2+}]_i$. Several factors may contribute to the disagreement with the data in this Chapter. Firstly, in contrast to Fura-2, Fluo-4 is a non-ratiometric $Ca^{2+}$ fluorescence indicator with a lower affinity ($K_d$ = 300 nM) (Gee *et al.*, 2000). Fluo-4 may be less sensitive than Fura-2 but does not chelate $[Ca^{2+}]_i$ as strongly as Fura-2 (Takahashi *et al.*, 1999). Hence, compared with Fura-2, Fluo-4 may be more suitable for recording

Ca$^{2+}$ activities that depend on free cytosolic Ca$^{2+}$, such as store-operated Ca$^{2+}$ entry (SOCE) through Ca$^{2+}$-release activated Ca$^{2+}$ (CRAC) channels (Takahashi *et al.*, 1999). Future experiments should directly compare these Ca$^{2+}$ fluorescence indicators. Secondly, the high KCl-induced Ca$^{2+}$ increase reported by Dr Fraser suggests the presence of depolarisation-induced Ca$^{2+}$ entry or release from stores. The machinery that carries the Ca$^{2+}$ influx in MDA-MB-231 cells needs to be further investigated. In the present study, VGCCs were not detected in MDA-MB-231 cells. The scenario that the Ca$^{2+}$ was released from the store is also unlikely, because as a low affinity Ca$^{2+}$ indicator, Fluo-4 can bind to Ca$^{2+}$ in organelles in the first place (Takahashi *et al.*, 1999; Lambert, 2006), therefore, any Ca$^{2+}$ release from the store/organelle should be reflected as redistribution rather than an increase of Fluo-4 signal intensity. Clearly, the link between VGSC/$V_m$ and [Ca$^{2+}$]$_i$ in MDA-MB-231 cells needs further investigation, using multiple Ca$^{2+}$ indicators.

### 4.3.2  BK$_{Ca}$ channels hyperpolarise the $V_m$ of MDA-MB-231 cells

Experiments in this Chapter investigated whether the depolarised $V_m$ *per se* is a functional factor in promoting cancer cell metastatic behaviours by modulating endogenous BK$_{Ca}$ channels. Unexpectedly, while searching for a suitable protocol to record the BK$_{Ca}$ current, a voltage-dependent persistent inward current was discovered in MDA-MB-231 cells when the [Ca$^{2+}$]$_i$ was buffered at 7.8 µM. The current is not sensitive to VGCC blockers nifedipine and Cd$^{2+}$, but is abolished by Ba$^{2+}$, which inhibits BK$_{Ca}$ channels. Other groups have also recorded similar inward current while studying BK$_{Ca}$ channels by applying [Ca$^{2+}$]$_i$ in the micromolar range (Cui *et al.*, 1997; Xia *et al.*, 2002), and mutations in the BK$_{Ca}$ intracellular regulator of the conductance of K$^+$ (RCK) domain abolish this inward current (Xia *et al.*, 2002). The persistent inward current may also be mediated by other types of Ca$^{2+}$-sensitive currents, such as Ca$^{2+}$-activated Cl$^-$

current and CRAC (Hartzell *et al.*, 2005; Motiani *et al.*, 2010). Future work is required to establish whether this inward current is a feature of endogenous $BK_{Ca}$ channels, or is due to indirect activation of another type of channel, e.g. ClC3 (Habela *et al.*, 2008).

In whole-cell patch clamp mode, by buffering the $[Ca^{2+}]$ in the intracellular solution to 100 nM, which is close to the physiological $[Ca^{2+}]_i$ reported in MDA-MB-231 cells (Sareen *et al.*, 2007; Winnicka *et al.*, 2008), $BK_{Ca}$ current can be recorded from MDA-MB-231 cells, in agreement with a previous study (Roger *et al.*, 2004). However, the perforated patch clamp technique leaves the $[Ca^{2+}]_i$ uncontaminated by components in the recording pipette, and this technique delivered better success rate in recording $BK_{Ca}$ currents from MDA-MB-231 cells. The current-voltage relationship obtained is similar to that reported previously (Roger *et al.*, 2004). Activating $BK_{Ca}$ channels using NS-1619 at various concentrations hyperpolarised the $V_m$. Interestingly, activating $BK_{Ca}$ channels in MDA-MB-231 cells using 40 µM NS-1619 yielded a $V_m$ at ~-52 mV, similar to that in non-tumourigenic mammary epithelial MCF-10A cells where various types of $K^+$ channels are present (Fraser *et al.*, 2005). This suggests that the depolarised $V_m$ (~-10 mV) recorded from MDA-MB-231 cells should be attributed to the $Na^+$ influx carried by VGSCs as well as the low activity of $V_m$-hyperpolarising $K^+$ channels.

### 4.3.3 $V_m$ hyperpolarisation does not inhibit MDA-MB-231 cell proliferation

Although $V_m$ can function as an instructive signal in promoting cell cycle progression, previous reports have shown that blocking VGSCs with TTX or phenytoin does not affect cancer cell proliferation *in vitro* (Roger *et al.*, 2003; Fraser *et al.*, 2005; Yang *et al.*, 2012; Aktas *et al.*, 2015). In the present study, hyperpolarising the $V_m$ using NS-1619 did not affect MDA-MB-231 cell proliferation. However, another study reported that NS-1619 at 50 µM reduced MDA-MB-231 cell growth by 40 % (Roger *et al.*, 2004). This discrepancy is probably due to the higher concentration and the

different incubation period adopted [5 days in (Roger *et al.,* 2004) vs. 1 day in the present study]. Since $V_m$ hyperpolarisation inhibits MDA-MB-231 cell migration (Section 4.2.7), the cell colonies may expand more slowly and therefore longer incubation leads to higher cell population density, which may induce contact inhibition of proliferation and locomotion, as well as apoptosis (Bates *et al.,* 1994). Future work needs to determine whether in MDA-MB-231 cells, $V_m$ regulates cell proliferation in a cell-density dependent manner.

In rat cerebellar neurones, $V_m$-dependent cell cycle progression is partly dependent on promoting the activity of VGCCs that trigger downstream $Ca^{2+}$ signalling by carrying $Ca^{2+}$ influx upon $V_m$ depolarisation (Borodinsky & Fiszman, 1998). However, in MDA-MB-231 cells, there is no evidence showing the presence of VGCCs. In addition, $Ca^{2+}$ imaging data show that $V_m$ hyperpolarisation, which is thought to be able to increase the driving force of $Ca^{2+}$ entry, does not significantly alter the $[Ca^{2+}]_i$ of MDA-MB-231 cells (Section 4.2.2), suggesting $V_m$ may not play an important role in $Ca^{2+}$-dependent proliferation of MDA-MB-231 cells.


### 4.3.4  $V_m$ hyperpolarisation reduces migration but not invasion

In MDA-MB-231 cells, $V_m$ depolarisation caused by VGSCs promotes cell motility, because TTX (30 µM) or NS-1619 (1 µM) hyperpolarised the $V_m$ to a similar degree and decreased migration to comparable levels. Activating $BK_{Ca}$ channels has been previously reported to reduce migration of glioma cells, although the molecular mechanism was unclear (Bordey *et al.,* 2000; Kraft *et al.,* 2003). However, another study using the same 1321N glioma cells as in Kraft *et al.,* 2003 demonstrated that inhibiting $BK_{Ca}$ channels reduced cell transwell migration (Weaver *et al.,* 2004). The authors proposed that this is because $BK_{Ca}$ channel activity is necessary for regulating cell volume (Schwab *et al.,* 1994; Weskamp *et al.,* 2000; Schwab, 2001), which is

important while the cells are migrating through the 8 µm-sized pores on the polyethylene terephthalate membrane. In this Chapter, ptychography was used to measure the change in MDA-MB-231 cell volume in wound healing assays, and 1 µM NS-1619 did not significantly alter the cell volume compared to control. Therefore, it is possible that the role of $BK_{Ca}$ channels in controlling cell volume is more significant in transwell migration than in lateral migration.

Interestingly, the inactivation of $BK_{Ca}$ channels in MDA-MB-231 cells grown on monolayers of human brain microvasculature endothelial HCMEC/D3 cells reduced transendothelial migration (Khaitan *et al.*, 2009). This suggests that the functionality of $BK_{Ca}$ channels during MDA-MB-231 cell migration is dependent on the culture conditions and the extracellular environment. MDA-MB-231 cell invasion was not affected by hyperpolarising the $V_m$ using NS-1619, however, TTX reduced invasion by ~42 % (Section 4.2.8), consistent with previous reports (Fraser *et al.*, 2005; Brackenbury *et al.*, 2007). Thus, the data in this Chapter suggest that VGSCs control MDA-MB-231 cell migration and invasion via different pathways: VGSC-mediated $V_m$ depolarisation promotes cell migration, whereas $Na^+$ itself may lead to a more invasive phenotype in MDA-MB-231 cells, independent of regulating the $V_m$. Indeed, a model previously proposed by Dr Sebastien Roger's group argues that $Na^+$ allosterically regulates NHE1 at the MDA-MB-231 cell plasma membrane, which acidifies extracellular pH and therefore promotes cysteine cathepsin B and S proteolytic activity, leading to a more invasive phenotype (Gillet *et al.*, 2009; Brisson *et al.*, 2011).

### 4.3.5 $V_m$ hyperpolarisation reduces the active Rac1 level at the leading edge

The relationship between VGSCs and small GTPase Rac1 was recently reported, where researchers demonstrated that in ATP-stimulated microglia, VGSCs increased

[Ca$^{2+}$]$_i$ via NCX and subsequently activated ERK and Rac1, which led to migration (Persson *et al.*, 2014). However, data here show that in MDA-MB-231 cells, hyperpolarising the V$_m$ using TTX and NS-1619 both reduced the active Rac1 level at the cell leading edge, but the [Ca$^{2+}$]$_i$ did not significantly change after ChoCl or TTX treatment. This suggests that NCX activity may not be involved in the V$_m$-dependent [Ca$^{2+}$]$_i$ regulation in the context of MDA-MB-231 cells, and Rac1 may be regulated by V$_m$/VGSCs but not Ca$^{2+}$.

The VGSC-V$_m$-Rac1 signalling axis fits well in a previously proposed model in MDA-MB-231 cells in which VGSCs potentiate the phosphorylation of src kinase and cortactin (Brisson *et al.*, 2013). Src kinase can promote cortactin phosphorylation via Rac1 activation (Head *et al.*, 2003; Servitja *et al.*, 2003), which ultimately facilitates lamellipodia formation by activating the Arp2/3 complex (Miki *et al.*, 1998; Krueger *et al.*, 2003). Interestingly, it has been reported that VGSC activity caused the activation of the small GTPase Rap1B in SW620 cells (House *et al.*, 2015). Further experiments should explore whether the activation of Rap1B is due to the V$_m$-depolarising role of VGSCs in these cells.

The detailed mechanism by which V$_m$ regulates Rac1 activation and/or distribution is not yet clear. V$_m$ may regulate Rac1 activity via controlling GEFs, For example, GEF-H1 (a Rho GEF) is activated upon V$_m$ depolarisation (Waheed *et al.*, 2010). In addition, the V$_m$ depolarisation-induced activation of Ras and Rap1 has been reported in mouse cortical neurones (Baldassa *et al.*, 2003). In PC12 cells, V$_m$ depolarisation activates Ras in a PKA-dependent manner (Obara *et al.*, 2007). Given that VGSCs activate PKA in MDA-MB-231 and Mat-LyLu cells (Brackenbury & Djamgoz, 2006; Chioni *et al.*, 2010), activation of Rac1 may be through this pathway. More recently, a study has demonstrated that V$_m$ depolarisation enhances phosphatidylserine and K-Ras nanoclustering in baby hamster kidney cells, and K-Ras nanoclustering upon V$_m$ depolarisation activates the MAPK signalling pathway (Zhou *et*

*al.*, 2015). Taken together, emerging data suggest that a depolarised $V_m$ is a functional signal in activating small GTPases. It may consequently and/or concurrently promote the MAPK signalling pathway, which in turn controls key cellular behaviours including proliferation, differentiation and development (Shaul & Seger, 2007).

## 4.4 Conclusion

The data in this Chapter show that $V_m$ hyperpolarisation and blockade of VGSC have no impact on $[Ca^{2+}]_i$ of MDA-MB-231 cells. Modulating the $V_m$ using TTX and NS-1619 has revealed a role for $V_m$ depolarisation in promoting migration but not invasion of MDA-MB-231 cells. TTX and NS-1619 both reduce lamellipodium formation and cause a round morphology in these cells, likely through reducing the active Rac1 level at the leading edge of lamellipodia (Figure 4.18). Further studies should elucidate the detailed molecular mechanism(s) by which a depolarised $V_m$ activates Rac1 in BCa cells.
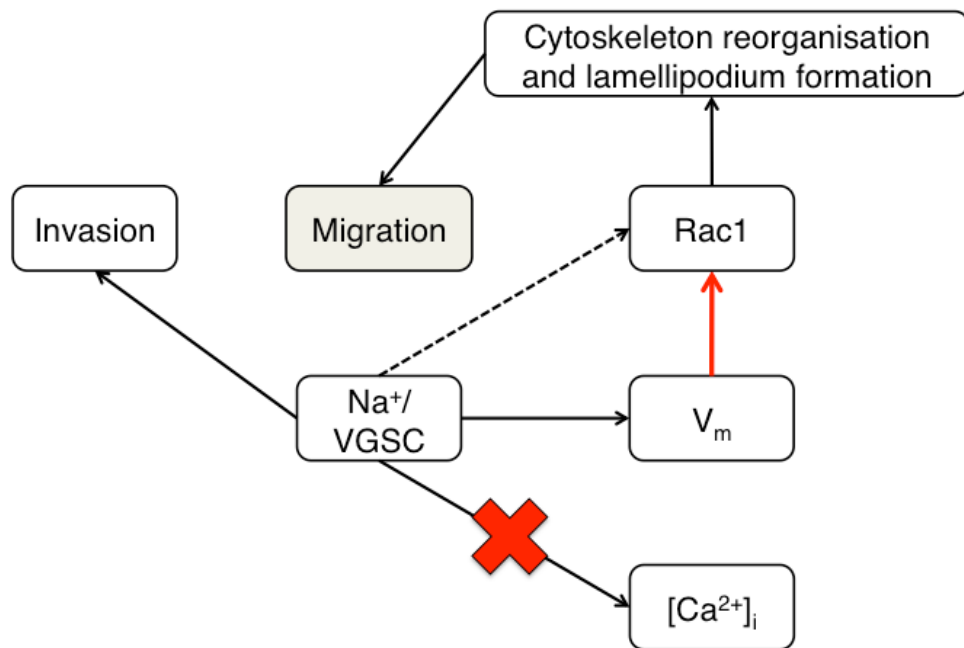
Figure 4.18. Depolarised membrane potential ($V_m$) increases MDA-MB-231 cell migration.

This Chapter demonstrated that blocking voltage-gated Na$^+$ channels (VGSCs) or hyperpolarising the $V_m$ does not change intracellular Ca$^{2+}$ concentration ([Ca$^{2+}$]$_i$, red cross). However, VGSC activity and depolarised $V_m$ promotes lamellipodium formation and cell migration by increasing active Rac1 level at MDA-MB-231 cell leading edge (red arrow). Whether Na$^+$/VGSC regulates Rac1 activity independent of $V_m$ is not clear (dashed line). Figure is adapted from (Yang & Brackenbury, 2013).

# Chapter 5: Investigating the $I_{Na}$ and $V_m$ in tumour tissue slices

## 5.1 Introduction

$Na^+$ accumulation in tumour cells was reported in the 1980s: X-ray microanalyses of freeze-dried tissue sections revealed that cancer cells have a higher $[Na^+]_i$: the mean $[Na^+]_i$ of H6 mouse hepatoma, 7777 rat hepatoma, C3H mouse adenocarcinoma and 13762 HF rat adenocarcinoma is 451 mmol/kg in freeze-dried tissue sections, which is significantly higher than that in their non-cancerous counterparts (138 mmol/kg) (Cameron *et al.*, 1980). In addition, rapidly proliferating cells, including neonatal mouse cardiomyocytes and rat thymus cortex cells, have significantly higher $[Na^+]_i$ (196 mmol/kg) than slowly proliferating cells, such as rat thymus medulla and mouse/rat mammary epithelial cells (140 mmol/kg), but have significantly lower $[Na^+]_i$ than cancer cells (Cameron *et al.*, 1980). Electron probe X-ray analysis revealed that daily injection of amiloride to H6 hepatoma-bearing mice reduces intranuclear $[Na^+]_i$ from 499 mmol/kg to 275 mmol/kg and significantly decreases tumour growth (Sparks *et al.*, 1983). In *Xenopus laevis*, $Na^+$ accumulation appears in regions where cells over-proliferate (Lobikin *et al.*, 2012). Moreover, quantitative magnetic resonance imaging (MRI) has shown that the total tissue $Na^+$ concentration in patients' BCa lesions is 53 mmol/l, which is significantly elevated compared to benign lesions (26 mmol/l) (Ouwerkerk *et al.*, 2007).

How $Na^+$ accumulates in cancer cells is not clear. Recently, it is reported that VGSCs increase the $[Na^+]_i$ in lung cancer cells: compared to VGSC-expressing H460 NSCLC cells, the $[Na^+]_i$ of VGSC-lacking normal NL-20 cells or non-invasive A549 cells is significantly lower (Roger *et al.*, 2007; Campbell *et al.*, 2013). Blocking VGSCs in H460 cells with TTX reduces the $[Na^+]_i$ from 22.3 mM to 10.8 mM (Campbell *et al.*, 2013). Therefore, considering the correlation between increased $[Na^+]_i$ and

tumourigenesis (Pool *et al.*, 1981; Sparks *et al.*, 1983), it is possible that the high malignancy of MDA-MB-231 cells may be partly due to a high $[Na^+]_i$ caused by VGSCs. Indeed, VGSCs increase MDA-MB-231 cell migration by depolarising the $V_m$, but $Na^+$ *per se* may be important in potentiating cell invasion. Thus, it is likely that VGSCs may also regulate $[Na^+]_i$ in MDA-MB-231 cells.

In mouse BCa models, inhibiting $Na_v1.5$ with phenytoin or ranolazine reduces tumour growth (Nelson *et al.*, 2015a) and metastasis (Yildirim *et al.*, 2012; Driffort *et al.*, 2014; Nelson *et al.*, 2015a; Nelson *et al.*, 2015b). Together with the *in vitro* data (Fraser *et al.*, 2005; Brackenbury *et al.*, 2007; Yang *et al.*, 2012), these studies suggest that VGSCs may be potential therapeutic targets in cancer treatment. However, the functional activity of VGSCs in tumours *in vivo* has not been explored. In this Chapter, whole-cell slice recording, which has been frequently used to study neuronal activities in the brain (Blanton *et al.*, 1989), was performed on BCa tissue slices to study the $I_{Na}$ and $V_m$ in cancer cells *ex vivo*. The whole-cell recording technique has been previously used in slices to investigate the electrophysiological properties of single cancer cells. For example, $Cl^-$ currents were recorded in human glioma cells in patient tissue slices (Ullrich *et al.*, 1998), and action potentials were recorded from human oligodendroglioma and oligoastrocytoma cells in brain slices (Patt *et al.*, 1996). However, VGSC activity in BCa cells in tissue slices has not been studied.

A previous study used sharp electrode to measure the $V_m$ of human breast cells in slices from biopsies and reported that the $V_m$ is significantly more depolarised in biopsies from patients who are diagnosed with infiltrating ductal carcinoma compared to patients with benign breast disease (Marino *et al.*, 1994). The same study also showed that in comparison to normal fibroblasts, chemically transformed fibroblasts have more depolarised $V_m$ (Marino *et al.*, 1994). In *Xenopus laevis*, $V_m$ depolarisation can induce tumourigenesis *in vivo* (Lobikin *et al.*, 2012). During development, melanocytes with artificially depolarised $V_m$ exhibit a neoplastic phenotype in the tadpole neural crest,

including over-proliferation, arborized cell morphology and increased local invasion (Blackiston *et al.*, 2011). It is proposed that depolarised $V_m$ increases serotonin export at the melanocyte plasma membrane, resulting in an increase in serotonin concentration in the extracellular microenvironment. Serotonin receptors on nearby melanocytes and on pituitary melanotrope cells are then activated, increasing the expression of TFs, including *Sox10* and *Slug*, ultimately resulting in cellular over-proliferation (Lobikin *et al.*, 2015).

Given the functional expression of VGSCs in MDA-MB-231 cells *in vitro*, $I_{Na}$ carried by VGSCs should also be present in MDA-MB-231 tumour xenografts *in vivo*. Additionally, since the depolarised $V_m$ and $Na^+$ influx have pro-migratory and pro-invasive roles *in vitro*, cancer cells at the periphery of tumour tissue may have larger $I_{Na}$ and/or more depolarised $V_m$ during their invasion into surrounding non-tumour tissue.

### 5.1.1 Hypotheses and aims

The hypotheses in this Chapter were (1) VGSCs regulate $[Na^+]_i$ in MDA-MB-231 cells *in vitro*, and (2) VGSCs are functionally active *in vivo*. The aims in this Chapter were:

(1)  To use the $Na^+$ reporting fluorescent probe SBFI to measure the steady-state $[Na^+]_i$ of MDA-MB-231 cells.

(2)  To measure the $[Na^+]_i$ after extracellular $Na^+$ depletion, TTX or NS-1619 treatment.

(3)  To record the $I_{Na}$ and $V_m$ across various regions of mouse MDA-MB-231 primary tumour tissue.

(4)  To compare the tumour growth in shRNA control- and $Na_v1.5$-shRNA-bearing mice.

## 5.2 Results

### 5.2.1 Measurement of $[Na^+]_i$ in MDA-MB-231 cells *in vitro*

Tumour cells have higher $[Na^+]_i$ compared with normal cell types (Cameron *et al.*, 1980). VGSCs in MDA-MB-231 cells carry $I_{Na}$, but whether VGSCs regulate the $[Na^+]_i$ of MDA-MB-231 cells has not been investigated. Here, SBFI was used as the intracellular $Na^+$ fluorescent indicator to measure the $[Na^+]_i$. SBFI is a ratiometric $Na^+$-selective dye with $K_d$ for $Na^+$ of 7.4 mM in the presence of $K^+$ (Minta & Tsien, 1989). Upon $Na^+$ binding, SBFI shows an increase in the ratio of energy absorbed at 340 nm and 380 nm (Minta & Tsien, 1989). MDA-MB-231 cells were labelled with 5 μM SBFI in DMEM supplemented with 5 % FBS at 37 °C in the dark before being transferred to standard PSS for 2 min (Figure 5.1a). SBFI was alternately excited at 340 and 380 nm and the fluorescence emission at 512 nm was monitored using a Nikon Eclipse TE200 epi-fluorescence microscope as described in Section 2.9 (Figure 5.1b, top panel). After the incubation with the standard extracellular PSS, cells were treated with extracellular solution containing 10 mM $Na^+$ for 2 min in order to let the cells settle in a low $[Na^+]_o$ environment, before being consecutively perfused with 10 mM $Na^+$ extracellular solution plus 20 μM $Na^+$ ionophore gramicidin for 12 min, and then extracellular solution containing 20 mM $Na^+$ plus 20 μM gramicidin for a further 12 min (Figure 5.1a).

As shown in Figure 5.1b, cells in the 20 mM $Na^+$ PSS showed increased 340/380 ratio compared to 10 mM $Na^+$ PSS, indicating an increase of $[Na^+]_i$ . Cells had higher 340/380 ratio in standard PSS than in 10 mM $Na^+$ PSS, but lower than in 20 mM $Na^+$ PSS, suggesting that the $[Na^+]_i$ in standard PSS is between 10 mM and 20 mM. The $[Na^+]_i$ was determined for individual cells. Figure 5.1c shows the calculation of $[Na^+]_i$ in a representative cell. The mean 340/380 ratios over the last 60 s of PSS, 10 mM and 20 mM $Na^+$ extracellular solution treatment were 1.31, 1.23 and 1.34, respectively. A linear relationship between 340/380 ratio and $[Na^+]_i$ was derived by plotting $[Na^+]_i$ at 10 mM and 20 mM with the corresponding 340/380 ratios, giving:

**a**

Standard PSS → 10 mM Na$^+$ → 10 mM Na$^+$ + gramicidin → 20 mM Na$^+$ + gramicidin

2 min — 2 min — 12 min — 12 min

**b**

Excitation = 340 nm    Excitation = 380 nm

Standard PSS

10 mM Na$^+$ + gramicidin

20 mM Na$^+$ + gramicidin

**c**

340/380 ratio vs [Na$^+$]$_i$ (mM)
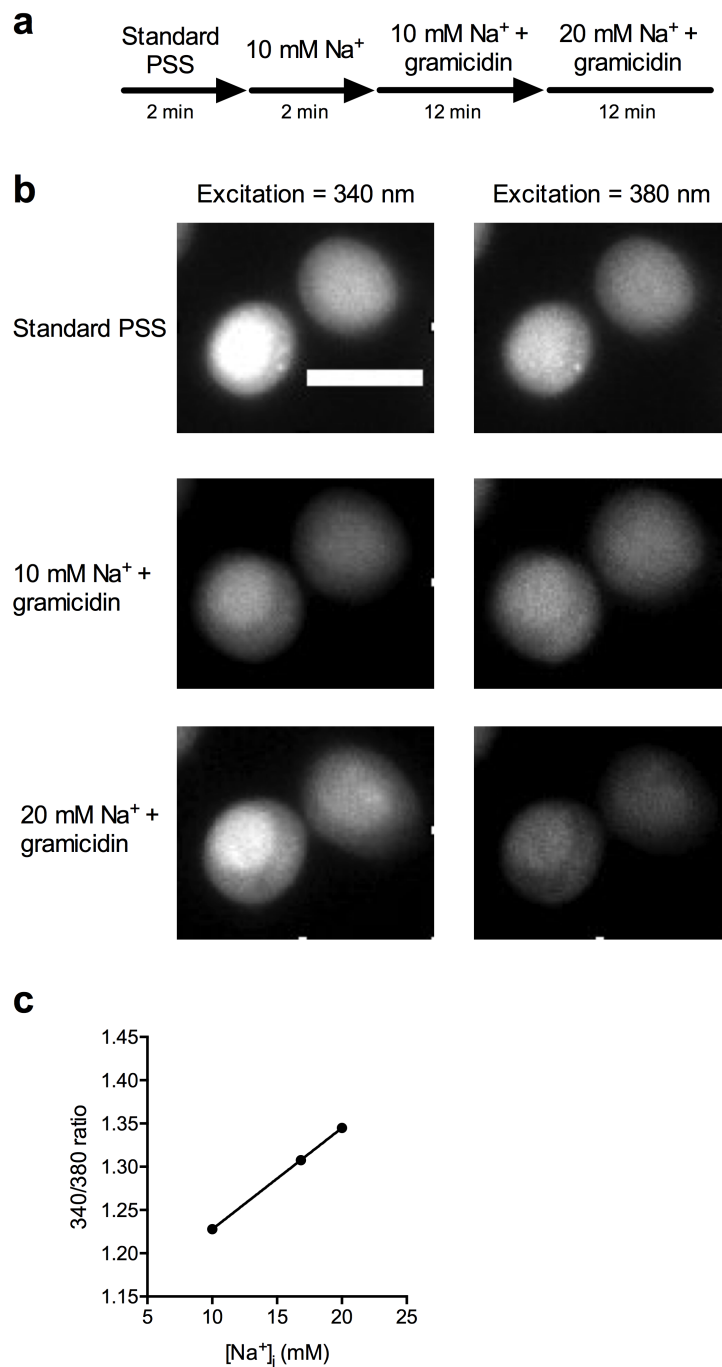
Figure 5.1. Measurement of intracellular Na$^+$ concentration ([Na$^+$]$_i$) of MDA-MB-231 cells.

(**a**) Na$^+$ imaging experimental outline. (**b**) Representative SBFI fluorescence intensity at excitation = 340 nm and 380 nm when cells were perfused with standard PSS (top panel), extracellular solution containing 10 mM Na$^+$ plus 20 µM gramicidin (middle panel) and extracellular solution containing 20 mM Na$^+$ plus 20 µM gramicidin (bottom panel). (**c**) Relationship between SBFI fluorescence intensity (340/380 ratio) and [Na$^+$]$_i$ in a representative cell. Scale bar = 10 µm.

$$340/380 \ ratio = \ 0.01171 \times [Na^+]_i + 1.111 \qquad \text{(Equation 5.1)}$$

Hence, the $[Na^+]_i$ of the cell in standard PSS was calculated as $(1.31 - 1.111) \div 0.01171$ = 17.0 mM for this cell. Six technical repeats were performed. In each repeat, $[Na^+]_i$ of 8 - 20 cells was calculated individually and averaged in each of the experiment, giving a steady-state $[Na^+]_i$ of MDA-MB-231 cells of 15.6 ± 0.7 mM (Figure 5.2b; n = 6).

Next, the effect of replacing extracellular NaCl with NMDG on the $[Na^+]_i$ of MDA-MB-231 cells was investigated. After labelling the cells with SBFI (5 µM), cells were immediately transferred to NMDG saline solution where NaCl was replaced with equimolar NMDG. After 2 min, cells were consecutively perfused with 10 mM $Na^+$ extracellular solution for 2 min, 10 mM $Na^+$ extracellular solution plus 20 µM gramicidin for 12 min, and 20 mM $Na^+$ extracellular solution plus 20 µM gramicidin for 12 min (Figure 5.2a). The 340/380 ratios were obtained, and the $[Na^+]_i$ was calculated as described above. The steady-state $[Na^+]_i$ of MDA-MB-231 cells after extracellular $Na^+$ depletion was 7.6 ± 1.7 mM, which was significantly lower than in control (Figure 5.2; P < 0.05; ANOVA with Tukey *post hoc* test; n = 6 in standard PSS and n = 3 in NMDG).

The effect of VGSC activity on $[Na^+]_i$ in MDA-MB-231 cells was also examined. Cells were pre-incubated with 30 µM TTX for 48 h before imaging. TTX was also present during the labelling the cells with SBFI and in the first 2 min after the cells were perfused with standard PSS. TTX was then washed out with 10 mM $Na^+$ extracellular solution before 10 mM and 20 mM $Na^+$ PSS plus gramicidin were consecutively applied. Compared with standard PSS, TTX significantly reduced the steady-state $[Na^+]_i$ of MDA-MB-231 cells from 15.6 ± 0.7 mM to 11.3 ± 0.5 mM (Figure 5.2b; P < 0.05; ANOVA with Tukey *post hoc* test; n = 6 in standard PSS and n = 3 in TTX). However, the $[Na^+]_i$ of MDA-MB-231 cells was not significantly different comparing TTX and NMDG treatment (Figure 5.2b; P = 0.08; ANOVA with Tukey *post hoc* test; n = 3 in both conditions). In

**a**

Standard PSS → 10 mM Na$^+$ → 10 mM Na$^+$ + gramicidin → 20 mM Na$^+$ + gramicidin

2 min — 2 min — 12 min — 12 min

NMDG → 10 mM Na$^+$ → 10 mM Na$^+$ + gramicidin → 20 mM Na$^+$ + gramicidin

2 min — 2 min — 12 min — 12 min

TTX ⋯ → TTX → 10 mM Na$^+$ → 10 mM Na$^+$ + gramicidin → 20 mM Na$^+$ + gramicidin

48 h — 2 min — 2 min — 12 min — 12 min

**b**
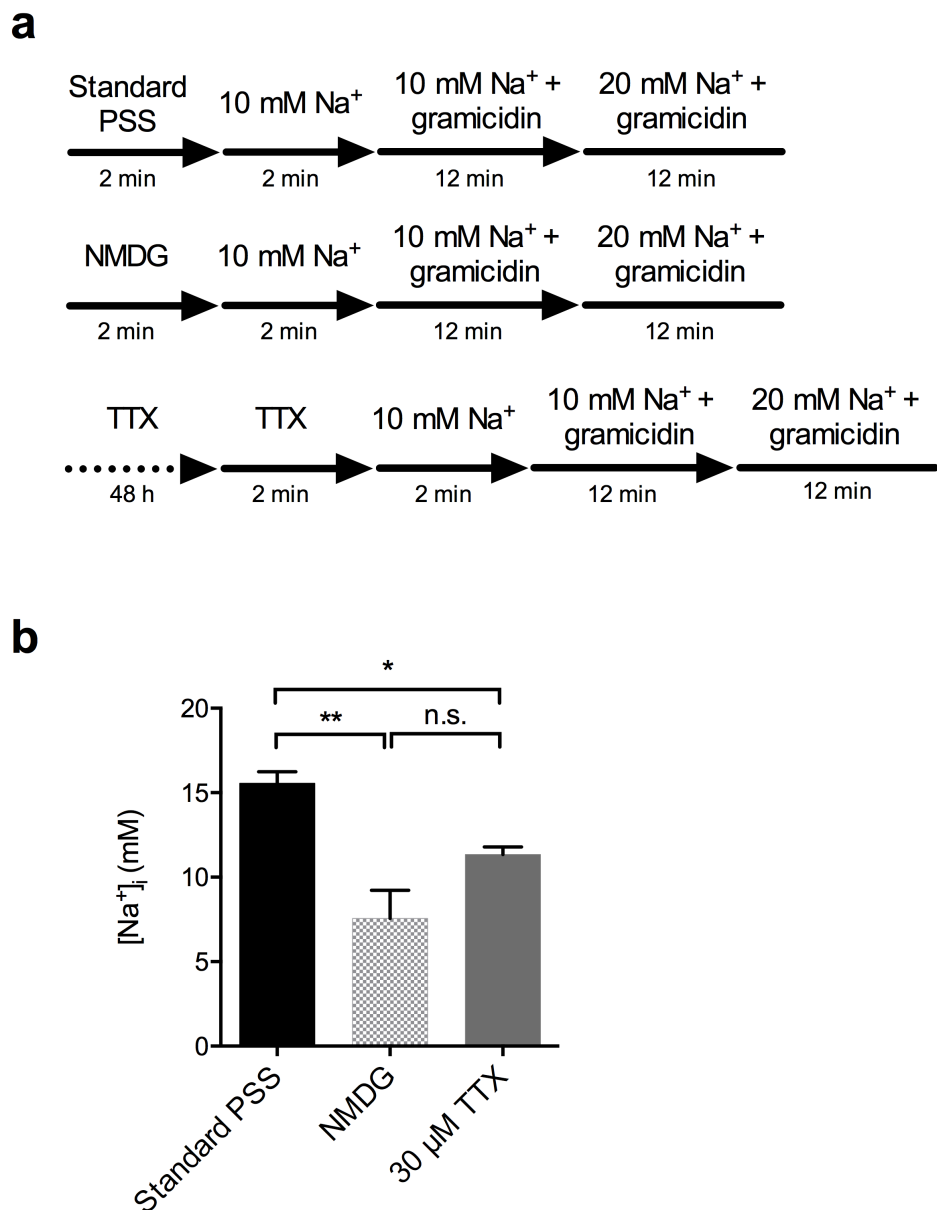


Figure 5.2. Depletion of extracellular Na$^+$ and tetrodotoxin (TTX) pre-treatment reduced the Na$^+$ concentration ([Na$^+$]$_i$) of MDA-MB-231 cells.

(**a**) Na$^+$ imaging experimental outline. Cells were perfused with N-methyl-D-glucamine (NMDG)-containing extracellular solution or TTX (30 µM) for 2 min, before perfusion in 10 mM Na$^+$ extracellular solution and then gramicidin-containing extracellular solutions. For TTX, cells were pre-incubated with 30 µM TTX for 48 h. (**b**) The comparison of the steady-state [Na$^+$]$_i$ in standard extracellular physiological saline solution (PSS), in NMDG extracellular solution, and after TTX (30 µM) treatment. (*) $P < 0.05$; (**) $P < 0.01$; ANOVA with Tukey *post hoc* test (n = 6 in standard PSS and n = 3 in NMDG and TTX). Data are mean ± SEM.

summary, extracellular $Na^+$ depletion and incubation with TTX (30 µM) both reduced the $[Na^+]_i$.

## 5.2.2 Suppressing $Na_v1.5$ expression using shRNA reduces $[Na^+]_i$ in MDA-MB-231 cells

The steady-state $[Na^+]_i$ of $Na_v1.5$-shRNA and shRNA control cells was measured as described in Section 5.2.1. The $[Na^+]_i$ of shRNA control and $Na_v1.5$-shRNA cells was 13.5 ± 0.4 mM and 9.4 ± 0.7 mV (n = 3 in both conditions), respectively, showing a significant difference (Figure 5.3; P < 0.01; t-test; n = 3 in both conditions). Therefore, these data suggest that $Na_v1.5$, by carrying a sustained $Na^+$ influx, causes an increase in the steady-state $[Na^+]_i$ in MDA-MB-231 cells.

## 5.2.3 NS1619 (1 µM) does not significantly alter the $[Na^+]_i$ in MDA-MB-231 cells

Both 30 µM TTX and 1 µM NS-1619 hyperpolarised the $V_m$ of MDA-MB-231 cells to a similar degree, and $V_m$ hyperpolarisation inhibited cell migration and reduced active Rac1 levels at cell leading edge (Section 4.3.5), suggesting that VGSCs potentiate MDA-MB-231 cell migration by depolarising the $V_m$. In order to investigate whether 1 µM NS-1619 hyperpolarises the $V_m$ without altering $[Na^+]_i$, SBFI-labelled MDA-MB-231 cells were perfused with 1 µM NS-1619 for 5 min (Figure 5.4a). The mean $[Na^+]_i$ both before and after NS-1619 treatment was 14.3 ± 1.0 mM (Figure 5.4b; P = 0.93; t-test; n = 22 from three technical repeats). In summary, in MDA-MB-231 cells, depleting extracellular $Na^+$ or blocking VGSCs reduced $[Na^+]_i$. Importantly, NS-1619 (1 µM) did not significantly change $[Na^+]_i$. Thus, the inhibitory role of NS-1619 (1 µM) on MDA-MB-231 cell migration (Section 4.2.7) is achieved via $V_m$ hyperpolarisation and not $[Na^+]_i$ regulation.

**a**

| Standard PSS | 10 mM Na$^+$ | 10 mM Na$^+$ + gramicidin | 20 mM Na$^+$ + gramicidin |
|:---:|:---:|:---:|:---:|
| 2 min | 2 min | 12 min | 12 min |
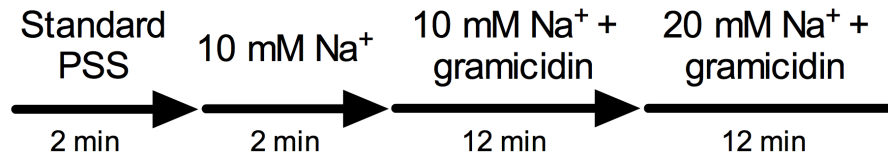
**b**
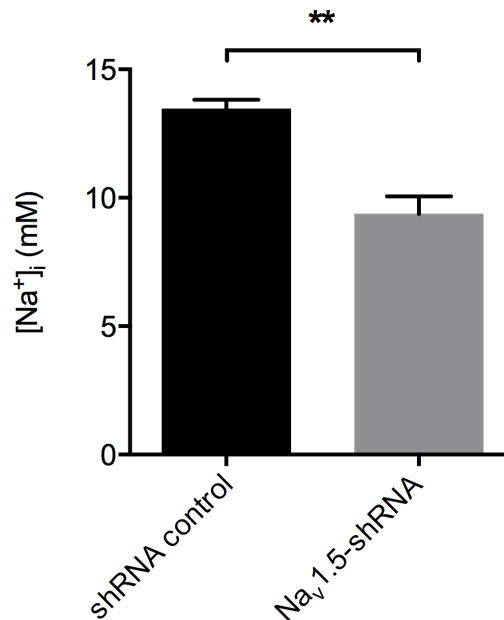


Figure 5.3. The intracellular Na$^+$ concentration ($[Na^+]_i$) of MDA-MB-231 cells is reduced when Na$_v$1.5 expression is suppressed by shRNA.

(**a**) Na$^+$ imaging experimental outline. Cells were perfused with standard saline solution (PSS) for 2 min before settled in 10 mM Na$^+$ extracellular solution and being perfused with gramicidin-containing extracellular solutions (**b**) The steady-state $[Na^+]_i$ of MDA-MB-231 cells where Na$_v$1.5 expression was suppressed by shRNA (Na$_v$1.5-shRNA), and the scrambled RNA control (shRNA control). (**) $P < 0.01$; t-test (n = 3 in both conditions). Data are mean ± SEM.

**a**

Standard PSS → 1 μM NS-1619 → 10 mM Na$^+$ → 10 mM Na$^+$ + gramicidin → 20 mM Na$^+$ + gramicidin

2 min | 5 min | 2 min | 12 min | 12 min
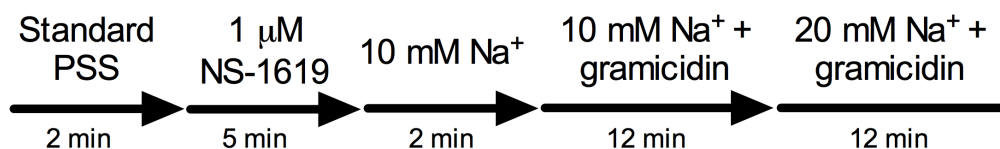
**b**
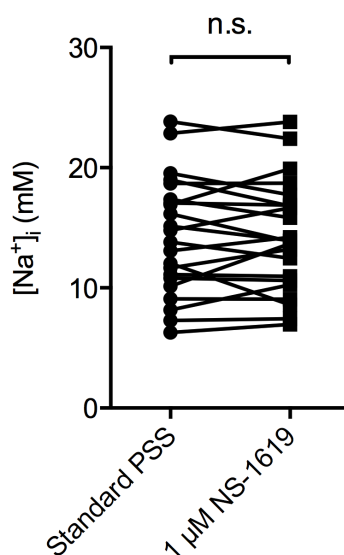


Figure 5.4. NS-1619 (1 μM) application does not change the intracellular Na$^+$ concentration ([Na$^+$]$_i$) in MDA-MB-231 cells.

(**a**) Na$^+$ imaging experimental outline. Cells were treated with standard PSS (2 min) followed by 1 μM NS-1619 (5 min), before perfusion with 10 mM Na$^+$ extracellular solution and then gramicidin-containing extracellular solutions. (**b**) [Na$^+$]$_i$ of individual MDA-MB-231 cells after NS-1619 (1 μM) treatment. n.s. not significant; t-test (n = 22 cells from three technical repeats). Data are mean only.

### 5.2.4 Recording the $I_{Na}$ and $V_m$ from cells in tumour tissue slices

Although many *in vitro* studies have recorded the $I_{Na}$ carried by VGSCs from cancer cells with different tissue origins, functional VGSC activity has not been studied in intact tumour tissue before. Here, the whole-cell patch clamp technique was used to study the $I_{Na}$ and $V_m$ of shRNA control cells xenografted in mice. GFP-expressing shRNA control cells were mixed with Matrigel/PBS and were orthotopically injected in the fourth left inguinal fat pad (Section 2.3.3). Tumours were allowed to grow for 20–37 days before being removed following euthanisation (Figure 5.5a). The fur and surrounding muscle tissue were gently removed from the tumour using a blade (Figure 5.5b), and the processed tumour was fixed onto the pedestal of a vibratome using cyanoacrylate glue and was immersed in ice-cold standard extracellular PSS (Figure 5.5c). A 5 % agar block was fixed onto the pedestal to support the tumour (Figure 5.5c), and the tumour was sliced at 250 µm. Tumour slices were incubated in the standard extracellular PSS at room temperature for at least 20 min before being transferred into the electrophysiology recording chamber and tightly held using a slice anchor (Figure 5.5d). The slice was continuously perfused with standard PSS. The tumour slice was firstly examined at 10X (Figure 5.5e). Next, healthy, GFP-positive cells were located at 40X before they were sealed with recording pipette containing $Cs^+$-free standard intracellular solution (Figure 5.5f).

Similar to shRNA control cells recorded *in vitro*, tumour cells showed fast inward $I_{Na}$ *ex vivo*. The current-voltage relationship from a representative cell is shown in (Figure 5.6a and b). Among all the 60 cells recorded from 18 mice across six cages, 39 cells (65 %) showed detectable $I_{Na}$. The current was inhibited by applying 30 µM TTX (Figure 5.6c; n = 3), and was recovered after subsequent washout using the standard extracellular PSS (Figure 5.6d; n = 3), suggesting that the fast inward current is carried by VGSCs. The current-voltage relationship of all the cells with $I_{Na}$ is shown in Figure 5.6e (n = 39). The relationships between $I_{Na}$ conductance/availability and voltage were
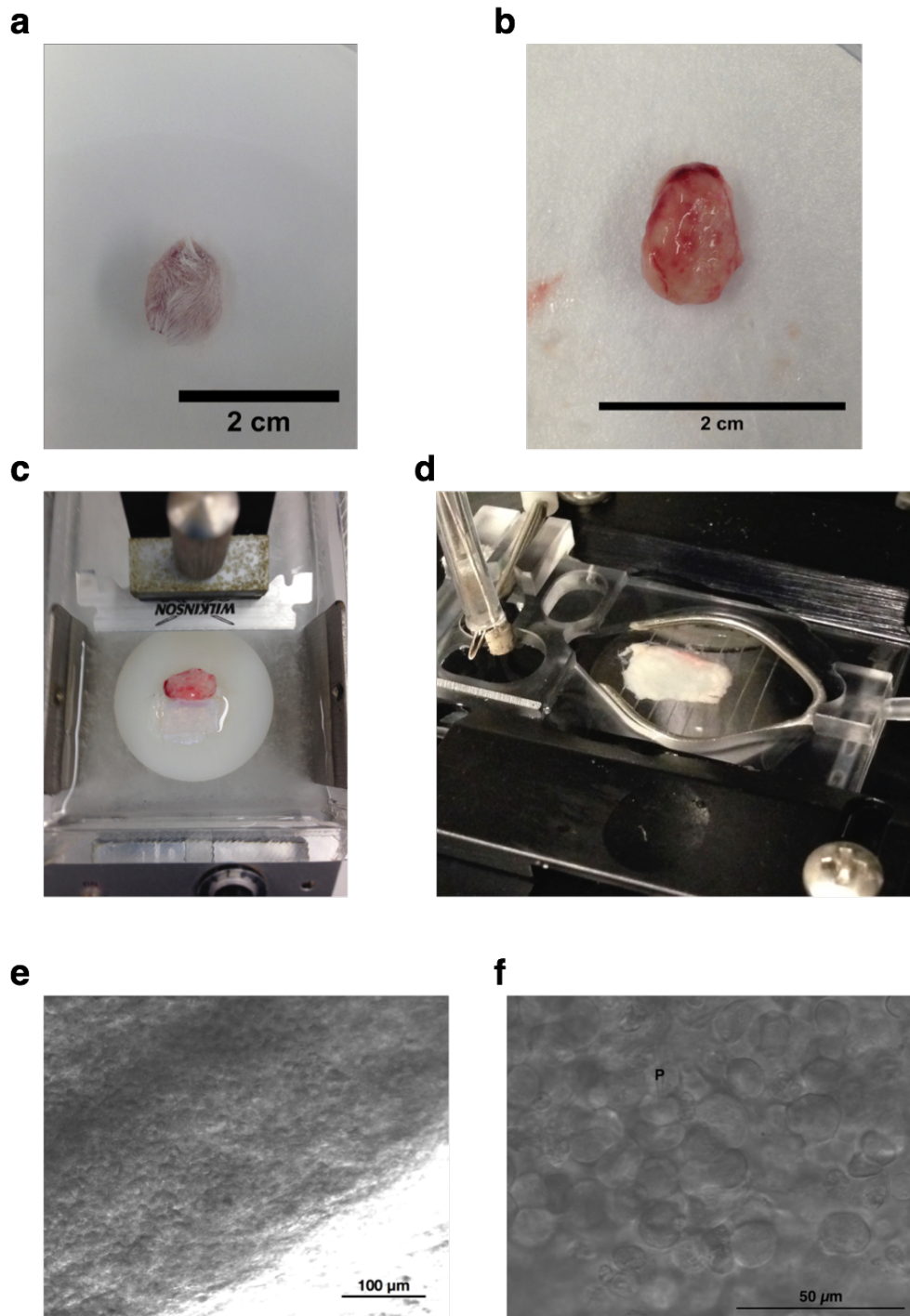
Figure 5.5. Performing electrophysiological study on mouse tumour tissue slices.

Tumour tissue was processed, sliced and mounted on an electrophysiology recording chamber. (**a**) The primary tumour was dissected from a euthanised mouse. (**b**) The fur and surrounding muscle tissue were removed from the tumour using a blade. (**c**) The tumour was fixed onto the pedestal of vibratome and was immersed in ice-cold physiological saline solution (PSS). (**d**) Tumour was sliced and incubated with PSS in a holding chamber at room temperature at least 20 min before being transferred to the electrophysiology recording chamber, and held with a slice anchor. (**e** and **f**) Bright field images of tumour tissue at 10X (e) and 40X (f). P in (f) shows the recording pipette.

fitted with Boltzmann functions (Figure 5.6f): the $V_{1/2}$ and the k for the conductance curve were -27.2 ± 1.4 mV and 3.9 ± 0.5 mV (n = 39), respectively. For the availability curve, $V_{1/2}$ was -87.4 ± 2.4 mV and the k was -0.7 ± 2.2 mV (n = 12).

The relationship between peak $I_{Na}$ density and the number of days following tumour implantation was also investigated (Figure 5.7a). The linear regression shows that the number of days after surgery did not correlate with size of the peak $I_{Na}$ density (Figure 5.7a; Pearson r = 0.27; P = 0.09; n = 39). Moreover, the size of tumours did not correlate with peak $I_{Na}$ density (Figure 5.7b; Pearson r = 0.11; P = 0.49; n = 39).

Compared with recording shRNA control cells cultured *in vitro*, tumour cells *in vivo* had subtly different electrophysiological properties. To begin with, the whole-cell capacitance recorded from cells on tissue slices was 11.7 ± 0.5 pF, which is significantly less than that recorded *in vitro* (23.1 ± 2.0 pF; Figure 5.8a; P < 0.001; t-test; n = 8 in *in vitro* and n = 60 in *ex vivo*). Since whole-cell capacitance is determined by cell surface area (Hille, 2001), the data suggest that compared with *in vitro* 2D culture, the average size of cells was significantly smaller when growing *in vivo*. However, the peak $I_{Na}$ density was not significantly different comparing *in vitro* and *ex vivo* (-14.9 ± 2.1 pA/pF vs. -11.8 ± 1.6 pA/pF; Figure 5.8b; P = 0.39; n = 8 in *in vitro* and 39 in *ex vivo*). Interestingly, the $V_m$ of cells on tissue slices was more depolarised than for *in vitro* recordings (-7.8 ± 0.5 mV vs. -12.6 ± 0.9 mV; Figure 5.8c; P < 0.001; n = 16 in *in vitro* and 60 in *ex vivo*).
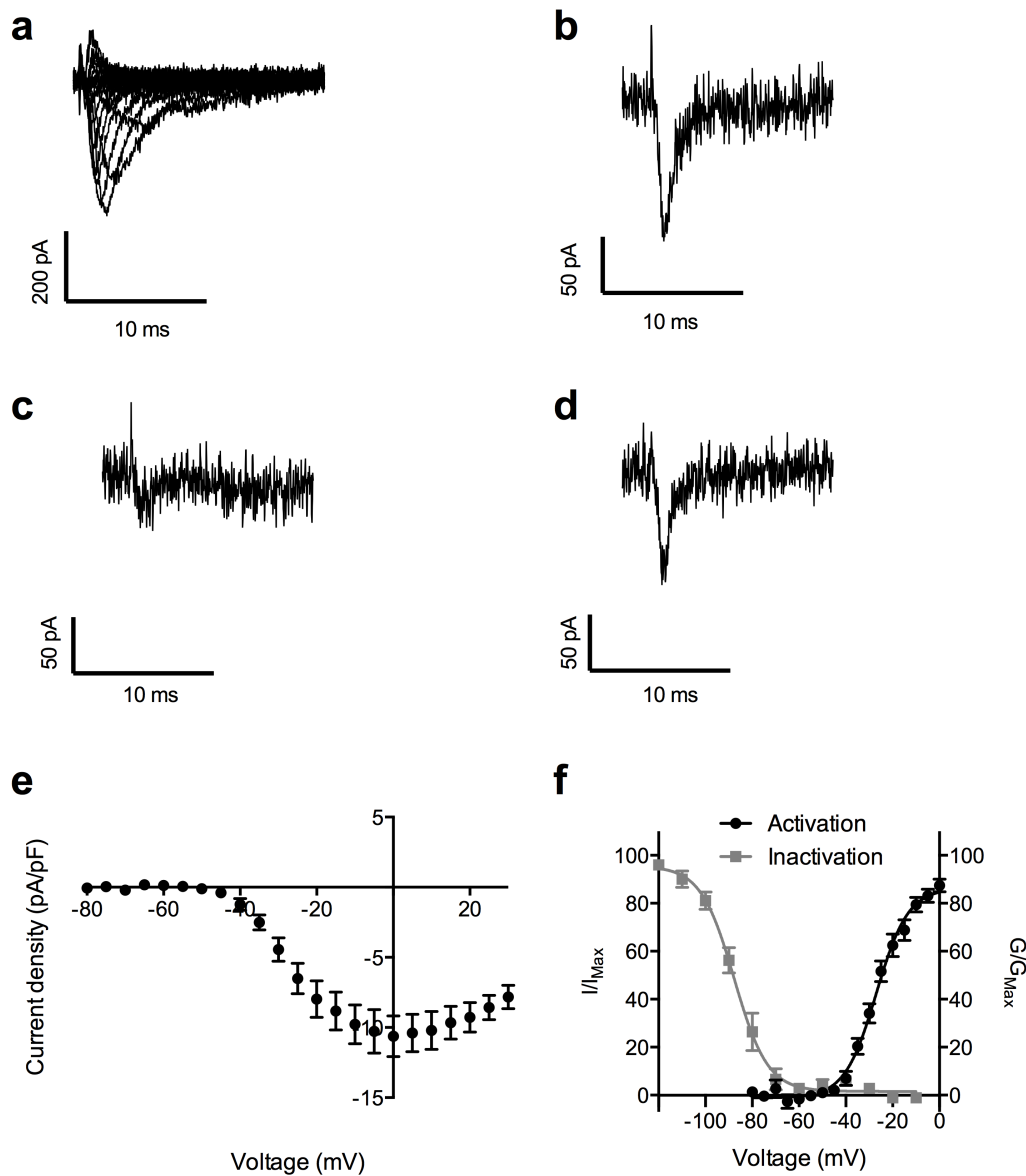
Figure 5.6. Na$^+$ current (I$_{Na}$) recorded from tumour tissue slices.

(a) I$_{Na}$ recorded from a representative cell from a tumour tissue slice. (b) The fast inward current was abolished by (c) TTX (30 µM) application, and (d) the current was recovered after subsequent washout. (e) The current-voltage relationship of I$_{Na}$ recorded (n = 39; 18 mice from six independent cages). (f) Normalised I$_{Na}$ availability and conductance plotted against voltage. Data are fitted with Boltzmann functions (n = 39 in conductance and 14 in availability). For (a), (e) and activation in (f), cells were depolarised from a -120 mV pre-pulse (250 ms) to voltages between -80 and 0 mV for 50 ms in 5 mV increments. For inactivation in (f), cells were held at various pre-pulses ranging from -120 mV to -10 mV for 250 ms before depolarisation to -10 mV for 50 ms. Data are mean ± SEM in (e) and (f).
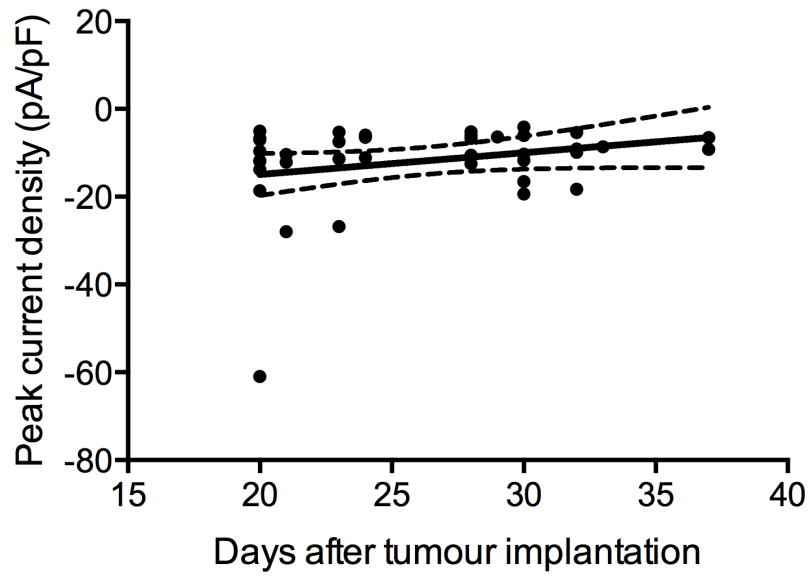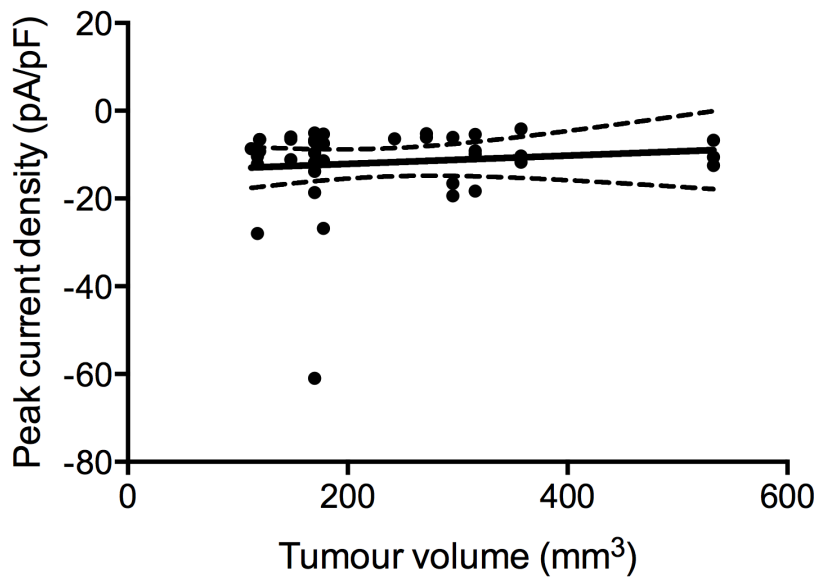
Figure 5.7. The relationship between tumour volume/stage and peak Na$^+$ current ($I_{Na}$) density.

(**a**) The relationship between peak $I_{Na}$ density and the number of days after tumour implantation (n = 39). (**b**) The relationship between peak $I_{Na}$ density and tumour volume (n = 39). Solid line shows linear regression and broken lines 95 % confidence intervals. Pearson r = 0.27 (P = 0.09) in (a), and Pearson r = 0.11 (P = 0.49) in (b).
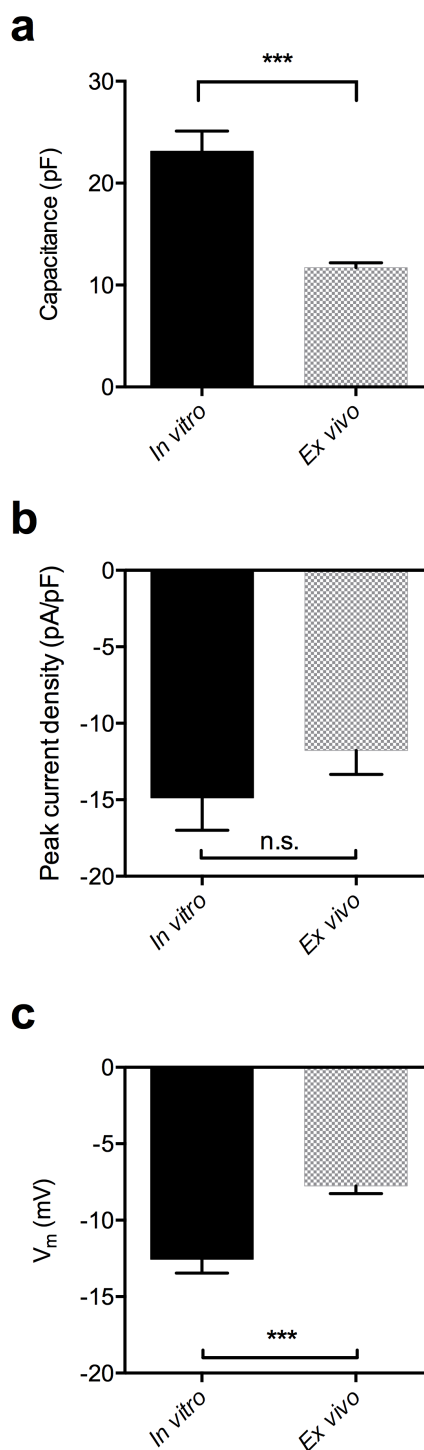
Figure 5.8. Cell capacitance, Na⁺ current ($I_{Na}$) density and membrane potential ($V_m$) *in vitro* and *ex vivo*.

The comparison of (**a**) cell capacitance, (**b**) peak $I_{Na}$ density and (**c**) $V_m$ recorded using whole cell patch clamp *in vitro* and *ex vivo*. (\*\*\*) P < 0.001. n.s. not significant; t-test. (a) n = 8 in *in vitro* and n = 60 in *ex vivo.* (b) n = 8 in *in vitro* and n = 39 in *ex vivo.* (c) n = 16 in *in vitro* and n = 60 in *ex vivo.* Liquid junction potential is compensated in (c). Data are mean ± SEM.

### 5.2.5  Investigating the $I_{Na}$ from cells across various regions of the tumour

Previously published *in vitro* evidence shows that VGSCs potentiate local invasion of MDA-MB-231 cells by enhancing the activity of cysteine cathepsins B and S (Gillet *et al.,* 2009; Brisson *et al.,* 2013). Additionally, VGSCs increase MDA-MB-231 cell motility by depolarising the cell $V_m$ (Section 4.2.7). Therefore, since $I_{Na}/V_m$ lead to cancer cell migration and invasion, next, the $I_{Na}$ and $V_m$ were compared across central and peripheral regions of orthotopic primary tumours of shRNA control cells.

Slices from primary tumours were categorised into three regions, namely periphery, intermediate region and centre, according to distance from the edge of the tumour. The distance between recorded cells and the tumour edge was determined using an eyepiece reticule. Cells that were ≤ 1 mm from the edge were categorised as in the periphery; those > 1mm and ≤ 1.5 mm as in the intermediate region; and those ≥ 1.5 mm as in the centre (Figure 5.9a). The whole-cell capacitance was 11.8 ± 0.6 pF, 11.4 ± 0.9 pF and 12.1 ± 1.1 pF in periphery, intermediate region and centre, respectively, showing no statistically significant difference across regions (Figure 5.9b; P = 0.87; ANOVA with Tukey *post hoc* test; n = 25, 20 and 15, respectively). Moreover, the peak $I_{Na}$ density in the periphery was -11.44 ± 1.3 pA/pF, which was not different from that in the intermediate region (-12.44 ± 4.3 pA/pF) or in the centre (-10.9 ± 1.8 pA/pF; P = 0.93; ANOVA with Tukey *post hoc* test; n = 20, 12 and 7, respectively).

The $I_{Na}$ conductance and availability in the periphery (Figure 5.10a; n = 20 in activation and n = 3 in inactivation), the intermediate region (Figure 5.10b; n = 12 in activation and n = 3 in inactivation) and centre (Figure 5.10c; n = 7 in activation and n = 3 in inactivation) were analysed by plotting the normalised $I_{Na}$ or conductance against voltage. The activation/inactivation $V_{1/2}$ and slope factor k did not differ across tumour regions (Table 5.1; ANOVA with Tukey *post hoc* test; conductance: n = 20, 12 and 7 in periphery, intermediate region and centre; availability: n = 3 in all these regions).
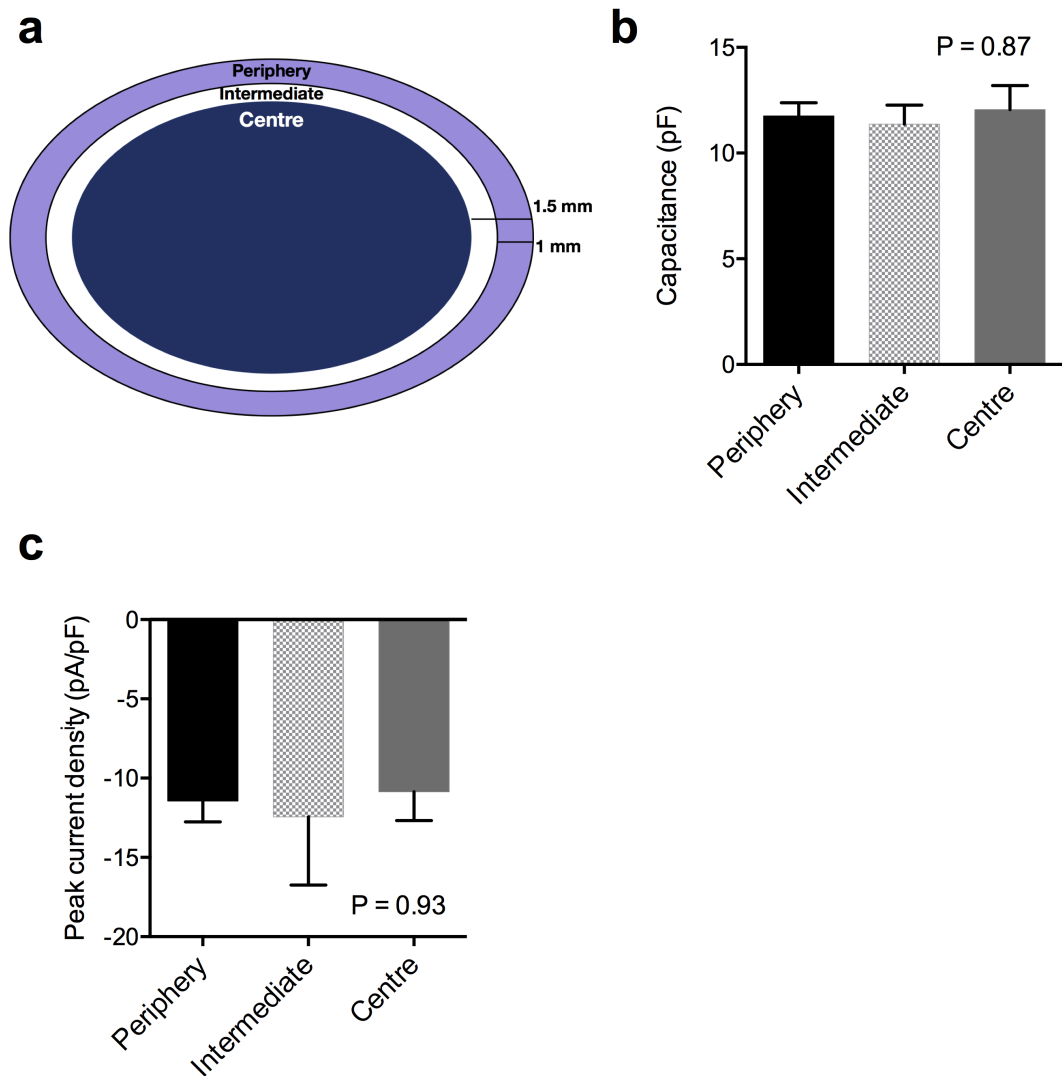
Figure 5.9. Na$^+$ current (I$_{Na}$) density across various regions of tumour tissue slices.

(**a**) Diagram showing the definition of the periphery ($\leq$ 1 mm from the edge of tumour tissue slice), intermediate region (> 1 and $\leq$ 1.5 mm from the edge of tissue slice) and centre (> 1.5 mm from the edge) regions of the tumour. (**b**) Comparison of whole-cell capacitance and (**c**) peak I$_{Na}$ density across the periphery, intermediate region and centre of tumour. ANOVA with Tukey *post hoc* test. n = 25, 20 and 15 in periphery, intermediate region and centre, respectively).
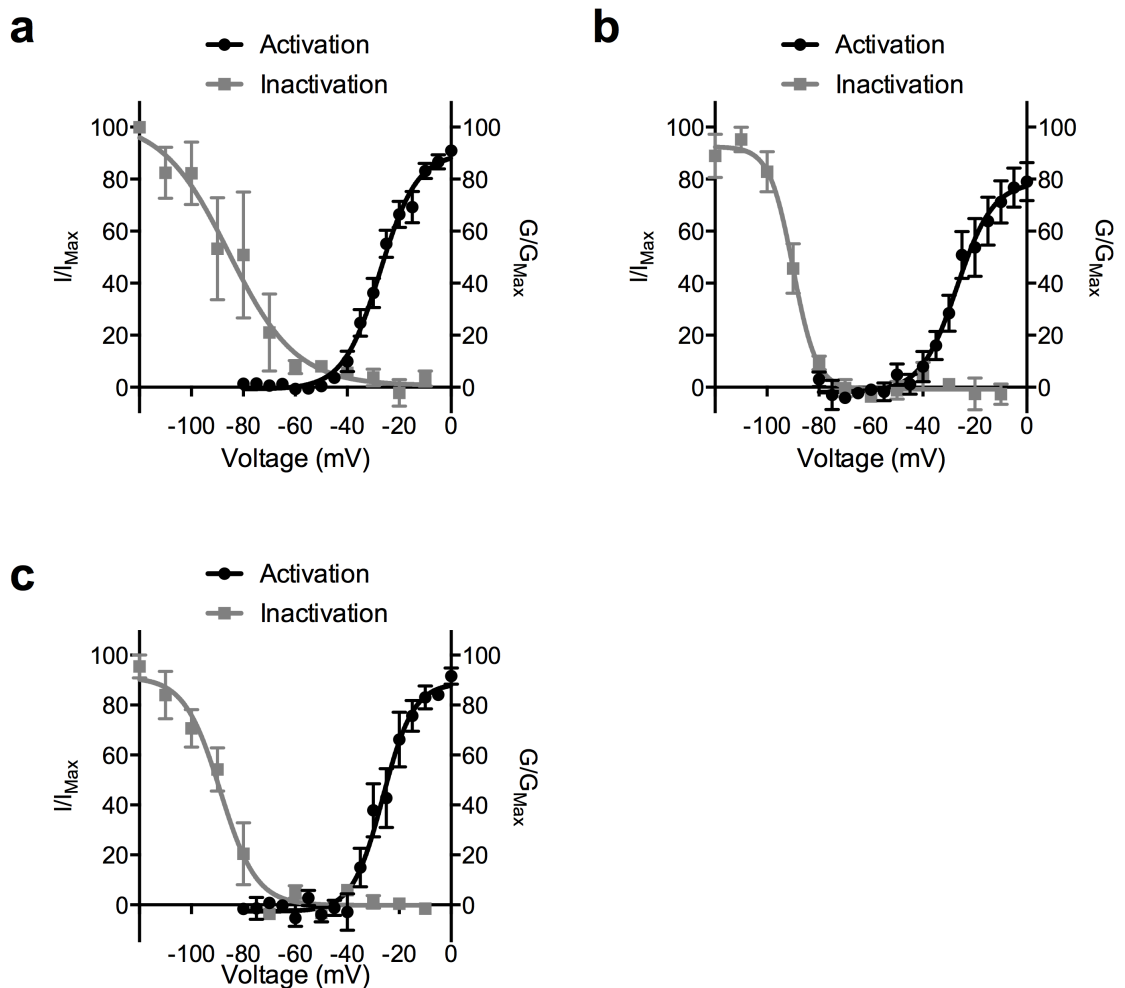
Figure 5.10. Na$^+$ current (I$_{Na}$) availability and conductance across various regions of tumour tissue slices.

The normalised I$_{Na}$ availability and conductance in the (**a**) periphery, (**b**) intermediate region and the (**c**) centre plotted against voltage. Data are fitted with Boltzmann functions. (a) n = 20 in conductance and 3 in availability. (b) n = 12 in conductance and 3 in availability. (c) n = 7 in conductance and n = 3 in availability. For activation, cells were depolarised from a -120 mV pre-pulse (250 ms) to voltages between -80 mV and +30 mV for 50 ms in 5 mV increments. For inactivation, cells were held at various voltages ranging from -120 mV to -10 mV for 250 ms before depolarisation to -10 mV for 50 ms. Data are mean ± SEM.

| Table 5.1 Characteristics of Na$^+$ current recorded in various tumour regions. | | | | |
|---|---|---|---|---|
| | **Periphery** | **Intermediate region** | **Centre** | **P** |
| **$V_a$ (mV)** | -31.0 ± 1.8 | -27.9 ± 3.1 | -27.9 ± 0.4 | 0.55 |
| **$V_p$ (mV)** | 9.8 ± 1.9 | 10.0 ± 3.4 | 9.3 ± 3.2 | 0.99 |
| **$T_p$ at 0 mV (ms)** | 1.41 ± 0.11 | 1.51 ± 0.41 | 1.01 ± 0.11 | 0.56 |
| **Activation $V_{1/2}$ (mV)** | -27.3 ± 0.9 | -26.9 ± 1.8 | -26.2 ± 1.8 | 0.88 |
| **Activation k (mV)** | 7.1 ± 0.8 | 7.0 ± 1.5 | 5.7 ± 1.5 | 0.74 |
| **Inactivation $V_{1/2}$ (mV)** | -85.6 ± 6.1 | -90.0 ± 1.0 | -89.1 ± 1.5 | 0.69 |
| **Inactivation k (mV)** | -13.0 ± 5.1 | -4.5 ± 1.0 | -5.9 ± 1.3 | 0.20 |
| $V_a$, activation voltage; $V_p$ voltage at current peak; $T_p$ time to peak; $V_{1/2}$, half activation or inactivation voltage; k: slope factor. Periphery: ≤ 1 mm from tumour edge; intermediate region: > 1 mm and ≤ 1.5 mm from the edge; centre: > 1.5 mm from the edge. ANOVA with Tukey *post hoc* test. Data are mean ± SEM. | | | | |

Other $I_{Na}$ characteristics including the activation voltage $V_a$, voltage at peak current $V_p$ and time to peak $T_p$ at 0 mV were not significantly different across the three tumour regions (Table 5.1; ANOVA with Tukey *post hoc* test; n = 20, 12 and 7 in periphery, intermediate and centre). Finally, the proportion of cells that had $I_{Na}$ was not significantly different across the three regions (Table 5.2; Fisher's exact tests with Bonferroni corrections). In summary, the data suggest that the whole-cell capacitance, peak $I_{Na}$ density, as well as the $I_{Na}$ characteristics, were not significantly different across various tumour regions.

### 5.2.6 Investigating the $V_m$ from cells across various regions of mouse primary tumour

The $V_m$ recorded from cells in orthotopic tumours is significantly more depolarised than cells cultured *in vitro* (Section 5.2.4). Next, the $V_m$ across the tumour periphery, intermediate region and centre was analysed. The $V_m$ was highly consistent across the three regions: cells in the periphery had a $V_m$ of -7.6 ± 0.6 mV (n = 26), and the $V_m$ of cells in the intermediate region and centre was -8.8 ± 1.3 mV (n = 18) and -7.2 ± 0.3 mV (n = 10), respectively (Figure 5.11; P = 0.53; ANOVA with Tukey *post hoc* test). The data suggest that in tumour tissues, the level of cell $V_m$ does not correlate with the position of the cell.

| Table 5.2. The proportion of cells with $Na^+$ current ($I_{Na}$) across tumour regions. | | | |
|---|---|---|---|
| | **Periphery** | **Intermediate region** | **Centre** |
| **Number of cells with $I_{Na}$** | 20 | 12 | 7 |
| **Number of cells without $I_{Na}$** | 6 | 6 | 9 |
| **Total** | 26 | 18 | 16 |
| Periphery: ≤ 1 mm from tumour edge; intermediate region: > 1 mm and ≤ 1.5 mm from the edge; centre: > 1.5 mm from the edge. No statistical difference in the proportions of cells with $I_{Na}$ across the regions. Fisher's exact test with Bonferroni corrections. | | | |
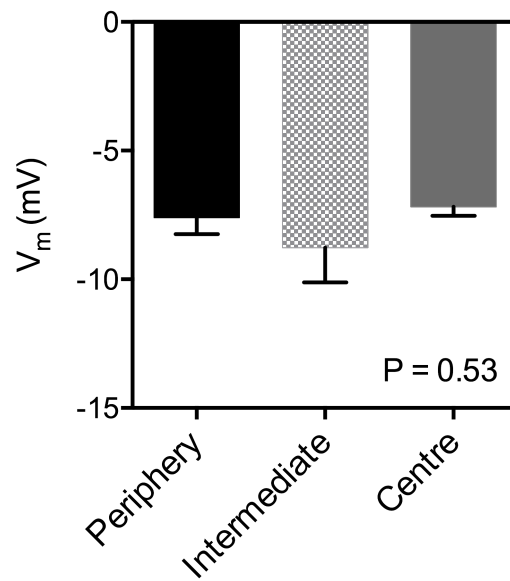
Figure 5.11. The tumour cell membrane potential ($V_m$) at various regions across orthotopic tumours.

The $V_m$ was measured using whole-cell patch clamp. Periphery: ≤ 1 mm from tumour edge; intermediate region: > 1 mm and ≤ 1.5 mm from the edge; centre: > 1.5 mm from the edge. ANOVA with Tukey *post hoc* test. n = 26, 18 and 10 in periphery, intermediate and centre, respectively. Data are mean ± SEM.

### 5.2.7  Na$_v$1.5-shRNA cells showed reduced tumour growth in mice

Blocking VGSCs decreases cancer cell migration and invasion *in vitro* (Brackenbury, 2012; Roger *et al.*, 2015). Recently, an increasing number of *in vivo* studies has demonstrated the potential therapeutic value of VGSCs in cancer treatment. For example, we have previously reported that using an orthotopic BCa model where MDA-MB-231 cells were implanted into mouse mammary fat pads, daily intraperitoneal injection of phenytoin reduced primary tumour growth and invasion and inhibited metastasis to lungs, liver and spleen (Nelson *et al.*, 2015a). Here, the effect of Na$_v$1.5 on tumour growth was investigated. The dimensions of the tumour (length and width) were determined using calliper measurement, and the volume of the tumour was calculated using Equation 2.2.

Mice developed palpable tumours typically 8–9 days after the surgery. As shown in Figure 5.12, two weeks following tumour cell implantation, the primary tumour development in Na$_v$1.5-shRNA cell-bearing mice was significantly less than in mice implanted with shRNA control cells. At the end of the experiment (typically 28 days after surgery), the tumour volume was $327.0 \pm 21.2$ mm$^3$ in mice with shRNA control cells and $155.3 \pm 18.4$ mm$^3$ in mice bearing Na$_v$1.5-shRNA cells (Figure 5.12; $P < 0.001$; t-test; n = 13 for shRNA control and n = 16 for Na$_v$1.5-shRNA cells). Therefore, Na$_v$1.5 promotes primary tumour growth *in vivo*.
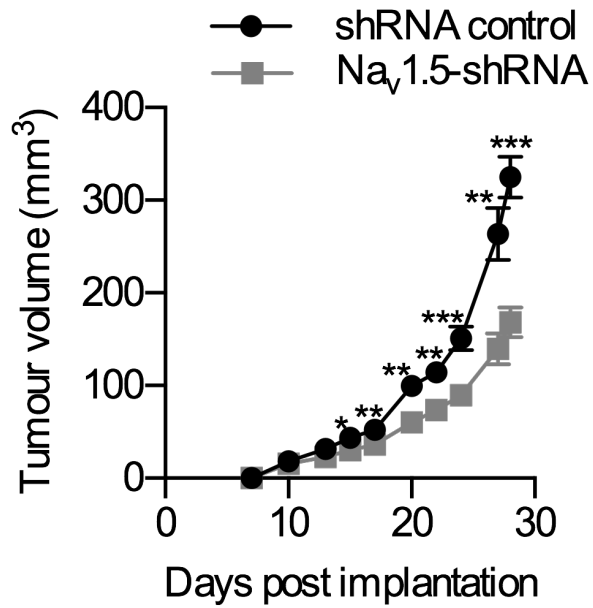
Figure 5.12. Suppressing $Na_v1.5$ expression using shRNA reduces primary tumour growth *in vivo*.

$Na_v1.5$-shRNA or shRNA control MDA-MB-231 cells ($5 \times 10^5$) were orthotopically implanted under the fourth left inguinal fat pad in immunodeficient mice. The dimensions of the tumour were measured using callipers, and the tumour volume was calculated as volume = 0.5 × (length × width$^2$). (*) $P < 0.05$; (**) $P < 0.01$; (***) $P < 0.001$; t-test (n = 13 and n = 16 in shRNA control and $Na_v1.5$-shRNA, respectively). Data are mean ± SEM.

## 5.3   Discussion

### 5.3.1   VGSCs increase [Na$^+$]$_i$ in MDA-MB-231 cells

Cancer cells are reported to have higher [Na$^+$]$_i$ compared to normal cells (Cone & Tongier, 1973; Smith *et al.*, 1978; Cameron *et al.*, 1980), and the implication of high [Na$^+$]$_i$ in tumourigenesis and/or mitogenesis has been reported since the late 1970's (Smith *et al.*, 1978; Pool *et al.*, 1981; Sparks *et al.*, 1983). Recently, quantitative Na$^+$ MRI has shown that the total tissue Na$^+$ concentration is higher in malignant BCa tissues than in benign lesions (Ouwerkerk *et al.*, 2007). In this Chapter, pre-incubation with 30 µM TTX for 48 h, or Na$_v$1.5 knockdown with shRNA both showed a similar reduction in [Na$^+$]$_i$ compared to controls, suggesting that VGSCs result in Na$^+$ accumulation in MDA-MB-231 cells. The result agrees with other studies on H460 NSCLC cells where VGSCs are expressed (Roger *et al.*, 2007; Campbell *et al.*, 2013). MDA-MB-231 cells treated with NMDG showed further but not statistically significant [Na$^+$]$_i$ reduction than reported in the TTX and Na$_v$1.5-shRNA experiment, suggesting that VGSCs are the predominant pathway that causes Na$^+$ accumulation in MDA-MB-231 cells. Future experiments should investigate how other Na$^+$ transporters, such as NHE1 (Brisson *et al.*, 2011), regulate [Na$^+$]$_i$, and whether or not leak I$_{Na}$ or ENaC are present in MDA-MB-231 cells and increase [Na$^+$]$_i$ (Kellenberger & Schild, 2002).

According to the Goldman-Hodgkin-Katz equation (Equation 1.1), increased [Na$^+$]$_i$ is an important factor that contributes to the depolarised V$_m$ in MDA-MB-231 cells. A calculation using the Nernst equation predicts that the reduced [Na$^+$]$_i$ (from 15.6 mM to 7.6 mM) after NMDG treatment would lead to a hyperpolarising shift in the Na$^+$ equilibrium potential of -18.3 mV, which is close to the V$_m$ hyperpolarisation (~-15 mV) recorded using whole-cell patch clamp technique (Section 3.2.1). However, the calculated V$_m$ hyperpolarisation based on the decreased [Na$^+$]$_i$ in TTX-treated cells and shRNA control cells is -8.2 mV and -12.8 mV, respectively, which is more than 2-fold greater than the electrophysiology data (Section 3.2.3 and Section 3.2.6). This may be

due to the limited resolution of SBFI and/or epi-fluorescence microscopy when determining changes in $[Na^+]_i$ at a few mV. Future experiments should address this discrepancy by using alternative $Na^+$-sensitive fluorescent indicator, using a confocal microscope, or using methods that are more sensitive to small changes in the $[Na^+]_i$, such as the intracellular ion-selective microelectrode (ISME) technique (Shattock & Bers, 1989).

A recent study showed that $Na^+$ accumulated at the "regeneration bud" during tail regeneration in *Xenopus laevis* (Tseng *et al.*, 2010). In the tadpole tail amputation model, application of the $Na^+$ ionophore monensin with $Na^+$ gluconate increased the level of MSX-1, a regenerative marker, at the wound, and eventually facilitated the regrowth of limbs at the amputation site (Tseng & Levin, 2013). Using the same animal model, high local $[Na^+]$ can be indicative of tumourigenesis *in vivo* (Lobikin *et al.*, 2012). Together, the evidence suggests a role for $[Na^+]_i$ in intracellular signalling. Indeed, data in Section 4.2.7 suggest that it was the $Na^+$ ions, rather than $V_m$, that increased the invasiveness of MDA-MB-231 cells *in vitro.* This agrees with the previously proposed $Na_v1.5$-$Na^+$-NHE1-cathepsin pathway in MDA-MB-231 cell invasion (Gillet *et al.*, 2009; Brisson *et al.*, 2011). Furthermore, $Na^+$ carried by VGSCs can also enhance the activity of NCX in microglia, which ultimately leads to $[Ca^{2+}]_i$ increase and ERK activation (Pappalardo *et al.*, 2014b; Persson *et al.*, 2014). In THP-1 macrophages, activating $Na_v1.6$ with veratridine increases $Na^+$ release from cationic vesicular compartments, which then increases mitochondrial $Ca^{2+}$ release via NCX (Carrithers *et al.*, 2009). Finally, how the increased $[Na^+]_i$ regulates the activity of other $Na^+$-related ion transporters and exchangers remains unclear in cancer cells. For example, in rat kidney tubules, $[Na^+]_i$ increases $Na^+$-$K^+$ ATPase activity and cell surface expression in a PKA-dependent manner (Vinciguerra *et al.,* 2003). Future experiments should address the potential $Na^+$-dependent regulation of transmembrane transportation of various types of ions and their role in downstream intracellular signals in cancer cells.

Considering the role of the depolarised $V_m$ in promoting cancer cell migration (Section 4.2.7) and the role of $Na^+$ in inducing tumourigenesis and cancer cell invasion, further experiments should explore whether combining $V_m$ hyperpolarisation with $[Na^+]_i$ reduction can reduce the malignancy of cancer cells both *in vitro* and *in vivo*. Data in Section 3.2.1 and Section 5.2.1 demonstrated the impact of the extracellular environment on $[Na^+]_i$ and $V_m$: MDA-MB-231 cells in a $Na^+$-free environment displayed significant $[Na^+]_i$ reduction as well as hyperpolarised $V_m$. The clinical value of reducing $[Na^+]_o$ in patient tumour tissue during cancer treatment should be investigated in the future.

### 5.3.2 Recording the $I_{Na}$ in tumour tissue

An increasing number of reports demonstrate the presence of VGSCs in various types of cancer cell lines and biopsies. Since 2012, the therapeutic potential of VGSCs in cancer treatment has been investigated *in vivo*. Application of VGSC blockers such as TTX (Yildirim *et al.*, 2012), ranolazine (Driffort *et al.*, 2014) and phenytoin (Nelson *et al.*, 2015a) reduced tumour progression *in vivo*. Agreeing with these previous reports, Section 5.2.7 showed that $Na_v1.5$-shRNA significantly decreased primary tumour growth compared to shRNA control cells. $Na_v1.5/I_{Na}$ increased the tumour growth probably by reducing cell apoptosis, since the density of activated caspase $3^+$ apoptotic cells was significantly lower in shRNA control tumours (Nelson *et al.*, 2015b). Additionally, $Na_v1.5$-shRNA cell-bearing mice showed reduced metastases to lungs, liver and spleen (Nelson *et al.*, 2015b), which is similar to the effects caused by phenytoin (Nelson *et al.*, 2015a). In spite of all the data showing the clinical relevance of targeting VGSCs in cancer treatment, until now, the $I_{Na}$ in cells in tumour tissue had not been studied. In the present study, by performing whole-cell patch clamp recording on tumour tissue slices, data in Section 5.2.4 provide the first direct evidence showing $I_{Na}$ carried by VGSCs in primary

tumour tissue. The tumour slice recording technique may have value when applied to recording $I_{Na}$ on tumour tissues from cancer patients in the future.

Compared to most mammalian tissues that exist at 2–9 % $O_2$ (Hockel & Vaupel, 2001; Bertout *et al.*, 2008), cells in solid tumours are thought to experience sustained hypoxia (defined as $\leq$ 2 % $O_2$) due to the restrained $O_2$ delivery (Hockel & Vaupel, 2001), which is the result of the structural abnormalities of tumour microvessels and disrupted microcirculation (Vaupel *et al.*, 1989). Surgical specimens of cervical tumours showed that compared to well-oxygenated tumours, hypoxic tumours exhibit a more invasive phenotype and more frequent parametrial spread, resulting in a worse survival rate (Hockel *et al.*, 1996). Hypoxia can modulate the function of VGSCs. In rat ventricular myocytes, hypoxia augmented the persistent $I_{Na}$ (Ju *et al.*, 1996); in rat glomus cells in the carotid body, chronic hypoxia for 1–2 weeks increased transient $I_{Na}$; and $Na_v1.5$-expressing HEK293 cells showed increased persistent $I_{Na}$ under acute hypoxia (Fearon & Brown, 2004). In MDA-MB-231 cells, acute hypoxia (2 % $O_2$) increases persistent $I_{Na}$, and 24 h hypoxic treatment increases Matrigel invasion (Djamgoz & Onkal, 2013). In the present study, the tumour tissue was divided into three regions, namely periphery, intermediate region and centre, and the characteristics of $I_{Na}$ were consistent across these regions. However, it was not possible to resolve hypoxia and/or distance from vasculature in this model. In a future experiment, transgenic mice with GFP-tagged VEGF (Kishimoto *et al.*, 2000), which serves as an angiogenesis marker (Hoeben *et al.*, 2004), could be used to study the $I_{Na}$ from tumour cells from regions with different blood vessel densities.

### 5.3.3  The unvarying $V_m$ across the tumour tissue

Given the pro-migratory role of the depolarised $V_m$ in MDA-MB-231 cell *in vitro*, it is logical to hypothesise that the $V_m$ of tumour cells at the edge of tumour tissue would be more depolarised. However, the $V_m$ was broadly unvarying across the tumour tissue.

Future experiments should perfuse the slices with TTX and test whether or not VGSCs regulate the $V_m$ in cells in tumour tissue. On the other hand, gap junctions are able to regulate $V_m$ at long-range (Chernet & Levin, 2014), and they may cause a unified $V_m$ across the cells in tumour tissue via transporting ions intercellularly. However, a group has performed dye injection experiments using Lucifer Yellow on MDA-MB-231 cell monolayers cultured *in vitro* (Qin *et al.*, 2002), where they found that the diffusion of dye was inefficient, given that only 6 % of cells exhibited dye transfer (Qin *et al.*, 2002), suggesting a limited role for gap junctions in intercellular communication in this cell line. Interestingly, although exogenously expressing Cx43 in MDA-MB-231 cells increased the proportion of cells with dye transfer to 37 % (Qin *et al.*, 2002), MDA-MB-231 cells over-expressing Cx43 did not form gap junctions *in vivo* (Qin *et al.*, 2002). Future experiments should block Cx43 connexon using pharmacological agents such as mefloquine (Juszczak & Swiergiel, 2009) or perform juxtapositional recordings on cells in tumour tissue to further investigate whether the $V_m$ of a target cell can be affected by artificially controlling the $V_m$ in its adjacent cell, and whether the depolarised, unvarying $V_m$ across tumour tissue is caused by the *in vivo* tumour microenvironment.

## 5.4   Conclusion

This Chapter has demonstrated that VGSCs not only depolarise the $V_m$ of MDA-MB-231 cells *in vitro*, but also cause $Na^+$ accumulation in these cells. Suppressing $Na_v1.5$ expression with shRNA significantly reduced tumour growth *in vivo*, supporting the value of targeting VGSCs in cancer treatment. For the first time, $I_{Na}$ carried by VGSCs has been recorded in tumour tissue slices, indicating the role of VGSCs in regulating $Na^+$ influx *in vivo* and suggesting that $V_m$ of tumour cells *in vivo* may not be intrinsically regulated. Future experiments should record $I_{Na}$ from tumour tissue samples from patients, and should address how cell $V_m$ is regulated *in vivo*.

# Chapter 6: Discussion

## 6.1 The knowledge gap in understanding VGSC-dependent metastasis

Cancer is a leading cause of death, given that 8.2 million cancer deaths occurred globally in 2012 (Torre *et al.*, 2015). Recently, an increasing number of ion channels and transporters have been identified in cancer cells and biopsies from patient tumours (Prevarskaya *et al.*, 2010; Lastraioli *et al.*, 2015; Stock & Schwab, 2015), where they regulate metastasis-related activities such as proliferation, apoptosis, adhesion, migration, invasion and gene expression (Brackenbury, 2012; Roger *et al.*, 2015; Stock & Schwab, 2015). Excitingly, studies have highlighted the therapeutic potential of ion channels as novel targets in cancer treatment (Prevarskaya *et al.*, 2011; Brackenbury, 2012; Huang & Jan, 2014; Turner & Sontheimer, 2014).

VGSCs were previously thought to be expressed only in excitable cells, such as neurones, skeletal muscle cells and cardiomyocytes, where they initiate the firing of action potentials (Catterall, 2000). VGSCs are also expressed predominantly in cancer cells with strong migration and/or invasion potential (Brackenbury, 2012; Roger *et al.*, 2015). Compared to less malignant cancer cells, highly metastatic or multidrug-resistant cancer cells exhibit $I_{Na}$ together with reduced outward $I_K$ (Yamashita *et al.*, 1987; Lee *et al.*, 1988; Fraser *et al.*, 2005; Fulgenzi *et al.*, 2006). Moreover, inhibiting VGSCs with pharmacological agents or shRNA/siRNA reduces proliferation and metastasis *in vivo* (Yildirim *et al.*, 2012; Driffort *et al.*, 2014; Nelson *et al.*, 2015a; Nelson *et al.*, 2015b), and cell metastatic behaviour *in vitro* (Roger *et al.*, 2003; Fraser *et al.*, 2005; Brackenbury *et al.*, 2007; Roger *et al.*, 2007; House *et al.*, 2010; Yang *et al.*, 2012; Campbell *et al.*, 2013; Xing *et al.*, 2014; House *et al.*, 2015). However, the detailed molecular mechanism(s) underlying VGSC-dependent cancer cell migration and invasion is not yet clear.

As in excitable cells, $Na^+$ influx carried by VGSCs through the cancer cell plasma membrane may cause two main physiological changes to the cell: increased $[Na^+]_i$ and depolarised $V_m$. It was reported over 30 years ago that cancer cells possess higher $[Na^+]_i$ compared to cells derived from healthy tissue (Smith *et al.*, 1978; Cameron *et al.*, 1980; Pool *et al.*, 1981), and reducing $[Na^+]_i$ in tumour cells slows tumour growth *in vivo* (Sparks *et al.*, 1983), suggesting the role of intracellular $Na^+$ in tumourigenesis. However, according to the Nernst equation (Equation 2.6), the increase of the $[Na^+]_i$ will also inevitably depolarise the $V_m$ of cells under physiological conditions.

$V_m$ is more than an epi-phenomenon that only indicates the difference of ionic concentration across cell plasma membrane. An increasing amount of evidence has shown that $V_m$ is a functional signal *per se* (Sundelacruz *et al.*, 2009; Yang & Brackenbury, 2013; Lobikin *et al.*, 2015; Zhou *et al.*, 2015). During cell proliferation, a depolarised $V_m$ is necessary for $G_1$/S transition in the cell cycle (Cone & Tongier, 1971), whereas a hyperpolarised $V_m$ is required at the $G_2$/M border (Habela *et al.*, 2008). $V_m$ depolarisation is able to induce mitogenesis/tumourigenesis both *in vitro* and *in vivo*. Sustained $V_m$ depolarisation (1–3 h) induces mitotic activity in terminally differentiated neurones (Stillwell *et al.*, 1973; Cone & Cone, 1976). In *Xenopus laevis* and *Dugesia japonica* planaria, $V_m$ depolarisation facilitates the regeneration of amputated tissues (Beane *et al.*, 2011; Beane *et al.*, 2013; Tseng & Levin, 2013). Artificially depolarising the $V_m$ in *Xenopus laevis* embryos induces tumour formation (Blackiston *et al.*, 2011; Lobikin *et al.*, 2012). Taken together, this evidence suggests a powerful role for a depolarised $V_m$ in promoting tumourigenesis. Therefore, it is not surprising that cancer cells generally display a depolarised $V_m$, and that the cells from cancer tissue possess a more depolarised $V_m$ compared to those from normal tissue of the same origin (Binggeli & Weinstein, 1986; Yang & Brackenbury, 2013).

Given the importance of $V_m$ in regulating cellular behaviours, this PhD Thesis aimed to explore the relationship between VGSCs and the depolarised $V_m$ reported in

MDA-MB-231 cells and investigate whether VGSC-mediated cell migration/invasion is also dependent on the $V_m$ in these cells.

## 6.2 VGSCs depolarise the $V_m$ and therefore increase cell motility in *vitro*

Before this study, there was no evidence showing whether VGSCs potentiate cancer cell migration and/or invasion due to $Na^+$ *per se* or via their possible role in altering the $V_m$. The involvement of VGSCs in $V_m$ regulation was examined in MDA-MB-231 cells. Blocking VGSCs using phenytoin or TTX causes a 3–4 mV $V_m$ hyperpolarisation. $Na_v1.5$-shRNA cells are 3.4 mV more hyperpolarised than control cells, suggesting that $Na_v1.5$ causes a steady-state $V_m$ depolarisation, and that the depolarised $V_m$ caused by $Na_v1.5$ is not compensated by other ion-permeable pathways when the $Na^+$ conductance through $Na_v1.5$ is shut down. Since the $V_m$ of MDA-MB-231 cells is at approximately -10 mV, blocking $Na_v1.5$ leads to a 40 % increase in the transmembrane voltage. Extracellular $Na^+$ depletion causes a much larger $V_m$ hyperpolarisation of 10–15 mV, which points to other $Na^+$ permeable pathways in MDA-MB-231 cells that contribute to the depolarised $V_m$, in addition to VGSCs. Future experiments should address the involvement of $Na^+$-$K^+$ ATPase (Winnicka *et al.*, 2008) and NHE1 (Brisson *et al.*, 2011) in $Na^+$-dependent $V_m$ regulation in MDA-MB-231 cells. Additionally, the presence of other $Na^+$-permeable ion channels/ transporters, such as ENaC, NCX and $Na^+$-$K^+$-$2Cl^-$ co-transporter, has not been reported in MDA-MB-231 cells, and whether or not they contribute to $Na^+$-dependent $V_m$ regulation should be investigated in future studies. Another study showed that blocking $Na_v1.7$ in H460 non-small cell lung cancer cells hyperpolarises the $V_m$ by 10 mV (Campbell *et al.*, 2013). Taken together, VGSCs are now known to cause $V_m$ depolarisation not only in excitable cells during action potential firing, but also in non-excitable cancer cells.

In order to study the role of $V_m$ without interfering with $[Na^+]_i$, subsequent experiments modulated the endogenously expressed $BK_{Ca}$ channels in MDA-MB-231

cells (Section 0). The activity of $BK_{Ca}$ channels is weak in MDA-MB-231 cells (Section 0), probably because the $[Ca^{2+}]_i$ is not sufficiently high to fully activate the channel (Barrett *et al.*, 1982). Activating $BK_{Ca}$ channels in MDA-MB-231 cells using 40 µM NS-1619 yielded a $V_m$ of -52 mV, similar to that in MCF-10A cells where various types of $K^+$ channels are present (Fraser *et al.*, 2005). A previous report showed that suppressing hEAG1 channels in MDA-MB-231 cells depolarises the $V_m$ by 18 mV (Hammadi *et al.*, 2012). Therefore, the depolarised $V_m$ (~-10 mV) recorded from MDA-MB-231 cells should be attributed to the increased permeability to $Na^+$ via VGSCs as well as the weak activity of $V_m$-hyperpolarising $K^+$ channels.

NS-1619 at 1 µM hyperpolarised the steady-state $V_m$ of MDA-MB-231 cells by approximately 4 mV, replicating the effect of 30 µM TTX in these cells. Importantly, 1 µM NS-1619 did not significantly alter the $[Na^+]_i$ (Section 5.2.3). In a wound healing assay, NS-1619 (1 µM) and TTX (30 µM) reduced cell migration *in vitro* to a strikingly similar extent (Section 4.2.7). However, while 30 µM TTX showed a strong inhibitory effect on invasion through Matrigel, NS-1619, at both 1 µM and 40 µM, did not have any effect (Section 4.2.7). These data suggest that VGSC-mediated $V_m$ depolarisation leads to increased cell migration, whilst VGSC-dependent cell invasion is $Na^+$- but not $V_m$-dependent. $Na^+$ may promote cell invasion via the previously proposed $Na_v1.5$-NHE1-cathepsins pathway (Gillet *et al.*, 2009; Brisson *et al.*, 2011; Brisson *et al.*, 2013). For the first time, data presented in this Thesis show that $Na_v1.5$ potentiates cancer cell migration and invasion via different mechanisms.

## 6.3 $V_m$ and $[Ca^{2+}]_i$ regulation

$V_m$ is a double-edged sword in regulating $[Ca^{2+}]_i$ (Schwab *et al.*, 2012; Yang & Brackenbury, 2013). On one hand, a depolarised $V_m$ can activate VGCCs, which then causes $Ca^{2+}$ influx (Borodinsky & Fiszman, 1998). On the other hand, a hyperpolarised $V_m$ may increase the driving force of passive $Ca^{2+}$ entry via $Ca^{2+}$-permeable, voltage-

independent channels (Prevarskaya *et al.*, 2011; Schwab *et al.*, 2012). For example, in MDA-MB-231 cells, hEAG1 channels cause a hyperpolarised $V_m$, and blocking these channels reduces $Ca^{2+}$ entry via Orai1 (Hammadi *et al.*, 2012), suggesting that $V_m$-hyperpolarisation increases $[Ca^{2+}]_i$ in MDA-MB-231 cells. However, in the present study, replacing extracellular NaCl with ChoCl or blocking VGSCs with TTX, both hyperpolarising the $V_m$ (Section 3.2.1), did not significantly alter the $[Ca^{2+}]_i$ in MDA-MB-231 cells. It is possible that hEAG1-induced $Ca^{2+}$ entry requires a hEAG1-Orai1 interaction, whereas the hyperpolarised $V_m$ is not necessary. Indeed, ion channels can regulate intracellular signalling without conducting ions. For example, 3T3 fibroblasts transfected with *Drosophila* EAG channels show increased p38 MAPK activity and proliferation, which is independent of ion flux through the expressed EAG channels but depends on the position of the channel voltage sensor domain (Hegle *et al.*, 2006).

VGSCs are present in THP-1 macrophages (Carrithers *et al.*, 2009), rat cortical astrocytes (Pappalardo *et al.*, 2014b) and microglia (Persson *et al.*, 2014), where they play a role in $[Ca^{2+}]_i$ regulation by collaborating with NCX on the mitochondrial or plasma membrane. In human umbilical vein endothelial cells, $Ca^{2+}$ influx through NCX is required for VEGF-induced ERK1/2 activation, which requires $Na^+$ carried by VGSCs (Andrikopoulos *et al.*, 2011a; Andrikopoulos *et al.*, 2011b). In mouse cardiomyocytes, $I_{Na}$ potentiates $Ca^{2+}$ influx in wildtype but not NCX-knockout mice (Larbig *et al.*, 2010). It is noteworthy that the mode of action of NCX is $V_m$-dependent (Blaustein & Lederer, 1999): when the $V_m$ is more depolarised than the $V_{rev}$ of NCX, the exchanger works in its reverse mode, importing $Ca^{2+}$. Therefore, whether or not VGSCs potentiate NCX activity and then causes an increase of $[Ca^{2+}]_i$ in these cells should be studied in the future.

## 6.4  $V_m$ and the small GTPases

Work presented in this Thesis examined the possible underlying mechanism by which $V_m$ hyperpolarisation inhibited migration of MDA-MB-231 cells *in vitro*. The

proportion of cells with lamellipodia in NS-1619- and TTX-treated MDA-MB-231 cells was reduced; the cells had a less elongated morphology after treatment with either of the drugs, suggesting $V_m$ hyperpolarisation causes alterations in cytoskeletal components (Section 4.2.9). Active Rac1 at cell leading edge was reduced to a similar degree by TTX (30 µM) and NS-1619 (1 µM) treatment (Section 4.2.11). Therefore, the results suggest a functional role for the depolarised $V_m$ in increasing active Rac1 levels at the leading edge. However, whether this is due to the redistribution of active Rac1 in the cell body, or increased Rac1 activation at cell leading edge is not clear. Future experiments should examine the protein level of total Rac1 and active Rac1 upon $V_m$ depolarisation.

The relationship between VGSC activity and the small GTPase Rac1 was recently investigated in microglia, where VGSCs increase $[Ca^{2+}]_i$ via NCX and subsequently activate ERK and Rac1, which leads to migration in an ATP-dependent manner (Persson *et al.*, 2014). Since the $[Ca^{2+}]_i$ does not change after $V_m$ hyperpolarisation or blocking VGSCs in MDA-MB-231 cells (Section 0), the activation of Rac1 may be dependent on the depolarised $V_m$ *per se*.

A depolarised $V_m$ can activate small GTPases in both a $Ca^{2+}$-dependent and independent manner. For example, in mouse cortical neurones, $V_m$ depolarisation activates Ras and Rap1 via PKA and calmodulin, which subsequently induces ERK activation (Baldassa *et al.*, 2003). Similarly, $V_m$ depolarisation in PC12 cells induces c-fos expression via PKA and MAPK, and the process requires the $Ca^{2+}$-sensitive proline-rich tyrosine kinase 2 (Park *et al.*, 2000). In rat caudal arterial smooth muscle cells, the depolarised $V_m$ activates ROCK and downstream MLCK in a VGCC- dependent manner and ultimately leads to muscle contraction (Mita *et al.*, 2002; Mita *et al.*, 2013). On the other hand, in LLC-PK$_1$ kidney tubule epithelial cells, $V_m$ depolarisation induces MLC phosphorylation via a Rho- and ROCK-dependent but $Ca^{2+}$-independent pathway (Szaszi *et al.*, 2005). In this pathway, phosphorylation is caused by the activation of

GEFs upon $V_m$ depolarisation (Waheed *et al.*, 2010). More recently, a study has demonstrated that $V_m$ depolarisation enhances phosphatidylserine and K-Ras nanoclustering in baby hamster kidney cells, and K-Ras nanoclustering upon $V_m$ depolarisation activates MAPK signalling (Zhou *et al.*, 2015). Taken together, depolarised $V_m$ is emerging as a functional signal in activating small GTPases. These activated small GTPases can then increase the assembly of cytoskeletal components, or promote the MAPK signalling pathway, which controls key cellular behaviours including proliferation, differentiation and development (Shaul & Seger, 2007).

Interestingly, $Na_v1.5$ activity activates Rap1B in SW620 cells (House *et al.*, 2015). Given the capability of a depolarised $V_m$ in activating small GTPases, future experiments should explore whether the activation of Rap1B is due to the $V_m$-depolarising role of $Na_v1.5$ in SW620 cells. In order to fully understand the $V_m$-dependent small GTPase activation pathways in cancer cells, future experiments should also investigate the up-stream effectors of Rac1 that lead to its activation, such as GEFs, upon $V_m$ depolarisation. Moreover, since the activation of small GTPases may increase cancer malignancy by promoting cancer cell migration/invasion (Sahai & Marshall, 2002; Downward, 2003; Yamazaki *et al.*, 2005), how VGSCs/$V_m$ regulate other small GTPases in cancer cells should be further examined. Recently, it was reported that the $Na_v1.5$ level in MDA-MB-231 cells positively correlates to that of RhoA (Dulong *et al.*, 2014). In the future, one may expect that the relationships between VGSC/$V_m$ and other cancer-related small GTPases such as Rab (Cheng *et al.*, 2004), Ras (von Lintig *et al.*, 2000; Eckert *et al.*, 2004) and Arf (Hashimoto *et al.*, 2004) will be revealed.

## 6.5   The roles of VGSCs in cancer cells: an updated view

In MDA-MB-231 cells, the $Na_v1.5$-$V_m$-Rac1 signalling axis fits well in a previously proposed model that shows $Na_v1.5$ potentiates the phosphorylation of src kinase, cortactin and cofilin (Brisson *et al.*, 2013). Src kinase can promote cortactin

phosphorylation by increasing Rac1 activity (Servitja $et$ $al.$, 2003), and active Rac1 can potentiate cortactin phosphorylation (Head $et$ $al.$, 2003), which ultimately facilitates lamellipodia formation by activating the Arp2/3 complex (Miki $et$ $al.$, 1998; Krueger $et$ $al.$, 2003).

Together with other previously published data, more detail showing the downstream signals initiated by VGSC activity has been revealed (Figure 6.1). In Mat-LyLu PCa and MDA-MB-231 cells, $Na^+$ influx through $Na_v1.7$ or $Na_v1.5$ activates PKA, which consequently increases $Na_v1.7/Na_v1.5$ mRNA level and increases the trafficking of VGSC α subunit protein to the plasma membrane (Brackenbury & Djamgoz, 2006; Chioni $et$ $al.$, 2010). Additionally, $Na^+$ influx carried by $Na_v1.5$ allosterically potentiates the activity of NHE1 in MDA-MB-231 cells, which leads to an acidic extracellular environment, favouring the pH-dependent proteolytic activity of cysteine cathepsins B and S (Gillet $et$ $al.$, 2009; Brisson $et$ $al.$, 2011; Brisson $et$ $al.$, 2013).

Moreover, $Na_v1.5$ positively regulates the expression of the metastasis-promoting CD44 protein in MDA-MB-231 and SW620 cells (House $et$ $al.$, 2015; Nelson $et$ $al.$, 2015b), which may lead to the activation of src kinase (Bourguignon $et$ $al.$, 2001; Lee $et$ $al.$, 2008). Given that CD44 promotes invasion by up-regulating the cortactin mRNA level (Hill $et$ $al.$, 2006), taken together, these data suggest that the CD44-src-cortactin axis is regulated by $Na_v1.5$ in cancer cells.

In BCa cell lines, the expression of VGSCs appears to be associated with ER status: VGSCs are expressed in $ER^-$ MDA-MB-231 cells but not in $ER^+$ MCF-7 cells. Interestingly, down-regulation of ER in MCF-7 cells induced functional expression of VGSCs, likely $Na_v1.5$ (Section 3.2.7) (Mohammed $et$ $al.$, 2015). Although microarray data show that $Na_v1.5$ mRNA levels do not correlate with ER status in BCa patient samples (Yang $et$ $al.$, 2012), ER down-regulation may increase functional channel activity and/or channel trafficking to plasma membrane of BCa cells, independent of mRNA regulation.
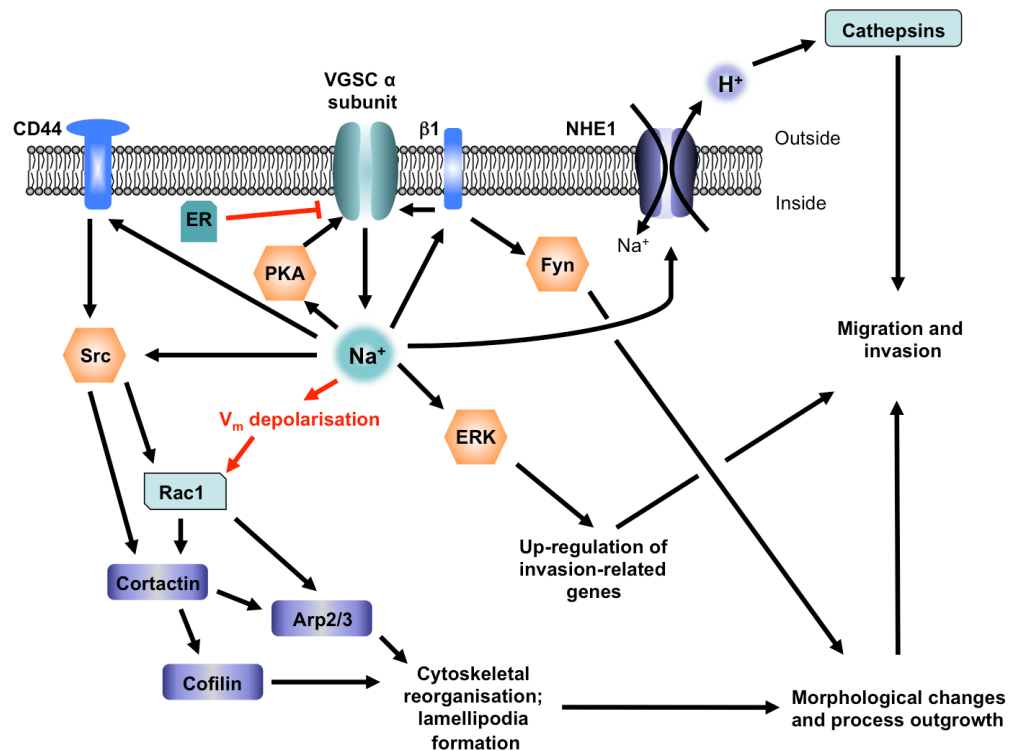
Figure 6.1. The roles of voltage-gated Na$^+$ channels in different cancer cells.

In MDA-MB-231 cells, Na$_v$1.5 carries Na$^+$ influx, which depolarises the V$_m$, increasing Rac1 activity (Section 4.2.11). VGSC activity also activates src kinase (Brisson *et al.*, 2013). Rac1 and src kinase control cytoskeletal modification by regulating the Arp2/3 complex and phosphorylation of cortactin and cofilin (Pollard, 2007; Stock & Schwab, 2015). Na$_v$1.5 positively regulates the expression of CD44 (Nelson *et al.*, 2015b), which may lead to src activation (Lee *et al.*, 2008). Na$^+$ also increases H$^+$ efflux through NHE1, which enhances cathepsin protease activity (Brisson *et al.*, 2011; Brisson *et al.*, 2013; Pardo & Stuhmer, 2014). In SW620 colon cancer cells, Na$_v$1.5 transcriptionally up-regulates invasion-related genes via an ERK signalling pathway (Schwab *et al.*, 2012; House *et al.*, 2015; Roger *et al.*, 2015). In MDA-MB-231 and Mat-LyLu prostate cells, Na$^+$ influx potentiates VGSC synthesis at transcription level and increases VGSC trafficking to the plasma membrane in a PKA-dependent manner (Brackenbury & Djamgoz, 2006; Chioni *et al.*, 2010). In addition, in MDA-MB-231 cells, ER down-regulation induces functional Na$_v$1.5 expression (Section 3.2.7). The auxiliary β1 subunit increases cancer cell process outgrowth via fyn kinase (Nelson *et al.*, 2014). β1 also increases I$_{Na}$ density in MDA-MB-231 cells (Chioni *et al.*, 2009). Red lines indicate the findings in this study.

219

In SW620 colon cancer cells, $Na_v1.5$ activity leads to persistent MAPK activation in a Rap1-dependent manner (House *et al.*, 2015), and it also transcriptionally activates the expression of invasion-related genes via an ERK/c-Jun pathway (House *et al.*, 2010; House *et al.*, 2015). Finally, the auxiliary β1 subunit can potentiate $Na^+$ influx through $Na_v1.5$ in MDA-MB-231 cells (Chioni *et al.*, 2009), and can also facilitate neurite-like process outgrowth on BCa cells *in vitro* in a fyn kinase-dependent manner, where $Na^+$ conductance through the α subunits is also required (Nelson *et al.*, 2014). In conclusion, a number of models have shown distinct downstream signalling pathways initiated by VGSCs in different cancer cells. Future studies should investigate whether these mechanisms are applicable to all cancers where VGSCs are present, or whether they are dependent on the cancer type or VGSC isoform.

## 6.6  $Na^+$ and tumourigenesis

In *Xenopus laevis*, $Na^+$ accumulation appears in regions where cells over-proliferate (Lobikin *et al.*, 2012). High $[Na^+]_i$ correlates with tumourigenesis in mammalian cell types (Cameron *et al.*, 1980; Pool *et al.*, 1981; Sparks *et al.*, 1983). Therefore, this study also investigated whether VGSCs regulate $[Na^+]_i$ in MDA-MB-231 cells. TTX and $Na_v1.5$-shRNA reduced $[Na^+]_i$, suggesting that $Na_v1.5$ not only depolarises the $V_m$ but also cause $Na^+$ accumulation in MDA-MB-231 cells (Section 0). This result agrees with another study using H460 NSCLC cells where $Na_v1.7$ is expressed, showing that blocking $Na_v1.7$ using TTX reduces $[Na^+]_i$ (Campbell *et al.*, 2013). However, how $Na^+$ *per se* contributes to tumourigenesis is less understood. As discussed above, $Na^+$ increases MDA-MB-231 cell invasion by allosterically regulating NHE1 (Gillet *et al.*, 2009; Brisson *et al.*, 2011; Brisson *et al.*, 2013), but how $Na^+$ regulates other ion channels/transporters in cancer is less studied. Increased $[Na^+]_i$ enhances the activity and cell surface expression of $Na^+$-$K^+$ ATPase in rat kidney cortical collecting duct cells and opossum kidney cells (Vinciguerra *et al.*, 2003; Sjostrom *et al.*, 2007). As discussed in Section 6.3,

$Na^+$ influx via VGSCs may increase $[Ca^{2+}]_i$ through NCX in human umbilical vein endothelial cells and mouse cardiomyocytes (Larbig *et al.*, 2010; Andrikopoulos *et al.*, 2011a; Andrikopoulos *et al.*, 2011b). Future work should investigate whether or not increased $Na^+$-$K^+$ ATPase and/or NCX activity leads to tumourigenesis.

## 6.7  Recording $I_{Na}$ and $V_m$ on cells from tumour tissue slices

In spite of all the *in vivo* evidence showing that suppressing VGSC expression or blocking VGSC activity reduces tumour growth and metastasis (Yildirim *et al.*, 2012; Driffort *et al.*, 2014; Nelson *et al.*, 2015a; Nelson *et al.*, 2015b), the $I_{Na}$ on cells in tumour tissue had not been previously studied. By performing whole-cell patch clamp recording on tumour tissue slices, this study provides direct evidence showing $I_{Na}$ carried by VGSCs in primary tumour tissue. The $I_{Na}$ characteristics did not differ across the tissue, suggesting that VGSCs are homogeneously expressed in orthotopically implanted tumours. *In vitro*, hypoxia increases persistent $I_{Na}$ in MDA-MB-231 cells (Djamgoz & Onkal, 2013), but VGSC activity in hypoxic regions of tumour tissue was not investigated. Future experiments using *Tie2*-promoter driven GFP in transgenic mice (Schlaeger *et al.*, 1997; Motoike *et al.*, 2000), where endothelial cells of vasculature are labelled with GFP, in order to study whether or not $I_{Na}$ differs in tumour regions with various blood vessel densities.

The $V_m$ recorded *ex vivo* was more depolarised than in cells cultured *in vitro* (Section 5.2.4), and the $V_m$ across tumour tissue did not vary. It is possible that the $V_m$ of cells in tumour tissue is regulated at a tissue-scale via gap junctions (Chernet *et al.*, 2014; Chernet & Levin, 2014). Cx43 is expressed in MDA-MB-231 cells (Qin *et al.*, 2002), and future experiments can apply Cx43 blockers such as mefloquine (Juszczak & Swiergiel, 2009) on tumour tissue and investigate whether or not inhibiting gap junctional intercellular communication causes different distributions of cell $V_m$ across tumour tissue.

## 6.8 Clinical relevance

Using an orthotopic mouse model, suppressing $Na_v1.5$ expression using shRNA reduced tumour growth (Section 5.2.7) and metastasis to liver, lungs and spleen in mice (Nelson *et al.*, 2015b). Moreover, phenytoin, an FDA-approved anticonvulsant, reduces tumour growth in mice bearing MDA-MB-231 cells, possibly by increasing cancer cell apoptosis (Nelson *et al.*, 2015a). In addition, phenytoin also reduced cancer cell invasion and metastasis to liver, lungs and spleen (Nelson *et al.*, 2015a). Additionally, ranolazine, another FDA-approved antiarrhythmic, reduces lung metastasis after injection of MDA-MB-231 cells into the tail vein (Driffort *et al.*, 2014). Similarly, subcutaneously implanted Mat-LyLu cells show reduced lung metastasis in rats following local injection with TTX (Yildirim *et al.*, 2012). In summary, using various tumour implantation models, inhibiting VGSCs results in reduced primary tumour growth and/or metastasis, suggesting the significance of repurposing VGSC-targeting antiarrhythmic antiepileptic drugs as a potential new cancer treatment. Further studies should investigate combining VGSC-blocking anti-arrhythmics with chemotherapy, radiation therapy and/or hormone therapy during cancer treatment in order to inhibit metastasis.

## 6.9 Future directions

Given the data presented in this study, a number of future experiments should be done to better illustrate the relationships between VGSC/$V_m$ and tumour progression both *in vitro* and *in vivo*.

To begin with, whether VGSCs regulate $V_m$ in other cancer cell types and thereby potentiate cancer cell migration by activating Rac1 should be studied. On the other hand, Rac1 may not be the only small GTPase that is activated upon $V_m$ depolarisation in cancer cells, and the activity of other cancer-related small GTPases should be investigated in response to changes in $V_m$. More importantly, how exactly a depolarised $V_m$ activates small GTPases in cancer is still unclear.

One of the limitations of the present study is that $V_m$ was determined in individual cells using the whole-cell patch clamp technique. In spite of their limited accuracy, $V_m$-sensitive fluorescent indicators are becoming popular in studying tissue-scale, temporal and spatial $V_m$ change *in vivo* (Adams & Levin, 2012). Future studies can combine $V_m$- and $Na^+$-/$Ca^{2+}$-sensitive fluorophores to investigate dynamics between $[Na^+]_i$, $V_m$ and $[Ca^{2+}]_i$.

The effector(s) of increased $[Na^+]_i$ in tumours is not completely clear. However, considering the pro-invasive role of intracellular $Na^+$ and the pro-migratory role of depolarised $V_m$, reducing $[Na^+]_o$ may have therapeutic value in cancer treatment, since replacement of extracellular NaCl with NMDG both hyperpolarises the $V_m$ and reduces $[Na^+]_i$. Future experiments should test this hypothesis both *in vitro* and *in vivo*.

Polyoma middle T oncoprotein-expressing (PyMT) mice can develop BCa and lung-metastasis spontaneously (Lin *et al.*, 2003; Fantozzi & Christofori, 2006). Interestingly, the BCa progression in PyMT mice accompanies loss of ER (Lin *et al.*, 2003). Given that suppressing ER expression leads to functional VGSC expression in MCF-7 cells (Section 3.2.7), the PyMT mouse is an ideal model to investigate how VGSCs are up-regulated during cancer progression.

In conclusion, given the significance of VGSC/$Na^+$/depolarised $V_m$ in promoting cancer progression both *in vitro* and *in vivo*, one may expect further elucidation of the VGSC-dependent metastasis pathways, as well as their potential exploration as therapeutic targets in cancer treatment.

## Abbreviations

AC: adenylyl cyclase

AIS: axon initial segment

ATX: sea-anemone toxins

BCa: breast cancer

$BK_{Ca}$ channels: large conductance $Ca^{2+}$-activated $K^+$ channels

BRCA1: breast cancer 1

$[Ca^{2+}]_i$: intracellular $Ca^{2+}$ concentration

CaM: calmodulin

CAM: cell adhesion molecule

CaMK: calmodulin kinase

CCD: charge-coupled device

CDK: cyclin-dependent kinases

CGN: cerebellar granule neuron

CHL cells: Chinese hamster lung cells

CHO cells: Chinese hamster ovary cells

ChoCl: choline chloride

CNS: the central nervous system

CRAC channels: $Ca^{2+}$-release activated $Ca^{2+}$ channels

CSC: cancer stem cell

DAPC: dystrophin-associated protein complex

DAPI: 4',6-diamidino-2-phenylindole

DMBA: 7,12-dimethylbenz(a)anthracene

DMEM: Dulbecco's modified eagle medium

DMSO: dimethyl sulfoxide

DRG: dorsal root ganglion

E2: β-oestradiol

EAG channels: *Ether à go-go* channels

ECM: extracellular matrix

EGF: epidermal growth factor

eGFP: enhanced green fluorescent protein

EGTA: ethylene glycol tetraacetic acid

ENaC: epithelial $Na^+$ channel

ER: oestrogen receptor

ERK: extracellular signal-regulated kinase

FAK: focal adhesion kinase

FBS: foetal bovine serum

FDA: the US Food and Drug Administration

$G_{\beta\gamma}$: the βγ subunits of G proteins

GEF: guanine nucleotide exchange factor

GEFS+: generalised epilepsy with febrile seizure plus

hEAG channels: human *Ether à go-go* channels

HEK: human embryonic kidney

HEPES: 4-(2-hydroxyethyl)-1-piperazineethanesulfonic acid

HER2: human epidermal growth factor receptor 2

HERG: human EAG-related gene

hMSC: human mesenchymal stem cell

$I_{BKCa}$: large conductance $Ca^{2+}$-activated $K^+$ channels current

IbTx: iberiotoxin

$IC_{50}$: the concentration of drug at which half of its maximal effect occurs

$I_{EAG}$: EAG current

IFM motif: isoleucine-phenylalanine-methionine motif

Ig: immunoglobulin

$I_{HERG}$: HERG current

$I_K$: $K^+$ current

$I_{Kir}$: inward rectifier $K^+$ current

IL: interleukin

$I_{Na}$: $Na^+$ current

$IP_3$: inositol 1,4,5-trisphosphate

IQ domain: isoleucine-glutamine domain

ISME: ion-selective microelectrode

JNK: ERK-Jun-amino-terminal kinase

k: slope factor

$K_{ATP}$ channels: ATP-sensitive $K^+$ channels

$K_{Ca}$ channels: $Ca^{2+}$-activated $K^+$ channels

$K_d$: dissociation constant

$K_{ir}$ channels: inward rectifier $K^+$ channels

MAP: mitogen-activated protein

MAPK: mitogen-activated protein kinase

MDR: multidrug-resistant

MEK: MAPK/ERK kinase

MLC: myosin regulatory light chain

MLCK: MLC kinase

MLK3: mixed lineage kinase 3

MMP: matrix metalloproteinases

MOG1: multicopy suppressor of *Gsp1*

MRI: magnetic resonance imaging

MTT: thiazolyl blue tetrazolium bromide

$[Na^+]_i$: intracellular $Na^+$ concentration

$[Na^+]_o$ : extracellular $Na^+$ concentration

$Na_v1.5$-shRNA: shRNA targeting $Na_v1.5$

NCX: $Na^+$-$Ca^{2+}$ exchanger

NFAT: nuclear factor of activated T cells

NGF: nerve growth factor

NHE1: $Na^+$-$H^+$ exchanger type 1

NMDG: N-methyl-D-glucamine

NMR: nuclear magnetic resonance

NSCLC: non-small cell lung cancer

p11: annexin II light chain

PARP: poly (ADP-ribose) polymerase

PBS: phosphate saline solution

PCa: prostate cancer

PKA: cAMP-dependent protein kinase

PKC: protein kinase C

PNS: the peripheral nervous system

PR: progesterone receptor

PSS: physiological saline solution

PTPH1: protein tyrosine phosphatase 1

PyMT: polyoma middle T

qPCR: real-time PCR

RCK: regulator of the conductance of $K^+$

ROCK: Rho-associated kinase

ROI: region of interest

RPTPβ: receptor protein kinase tyrosine phosphatase β

RTK: receptor tyrosine kinases

SCLC: small-cell lung cancer

SERT: serotonin transporter

shRNA: small-hairpin RNA

shRNA control: non-targeting shRNA control

siRNA: small-interfering RNA

SOCE: store-operated $Ca^{2+}$ entry

SPF: specific pathogen free

STX: saxitoxin

$t_{1/2}$: half time

TF: transcription factor

TGF: tumour growth factor

TNF: tumour necrosis factor

TNFR1: tumour necrosis factor receptor 1

$T_p$: time to peak

TRP: transient receptor potential

TTX: tetrodotoxin

$V_{1/2}$: the voltage at which half-maximal conductance or availability occurs

$V_a$: activation voltage

VEGF: vascular endothelial growth factor

VGCC: voltage-gated $Ca^{2+}$ channel

VGPC: voltage-gated $K^+$ channel

VGSC: voltage-gated $Na^+$ channel

$V_m$: membrane potential

$V_p$: voltage at current peak

$V_{rev}$: reversal potential

WAVE: Wiskott-Aldrich syndrome protein-family verprolin-homologous proteins

# References

Aaltomaa S, Lipponen P, Eskelinen M, Kosma VM, Marin S, Alhava E & Syrjanen K. (1991a). Hormone receptor status and mitotic activity as risk factors for recurrence and death in female breast carcinoma. *Anticancer Res* **11,** 1701-1706.

Aaltomaa S, Lipponen P, Eskelinen M, Kosma VM, Marin S, Alhava E & Syrjanen K. (1991b). Hormone receptors as prognostic factors in female breast cancer. *Ann Med* **23,** 643-648.

Abdul M & Hoosein N. (2002). Expression and activity of potassium ion channels in human prostate cancer. *Cancer Lett* **186,** 99-105.

Adachi K, Toyota M, Sasaki Y, Yamashita T, Ishida S, Ohe-Toyota M, Maruyama R, Hinoda Y, Saito T, Imai K, Kudo R & Tokino T. (2004). Identification of SCN3B as a novel p53-inducible proapoptotic gene. *Oncogene* **23,** 7791-7798.

Adams DS & Levin M. (2012). General principles for measuring resting membrane potential and ion concentration using fluorescent bioelectricity reporters. *Cold Spring Harb Protoc* **2012,** 385-397.

Agnew WS, Moore AC, Levinson SR & Raftery MA. (1980). Identification of a large molecular weight peptide associated with a tetrodotoxin binding protein from the electroplax of Electrophorus electricus. *Biochem Biophys Res Commun* **92,** 860-866.

Akaike N & Harata N. (1994). Nystatin perforated patch recording and its applications to analyses of intracellular mechanisms. *Jpn J Physiol* **44,** 433-473.

Aktas CC, Zeybek ND & Piskin AK. (2015). In vitro effects of phenytoin and DAPT on MDA-MB-231 breast cancer cells. *Acta Biochim Biophys Sin (Shanghai)*.

Albuquerque EX, Daly JW & Witkop B. (1971). Batrachotoxin: chemistry and pharmacology. *Science* **172,** 995-1002.

Allard B, Magloire H, Couble ML, Maurin JC & Bleicher F. (2006). Voltage-gated sodium channels confer excitability to human odontoblasts: possible role in tooth pain transmission. *J Biol Chem* **281,** 29002-29010.

Allinen M, Beroukhim R, Cai L, Brennan C, Lahti-Domenici J, Huang H, Porter D, Hu M, Chin L, Richardson A, Schnitt S, Sellers WR & Polyak K. (2004). Molecular characterization of the tumor microenvironment in breast cancer. *Cancer Cell* **6,** 17-32.

Alroy G, Su H & Yaari Y. (1999). Protein kinase C mediates muscarinic block of intrinsic bursting in rat hippocampal neurons. *J Physiol* **518 ( Pt 1),** 71-79.

Anders C & Carey LA. (2008). Understanding and treating triple-negative breast cancer. *Oncology (Williston Park)* **22,** 1233-1239; discussion 1239-1240, 1243.

Andrikopoulos P, Baba A, Matsuda T, Djamgoz MB, Yaqoob MM & Eccles SA. (2011a). Ca2+ influx through reverse mode Na+/Ca2+ exchange is critical for vascular endothelial growth factor-mediated extracellular signal-regulated kinase (ERK) 1/2 activation and angiogenic functions of human endothelial cells. *J Biol Chem* **286,** 37919-37931.

Andrikopoulos P, Fraser SP, Patterson L, Ahmad Z, Burcu H, Ottaviani D, Diss JK, Box C, Eccles SA & Djamgoz MB. (2011b). Angiogenic functions of voltage-gated Na+ Channels in human endothelial cells: modulation of vascular endothelial growth factor (VEGF) signaling. *J Biol Chem* **286,** 16846-16860.

Arcangeli A. (2005). Expression and role of hERG channels in cancer cells. *Novartis Foundation symposium* **266,** 225-232; discussion 232-224.

Arcangeli A, Bianchi L, Becchetti A, Faravelli L, Coronnello M, Mini E, Olivotto M & Wanke E. (1995). A novel inward-rectifying K+ current with a cell-cycle dependence governs the resting potential of mammalian neuroblastoma cells. *J Physiol* **489 ( Pt 2),** 455-471.

Arcangeli A, Rosati B, Cherubini A, Crociani O, Fontana L, Ziller C, Wanke E & Olivotto M. (1997). HERG- and IRK-like inward rectifier currents are sequentially expressed during neuronal development of neural crest cells and their derivatives. *Eur J Neurosci* **9,** 2596-2604.

Arcangeli A, Wanke E, Olivotto M, Camagni S & Ferroni A. (1987). Three types of ion channels are present on the plasma membrane of Friend erythroleukemia cells. *Biochem Biophys Res Commun* **146,** 1450-1457.

Armstrong CM & Bezanilla F. (1973). Currents related to movement of the gating particles of the sodium channels. *Nature* **242,** 459-461.

Armstrong CM & Bezanilla F. (1977). Inactivation of the sodium channel. II. Gating current experiments. *J Gen Physiol* **70,** 567-590.

Armstrong CM & Matteson DR. (1985). Two distinct populations of calcium channels in a clonal line of pituitary cells. *Science* **227,** 65-67.

Aronica E, Troost D, Rozemuller AJ, Yankaya B, Jansen GH, Isom LL & Gorter JA. (2003). Expression and regulation of voltage-gated sodium channel beta1 subunit protein in human gliosis-associated pathologies. *Acta Neuropathol* **105,** 515-523.

Azouz R, Jensen MS & Yaari Y. (1994). Muscarinic modulation of intrinsic burst firing in rat hippocampal neurons. *Eur J Neurosci* **6,** 961-966.

Bacac M & Stamenkovic I. (2008). Metastatic cancer cell. *Annu Rev Pathol* **3,** 221-247.

Baldassa S, Zippel R & Sturani E. (2003). Depolarization-induced signaling to Ras, Rap1 and MAPKs in cortical neurons. *Brain Res Mol Brain Res* **119,** 111-122.

Baptista-Hon DT, Robertson FM, Robertson GB, Owen SJ, Rogers GW, Lydon EL, Lee NH & Hales TG. (2014). Potent inhibition by ropivacaine of metastatic colon

cancer SW620 cell invasion and NaV1.5 channel function. *Br J Anaesth* **113 Suppl 1,** i39-i48.

Barnes S & Hille B. (1988). Veratridine modifies open sodium channels. *J Gen Physiol* **91,** 421-443.

Baroni D & Moran O. (2015). On the multiple roles of the voltage gated sodium channel beta1 subunit in genetic diseases. *Front Pharmacol* **6,** 108.

Barrett JN, Magleby KL & Pallotta BS. (1982). Properties of single calcium-activated potassium channels in cultured rat muscle. *J Physiol* **331,** 211-230.

Barry PH & Lynch JW. (1991). Liquid junction potentials and small cell effects in patch-clamp analysis. *J Membr Biol* **121,** 101-117.

Batcioglu K, Uyumlu AB, Satilmis B, Yildirim B, Yucel N, Demirtas H, Onkal R, Guzel RM & Djamgoz MB. (2012). Oxidative stress in the in vivo DMBA rat model of breast cancer: suppression by a voltage-gated sodium channel inhibitor (RS100642). *Basic Clin Pharmacol Toxicol* **111,** 137-141.

Bates RC, Buret A, van Helden DF, Horton MA & Burns GF. (1994). Apoptosis induced by inhibition of intercellular contact. *J Cell Biol* **125,** 403-415.

Beane WS, Morokuma J, Adams DS & Levin M. (2011). A chemical genetics approach reveals H,K-ATPase-mediated membrane voltage is required for planarian head regeneration. *Chem Biol* **18,** 77-89.

Beane WS, Morokuma J, Lemire JM & Levin M. (2013). Bioelectric signaling regulates head and organ size during planarian regeneration. *Development* **140,** 313-322.

Beck H & Yaari Y. (2008). Plasticity of intrinsic neuronal properties in CNS disorders. *Nat Rev Neurosci* **9,** 357-369.

Beckh S, Noda M, Lubbert H & Numa S. (1989). Differential regulation of three sodium channel messenger RNAs in the rat central nervous system during development. *EMBO J* **8,** 3611-3616.

Belcher SM, Zerillo CA, Levenson R, Ritchie JM & Howe JR. (1995). Cloning of a sodium channel alpha subunit from rabbit Schwann cells. *Proc Natl Acad Sci U S A* **92,** 11034-11038.

Beneski DA & Catterall WA. (1980). Covalent labeling of protein components of the sodium channel with a photoactivable derivative of scorpion toxin. *Proc Natl Acad Sci U S A* **77,** 639-643.

Bennett E, Urcan MS, Tinkle SS, Koszowski AG & Levinson SR. (1997). Contribution of sialic acid to the voltage dependence of sodium channel gating. A possible electrostatic mechanism. *J Gen Physiol* **109,** 327-343.

Bennett ES. (2002). Isoform-specific effects of sialic acid on voltage-dependent Na+ channel gating: functional sialic acids are localized to the S5-S6 loop of domain I. *J Physiol* **538,** 675-690.

Bennett ES, Smith BA & Harper JM. (2004). Voltage-gated Na+ channels confer invasive properties on human prostate cancer cells. *Pflugers Arch* **447,** 908-914.

Benoit E, Legrand AM & Dubois JM. (1986). Effects of ciguatoxin on current and voltage clamped frog myelinated nerve fibre. *Toxicon* **24,** 357-364.

Bertout JA, Patel SA & Simon MC. (2008). The impact of O2 availability on human cancer. *Nat Rev Cancer* **8,** 967-975.

Besson P, Driffort V, Bon E, Gradek F, Chevalier S & Roger S. (2015). How do voltage-gated sodium channels enhance migration and invasiveness in cancer cells? *Biochim Biophys Acta* **1848,** 2493-2501.

Bezanilla F. (2000). The voltage sensor in voltage-dependent ion channels. *Physiol Rev* **80,** 555-592.

Biagiotti T, D'Amico M, Marzi I, Di Gennaro P, Arcangeli A, Wanke E & Olivotto M. (2006). Cell renewing in neuroblastoma: electrophysiological and immunocytochemical characterization of stem cells and derivatives. *Stem Cells* **24,** 443-453.

Bianchi L, Wible B, Arcangeli A, Taglialatela M, Morra F, Castaldo P, Crociani O, Rosati B, Faravelli L, Olivotto M & Wanke E. (1998). herg encodes a K+ current highly conserved in tumors of different histogenesis: a selective advantage for cancer cells? *Cancer Res* **58,** 815-822.

Binggeli R & Cameron IL. (1980). Cellular potentials of normal and cancerous fibroblasts and hepatocytes. *Cancer Res* **40,** 1830-1835.

Binggeli R & Weinstein RC. (1985). Deficits in elevating membrane potential of rat fibrosarcoma cells after cell contact. *Cancer Res* **45,** 235-241.

Binggeli R & Weinstein RC. (1986). Membrane potentials and sodium channels: hypotheses for growth regulation and cancer formation based on changes in sodium channels and gap junctions. *J Theor Biol* **123,** 377-401.

Biswas S, Deschenes I, Disilvestre D, Tian Y, Halperin VL & Tomaselli GF. (2008). Calmodulin regulation of Nav1.4 current: role of binding to the carboxyl terminus. *J Gen Physiol* **131,** 197-209.

Biswas S, DiSilvestre D, Tian Y, Halperin VL & Tomaselli GF. (2009). Calcium-mediated dual-mode regulation of cardiac sodium channel gating. *Circ Res* **104,** 870-878.

Black JA, Liu S & Waxman SG. (2009). Sodium channel activity modulates multiple functions in microglia. *Glia* **57,** 1072-1081.

Black JA & Waxman SG. (2013). Noncanonical roles of voltage-gated sodium channels. *Neuron* **80,** 280-291.

Black JA, Westenbroek RE, Catterall WA & Waxman SG. (1995). Type II brain sodium channel expression in non-neuronal cells: embryonic rat osteoblasts. *Brain Res Mol Brain Res* **34,** 89-98.

Blackiston D, Adams DS, Lemire JM, Lobikin M & Levin M. (2011). Transmembrane potential of GlyCl-expressing instructor cells induces a neoplastic-like conversion of melanocytes via a serotonergic pathway. *Dis Model Mech* **4,** 67-85.

Blackiston DJ, McLaughlin KA & Levin M. (2009). Bioelectric controls of cell proliferation: ion channels, membrane voltage and the cell cycle. *Cell Cycle* **8,** 3519-3528.

Blandino JK, Viglione MP, Bradley WA, Oie HK & Kim YI. (1995). Voltage-dependent sodium channels in human small-cell lung cancer cells: role in action potentials and inhibition by Lambert-Eaton syndrome IgG. *J Membr Biol* **143,** 153-163.

Blanton MG, Lo Turco JJ & Kriegstein AR. (1989). Whole cell recording from neurons in slices of reptilian and mammalian cerebral cortex. *J Neurosci Methods* **30,** 203-210.

Blaustein MP & Lederer WJ. (1999). Sodium/calcium exchange: its physiological implications. *Physiol Rev* **79,** 763-854.

Boiko T, Rasband MN, Levinson SR, Caldwell JH, Mandel G, Trimmer JS & Matthews G. (2001). Compact myelin dictates the differential targeting of two sodium channel isoforms in the same axon. *Neuron* **30,** 91-104.

Boonstra J, Mummery CL, Tertoolen LG, Van Der Saag PT & De Laat SW. (1981). Cation transport and growth regulation in neuroblastoma cells. Modulations of K+ transport and electrical membrane properties during the cell cycle. *J Cell Physiol* **107,** 75-83.

Bootman MD, Rietdorf K, Collins T, Walker S & Sanderson M. (2013). Ca2+-sensitive fluorescent dyes and intracellular Ca2+ imaging. *Cold Spring Harb Protoc* **2013,** 83-99.

Bordey A, Sontheimer H & Trouslard J. (2000). Muscarinic activation of BK channels induces membrane oscillations in glioma cells and leads to inhibition of cell migration. *J Membr Biol* **176,** 31-40.

Borodinsky LN & Fiszman ML. (1998). Extracellular potassium concentration regulates proliferation of immature cerebellar granule cells. *Brain Res Dev Brain Res* **107,** 43-48.

Borowiec AS, Hague F, Harir N, Guenin S, Guerineau F, Gouilleux F, Roudbaraki M, Lassoued K & Ouadid-Ahidouch H. (2007). IGF-1 activates hEAG K(+) channels through an Akt-dependent signaling pathway in breast cancer cells: role in cell proliferation. *J Cell Physiol* **212,** 690-701.

Bourguignon LY, Zhu H, Shao L & Chen YW. (2001). CD44 interaction with c-Src kinase promotes cortactin-mediated cytoskeleton function and hyaluronic acid-dependent ovarian tumor cell migration. *J Biol Chem* **276,** 7327-7336.

Brackenbury WJ. (2012). Voltage-gated sodium channels and metastatic disease. *Channels (Austin)* **6,** 352-361.

Brackenbury WJ, Calhoun JD, Chen C, Miyazaki H, Nukina N, Oyama F, Ranscht B & Isom LL. (2010). Functional reciprocity between Na+ channel Nav1.6 and beta1

subunits in the coordinated regulation of excitability and neurite outgrowth. *Proc Natl Acad Sci U S A* **107,** 2283-2288.

Brackenbury WJ, Chioni AM, Diss JK & Djamgoz MB. (2007). The neonatal splice variant of Nav1.5 potentiates in vitro invasive behaviour of MDA-MB-231 human breast cancer cells. *Breast Cancer Res Treat* **101,** 149-160.

Brackenbury WJ, Davis TH, Chen C, Slat EA, Detrow MJ, Dickendesher TL, Ranscht B & Isom LL. (2008). Voltage-gated Na+ channel beta1 subunit-mediated neurite outgrowth requires Fyn kinase and contributes to postnatal CNS development in vivo. *J Neurosci* **28,** 3246-3256.

Brackenbury WJ & Djamgoz MB. (2006). Activity-dependent regulation of voltage-gated Na+ channel expression in Mat-LyLu rat prostate cancer cell line. *J Physiol* **573,** 343-356.

Brackenbury WJ & Djamgoz MB. (2007). Nerve growth factor enhances voltage-gated Na+ channel activity and Transwell migration in Mat-LyLu rat prostate cancer cell line. *J Cell Physiol* **210,** 602-608.

Brackenbury WJ & Isom LL. (2011). Na Channel beta Subunits: Overachievers of the Ion Channel Family. *Front Pharmacol* **2,** 53.

Brackenbury WJ, Yuan Y, O'Malley HA, Parent JM & Isom LL. (2013). Abnormal neuronal patterning occurs during early postnatal brain development of Scn1b-null mice and precedes hyperexcitability. *Proc Natl Acad Sci U S A* **110,** 1089-1094.

Brancho D, Ventura JJ, Jaeschke A, Doran B, Flavell RA & Davis RJ. (2005). Role of MLK3 in the regulation of mitogen-activated protein kinase signaling cascades. *Mol Cell Biol* **25,** 3670-3681.

Brisson L, Driffort V, Benoist L, Poet M, Counillon L, Antelmi E, Rubino R, Besson P, Labbal F, Chevalier S, Reshkin SJ, Gore J & Roger S. (2013). NaV1.5 Na(+) channels allosterically regulate the NHE-1 exchanger and promote the activity of breast cancer cell invadopodia. *J Cell Sci* **126,** 4835-4842.

Brisson L, Gillet L, Calaghan S, Besson P, Le Guennec JY, Roger S & Gore J. (2011). Na(V)1.5 enhances breast cancer cell invasiveness by increasing NHE1-dependent H(+) efflux in caveolae. *Oncogene* **30,** 2070-2076.

Brundage RA, Fogarty KE, Tuft RA & Fay FS. (1991). Calcium gradients underlying polarization and chemotaxis of eosinophils. *Science* **254,** 703-706.

Brysch W, Creutzfeldt OD, Luno K, Schlingensiepen R & Schlingensiepen KH. (1991). Regional and temporal expression of sodium channel messenger RNAs in the rat brain during development. *Exp Brain Res* **86,** 562-567.

Buchwald HD, Durham L, Fischer HG, Harada R, Mosher HS, Kao CY & Fuhrman FA. (1964). Identity of Tarichatoxin and Tetrodotoxin. *Science* **143,** 474-475.

Buffington SA & Rasband MN. (2013). Na+ channel-dependent recruitment of Navbeta4 to axon initial segments and nodes of Ranvier. *J Neurosci* **33,** 6191-6202.

Calderone V. (2002). Large-conductance, ca(2+)-activated k(+) channels: function, pharmacology and drugs. *Curr Med Chem* **9,** 1385-1395.

Cameron IL, Smith NK, Pool TB & Sparks RL. (1980). Intracellular concentration of sodium and other elements as related to mitogenesis and oncogenesis in vivo. *Cancer Res* **40,** 1493-1500.

Camougis G, Takman BH & Tasse JR. (1967). Potency difference between the zwitterion form and the cation forms of tetrodotoxin. *Science* **156,** 1625-1627.

Campbell TM, Main MJ & Fitzgerald EM. (2013). Functional expression of the voltage-gated Na(+)-channel Nav1.7 is necessary for EGF-mediated invasion in human non-small cell lung cancer cells. *J Cell Sci* **126,** 4939-4949.

Canady KS, Ali-Osman F & Rubel EW. (1990). Extracellular potassium influences DNA and protein syntheses and glial fibrillary acidic protein expression in cultured glial cells. *Glia* **3,** 368-374.

Cantrell AR & Catterall WA. (2001). Neuromodulation of Na+ channels: an unexpected form of cellular plasticity. *Nat Rev Neurosci* **2,** 397-407.

Cantrell AR, Smith RD, Goldin AL, Scheuer T & Catterall WA. (1997). Dopaminergic modulation of sodium current in hippocampal neurons via cAMP-dependent phosphorylation of specific sites in the sodium channel alpha subunit. *J Neurosci* **17,** 7330-7338.

Carragher NO, Westhoff MA, Fincham VJ, Schaller MD & Frame MC. (2003). A novel role for FAK as a protease-targeting adaptor protein: regulation by p42 ERK and Src. *Curr Biol* **13,** 1442-1450.

Carrithers MD, Chatterjee G, Carrithers LM, Offoha R, Iheagwara U, Rahner C, Graham M & Waxman SG. (2009). Regulation of podosome formation in macrophages by a splice variant of the sodium channel SCN8A. *J Biol Chem* **284,** 8114-8126.

Carrithers MD, Dib-Hajj S, Carrithers LM, Tokmoulina G, Pypaert M, Jonas EA & Waxman SG. (2007). Expression of the voltage-gated sodium channel NaV1.5 in the macrophage late endosome regulates endosomal acidification. *J Immunol* **178,** 7822-7832.

Cass A & Dalmark M. (1973). Equilibrium dialysis of ions in nystatin-treated red cells. *Nat New Biol* **244,** 47-49.

Catterall WA. (1977). Activation of the action potential Na+ ionophore by neurotoxins. An allosteric model. *J Biol Chem* **252,** 8669-8676.

Catterall WA. (1980). Neurotoxins that act on voltage-sensitive sodium channels in excitable membranes. *Annu Rev Pharmacol Toxicol* **20,** 15-43.

Catterall WA. (2000). From ionic currents to molecular mechanisms: the structure and function of voltage-gated sodium channels. *Neuron* **26,** 13-25.

Catterall WA. (2012). Voltage-gated sodium channels at 60: structure, function and pathophysiology. *J Physiol* **590,** 2577-2589.

Catterall WA & Beress L. (1978). Sea anemone toxin and scorpion toxin share a common receptor site associated with the action potential sodium ionophore. *J Biol Chem* **253,** 7393-7396.

Cestele S & Catterall WA. (2000). Molecular mechanisms of neurotoxin action on voltage-gated sodium channels. *Biochimie* **82,** 883-892.

Cestele S, Qu Y, Rogers JC, Rochat H, Scheuer T & Catterall WA. (1998). Voltage sensor-trapping: enhanced activation of sodium channels by beta-scorpion toxin bound to the S3-S4 loop in domain II. *Neuron* **21,** 919-931.

Chagot B, Potet F, Balser JR & Chazin WJ. (2009). Solution NMR structure of the C-terminal EF-hand domain of human cardiac sodium channel NaV1.5. *J Biol Chem* **284,** 6436-6445.

Chahine M, Sirois J, Marcotte P, Chen L & Kallen RG. (1998). Extrapore residues of the S5-S6 loop of domain 2 of the voltage-gated skeletal muscle sodium channel (rSkM1) contribute to the mu-conotoxin GIIIA binding site. *Biophys J* **75,** 236-246.

Chan KT, Bennin DA & Huttenlocher A. (2010). Regulation of adhesion dynamics by calpain-mediated proteolysis of focal adhesion kinase (FAK). *J Biol Chem* **285,** 11418-11426.

Chang KW, Yuan TC, Fang KP, Yang FS, Liu CJ, Chang CS & Lin SC. (2003). The increase of voltage-gated potassium channel Kv3.4 mRNA expression in oral squamous cell carcinoma. *J Oral Pathol Med* **32,** 606-611.

Chantome A, Girault A, Potier M, Collin C, Vaudin P, Pages JC, Vandier C & Joulin V. (2009). KCa2.3 channel-dependent hyperpolarization increases melanoma cell motility. *Exp Cell Res* **315,** 3620-3630.

Chatelier A, Mercier A, Tremblier B, Theriault O, Moubarak M, Benamer N, Corbi P, Bois P, Chahine M & Faivre JF. (2012). A distinct de novo expression of Nav1.5 sodium channels in human atrial fibroblasts differentiated into myofibroblasts. *J Physiol* **590,** 4307-4319.

Chen C, Bharucha V, Chen Y, Westenbroek RE, Brown A, Malhotra JD, Jones D, Avery C, Gillespie PJ, 3rd, Kazen-Gillespie KA, Kazarinova-Noyes K, Shrager P, Saunders TL, Macdonald RL, Ransom BR, Scheuer T, Catterall WA & Isom LL. (2002). Reduced sodium channel density, altered voltage dependence of inactivation, and increased susceptibility to seizures in mice lacking sodium channel beta 2-subunits. *Proc Natl Acad Sci U S A* **99,** 17072-17077.

Chen C, Calhoun JD, Zhang Y, Lopez-Santiago L, Zhou N, Davis TH, Salzer JL & Isom LL. (2012). Identification of the cysteine residue responsible for disulfide linkage of Na+ channel alpha and beta2 subunits. *J Biol Chem* **287,** 39061-39069.

Chen C, Westenbroek RE, Xu X, Edwards CA, Sorenson DR, Chen Y, McEwen DP, O'Malley HA, Bharucha V, Meadows LS, Knudsen GA, Vilaythong A, Noebels JL, Saunders TL, Scheuer T, Shrager P, Catterall WA & Isom LL. (2004). Mice

lacking sodium channel beta1 subunits display defects in neuronal excitability, sodium channel expression, and nodal architecture. *J Neurosci* **24,** 4030-4042.

Chen TC, Law B, Kondratyuk T & Rossie S. (1995). Identification of soluble protein phosphatases that dephosphorylate voltage-sensitive sodium channels in rat brain. *J Biol Chem* **270,** 7750-7756.

Cheng KW, Lahad JP, Kuo WL, Lapuk A, Yamada K, Auersperg N, Liu J, Smith-McCune K, Lu KH, Fishman D, Gray JW & Mills GB. (2004). The RAB25 small GTPase determines aggressiveness of ovarian and breast cancers. *Nat Med* **10,** 1251-1256.

Chernet BT, Fields C & Levin M. (2014). Long-range gap junctional signaling controls oncogene-mediated tumorigenesis in Xenopus laevis embryos. *Front Physiol* **5,** 519.

Chernet BT & Levin M. (2013). Transmembrane voltage potential is an essential cellular parameter for the detection and control of tumor development in a Xenopus model. *Dis Model Mech* **6,** 595-607.

Chernet BT & Levin M. (2014). Transmembrane voltage potential of somatic cells controls oncogene-mediated tumorigenesis at long-range. *Oncotarget* **5,** 3287-3306.

Chifflet S, Correa V, Nin V, Justet C & Hernandez JA. (2004). Effect of membrane potential depolarization on the organization of the actin cytoskeleton of eye epithelia. The role of adherens junctions. *Exp Eye Res* **79,** 769-777.

Chifflet S, Hernandez JA & Grasso S. (2005). A possible role for membrane depolarization in epithelial wound healing. *Am J Physiol Cell Physiol* **288,** C1420-1430.

Chifflet S, Hernandez JA, Grasso S & Cirillo A. (2003). Nonspecific depolarization of the plasma membrane potential induces cytoskeletal modifications of bovine corneal endothelial cells in culture. *Exp Cell Res* **282,** 1-13.

Chioni AM, Brackenbury WJ, Calhoun JD, Isom LL & Djamgoz MB. (2009). A novel adhesion molecule in human breast cancer cells: voltage-gated Na+ channel beta1 subunit. *Int J Biochem Cell Biol* **41,** 1216-1227.

Chioni AM, Fraser SP, Pani F, Foran P, Wilkin GP, Diss JK & Djamgoz MB. (2005). A novel polyclonal antibody specific for the Na(v)1.5 voltage-gated Na(+) channel 'neonatal' splice form. *J Neurosci Methods* **147,** 88-98.

Chioni AM, Shao D, Grose R & Djamgoz MB. (2010). Protein kinase A and regulation of neonatal Nav1.5 expression in human breast cancer cells: activity-dependent positive feedback and cellular migration. *Int J Biochem Cell Biol* **42,** 346-358.

Choi J, Chiang A, Taulier N, Gros R, Pirani A & Husain M. (2006). A calmodulin-binding site on cyclin E mediates Ca2+-sensitive G1/s transitions in vascular smooth muscle cells. *Circ Res* **98,** 1273-1281.

Chou JJ, Li S, Klee CB & Bax A. (2001). Solution structure of Ca(2+)-calmodulin reveals flexible hand-like properties of its domains. *Nat Struct Biol* **8,** 990-997.

Claes L, Del-Favero J, Ceulemans B, Lagae L, Van Broeckhoven C & De Jonghe P. (2001). De novo mutations in the sodium-channel gene SCN1A cause severe myoclonic epilepsy of infancy. *Am J Hum Genet* **68,** 1327-1332.

Cleator S, Heller W & Coombes RC. (2007). Triple-negative breast cancer: therapeutic options. *Lancet Oncol* **8,** 235-244.

Cole KS & Curtis HJ. (1939). Electric Impedance of the Squid Giant Axon during Activity. *J Gen Physiol* **22,** 649-670.

Cole KS & Hodgkin AL. (1939). Membrane and Protoplasm Resistance in the Squid Giant Axon. *J Gen Physiol* **22,** 671-687.

Cone CD, Jr. (1969). Electroosmotic interactions accompanying mitosis initation in sarcoma cells in vitro. *Trans N Y Acad Sci* **31,** 404-427.

Cone CD, Jr. (1970). Variation of the transmembrane potential level as a basic mechanism of mitosis control. *Oncology* **24,** 438-470.

Cone CD, Jr. (1971). Unified theory on the basic mechanism of normal mitotic control and oncogenesis. *J Theor Biol* **30,** 151-181.

Cone CD, Jr. & Cone CM. (1976). Induction of mitosis in mature neurons in central nervous system by sustained depolarization. *Science* **192,** 155-158.

Cone CD, Jr. & Tongier M, Jr. (1971). Control of somatic cell mitosis by simulated changes in the transmembrane potential level. *Oncology* **25,** 168-182.

Cone CD, Jr. & Tongier M, Jr. (1973). Contact inhibition of division: involvement of the electrical transmembrane potential. *J Cell Physiol* **82,** 373-386.

Copley RR. (2004). Evolutionary convergence of alternative splicing in ion channels. *Trends Genet* **20,** 171-176.

Coso OA, Chiariello M, Yu JC, Teramoto H, Crespo P, Xu N, Miki T & Gutkind JS. (1995). The small GTP-binding proteins Rac1 and Cdc42 regulate the activity of the JNK/SAPK signaling pathway. *Cell* **81,** 1137-1146.

Costa MR, Casnellie JE & Catterall WA. (1982). Selective phosphorylation of the alpha subunit of the sodium channel by cAMP-dependent protein kinase. *J Biol Chem* **257,** 7918-7921.

Costa MR & Catterall WA. (1984a). Cyclic AMP-dependent phosphorylation of the alpha subunit of the sodium channel in synaptic nerve ending particles. *J Biol Chem* **259,** 8210-8218.

Costa MR & Catterall WA. (1984b). Phosphorylation of the alpha subunit of the sodium channel by protein kinase C. *Cell Mol Neurobiol* **4,** 291-297.

Coward K, Jowett A, Plumpton C, Powell A, Birch R, Tate S, Bountra C & Anand P. (2001). Sodium channel beta1 and beta2 subunits parallel SNS/PN3 alpha-subunit changes in injured human sensory neurons. *Neuroreport* **12,** 483-488.

Cox JJ, Reimann F, Nicholas AK, Thornton G, Roberts E, Springell K, Karbani G, Jafri H, Mannan J, Raashid Y, Al-Gazali L, Hamamy H, Valente EM, Gorman S, Williams R, McHale DP, Wood JN, Gribble FM & Woods CG. (2006). An SCN9A channelopathy causes congenital inability to experience pain. *Nature* **444,** 894-898.

Craner MJ, Damarjian TG, Liu S, Hains BC, Lo AC, Black JA, Newcombe J, Cuzner ML & Waxman SG. (2005). Sodium channels contribute to microglia/macrophage activation and function in EAE and MS. *Glia* **49,** 220-229.

Crociani O, Cherubini A, Piccini E, Polvani S, Costa L, Fontana L, Hofmann G, Rosati B, Wanke E, Olivotto M & Arcangeli A. (2000). erg gene(s) expression during development of the nervous and muscular system of quail embryos. *Mech Dev* **95,** 239-243.

Crook T, Crossland S, Crompton MR, Osin P & Gusterson BA. (1997). p53 mutations in BRCA1-associated familial breast cancer. *Lancet* **350,** 638-639.

Crowe JP, Jr., Gordon NH, Hubay CA, Shenk RR, Zollinger RM, Brumberg DJ, McGuire WL & Shuck JM. (1991). Estrogen receptor determination and long term survival of patients with carcinoma of the breast. *Surg Gynecol Obstet* **173,** 273-278.

Cui J, Cox DH & Aldrich RW. (1997). Intrinsic voltage dependence and Ca2+ regulation of mslo large conductance Ca-activated K+ channels. *J Gen Physiol* **109,** 647-673.

Dang I, Gorelik R, Sousa-Blin C, Derivery E, Guerin C, Linkner J, Nemethova M, Dumortier JG, Giger FA, Chipysheva TA, Ermilova VD, Vacher S, Campanacci V, Herrada I, Planson AG, Fetics S, Henriot V, David V, Oguievetskaia K, Lakisic G, Pierre F, Steffen A, Boyreau A, Peyrieras N, Rottner K, Zinn-Justin S, Cherfils J, Bieche I, Alexandrova AY, David NB, Small JV, Faix J, Blanchoin L & Gautreau A. (2013). Inhibitory signalling to the Arp2/3 complex steers cell migration. *Nature* **503,** 281-284.

Danielsson BR, Lansdell K, Patmore L & Tomson T. (2003). Phenytoin and phenobarbital inhibit human HERG potassium channels. *Epilepsy Res* **55,** 147-157.

Dascal N & Lotan I. (1991). Activation of protein kinase C alters voltage dependence of a Na+ channel. *Neuron* **6,** 165-175.

Davis TH, Chen C & Isom LL. (2004). Sodium channel beta1 subunits promote neurite outgrowth in cerebellar granule neurons. *J Biol Chem* **279,** 51424-51432.

Dent R, Trudeau M, Pritchard KI, Hanna WM, Kahn HK, Sawka CA, Lickley LA, Rawlinson E, Sun P & Narod SA. (2007). Triple-negative breast cancer: clinical features and patterns of recurrence. *Clin Cancer Res* **13,** 4429-4434.

Deschenes I, Neyroud N, DiSilvestre D, Marban E, Yue DT & Tomaselli GF. (2002). Isoform-specific modulation of voltage-gated Na(+) channels by calmodulin. *Circ Res* **90,** E49-57.

Diaz D, Delgadillo DM, Hernandez-Gallegos E, Ramirez-Dominguez ME, Hinojosa LM, Ortiz CS, Berumen J, Camacho J & Gomora JC. (2007). Functional expression of voltage-gated sodium channels in primary cultures of human cervical cancer. *J Cell Physiol* **210,** 469-478.

Dib-Hajj SD, Binshtok AM, Cummins TR, Jarvis MF, Samad T & Zimmermann K. (2009a). Voltage-gated sodium channels in pain states: role in pathophysiology and targets for treatment. *Brain Res Rev* **60,** 65-83.

Dib-Hajj SD, Black JA & Waxman SG. (2009b). Voltage-gated sodium channels: therapeutic targets for pain. *Pain Med* **10,** 1260-1269.

Dib-Hajj SD, Black JA & Waxman SG. (2015). NaV1.9: a sodium channel linked to human pain. *Nat Rev Neurosci* **16,** 511-519.

Dib-Hajj SD, Tyrrell L, Cummins TR, Black JA, Wood PM & Waxman SG. (1999a). Two tetrodotoxin-resistant sodium channels in human dorsal root ganglion neurons. *FEBS Lett* **462,** 117-120.

Dib-Hajj SD, Tyrrell L, Escayg A, Wood PM, Meisler MH & Waxman SG. (1999b). Coding sequence, genomic organization, and conserved chromosomal localization of the mouse gene Scn11a encoding the sodium channel NaN. *Genomics* **59,** 309-318.

Ding Y, Brackenbury WJ, Onganer PU, Montano X, Porter LM, Bates LF & Djamgoz MB. (2008). Epidermal growth factor upregulates motility of Mat-LyLu rat prostate cancer cells partially via voltage-gated Na+ channel activity. *J Cell Physiol* **215,** 77-81.

Ding Y & Djamgoz MB. (2004). Serum concentration modifies amplitude and kinetics of voltage-gated Na+ current in the Mat-LyLu cell line of rat prostate cancer. *Int J Biochem Cell Biol* **36,** 1249-1260.

Diss JK, Archer SN, Hirano J, Fraser SP & Djamgoz MB. (2001). Expression profiles of voltage-gated Na(+) channel alpha-subunit genes in rat and human prostate cancer cell lines. *Prostate* **48,** 165-178.

Diss JK, Fraser SP & Djamgoz MB. (2004). Voltage-gated Na+ channels: multiplicity of expression, plasticity, functional implications and pathophysiological aspects. *Eur Biophys J* **33,** 180-193.

Diss JK, Fraser SP, Walker MM, Patel A, Latchman DS & Djamgoz MB. (2008). Beta-subunits of voltage-gated sodium channels in human prostate cancer: quantitative in vitro and in vivo analyses of mRNA expression. *Prostate Cancer Prostatic Dis* **11,** 325-333.

Diss JK, Stewart D, Fraser SP, Black JA, Dib-Hajj S, Waxman SG, Archer SN & Djamgoz MB. (1998). Expression of skeletal muscle-type voltage-gated Na+ channel in rat and human prostate cancer cell lines. *FEBS Lett* **427,** 5-10.

Diss JK, Stewart D, Pani F, Foster CS, Walker MM, Patel A & Djamgoz MB. (2005). A potential novel marker for human prostate cancer: voltage-gated sodium channel expression in vivo. *Prostate Cancer Prostatic Dis* **8,** 266-273.

Djamgoz MB & Onkal R. (2013). Persistent current blockers of voltage-gated sodium channels: a clinical opportunity for controlling metastatic disease. *Recent Pat Anticancer Drug Discov* **8,** 66-84.

Djamgoz MBA, Mycielska M, Madeja Z, Fraser SP & Korohoda W. (2001). Directional movement of rat prostate cancer cells in direct-current electric field: involvement of voltagegated Na+ channel activity. *J Cell Sci* **114,** 2697-2705.

Do K & Chen AP. (2013). Molecular pathways: targeting PARP in cancer treatment. *Clin Cancer Res* **19,** 977-984.

Donatsch P, Lowe DA, Richardson BP & Taylor P. (1977). The functional significance of sodium channels in pancreatic beta-cell membranes. *J Physiol* **267,** 357-376.

Downward J. (2003). Targeting RAS signalling pathways in cancer therapy. *Nat Rev Cancer* **3,** 11-22.

Driffort V, Gillet L, Bon E, Marionneau-Lambot S, Oullier T, Joulin V, Collin C, Pages JC, Jourdan ML, Chevalier S, Bougnoux P, Le Guennec JY, Besson P & Roger S. (2014). Ranolazine inhibits NaV1.5-mediated breast cancer cell invasiveness and lung colonization. *Mol Cancer* **13,** 264.

Dulong C, Fang YJ, Gest C, Zhou MH, Patte-Mensah C, Mensah-Nyagan AG, Vannier JP, Lu H, Soria C, Cazin L, Mei YA, Varin R & Li H. (2014). The small GTPase RhoA regulates the expression and function of the sodium channel Nav1.5 in breast cancer cells. *Int J Oncol* **44,** 539-547.

Dunnwald LK, Rossing MA & Li CI. (2007). Hormone receptor status, tumor characteristics, and prognosis: a prospective cohort of breast cancer patients. *Breast Cancer Res* **9,** R6.

Eckert LB, Repasky GA, Ulku AS, McFall A, Zhou H, Sartor CI & Der CJ. (2004). Involvement of Ras activation in human breast cancer cell signaling, invasion, and anoikis. *Cancer Res* **64,** 4585-4592.

Egeblad M & Werb Z. (2002). New functions for the matrix metalloproteinases in cancer progression. *Nat Rev Cancer* **2,** 161-174.

Escayg A, MacDonald BT, Meisler MH, Baulac S, Huberfeld G, An-Gourfinkel I, Brice A, LeGuern E, Moulard B, Chaigne D, Buresi C & Malafosse A. (2000). Mutations of SCN1A, encoding a neuronal sodium channel, in two families with GEFS+2. *Nat Genet* **24,** 343-345.

Fantozzi A & Christofori G. (2006). Mouse models of breast cancer metastasis. *Breast Cancer Res* **8,** 212.

Farias LM, Ocana DB, Diaz L, Larrea F, Avila-Chavez E, Cadena A, Hinojosa LM, Lara G, Villanueva LA, Vargas C, Hernandez-Gallegos E, Camacho-Arroyo I, Duenas-

Gonzalez A, Perez-Cardenas E, Pardo LA, Morales A, Taja-Chayeb L, Escamilla J, Sanchez-Pena C & Camacho J. (2004). Ether a go-go potassium channels as human cervical cancer markers. *Cancer Res* **64,** 6996-7001.

Fearon IM & Brown ST. (2004). Acute and chronic hypoxic regulation of recombinant hNa(v)1.5 alpha subunits. *Biochem Biophys Res Commun* **324,** 1289-1295.

Felts PA, Yokoyama S, Dib-Hajj S, Black JA & Waxman SG. (1997). Sodium channel alpha-subunit mRNAs I, II, III, NaG, Na6 and hNE (PN1): different expression patterns in developing rat nervous system. *Brain Res Mol Brain Res* **45,** 71-82.

Fitzgerald EM, Okuse K, Wood JN, Dolphin AC & Moss SJ. (1999). cAMP-dependent phosphorylation of the tetrodotoxin-resistant voltage-dependent sodium channel SNS. *J Physiol* **516 ( Pt 2),** 433-446.

Fraser SP, Ding Y, Liu A, Foster CS & Djamgoz MB. (1999). Tetrodotoxin suppresses morphological enhancement of the metastatic MAT-LyLu rat prostate cancer cell line. *Cell Tissue Res* **295,** 505-512.

Fraser SP, Diss JK, Chioni AM, Mycielska ME, Pan H, Yamaci RF, Pani F, Siwy Z, Krasowska M, Grzywna Z, Brackenbury WJ, Theodorou D, Koyuturk M, Kaya H, Battaloglu E, De Bella MT, Slade MJ, Tolhurst R, Palmieri C, Jiang J, Latchman DS, Coombes RC & Djamgoz MB. (2005). Voltage-gated sodium channel expression and potentiation of human breast cancer metastasis. *Clin Cancer Res* **11,** 5381-5389.

Fraser SP, Diss JK, Lloyd LJ, Pani F, Chioni AM, George AJ & Djamgoz MB. (2004). T-lymphocyte invasiveness: control by voltage-gated Na+ channel activity. *FEBS Lett* **569,** 191-194.

Fraser SP, Grimes JA & Djamgoz MB. (2000). Effects of voltage-gated ion channel modulators on rat prostatic cancer cell proliferation: comparison of strongly and weakly metastatic cell lines. *Prostate* **44,** 61-76.

Fraser SP, Ozerlat-Gunduz I, Onkal R, Diss JK, Latchman DS & Djamgoz MB. (2010). Estrogen and non-genomic upregulation of voltage-gated Na(+) channel activity in MDA-MB-231 human breast cancer cells: role in adhesion. *J Cell Physiol* **224,** 527-539.

Fraser SP, Rizaner N, Corro C, Al Jayoosi F & Djamgoz MB. (2015). Systems pathophysiology of voltage-gated sodium channel in breast cancer. In *An International Meeting on Ion Channels, Transporters & Cancer*. Imperial College London.

Fraser SP, Salvador V, Manning EA, Mizal J, Altun S, Raza M, Berridge RJ & Djamgoz MB. (2003). Contribution of functional voltage-gated Na+ channel expression to cell behaviors involved in the metastatic cascade in rat prostate cancer: I. Lateral motility. *J Cell Physiol* **195,** 479-487.

Freedman BD, Price MA & Deutsch CJ. (1992). Evidence for voltage modulation of IL-2 production in mitogen-stimulated human peripheral blood lymphocytes. *J Immunol* **149,** 3784-3794.

French CR, Sah P, Buckett KJ & Gage PW. (1990). A voltage-dependent persistent sodium current in mammalian hippocampal neurons. *J Gen Physiol* **95,** 1139-1157.

Fulgenzi G, Graciotti L, Faronato M, Soldovieri MV, Miceli F, Amoroso S, Annunziato L, Procopio A & Taglialatela M. (2006). Human neoplastic mesothelial cells express voltage-gated sodium channels involved in cell motility. *Int J Biochem Cell Biol* **38,** 1146-1159.

Furukawa T, Yamakawa T, Midera T, Sagawa T, Mori Y & Nukada T. (1999). Selectivities of dihydropyridine derivatives in blocking Ca(2+) channel subtypes expressed in Xenopus oocytes. *J Pharmacol Exp Ther* **291,** 464-473.

Gabelli SB, Boto A, Kuhns VH, Bianchet MA, Farinelli F, Aripirala S, Yoder J, Jakoncic J, Tomaselli GF & Amzel LM. (2014). Regulation of the NaV1.5 cytoplasmic domain by calmodulin. *Nat Commun* **5,** 5126.

Gabelli SB, Yoder JB, Tomaselli GF & Amzel LM. (2015). Calmodulin and Ca control of voltage gated Na channels. *Channels (Austin)***,** 0.

Ganz PA. (2005). Breast cancer, menopause, and long-term survivorship: critical issues for the 21st century. *Am J Med* **118 Suppl 12B,** 136-141.

Ganz PA, Greendale GA, Petersen L, Kahn B & Bower JE. (2003). Breast cancer in younger women: reproductive and late health effects of treatment. *J Clin Oncol* **21,** 4184-4193.

Gao R, Shen Y, Cai J, Lei M & Wang Z. (2010). Expression of voltage-gated sodium channel alpha subunit in human ovarian cancer. *Oncol Rep* **23,** 1293-1299.

Gavillet B, Rougier JS, Domenighetti AA, Behar R, Boixel C, Ruchat P, Lehr HA, Pedrazzini T & Abriel H. (2006). Cardiac sodium channel Nav1.5 is regulated by a multiprotein complex composed of syntrophins and dystrophin. *Circ Res* **99,** 407-414.

Geback T, Schulz MM, Koumoutsakos P & Detmar M. (2009). TScratch: a novel and simple software tool for automated analysis of monolayer wound healing assays. *BioTechniques* **46,** 265-274.

Gee KR, Brown KA, Chen WN, Bishop-Stewart J, Gray D & Johnson I. (2000). Chemical and physiological characterization of fluo-4 Ca(2+)-indicator dyes. *Cell Calcium* **27,** 97-106.

Gee SH, Madhavan R, Levinson SR, Caldwell JH, Sealock R & Froehner SC. (1998). Interaction of muscle and brain sodium channels with multiple members of the syntrophin family of dystrophin-associated proteins. *J Neurosci* **18,** 128-137.

Gellens ME, George AL, Jr., Chen LQ, Chahine M, Horn R, Barchi RL & Kallen RG. (1992). Primary structure and functional expression of the human cardiac tetrodotoxin-insensitive voltage-dependent sodium channel. *Proc Natl Acad Sci U S A* **89,** 554-558.

George AL, Jr., Knittle TJ & Tamkun MM. (1992). Molecular cloning of an atypical voltage-gated sodium channel expressed in human heart and uterus: evidence for a distinct gene family. *Proc Natl Acad Sci U S A* **89,** 4893-4897.

George AL, Jr., Ledbetter DH, Kallen RG & Barchi RL. (1991). Assignment of a human skeletal muscle sodium channel alpha-subunit gene (SCN4A) to 17q23.1-25.3. *Genomics* **9,** 555-556.

George AL, Jr., Varkony TA, Drabkin HA, Han J, Knops JF, Finley WH, Brown GB, Ward DC & Haas M. (1995). Assignment of the human heart tetrodotoxin-resistant voltage-gated Na+ channel alpha-subunit gene (SCN5A) to band 3p21. *Cytogenet Cell Genet* **68,** 67-70.

Gessner G, Schonherr K, Soom M, Hansel A, Asim M, Baniahmad A, Derst C, Hoshi T & Heinemann SH. (2005). BKCa channels activating at resting potential without calcium in LNCaP prostate cancer cells. *J Membr Biol* **208,** 229-240.

Giancotti FG & Ruoslahti E. (1999). Integrin signaling. *Science* **285,** 1028-1032.

Gillet L, Roger S, Besson P, Lecaille F, Gore J, Bougnoux P, Lalmanach G & Le Guennec JY. (2009). Voltage-gated Sodium Channel Activity Promotes Cysteine Cathepsin-dependent Invasiveness and Colony Growth of Human Cancer Cells. *J Biol Chem* **284,** 8680-8691.

Gold MS, Levine JD & Correa AM. (1998). Modulation of TTX-R INa by PKC and PKA and their role in PGE2-induced sensitization of rat sensory neurons in vitro. *J Neurosci* **18,** 10345-10355.

Goldin AL. (2001). Resurgence of sodium channel research. *Annu Rev Physiol* **63,** 871-894.

Goldman DE. (1943). Potential, Impedance, and Rectification in Membranes. *J Gen Physiol* **27,** 37-60.

Gong B, Rhodes KJ, Bekele-Arcuri Z & Trimmer JS. (1999). Type I and type II Na(+) channel alpha-subunit polypeptides exhibit distinct spatial and temporal patterning, and association with auxiliary subunits in rat brain. *J Comp Neurol* **412,** 342-352.

Gorter JA, Zurolo E, Iyer A, Fluiter K, van Vliet EA, Baayen JC & Aronica E. (2010). Induction of sodium channel Na(x) (SCN7A) expression in rat and human hippocampus in temporal lobe epilepsy. *Epilepsia* **51,** 1791-1800.

Grimes JA, Fraser SP, Stephens GJ, Downing JE, Laniado ME, Foster CS, Abel PD & Djamgoz MB. (1995). Differential expression of voltage-activated Na+ currents in two prostatic tumour cell lines: contribution to invasiveness in vitro. *FEBS Lett* **369,** 290-294.

Groome JR. (2014). The voltage sensor module in sodium channels. *Handb Exp Pharmacol* **221,** 7-31.

Gruvberger S, Ringner M, Chen Y, Panavally S, Saal LH, Borg A, Ferno M, Peterson C & Meltzer PS. (2001). Estrogen receptor status in breast cancer is associated with remarkably distinct gene expression patterns. *Cancer Res* **61,** 5979-5984.

Gupta GP & Massague J. (2006). Cancer metastasis: building a framework. *Cell* **127,** 679-695.

Gustafson TA, Clevinger EC, O'Neill TJ, Yarowsky PJ & Krueger BK. (1993). Mutually exclusive exon splicing of type III brain sodium channel alpha subunit RNA generates developmentally regulated isoforms in rat brain. *J Biol Chem* **268,** 18648-18653.

Habela CW, Ernest NJ, Swindall AF & Sontheimer H. (2009). Chloride accumulation drives volume dynamics underlying cell proliferation and migration. *J Neurophysiol* **101,** 750-757.

Habela CW, Olsen ML & Sontheimer H. (2008). ClC3 is a critical regulator of the cell cycle in normal and malignant glial cells. *J Neurosci* **28,** 9205-9217.

Hainsworth AH, Randall AD & Stefani A. (2006). Whole-cell patch clamp recording of voltage-sensitive Ca2+ channel currents heterologous expression systems and dissociated brain neurons. *Methods Mol Biol* **312,** 161-179.

Hall A. (1998). Rho GTPases and the actin cytoskeleton. *Science* **279,** 509-514.

Hammadi M, Chopin V, Matifat F, Dhennin-Duthille I, Chasseraud M, Sevestre H & Ouadid-Ahidouch H. (2012). Human ether a-gogo K(+) channel 1 (hEag1) regulates MDA-MB-231 breast cancer cell migration through Orai1-dependent calcium entry. *J Cell Physiol* **227,** 3837-3846.

Hanahan D & Weinberg RA. (2011). Hallmarks of cancer: the next generation. *Cell* **144,** 646-674.

Haren N, Khorsi H, Faouzi M, Ahidouch A, Sevestre H & Ouadid-Ahidouch H. (2010). Intermediate conductance Ca2+ activated K+ channels are expressed and functional in breast adenocarcinomas: correlation with tumour grade and metastasis status. *Histol Histopathol* **25,** 1247-1255.

Hartshorne RP, Messner DJ, Coppersmith JC & Catterall WA. (1982). The saxitoxin receptor of the sodium channel from rat brain. Evidence for two nonidentical beta subunits. *J Biol Chem* **257,** 13888-13891.

Hartzell C, Putzier I & Arreola J. (2005). Calcium-activated chloride channels. *Annu Rev Physiol* **67,** 719-758.

Hashimoto S, Onodera Y, Hashimoto A, Tanaka M, Hamaguchi M, Yamada A & Sabe H. (2004). Requirement for Arf6 in breast cancer invasive activities. *Proc Natl Acad Sci U S A* **101,** 6647-6652.

Hasson A, Fainzilber M, Gordon D, Zlotkin E & Spira ME. (1993). Alteration of sodium currents by new peptide toxins from the venom of a molluscivorous Conus snail. *Eur J Neurosci* **5,** 56-64.

Hazelton B, Mitchell B & Tupper J. (1979). Calcium, magnesium, and growth control in the WI-38 human fibroblast cell. *J Cell Biol* **83,** 487-498.

Head JA, Jiang D, Li M, Zorn LJ, Schaefer EM, Parsons JT & Weed SA. (2003). Cortactin tyrosine phosphorylation requires Rac1 activity and association with the cortical actin cytoskeleton. *Mol Biol Cell* **14,** 3216-3229.

Hegle AP, Marble DD & Wilson GF. (2006). A voltage-driven switch for ion-independent signaling by ether-a-go-go K+ channels. *Proc Natl Acad Sci U S A* **103,** 2886-2891.

Heinemann SH, Terlau H, Stuhmer W, Imoto K & Numa S. (1992). Calcium channel characteristics conferred on the sodium channel by single mutations. *Nature* **356,** 441-443.

Hemmerlein B, Weseloh RM, Mello de Queiroz F, Knotgen H, Sanchez A, Rubio ME, Martin S, Schliephacke T, Jenke M, Heinz Joachim R, Stuhmer W & Pardo LA. (2006). Overexpression of Eag1 potassium channels in clinical tumours. *Molecular cancer* **5,** 41.

Hernandez-Plata E, Ortiz CS, Marquina-Castillo B, Medina-Martinez I, Alfaro A, Berumen J, Rivera M & Gomora JC. (2012). Overexpression of NaV 1.6 channels is associated with the invasion capacity of human cervical cancer. *Int J Cancer* **130,** 2013-2023.

Herzog RI, Liu C, Waxman SG & Cummins TR. (2003). Calmodulin binds to the C terminus of sodium channels Nav1.4 and Nav1.6 and differentially modulates their functional properties. *J Neurosci* **23,** 8261-8270.

Higashimori H & Sontheimer H. (2007). Role of Kir4.1 channels in growth control of glia. *Glia* **55,** 1668-1679.

Hill A, McFarlane S, Mulligan K, Gillespie H, Draffin JE, Trimble A, Ouhtit A, Johnston PG, Harkin DP, McCormick D & Waugh DJ. (2006). Cortactin underpins CD44-promoted invasion and adhesion of breast cancer cells to bone marrow endothelial cells. *Oncogene* **25,** 6079-6091.

Hille B. (1968). Pharmacological modifications of the sodium channels of frog nerve. *J Gen Physiol* **51,** 199-219.

Hille B. (1971). The permeability of the sodium channel to organic cations in myelinated nerve. *J Gen Physiol* **58,** 599-619.

Hille B. (1972). The permeability of the sodium channel to metal cations in myelinated nerve. *J Gen Physiol* **59,** 637-658.

Hille B. (1975). The receptor for tetrodotoxin and saxitoxin. A structural hypothesis. *Biophys J* **15,** 615-619.

Hille B. (1992). *Ionic channels of excitable membranes*. Sinauer Associates, Sunderland, Mass.

Hille B. (2001). *Ion channels of excitable membranes*. Sinauer, Sunderland, Mass.

Hirschberg B, Rovner A, Lieberman M & Patlak J. (1995). Transfer of twelve charges is needed to open skeletal muscle Na+ channels. *J Gen Physiol* **106,** 1053-1068.

Hockel M, Schlenger K, Aral B, Mitze M, Schaffer U & Vaupel P. (1996). Association between tumor hypoxia and malignant progression in advanced cancer of the uterine cervix. *Cancer Res* **56,** 4509-4515.

Hockel M & Vaupel P. (2001). Tumor hypoxia: definitions and current clinical, biologic, and molecular aspects. *J Natl Cancer Inst* **93,** 266-276.

Hodgkin AL. (1937). Evidence for electrical transmission in nerve: Part II. *J Physiol* **90,** 211-232.

Hodgkin AL. (1939). The relation between conduction velocity and the electrical resistance outside a nerve fibre. *J Physiol* **94,** 560-570.

Hodgkin AL & Huxley AF. (1952a). The components of membrane conductance in the giant axon of Loligo. *J Physiol* **116,** 473-496.

Hodgkin AL & Huxley AF. (1952b). Currents carried by sodium and potassium ions through the membrane of the giant axon of Loligo. *J Physiol* **116,** 449-472.

Hodgkin AL & Huxley AF. (1952c). The dual effect of membrane potential on sodium conductance in the giant axon of Loligo. *J Physiol* **116,** 497-506.

Hodgkin AL & Huxley AF. (1952d). A quantitative description of membrane current and its application to conduction and excitation in nerve. *J Physiol* **117,** 500-544.

Hodgkin AL, Huxley AF & Katz B. (1952). Measurement of current-voltage relations in the membrane of the giant axon of Loligo. *J Physiol* **116,** 424-448.

Hodgkin AL & Katz B. (1949). The effect of sodium ions on the electrical activity of giant axon of the squid. *J Physiol* **108,** 37-77.

Hoeben A, Landuyt B, Highley MS, Wildiers H, Van Oosterom AT & De Bruijn EA. (2004). Vascular endothelial growth factor and angiogenesis. *Pharmacol Rev* **56,** 549-580.

Hoffman JF, Dodson A, Wickrema A & Dib-Hajj SD. (2004). Tetrodotoxin-sensitive Na+ channels and muscarinic and purinergic receptors identified in human erythroid progenitor cells and red blood cell ghosts. *Proc Natl Acad Sci U S A* **101,** 12370-12374.

Holland KD, Kearney JA, Glauser TA, Buck G, Keddache M, Blankston JR, Glaaser IW, Kass RS & Meisler MH. (2008). Mutation of sodium channel SCN3A in a patient with cryptogenic pediatric partial epilepsy. *Neurosci Lett* **433,** 65-70.

Hotary KB, Allen ED, Brooks PC, Datta NS, Long MW & Weiss SJ. (2003). Membrane type I matrix metalloproteinase usurps tumor growth control imposed by the three-dimensional extracellular matrix. *Cell* **114,** 33-45.

House CD, Vaske CJ, Schwartz AM, Obias V, Frank B, Luu T, Sarvazyan N, Irby R, Strausberg RL, Hales TG, Stuart JM & Lee NH. (2010). Voltage-gated Na+ channel SCN5A is a key regulator of a gene transcriptional network that controls colon cancer invasion. *Cancer Res* **70,** 6957-6967.

House CD, Wang BD, Ceniccola K, Williams R, Simaan M, Olender J, Patel V, Baptista-Hon DT, Annunziata CM, Silvio Gutkind J, Hales TG & Lee NH. (2015). Voltage-gated Na(+) Channel Activity Increases Colon Cancer Transcriptional Activity and Invasion Via Persistent MAPK Signaling. *Sci Rep* **5,** 11541.

Howard-Anderson J, Ganz PA, Bower JE & Stanton AL. (2012). Quality of life, fertility concerns, and behavioral health outcomes in younger breast cancer survivors: a systematic review. *J Natl Cancer Inst* **104,** 386-405.

Hsia DA, Mitra SK, Hauck CR, Streblow DN, Nelson JA, Ilic D, Huang S, Li E, Nemerow GR, Leng J, Spencer KS, Cheresh DA & Schlaepfer DD. (2003). Differential regulation of cell motility and invasion by FAK. *J Cell Biol* **160,** 753-767.

Hu D, Barajas-Martinez H, Medeiros-Domingo A, Crotti L, Veltmann C, Schimpf R, Urrutia J, Alday A, Casis O, Pfeiffer R, Burashnikov E, Caceres G, Tester DJ, Wolpert C, Borggrefe M, Schwartz P, Ackerman MJ & Antzelevitch C. (2012). A novel rare variant in SCN1Bb linked to Brugada syndrome and SIDS by combined modulation of Na(v)1.5 and K(v)4.3 channel currents. *Heart Rhythm* **9,** 760-769.

Huang J, Han C, Estacion M, Vasylyev D, Hoeijmakers JG, Gerrits MM, Tyrrell L, Lauria G, Faber CG, Dib-Hajj SD, Merkies IS, Waxman SG & Group PS. (2014). Gain-of-function mutations in sodium channel Na(v)1.9 in painful neuropathy. *Brain* **137,** 1627-1642.

Huang JM, Wu CH & Baden DG. (1984). Depolarizing action of a red-tide dinoflagellate brevetoxin on axonal membranes. *J Pharmacol Exp Ther* **229,** 615-621.

Huang X & Jan LY. (2014). Targeting potassium channels in cancer. *J Cell Biol* **206,** 151-162.

Hynes RO. (2002). Integrins: bidirectional, allosteric signaling machines. *Cell* **110,** 673-687.

Igci YZ, Bozgeyik E, Borazan E, Pala E, Suner A, Ulasli M, Gurses SA, Yumrutas O, Balik AA & Igci M. (2015). Expression profiling of SCN8A and NDUFC2 genes in colorectal carcinoma. *Exp Oncol* **37,** 77-80.

Irvin WJ, Jr. & Carey LA. (2008). What is triple-negative breast cancer? *Eur J Cancer* **44,** 2799-2805.

Isbilen B, Fraser SP & Djamgoz MB. (2006). Docosahexaenoic acid (omega-3) blocks voltage-gated sodium channel activity and migration of MDA-MB-231 human breast cancer cells. *Int J Biochem Cell Biol* **38,** 2173-2182.

Ishibe S, Joly D, Liu ZX & Cantley LG. (2004). Paxillin serves as an ERK-regulated scaffold for coordinating FAK and Rac activation in epithelial morphogenesis. *Mol Cell* **16,** 257-267.

Isom LL. (2002). Beta subunits: players in neuronal hyperexcitability? *Novartis Found Symp* **241,** 124-138; discussion 138-143, 226-132.

Isom LL & Catterall WA. (1996). Na+ channel subunits and Ig domains. *Nature* **383,** 307-308.

Isom LL, De Jongh KS, Patton DE, Reber BF, Offord J, Charbonneau H, Walsh K, Goldin AL & Catterall WA. (1992). Primary structure and functional expression of the beta 1 subunit of the rat brain sodium channel. *Science* **256,** 839-842.

Isom LL, Ragsdale DS, De Jongh KS, Westenbroek RE, Reber BF, Scheuer T & Catterall WA. (1995a). Structure and function of the beta 2 subunit of brain sodium channels, a transmembrane glycoprotein with a CAM motif. *Cell* **83,** 433-442.

Isom LL, Scheuer T, Brownstein AB, Ragsdale DS, Murphy BJ & Catterall WA. (1995b). Functional co-expression of the beta 1 and type IIA alpha subunits of sodium channels in a mammalian cell line. *J Biol Chem* **270,** 3306-3312.

Jaffe AB & Hall A. (2005). Rho GTPases: biochemistry and biology. *Annu Rev Cell Dev Biol* **21,** 247-269.

Jansson KH, Lynch JE, Lepori-Bui N, Czymmek KJ, Duncan RL & Sikes RA. (2012). Overexpression of the VSSC-associated CAM, beta-2, enhances LNCaP cell metastasis associated behavior. *Prostate* **72,** 1080-1092.

Javle M & Curtin NJ. (2011). The role of PARP in DNA repair and its therapeutic exploitation. *Br J Cancer* **105,** 1114-1122.

Jeong SY, Goto J, Hashida H, Suzuki T, Ogata K, Masuda N, Hirai M, Isahara K, Uchiyama Y & Kanazawa I. (2000). Identification of a novel human voltage-gated sodium channel alpha subunit gene, SCN12A. *Biochem Biophys Res Commun* **267,** 262-270.

Jespersen T, Gavillet B, van Bemmelen MX, Cordonier S, Thomas MA, Staub O & Abriel H. (2006). Cardiac sodium channel Na(v)1.5 interacts with and is regulated by the protein tyrosine phosphatase PTPH1. *Biochem Biophys Res Commun* **348,** 1455-1462.

Joensuu H & Gligorov J. (2012). Adjuvant treatments for triple-negative breast cancers. *Ann Oncol* **23 Suppl 6,** vi40-45.

Johnson D, Montpetit ML, Stocker PJ & Bennett ES. (2004). The sialic acid component of the beta1 subunit modulates voltage-gated sodium channel function. *J Biol Chem* **279,** 44303-44310.

Johnstone BM. (1959). Micro-electrode penetration of ascites tumour cells. *Nature* **183,** 411.

Ju YK, Saint DA & Gage PW. (1996). Hypoxia increases persistent sodium current in rat ventricular myocytes. *J Physiol* **497 ( Pt 2),** 337-347.

Juszczak GR & Swiergiel AH. (2009). Properties of gap junction blockers and their behavioural, cognitive and electrophysiological effects: animal and human studies. *Prog Neuropsychopharmacol Biol Psychiatry* **33,** 181-198.

Kajita M, Itoh Y, Chiba T, Mori H, Okada A, Kinoh H & Seiki M. (2001). Membrane-type 1 matrix metalloproteinase cleaves CD44 and promotes cell migration. *J Cell Biol* **153,** 893-904.

Kallen RG, Sheng ZH, Yang J, Chen LQ, Rogart RB & Barchi RL. (1990). Primary structure and expression of a sodium channel characteristic of denervated and immature rat skeletal muscle. *Neuron* **4,** 233-242.

Kao CY & Nishiyama A. (1965). Actions of saxitoxin on peripheral neuromuscular systems. *J Physiol* **180,** 50-66.

Kaplan MR, Cho MH, Ullian EM, Isom LL, Levinson SR & Barres BA. (2001). Differential control of clustering of the sodium channels Na(v)1.2 and Na(v)1.6 at developing CNS nodes of Ranvier. *Neuron* **30,** 105-119.

Kaufmann SG, Westenbroek RE, Maass AH, Lange V, Renner A, Wischmeyer E, Bonz A, Muck J, Ertl G, Catterall WA, Scheuer T & Maier SK. (2013). Distribution and function of sodium channel subtypes in human atrial myocardium. *J Mol Cell Cardiol* **61,** 133-141.

Kazarinova-Noyes K, Malhotra JD, McEwen DP, Mattei LN, Berglund EO, Ranscht B, Levinson SR, Schachner M, Shrager P, Isom LL & Xiao ZC. (2001). Contactin associates with Na+ channels and increases their functional expression. *J Neurosci* **21,** 7517-7525.

Kazen-Gillespie KA, Ragsdale DS, D'Andrea MR, Mattei LN, Rogers KE & Isom LL. (2000). Cloning, localization, and functional expression of sodium channel beta1A subunits. *J Biol Chem* **275,** 1079-1088.

Keely PJ, Westwick JK, Whitehead IP, Der CJ & Parise LV. (1997). Cdc42 and Rac1 induce integrin-mediated cell motility and invasiveness through PI(3)K. *Nature* **390,** 632-636.

Kellenberger S, Scheuer T & Catterall WA. (1996). Movement of the Na+ channel inactivation gate during inactivation. *J Biol Chem* **271,** 30971-30979.

Kellenberger S & Schild L. (2002). Epithelial sodium channel/degenerin family of ion channels: a variety of functions for a shared structure. *Physiol Rev* **82,** 735-767.

Kellenberger S, West JW, Catterall WA & Scheuer T. (1997a). Molecular analysis of potential hinge residues in the inactivation gate of brain type IIA Na+ channels. *J Gen Physiol* **109,** 607-617.

Kellenberger S, West JW, Scheuer T & Catterall WA. (1997b). Molecular analysis of the putative inactivation particle in the inactivation gate of brain type IIA Na+ channels. *J Gen Physiol* **109,** 589-605.

Khaitan D, Sankpal UT, Weksler B, Meister EA, Romero IA, Couraud PO & Ningaraj NS. (2009). Role of KCNMA1 gene in breast cancer invasion and metastasis to brain. *BMC Cancer* **9,** 258.

Khanna R, Chang MC, Joiner WJ, Kaczmarek LK & Schlichter LC. (1999). hSK4/hIK1, a calmodulin-binding KCa channel in human T lymphocytes. Roles in proliferation and volume regulation. *J Biol Chem* **274,** 14838-14849.

Kiefer H, Blume AJ & Kaback HR. (1980). Membrane potential changes during mitogenic stimulation of mouse spleen lymphocytes. *Proc Natl Acad Sci U S A* **77,** 2200-2204.

Kim DY, Carey BW, Wang H, Ingano LA, Binshtok AM, Wertz MH, Pettingell WH, He P, Lee VM, Woolf CJ & Kovacs DM. (2007). BACE1 regulates voltage-gated sodium channels and neuronal activity. *Nat Cell Biol* **9,** 755-764.

Kim DY, Ingano LA, Carey BW, Pettingell WH & Kovacs DM. (2005). Presenilin/gamma-secretase-mediated cleavage of the voltage-gated sodium channel beta2-subunit regulates cell adhesion and migration. *J Biol Chem* **280,** 23251-23261.

Kimura K, Ito M, Amano M, Chihara K, Fukata Y, Nakafuku M, Yamamori B, Feng J, Nakano T, Okawa K, Iwamatsu A & Kaibuchi K. (1996). Regulation of myosin phosphatase by Rho and Rho-associated kinase (Rho-kinase). *Science* **273,** 245-248.

Kis-Toth K, Hajdu P, Bacskai I, Szilagyi O, Papp F, Szanto A, Posta E, Gogolak P, Panyi G & Rajnavolgyi E. (2011). Voltage-gated sodium channel Nav1.7 maintains the membrane potential and regulates the activation and chemokine-induced migration of a monocyte-derived dendritic cell subset. *J Immunol* **187,** 1273-1280.

Kishimoto J, Ehama R, Ge Y, Kobayashi T, Nishiyama T, Detmar M & Burgeson RE. (2000). In vivo detection of human vascular endothelial growth factor promoter activity in transgenic mouse skin. *Am J Pathol* **157,** 103-110.

Klugbauer N, Lacinova L, Flockerzi V & Hofmann F. (1995). Structure and functional expression of a new member of the tetrodotoxin-sensitive voltage-activated sodium channel family from human neuroendocrine cells. *EMBO J* **14,** 1084-1090.

Ko SH, Lenkowski PW, Lee HC, Mounsey JP & Patel MK. (2005). Modulation of Na(v)1.5 by beta1-- and beta3-subunit co-expression in mammalian cells. *Pflugers Arch* **449,** 403-412.

Kole MH, Ilschner SU, Kampa BM, Williams SR, Ruben PC & Stuart GJ. (2008). Action potential generation requires a high sodium channel density in the axon initial segment. *Nat Neurosci* **11,** 178-186.

Kraft R, Krause P, Jung S, Basrai D, Liebmann L, Bolz J & Patt S. (2003). BK channel openers inhibit migration of human glioma cells. *Pflugers Arch* **446,** 248-255.

Kranenburg O. (2005). The KRAS oncogene: past, present, and future. *Biochim Biophys Acta* **1756,** 81-82.

Krasowska M, Grzywna ZJ, Mycielska ME & Djamgoz MB. (2004). Patterning of endocytic vesicles and its control by voltage-gated Na+ channel activity in rat prostate cancer cells: fractal analyses. *Eur Biophys J* **33,** 535-542.

Krasowska M, Grzywna ZJ, Mycielska ME & Djamgoz MB. (2009). Fractal analysis and ionic dependence of endocytotic membrane activity of human breast cancer cells. *Eur Biophys J* **38,** 1115-1125.

Krueger EW, Orth JD, Cao H & McNiven MA. (2003). A dynamin-cortactin-Arp2/3 complex mediates actin reorganization in growth factor-stimulated cells. *Mol Biol Cell* **14,** 1085-1096.

Krueger JS, Keshamouni VG, Atanaskova N & Reddy KB. (2001). Temporal and quantitative regulation of mitogen-activated protein kinase (MAPK) modulates cell motility and invasion. *Oncogene* **20,** 4209-4218.

Kuo CC & Bean BP. (1994). Slow binding of phenytoin to inactivated sodium channels in rat hippocampal neurons. *Mol Pharmacol* **46,** 716-725.

Laedermann CJ, Syam N, Pertin M, Decosterd I & Abriel H. (2013). beta1- and beta3- voltage-gated sodium channel subunits modulate cell surface expression and glycosylation of Nav1.7 in HEK293 cells. *Front Cell Neurosci* **7,** 137.

Lakhani SR, Reis-Filho JS, Fulford L, Penault-Llorca F, van der Vijver M, Parry S, Bishop T, Benitez J, Rivas C, Bignon YJ, Chang-Claude J, Hamann U, Cornelisse CJ, Devilee P, Beckmann MW, Nestle-Kramling C, Daly PA, Haites N, Varley J, Lalloo F, Evans G, Maugard C, Meijers-Heijboer H, Klijn JG, Olah E, Gusterson BA, Pilotti S, Radice P, Scherneck S, Sobol H, Jacquemier J, Wagner T, Peto J, Stratton MR, McGuffog L, Easton DF & Breast Cancer Linkage C. (2005). Prediction of BRCA1 status in patients with breast cancer using estrogen receptor and basal phenotype. *Clin Cancer Res* **11,** 5175-5180.

Lakhani SR, Van De Vijver MJ, Jacquemier J, Anderson TJ, Osin PP, McGuffog L & Easton DF. (2002). The pathology of familial breast cancer: predictive value of immunohistochemical markers estrogen receptor, progesterone receptor, HER-2, and p53 in patients with mutations in BRCA1 and BRCA2. *J Clin Oncol* **20,** 2310- 2318.

Lambert DG. (2006). *Calcium signaling protocols*. Humana Press, Totowa, N.J.

Lampert A, O'Reilly AO, Reeh P & Leffler A. (2010). Sodium channelopathies and pain. *Pflugers Arch* **460,** 249-263.

Lan JY, Williams C, Levin M & Black LD, 3rd. (2014). Depolarization of Cellular Resting Membrane Potential Promotes Neonatal Cardiomyocyte Proliferation In Vitro. *Cell Mol Bioeng* **7,** 432-445.

Laniado ME, Lalani EN, Fraser SP, Grimes JA, Bhangal G, Djamgoz MB & Abel PD. (1997). Expression and functional analysis of voltage-activated Na+ channels in human prostate cancer cell lines and their contribution to invasion in vitro. *Am J Pathol* **150,** 1213-1221.

Larbig R, Torres N, Bridge JH, Goldhaber JI & Philipson KD. (2010). Activation of reverse Na+-Ca2+ exchange by the Na+ current augments the cardiac Ca2+ transient: evidence from NCX knockout mice. *J Physiol* **588,** 3267-3276.

Lastraioli E, Iorio J & Arcangeli A. (2015). Ion channel expression as promising cancer biomarker. *Biochim Biophys Acta* **1848,** 2685-2702.

Latorre R & Brauchi S. (2006). Large conductance Ca2+-activated K+ (BK) channel: activation by Ca2+ and voltage. *Biol Res* **39,** 385-401.

Lee I, Park C & Kang WK. (2010). Knockdown of inwardly rectifying potassium channel Kir2.2 suppresses tumorigenesis by inducing reactive oxygen species-mediated cellular senescence. *Mol Cancer Ther* **9,** 2951-2959.

Lee J, Ishihara A, Oxford G, Johnson B & Jacobson K. (1999). Regulation of cell movement is mediated by stretch-activated calcium channels. *Nature* **400,** 382-386.

Lee JL, Wang MJ, Sudhir PR & Chen JY. (2008). CD44 engagement promotes matrix-derived survival through the CD44-SRC-integrin axis in lipid rafts. *Mol Cell Biol* **28,** 5710-5723.

Lee SC, Deutsch C & Beck WT. (1988). Comparison of ion channels in multidrug-resistant and -sensitive human leukemic cells. *Proc Natl Acad Sci U S A* **85,** 2019-2023.

Leipold E, Liebmann L, Korenke GC, Heinrich T, Giesselmann S, Baets J, Ebbinghaus M, Goral RO, Stodberg T, Hennings JC, Bergmann M, Altmuller J, Thiele H, Wetzel A, Nurnberg P, Timmerman V, De Jonghe P, Blum R, Schaible HG, Weis J, Heinemann SH, Hubner CA & Kurth I. (2013). A de novo gain-of-function mutation in SCN11A causes loss of pain perception. *Nat Genet* **45,** 1399-1404.

Lemaillet G, Walker B & Lambert S. (2003). Identification of a conserved ankyrin-binding motif in the family of sodium channel alpha subunits. *J Biol Chem* **278,** 27333-27339.

Li M, West JW, Lai Y, Scheuer T & Catterall WA. (1992). Functional modulation of brain sodium channels by cAMP-dependent phosphorylation. *Neuron* **8,** 1151-1159.

Lin EY, Jones JG, Li P, Zhu L, Whitney KD, Muller WJ & Pollard JW. (2003). Progression to malignancy in the polyoma middle T oncoprotein mouse breast cancer model provides a reliable model for human diseases. *Am J Pathol* **163,** 2113-2126.

Lin NU, Claus E, Sohl J, Razzak AR, Arnaout A & Winer EP. (2008). Sites of distant recurrence and clinical outcomes in patients with metastatic triple-negative breast cancer: high incidence of central nervous system metastases. *Cancer* **113,** 2638-2645.

Linnertz R, Wurm A, Pannicke T, Krugel K, Hollborn M, Hartig W, Iandiev I, Wiedemann P, Reichenbach A & Bringmann A. (2011). Activation of voltage-gated Na(+) and Ca(2)(+) channels is required for glutamate release from retinal glial cells implicated in cell volume regulation. *Neuroscience* **188,** 23-34.

Liu C & Hermann TE. (1978). Characterization of ionomycin as a calcium ionophore. *J Biol Chem* **253,** 5892-5894.

Liu JH, Bijlenga P, Fischer-Lougheed J, Occhiodoro T, Kaelin A, Bader CR & Bernheim L. (1998). Role of an inward rectifier K+ current and of hyperpolarization in human myoblast fusion. *J Physiol* **510 ( Pt 2),** 467-476.

Liu M & Wood JN. (2011). The roles of sodium channels in nociception: implications for mechanisms of neuropathic pain. *Pain Med* **12 Suppl 3,** S93-99.

Liu S, Dontu G & Wicha MS. (2005). Mammary stem cells, self-renewal pathways, and carcinogenesis. *Breast Cancer Res* **7,** 86-95.

Liu X, Chang Y, Reinhart PH, Sontheimer H & Chang Y. (2002). Cloning and characterization of glioma BK, a novel BK channel isoform highly expressed in human glioma cells. *J Neurosci* **22,** 1840-1849.

Lo WL, Donermeyer DL & Allen PM. (2012). A voltage-gated sodium channel is essential for the positive selection of CD4(+) T cells. *Nat Immunol* **13,** 880-887.

Lobikin M, Chernet B, Lobo D & Levin M. (2012). Resting potential, oncogene-induced tumorigenesis, and metastasis: the bioelectric basis of cancer in vivo. *Phys Biol* **9,** 065002.

Lobikin M, Lobo D, Blackiston DJ, Martyniuk CJ, Tkachenko E & Levin M. (2015). Serotonergic regulation of melanocyte conversion: A bioelectrically regulated network for stochastic all-or-none hyperpigmentation. *Sci Signal* **8,** ra99.

Lombet A, Bidard JN & Lazdunski M. (1987). Ciguatoxin and brevetoxins share a common receptor site on the neuronal voltage-dependent Na+ channel. *FEBS Lett* **219,** 355-359.

Lopez-Santiago LF, Brackenbury WJ, Chen C & Isom LL. (2011). Na+ channel Scn1b gene regulates dorsal root ganglion nociceptor excitability in vivo. *J Biol Chem* **286,** 22913-22923.

Lopez-Santiago LF, Meadows LS, Ernst SJ, Chen C, Malhotra JD, McEwen DP, Speelman A, Noebels JL, Maier SK, Lopatin AN & Isom LL. (2007). Sodium channel Scn1b null mice exhibit prolonged QT and RR intervals. *J Mol Cell Cardiol* **43,** 636-647.

Lossin C, Wang DW, Rhodes TH, Vanoye CG & George AL, Jr. (2002). Molecular basis of an inherited epilepsy. *Neuron* **34,** 877-884.

Lu CM & Brown GB. (1998). Isolation of a human-brain sodium-channel gene encoding two isoforms of the subtype III alpha-subunit. *J Mol Neurosci* **10,** 67-70.

Lu CM, Han J, Rado TA & Brown GB. (1992). Differential expression of two sodium channel subtypes in human brain. *FEBS Lett* **303,** 53-58.

Lu J, Steeg PS, Price JE, Krishnamurthy S, Mani SA, Reuben J, Cristofanilli M, Dontu G, Bidaut L, Valero V, Hortobagyi GN & Yu D. (2009). Breast cancer metastasis: challenges and opportunities. *Cancer Res* **69,** 4951-4953.

Luqmani YA, Al Azmi A, Al Bader M, Abraham G & El Zawahri M. (2009). Modification of gene expression induced by siRNA targeting of estrogen receptor alpha in MCF7 human breast cancer cells. *Int J Oncol* **34,** 231-242.

Lymangrover J, Pearlmutter AF, Franco-Saenz R & Saffran M. (1975). Transmembrane potentials and steroidogenesis in normal and neoplastic human adrenocortical tissue. *J Clin Endocrinol Metab* **41,** 697-706.

Ma JY, Catterall WA & Scheuer T. (1997). Persistent sodium currents through brain sodium channels induced by G protein betagamma subunits. *Neuron* **19,** 443-452.

Ma YG, Liu WC, Dong S, Du C, Wang XJ, Li JS, Xie XP, Wu L, Ma DC, Yu ZB & Xie MJ. (2012). Activation of BK(Ca) channels in zoledronic acid-induced apoptosis of MDA-MB-231 breast cancer cells. *PLoS One* **7,** e37451.

MacDonald PL & Gardner RC. (2000). Type I Error Rate Comparisons of Post Hoc Procedures for I j Chi-Square Tables. *Educ Psychol Meas* **60,** 735-754.

MacFarlane SN & Sontheimer H. (2000). Changes in ion channel expression accompany cell cycle progression of spinal cord astrocytes. *Glia* **30,** 39-48.

Macmillan S, Sheridan RD, Chilvers ER & Patmore L. (1995). A comparison of the effects of SCA40, NS 004 and NS 1619 on large conductance Ca(2+)-activated K+ channels in bovine tracheal smooth muscle cells in culture. *Br J Pharmacol* **116,** 1656-1660.

Maier SK, Westenbroek RE, McCormick KA, Curtis R, Scheuer T & Catterall WA. (2004). Distinct subcellular localization of different sodium channel alpha and beta subunits in single ventricular myocytes from mouse heart. *Circulation* **109,** 1421-1427.

Malhotra JD, Kazen-Gillespie K, Hortsch M & Isom LL. (2000). Sodium channel beta subunits mediate homophilic cell adhesion and recruit ankyrin to points of cell-cell contact. *J Biol Chem* **275,** 11383-11388.

Malhotra JD, Koopmann MC, Kazen-Gillespie KA, Fettman N, Hortsch M & Isom LL. (2002). Structural requirements for interaction of sodium channel beta 1 subunits with ankyrin. *J Biol Chem* **277,** 26681-26688.

Malhotra JD, Thyagarajan V, Chen C & Isom LL. (2004). Tyrosine-phosphorylated and nonphosphorylated sodium channel beta1 subunits are differentially localized in cardiac myocytes. *J Biol Chem* **279,** 40748-40754.

Malo MS, Blanchard BJ, Andresen JM, Srivastava K, Chen XN, Li X, Jabs EW, Korenberg JR & Ingram VM. (1994a). Localization of a putative human brain sodium channel gene (SCN1A) to chromosome band 2q24. *Cytogenet Cell Genet* **67,** 178-186.

Malo MS, Srivastava K, Andresen JM, Chen XN, Korenberg JR & Ingram VM. (1994b). Targeted gene walking by low stringency polymerase chain reaction: assignment of a putative human brain sodium channel gene (SCN3A) to chromosome 2q24-31. *Proc Natl Acad Sci U S A* **91,** 2975-2979.

Mantegazza M & Catterall WA. (2012). Voltage-Gated Na+ Channels: Structure, Function, and Pathophysiology. In *Jasper's Basic Mechanisms of the Epilepsies*, 4th edn, ed. Noebels JL, Avoli M, Rogawski MA, Olsen RW & Delgado-Escueta AV. Bethesda (MD).

Mantegazza M, Curia G, Biagini G, Ragsdale DS & Avoli M. (2010a). Voltage-gated sodium channels as therapeutic targets in epilepsy and other neurological disorders. *Lancet Neurol* **9,** 413-424.

Mantegazza M, Rusconi R, Scalmani P, Avanzini G & Franceschetti S. (2010b). Epileptogenic ion channel mutations: from bedside to bench and, hopefully, back again. *Epilepsy Res* **92,** 1-29.

Marino AA, Iliev IG, Schwalke MA, Gonzalez E, Marler KC & Flanagan CA. (1994). Association between cell membrane potential and breast cancer. *Tumour Biol* **15,** 82-89.

Marrison J, Raty L, Marriott P & O'Toole P. (2013). Ptychography--a label free, high-contrast imaging technique for live cells using quantitative phase information. *Sci Rep* **3,** 2369.

Masters JR, Thomson JA, Daly-Burns B, Reid YA, Dirks WG, Packer P, Toji LH, Ohno T, Tanabe H, Arlett CF, Kelland LR, Harrison M, Virmani A, Ward TH, Ayres KL & Debenham PG. (2001). Short tandem repeat profiling provides an international reference standard for human cell lines. *Proc Natl Acad Sci U S A* **98,** 8012-8017.

Matthews E, Tan SV, Fialho D, Sweeney MG, Sud R, Haworth A, Stanley E, Cea G, Davis MB & Hanna MG. (2008). What causes paramyotonia in the United Kingdom? Common and new SCN4A mutations revealed. *Neurology* **70,** 50-53.

Maxmen A. (2012). The hard facts. *Nature* **485,** S50-51.

McCormick KA, Isom LL, Ragsdale D, Smith D, Scheuer T & Catterall WA. (1998). Molecular determinants of Na+ channel function in the extracellular domain of the beta1 subunit. *J Biol Chem* **273,** 3954-3962.

McCusker EC, Bagneris C, Naylor CE, Cole AR, D'Avanzo N, Nichols CG & Wallace BA. (2012). Structure of a bacterial voltage-gated sodium channel pore reveals mechanisms of opening and closing. *Nat Commun* **3,** 1102.

McEwen DP, Chen C, Meadows LS, Lopez-Santiago L & Isom LL. (2009). The voltage-gated Na+ channel beta3 subunit does not mediate trans homophilic cell adhesion or associate with the cell adhesion molecule contactin. *Neurosci Lett* **462,** 272-275.

McEwen DP & Isom LL. (2004). Heterophilic interactions of sodium channel beta1 subunits with axonal and glial cell adhesion molecules. *J Biol Chem* **279,** 52744-52752.

McEwen DP, Meadows LS, Chen C, Thyagarajan V & Isom LL. (2004). Sodium channel beta1 subunit-mediated modulation of Nav1.2 currents and cell surface density is dependent on interactions with contactin and ankyrin. *J Biol Chem* **279,** 16044-16049.

McFarlane S, Coulter JA, Tibbits P, O'Grady A, McFarlane C, Montgomery N, Hill A, McCarthy HO, Young LS, Kay EW, Isacke CM & Waugh DJ. (2015). CD44 increases the efficiency of distant metastasis of breast cancer. *Oncotarget* **6,** 11465-11476.

Meadows L, Malhotra JD, Stetzer A, Isom LL & Ragsdale DS. (2001). The intracellular segment of the sodium channel beta 1 subunit is required for its efficient association with the channel alpha subunit. *J Neurochem* **76,** 1871-1878.

Meadows LS, Chen YH, Powell AJ, Clare JJ & Ragsdale DS. (2002). Functional modulation of human brain Nav1.3 sodium channels, expressed in mammalian cells, by auxiliary beta 1, beta 2 and beta 3 subunits. *Neuroscience* **114,** 745-753.

Medeiros-Domingo A, Kaku T, Tester DJ, Iturralde-Torres P, Itty A, Ye B, Valdivia C, Ueda K, Canizales-Quinteros S, Tusie-Luna MT, Makielski JC & Ackerman MJ. (2007). SCN4B-encoded sodium channel beta4 subunit in congenital long-QT syndrome. *Circulation* **116,** 134-142.

Meera P, Wallner M, Jiang Z & Toro L. (1996). A calcium switch for the functional coupling between alpha (hslo) and beta subunits (KV,Ca beta) of maxi K channels. *FEBS Lett* **382,** 84-88.

Meera P, Wallner M, Song M & Toro L. (1997). Large conductance voltage- and calcium-dependent K+ channel, a distinct member of voltage-dependent ion channels with seven N-terminal transmembrane segments (S0-S6), an extracellular N terminus, and an intracellular (S9-S10) C terminus. *Proc Natl Acad Sci U S A* **94,** 14066-14071.

Melczer N & Kiss J. (1957). Electrical method for detection of early cancerous growth of the skin. *Nature* **179,** 1177-1179.

Menendez ST, Rodrigo JP, Allonca E, Garcia-Carracedo D, Alvarez-Alija G, Casado-Zapico S, Fresno MF, Rodriguez C, Suarez C & Garcia-Pedrero JM. (2010). Expression and clinical significance of the Kv3.4 potassium channel subunit in the development and progression of head and neck squamous cell carcinomas. *J Pathol* **221,** 402-410.

Messner DJ & Catterall WA. (1985). The sodium channel from rat brain. Separation and characterization of subunits. *J Biol Chem* **260,** 10597-10604.

Meyer R & Heinemann SH. (1998). Characterization of an eag-like potassium channel in human neuroblastoma cells. *J Physiol* **508 ( Pt 1),** 49-56.

Miki H, Suetsugu S & Takenawa T. (1998). WAVE, a novel WASP-family protein involved in actin reorganization induced by Rac. *EMBO J* **17,** 6932-6941.

Miller C. (2000). An overview of the potassium channel family. *Genome Biol* **1,** REVIEWS0004.

Mills B & Tupper JT. (1976). Cell cycle dependent changes in potassium transport. *J Cell Physiol* **89,** 123-132.

Miloushev VZ, Levine JA, Arbing MA, Hunt JF, Pitt GS & Palmer AG, 3rd. (2009). Solution structure of the NaV1.2 C-terminal EF-hand domain. *J Biol Chem* **284,** 6446-6454.

Minta A & Tsien RY. (1989). Fluorescent indicators for cytosolic sodium. *J Biol Chem* **264,** 19449-19457.

Misra SN, Kahlig KM & George AL, Jr. (2008). Impaired NaV1.2 function and reduced cell surface expression in benign familial neonatal-infantile seizures. *Epilepsia* **49,** 1535-1545.

Mita M, Tanaka H, Yanagihara H, Nakagawa J, Hishinuma S, Sutherland C, Walsh MP & Shoji M. (2013). Membrane depolarization-induced RhoA/Rho-associated kinase activation and sustained contraction of rat caudal arterial smooth muscle involves genistein-sensitive tyrosine phosphorylation. *J Smooth Muscle Res* **49,** 26-45.

Mita M, Yanagihara H, Hishinuma S, Saito M & Walsh MP. (2002). Membrane depolarization-induced contraction of rat caudal arterial smooth muscle involves Rho-associated kinase. *Biochem J* **364,** 431-440.

Mitra SK & Schlaepfer DD. (2006). Integrin-regulated FAK-Src signaling in normal and cancer cells. *Curr Opin Cell Biol* **18,** 516-523.

Miyazaki H, Oyama F, Inoue R, Aosaki T, Abe T, Kiyonari H, Kino Y, Kurosawa M, Shimizu J, Ogiwara I, Yamakawa K, Koshimizu Y, Fujiyama F, Kaneko T, Shimizu H, Nagatomo K, Yamada K, Shimogori T, Hattori N, Miura M & Nukina N. (2014). Singular localization of sodium channel beta4 subunit in unmyelinated fibres and its role in the striatum. *Nat Commun* **5,** 5525.

Mohammed FH, Khajah MA, Yang M, Brackenbury WJ & Luqmani YA. (2015). Blockade of voltage-gated sodium channels inhibits invasion of endocrine-resistant breast cancer cells. *Int J Oncol* **In press**.

Montell DJ, Yoon WH & Starz-Gaiano M. (2012). Group choreography: mechanisms orchestrating the collective movement of border cells. *Nat Rev Mol Cell Biol* **13,** 631-645.

Morgan K, Stevens EB, Shah B, Cox PJ, Dixon AK, Lee K, Pinnock RD, Hughes J, Richardson PJ, Mizuguchi K & Jackson AP. (2000). beta 3: an additional auxiliary subunit of the voltage-sensitive sodium channel that modulates channel gating with distinct kinetics. *Proc Natl Acad Sci U S A* **97,** 2308-2313.

Mori H, Tomari T, Koshikawa N, Kajita M, Itoh Y, Sato H, Tojo H, Yana I & Seiki M. (2002). CD44 directs membrane-type 1 matrix metalloproteinase to lamellipodia by associating with its hemopexin-like domain. *EMBO J* **21,** 3949-3959.

Morris TA, DeLorenzo RJ & Tombes RM. (1998). CaMK-II inhibition reduces cyclin D1 levels and enhances the association of p27kip1 with Cdk2 to cause G1 arrest in NIH 3T3 cells. *Exp Cell Res* **240,** 218-227.

Motiani RK, Abdullaev IF & Trebak M. (2010). A novel native store-operated calcium channel encoded by Orai3: selective requirement of Orai3 versus Orai1 in estrogen receptor-positive versus estrogen receptor-negative breast cancer cells. *J Biol Chem* **285,** 19173-19183.

Motoike T, Loughna S, Perens E, Roman BL, Liao W, Chau TC, Richardson CD, Kawate T, Kuno J, Weinstein BM, Stainier DY & Sato TN. (2000). Universal GFP reporter for the study of vascular development. *Genesis* **28,** 75-81.

Murphy BJ, Rossie S, De Jongh KS & Catterall WA. (1993). Identification of the sites of selective phosphorylation and dephosphorylation of the rat brain Na+ channel alpha subunit by cAMP-dependent protein kinase and phosphoprotein phosphatases. *J Biol Chem* **268,** 27355-27362.

Mycielska ME, Fraser SP, Szatkowski M & Djamgoz MB. (2003). Contribution of functional voltage-gated Na+ channel expression to cell behaviors involved in the metastatic cascade in rat prostate cancer: II. Secretory membrane activity. *J Cell Physiol* **195,** 461-469.

Mycielska ME, Palmer CP, Brackenbury WJ & Djamgoz MB. (2005). Expression of Na+-dependent citrate transport in a strongly metastatic human prostate cancer PC-3M cell line: regulation by voltage-gated Na+ channel activity. *J Physiol* **563,** 393-408.

Narahashi T, Moore JW & Scott WR. (1964). Tetrodotoxin Blockage of Sodium Conductance Increase in Lobster Giant Axons. *J Gen Physiol* **47,** 965-974.

Nelson M, Millican-Slater R, Forrest LC & Brackenbury WJ. (2014). The sodium channel beta1 subunit mediates outgrowth of neurite-like processes on breast cancer cells and promotes tumour growth and metastasis. *Int J Cancer* **135,** 2338-2351.

Nelson M, Yang M, Dowle AA, Thomas JR & Brackenbury WJ. (2015a). The sodium channel-blocking antiepileptic drug phenytoin inhibits breast tumour growth and metastasis. *Mol Cancer* **14,** 13.

Nelson M, Yang M, Millican-Slater R & Brackenbury WJ. (2015b). Nav1.5 regulates breast tumor growth and metastatic dissemination in vivo. *Oncotarget* **6,** 32914-32929.

Neyton J & Miller C. (1988). Potassium blocks barium permeation through a calcium-activated potassium channel. *J Gen Physiol* **92,** 549-567.

Nilius B & Wohlrab W. (1992). Potassium channels and regulation of proliferation of human melanoma cells. *J Physiol* **445,** 537-548.

Niwinska A, Murawska M & Pogoda K. (2010). Breast cancer brain metastases: differences in survival depending on biological subtype, RPA RTOG prognostic class and systemic treatment after whole-brain radiotherapy (WBRT). *Ann Oncol* **21,** 942-948.

Nobes CD & Hall A. (1995). Rho, rac, and cdc42 GTPases regulate the assembly of multimolecular focal complexes associated with actin stress fibers, lamellipodia, and filopodia. *Cell* **81,** 53-62.

Noda M, Shimizu S, Tanabe T, Takai T, Kayano T, Ikeda T, Takahashi H, Nakayama H, Kanaoka Y, Minamino N & et al. (1984). Primary structure of Electrophorus electricus sodium channel deduced from cDNA sequence. *Nature* **312,** 121-127.

Noda M, Suzuki H, Numa S & Stuhmer W. (1989). A single point mutation confers tetrodotoxin and saxitoxin insensitivity on the sodium channel II. *FEBS Lett* **259,** 213-216.

Numann R, Catterall WA & Scheuer T. (1991). Functional modulation of brain sodium channels by protein kinase C phosphorylation. *Science* **254,** 115-118.

Obara Y, Horgan AM & Stork PJ. (2007). The requirement of Ras and Rap1 for the activation of ERKs by cAMP, PACAP, and KCl in cerebellar granule cells. *J Neurochem* **101,** 470-482.

Oesterreich S, Zhang P, Guler RL, Sun X, Curran EM, Welshons WV, Osborne CK & Lee AV. (2001). Re-expression of estrogen receptor alpha in estrogen receptor alpha-negative MCF-7 cells restores both estrogen and insulin-like growth factor-mediated signaling and growth. *Cancer Res* **61,** 5771-5777.

Offermanns S & Rosenthal W. (2008). *Encyclopedia of molecular pharmacology*. Springer, Berlin ; New York.

Ogiwara I, Nakayama T, Yamagata T, Ohtani H, Mazaki E, Tsuchiya S, Inoue Y & Yamakawa K. (2012). A homozygous mutation of voltage-gated sodium channel beta(I) gene SCN1B in a patient with Dravet syndrome. *Epilepsia* **53,** e200-203.

Oh Y, Black JA & Waxman SG. (1994). Rat brain Na+ channel mRNAs in non-excitable Schwann cells. *FEBS Lett* **350,** 342-346.

Oh Y & Waxman SG. (1995). Differential Na+ channel beta 1 subunit mRNA expression in stellate and flat astrocytes cultured from rat cortex and cerebellum: a combined in situ hybridization and immunocytochemistry study. *Glia* **13,** 166-173.

Oktay M, Wary KK, Dans M, Birge RB & Giancotti FG. (1999). Integrin-mediated activation of focal adhesion kinase is required for signaling to Jun NH2-terminal kinase and progression through the G1 phase of the cell cycle. *J Cell Biol* **145,** 1461-1469.

Okuse K, Malik-Hall M, Baker MD, Poon WY, Kong H, Chao MV & Wood JN. (2002). Annexin II light chain regulates sensory neuron-specific sodium channel expression. *Nature* **417,** 653-656.

Olson MF & Sahai E. (2009). The actin cytoskeleton in cancer cell motility. *Clin Exp Metastasis* **26,** 273-287.

Olson TM, Michels VV, Ballew JD, Reyna SP, Karst ML, Herron KJ, Horton SC, Rodeheffer RJ & Anderson JL. (2005). Sodium channel mutations and susceptibility to heart failure and atrial fibrillation. *JAMA* **293,** 447-454.

Onganer PU, Seckl MJ & Djamgoz MB. (2005). Neuronal characteristics of small-cell lung cancer. *Br J Cancer* **93,** 1197-1201.

Orr CW, Yoshikawa-Fukada M & Ebert JD. (1972). Potassium: effect on DNA synthesis and multiplication of baby-hamster kidney cells: (cell cycle-membrane potential-synchronization-transformation). *Proc Natl Acad Sci U S A* **69,** 243-247.

Ortiz CS, Montante-Montes D, Saqui-Salces M, Hinojosa LM, Gamboa-Dominguez A, Hernandez-Gallegos E, Martinez-Benitez B, Del Rosario Solis-Pancoatl M, Garcia-Villa E, Ramirez A, Aguilar-Guadarrama R, Gariglio P, Pardo LA, Stuhmer W & Camacho J. (2011). Eag1 potassium channels as markers of cervical dysplasia. *Oncology reports* **26,** 1377-1383.

Ou SW, Kameyama A, Hao LY, Horiuchi M, Minobe E, Wang WY, Makita N & Kameyama M. (2005). Tetrodotoxin-resistant Na+ channels in human neuroblastoma cells are encoded by new variants of Nav1.5/SCN5A. *Eur J Neurosci* **22,** 793-801.

Ouadid-Ahidouch H & Ahidouch A. (2008). K+ channel expression in human breast cancer cells: involvement in cell cycle regulation and carcinogenesis. *J Membr Biol* **221,** 1-6.

Ouadid-Ahidouch H, Chaussade F, Roudbaraki M, Slomianny C, Dewailly E, Delcourt P & Prevarskaya N. (2000). KV1.1 K(+) channels identification in human breast carcinoma cells: involvement in cell proliferation. *Biochem Biophys Res Commun* **278,** 272-277.

Ouadid-Ahidouch H, Le Bourhis X, Roudbaraki M, Toillon RA, Delcourt P & Prevarskaya N. (2001). Changes in the K+ current-density of MCF-7 cells during progression through the cell cycle: possible involvement of a h-ether.a-gogo K+ channel. *Receptors Channels* **7,** 345-356.

Ousingsawat J, Spitzner M, Puntheeranurak S, Terracciano L, Tornillo L, Bubendorf L, Kunzelmann K & Schreiber R. (2007). Expression of voltage-gated potassium channels in human and mouse colonic carcinoma. *Clin Cancer Res* **13,** 824-831.

Ouwerkerk R, Jacobs MA, Macura KJ, Wolff AC, Stearns V, Mezban SD, Khouri NF, Bluemke DA & Bottomley PA. (2007). Elevated tissue sodium concentration in malignant breast lesions detected with non-invasive 23Na MRI. *Breast Cancer Res Treat* **106,** 151-160.

Oyama F, Miyazaki H, Sakamoto N, Becquet C, Machida Y, Kaneko K, Uchikawa C, Suzuki T, Kurosawa M, Ikeda T, Tamaoka A, Sakurai T & Nukina N. (2006). Sodium channel beta4 subunit: down-regulation and possible involvement in neuritic degeneration in Huntington's disease transgenic mice. *J Neurochem* **98,** 518-529.

Pai VP, Lemire JM, Pare JF, Lin G, Chen Y & Levin M. (2015). Endogenous gradients of resting potential instructively pattern embryonic neural tissue via Notch signaling and regulation of proliferation. *J Neurosci* **35,** 4366-4385.

Palazzo AF, Eng CH, Schlaepfer DD, Marcantonio EE & Gundersen GG. (2004). Localized stabilization of microtubules by integrin- and FAK-facilitated Rho signaling. *Science* **303,** 836-839.

Palmer CP, Mycielska ME, Burcu H, Osman K, Collins T, Beckerman R, Perrett R, Johnson H, Aydar E & Djamgoz MB. (2008). Single cell adhesion measuring apparatus (SCAMA): application to cancer cell lines of different metastatic potential and voltage-gated Na+ channel expression. *Eur Biophys J* **37,** 359-368.

Pancrazio JJ, Viglione MP, Tabbara IA & Kim YI. (1989). Voltage-dependent ion channels in small-cell lung cancer cells. *Cancer Res* **49,** 5901-5906.

Pappalardo LW, Liu S, Black JA & Waxman SG. (2014a). Dynamics of sodium channel Nav1.5 expression in astrocytes in mouse models of multiple sclerosis. *Neuroreport* **25,** 1208-1215.

Pappalardo LW, Samad OA, Black JA & Waxman SG. (2014b). Voltage-gated sodium channel Nav 1.5 contributes to astrogliosis in an in vitro model of glial injury via reverse Na+ /Ca2+ exchange. *Glia* **62,** 1162-1175.

Pardo LA, Contreras-Jurado C, Zientkowska M, Alves F & Stuhmer W. (2005). Role of voltage-gated potassium channels in cancer. *J Membr Biol* **205,** 115-124.

Pardo LA, del Camino D, Sanchez A, Alves F, Bruggemann A, Beckh S & Stuhmer W. (1999). Oncogenic potential of EAG K(+) channels. *EMBO J* **18,** 5540-5547.

Pardo LA & Stuhmer W. (2014). The roles of K(+) channels in cancer. *Nat Rev Cancer* **14,** 39-48.

Park JH, Park JK, Bae KW & Park HT. (2000). Protein kinase A activity is required for depolarization-induced proline-rich tyrosine kinase 2 and mitogen-activated protein kinase activation in PC12 cells. *Neurosci Lett* **290,** 25-28.

Park JH, Park SJ, Chung MK, Jung KH, Choi MR, Kim Y, Chai YG, Kim SJ & Park KS. (2010). High expression of large-conductance Ca2+-activated K+ channel in the CD133+ subpopulation of SH-SY5Y neuroblastoma cells. *Biochem Biophys Res Commun* **396,** 637-642.

Parl FF, Schmidt BP, Dupont WD & Wagner RK. (1984). Prognostic significance of estrogen receptor status in breast cancer in relation to tumor stage, axillary node metastasis, and histopathologic grading. *Cancer* **54,** 2237-2242.

Patino GA, Brackenbury WJ, Bao Y, Lopez-Santiago LF, O'Malley HA, Chen C, Calhoun JD, Lafreniere RG, Cossette P, Rouleau GA & Isom LL. (2011). Voltage-gated Na+ channel beta1B: a secreted cell adhesion molecule involved in human epilepsy. *J Neurosci* **31,** 14577-14591.

Patino GA, Claes LR, Lopez-Santiago LF, Slat EA, Dondeti RS, Chen C, O'Malley HA, Gray CB, Miyazaki H, Nukina N, Oyama F, De Jonghe P & Isom LL. (2009). A functional null mutation of SCN1B in a patient with Dravet syndrome. *J Neurosci* **29,** 10764-10778.

Patt S, Labrakakis C, Bernstein M, Weydt P, Cervos-Navarro J, Nisch G & Kettenmann H. (1996). Neuron-like physiological properties of cells from human oligodendroglial tumors. *Neuroscience* **71,** 601-611.

Patton DE, Isom LL, Catterall WA & Goldin AL. (1994). The adult rat brain beta 1 subunit modifies activation and inactivation gating of multiple sodium channel alpha subunits. *J Biol Chem* **269,** 17649-17655.

Payandeh J, Gamal El-Din TM, Scheuer T, Zheng N & Catterall WA. (2012). Crystal structure of a voltage-gated sodium channel in two potentially inactivated states. *Nature* **486,** 135-139.

Payandeh J, Scheuer T, Zheng N & Catterall WA. (2011). The crystal structure of a voltage-gated sodium channel. *Nature* **475,** 353-358.

Perou CM, Sorlie T, Eisen MB, van de Rijn M, Jeffrey SS, Rees CA, Pollack JR, Ross DT, Johnsen H, Akslen LA, Fluge O, Pergamenschikov A, Williams C, Zhu SX, Lonning PE, Borresen-Dale AL, Brown PO & Botstein D. (2000). Molecular portraits of human breast tumours. *Nature* **406,** 747-752.

Persson AK, Estacion M, Ahn H, Liu S, Stamboulian-Platel S, Waxman SG & Black JA. (2014). Contribution of sodium channels to lamellipodial protrusion and Rac1 and ERK1/2 activation in ATP-stimulated microglia. *Glia* **62,** 2080-2095.

Pettit EJ & Fay FS. (1998). Cytosolic free calcium and the cytoskeleton in the control of leukocyte chemotaxis. *Physiol Rev* **78,** 949-967.

Plummer HK, 3rd, Dhar MS, Cekanova M & Schuller HM. (2005). Expression of G-protein inwardly rectifying potassium channels (GIRKs) in lung cancer cell lines. *BMC Cancer* **5,** 104.

Plummer HK, 3rd, Yu Q, Cakir Y & Schuller HM. (2004). Expression of inwardly rectifying potassium channels (GIRKs) and beta-adrenergic regulation of breast cancer cell lines. *BMC Cancer* **4,** 93.

Plummer NW, McBurney MW & Meisler MH. (1997). Alternative splicing of the sodium channel SCN8A predicts a truncated two-domain protein in fetal brain and non-neuronal cells. *J Biol Chem* **272,** 24008-24015.

Pollard TD. (2007). Regulation of actin filament assembly by Arp2/3 complex and formins. *Annu Rev Biophys Biomol Struct* **36,** 451-477.

Pool TB, Cameron IL, Smith N & Sparks R. (1981). Intracellular sodium and growth control: a comparison of normal and transformed cells. *The Transformed Cell*, 398.

Potier M, Joulin V, Roger S, Besson P, Jourdan ML, Leguennec JY, Bougnoux P & Vandier C. (2006). Identification of SK3 channel as a new mediator of breast cancer cell migration. *Mol Cancer Ther* **5,** 2946-2953.

Poullet P, Gautreau A, Kadare G, Girault JA, Louvard D & Arpin M. (2001). Ezrin interacts with focal adhesion kinase and induces its activation independently of cell-matrix adhesion. *J Biol Chem* **276,** 37686-37691.

Pressel DM & Misler S. (1991). Role of voltage-dependent ionic currents in coupling glucose stimulation to insulin secretion in canine pancreatic islet B-cells. *J Membr Biol* **124,** 239-253.

Prevarskaya N, Ouadid-Ahidouch H, Skryma R & Shuba Y. (2014). Remodelling of Ca2+ transport in cancer: how it contributes to cancer hallmarks? *Philos Trans R Soc Lond B Biol Sci* **369,** 20130097.

Prevarskaya N, Skryma R & Shuba Y. (2010). Ion channels and the hallmarks of cancer. *Trends Mol Med* **16,** 107-121.

Prevarskaya N, Skryma R & Shuba Y. (2011). Calcium in tumour metastasis: new roles for known actors. *Nat Rev Cancer* **11,** 609-618.

Prevarskaya N, Zhang L & Barritt G. (2007). TRP channels in cancer. *Biochim Biophys Acta* **1772,** 937-946.

Price M, Lee SC & Deutsch C. (1989). Charybdotoxin inhibits proliferation and interleukin 2 production in human peripheral blood lymphocytes. *Proc Natl Acad Sci U S A* **86,** 10171-10175.

Prior HM, Yates MS & Beech DJ. (1998). Functions of large conductance Ca2+-activated (BKCa), delayed rectifier (KV) and background K+ channels in the control of membrane potential in rabbit renal arcuate artery. *J Physiol* **511 ( Pt 1),** 159-169.

Probst V, Kyndt F, Potet F, Trochu JN, Mialet G, Demolombe S, Schott JJ, Baro I, Escande D & Le Marec H. (2003). Haploinsufficiency in combination with aging causes SCN5A-linked hereditary Lenegre disease. *J Am Coll Cardiol* **41,** 643-652.

Qin H, Shao Q, Curtis H, Galipeau J, Belliveau DJ, Wang T, Alaoui-Jamali MA & Laird DW. (2002). Retroviral delivery of connexin genes to human breast tumor cells inhibits in vivo tumor growth by a mechanism that is independent of significant gap junctional intercellular communication. *J Biol Chem* **277,** 29132-29138.

Qin N, D'Andrea MR, Lubin ML, Shafaee N, Codd EE & Correa AM. (2003). Molecular cloning and functional expression of the human sodium channel beta1B subunit, a novel splicing variant of the beta1 subunit. *Eur J Biochem* **270,** 4762-4770.

Quick DC & Waxman SG. (1977). Specific staining of the axon membrane at nodes of Ranvier with ferric ion and ferrocyanide. *J Neurol Sci* **31,** 1-11.

Rabert DK, Koch BD, Ilnicka M, Obernolte RA, Naylor SL, Herman RC, Eglen RM, Hunter JC & Sangameswaran L. (1998). A tetrodotoxin-resistant voltage-gated

sodium channel from human dorsal root ganglia, hPN3/SCN10A. *Pain* **78,** 107-114.

Raftopoulou M & Hall A. (2004). Cell migration: Rho GTPases lead the way. *Dev Biol* **265,** 23-32.

Ragsdale DS, McPhee JC, Scheuer T & Catterall WA. (1994). Molecular determinants of state-dependent block of Na+ channels by local anesthetics. *Science* **265,** 1724-1728.

Ragsdale DS, McPhee JC, Scheuer T & Catterall WA. (1996). Common molecular determinants of local anesthetic, antiarrhythmic, and anticonvulsant block of voltage-gated Na+ channels. *Proc Natl Acad Sci U S A* **93,** 9270-9275.

Ragsdale DS, Scheuer T & Catterall WA. (1991). Frequency and voltage-dependent inhibition of type IIA Na+ channels, expressed in a mammalian cell line, by local anesthetic, antiarrhythmic, and anticonvulsant drugs. *Mol Pharmacol* **40,** 756-765.

Rasband MN. (2010). The axon initial segment and the maintenance of neuronal polarity. *Nat Rev Neurosci* **11,** 552-562.

Ratcliffe CF, Qu Y, McCormick KA, Tibbs VC, Dixon JE, Scheuer T & Catterall WA. (2000). A sodium channel signaling complex: modulation by associated receptor protein tyrosine phosphatase beta. *Nat Neurosci* **3,** 437-444.

Ratcliffe CF, Westenbroek RE, Curtis R & Catterall WA. (2001). Sodium channel beta1 and beta3 subunits associate with neurofascin through their extracellular immunoglobulin-like domain. *J Cell Biol* **154,** 427-434.

Redmann K, Muller V, Tanneberger S & Kalkoff W. (1972). The membrane potential of primary ovarian tumor cells in vitro and its dependence on the cell cycle. *Acta Biol Med Ger* **28,** 853-856.

Ridley AJ. (2011). Life at the leading edge. *Cell* **145,** 1012-1022.

Ridley AJ. (2015). Rho GTPase signalling in cell migration. *Curr Opin Cell Biol* **36,** 103-112.

Ridley AJ, Schwartz MA, Burridge K, Firtel RA, Ginsberg MH, Borisy G, Parsons JT & Horwitz AR. (2003). Cell migration: integrating signals from front to back. *Science* **302,** 1704-1709.

Ritchie JM & Rogart RB. (1977a). The binding of saxitoxin and tetrodotoxin to excitable tissue. *Rev Physiol Biochem Pharmacol* **79,** 1-50.

Ritchie JM & Rogart RB. (1977b). Density of sodium channels in mammalian myelinated nerve fibers and nature of the axonal membrane under the myelin sheath. *Proc Natl Acad Sci U S A* **74,** 211-215.

Roderick HL & Cook SJ. (2008). Ca2+ signalling checkpoints in cancer: remodelling Ca2+ for cancer cell proliferation and survival. *Nat Rev Cancer* **8,** 361-375.

Rodriguez-Rasgado JA, Acuna-Macias I & Camacho J. (2012). Eag1 channels as potential cancer biomarkers. *Sensors* **12,** 5986-5995.

Roger S, Besson P & Le Guennec JY. (2003). Involvement of a novel fast inward sodium current in the invasion capacity of a breast cancer cell line. *Biochim Biophys Acta* **1616,** 107-111.

Roger S, Gillet L, Le Guennec JY & Besson P. (2015). Voltage-gated sodium channels and cancer: is excitability their primary role? *Front Pharmacol* **6,** 152.

Roger S, Potier M, Vandier C, Le Guennec JY & Besson P. (2004). Description and role in proliferation of iberiotoxin-sensitive currents in different human mammary epithelial normal and cancerous cells. *Biochim Biophys Acta* **1667,** 190-199.

Roger S, Rollin J, Barascu A, Besson P, Raynal PI, Iochmann S, Lei M, Bougnoux P, Gruel Y & Le Guennec JY. (2007). Voltage-gated sodium channels potentiate the invasive capacities of human non-small-cell lung cancer cell lines. *Int J Biochem Cell Biol* **39,** 774-786.

Rogers JC, Qu Y, Tanada TN, Scheuer T & Catterall WA. (1996). Molecular determinants of high affinity binding of alpha-scorpion toxin and sea anemone toxin in the S3-S4 extracellular loop in domain IV of the Na+ channel alpha subunit. *J Biol Chem* **271,** 15950-15962.

Rohl CA, Boeckman FA, Baker C, Scheuer T, Catterall WA & Klevit RE. (1999). Solution structure of the sodium channel inactivation gate. *Biochemistry* **38,** 855-861.

Rosenberg RL, Hess P & Tsien RW. (1988). Cardiac calcium channels in planar lipid bilayers. L-type channels and calcium-permeable channels open at negative membrane potentials. *J Gen Physiol* **92,** 27-54.

Rouzaire-Dubois B, Milandri JB, Bostel S & Dubois JM. (2000). Control of cell proliferation by cell volume alterations in rat C6 glioma cells. *Pflugers Arch* **440,** 881-888.

Sachs HG, Stambrook PJ & Ebert JD. (1974). Changes in membrane potential during the cell cycle. *Exp Cell Res* **83,** 362-366.

Sahai E & Marshall CJ. (2002). RHO-GTPases and cancer. *Nat Rev Cancer* **2,** 133-142.

Salkoff L, Butler A, Ferreira G, Santi C & Wei A. (2006). High-conductance potassium channels of the SLO family. *Nat Rev Neurosci* **7,** 921-931.

Sanguinetti MC & Jurkiewicz NK. (1990). Two components of cardiac delayed rectifier K+ current. Differential sensitivity to block by class III antiarrhythmic agents. *J Gen Physiol* **96,** 195-215.

Santella L, Ercolano E & Nusco GA. (2005). The cell cycle: a new entry in the field of Ca2+ signaling. *Cell Mol Life Sci* **62,** 2405-2413.

Sarao R, Gupta SK, Auld VJ & Dunn RJ. (1991). Developmentally regulated alternative RNA splicing of rat brain sodium channel mRNAs. *Nucleic Acids Res* **19,** 5673-5679.

Sareen D, Darjatmoko SR, Albert DM & Polans AS. (2007). Mitochondria, calcium, and calpain are key mediators of resveratrol-induced apoptosis in breast cancer. *Mol Pharmacol* **72,** 1466-1475.

Sarhan MF, Tung CC, Van Petegem F & Ahern CA. (2012). Crystallographic basis for calcium regulation of sodium channels. *Proc Natl Acad Sci U S A* **109,** 3558-3563.

Sarhan MF, Van Petegem F & Ahern CA. (2009). A double tyrosine motif in the cardiac sodium channel domain III-IV linker couples calcium-dependent calmodulin binding to inactivation gating. *J Biol Chem* **284,** 33265-33274.

Sato M, Suzuki K, Yamazaki H & Nakanishi S. (2005). A pivotal role of calcineurin signaling in development and maturation of postnatal cerebellar granule cells. *Proc Natl Acad Sci U S A* **102,** 5874-5879.

Savio-Galimberti E, Gollob MH & Darbar D. (2012). Voltage-gated sodium channels: biophysics, pharmacology, and related channelopathies. *Front Pharmacol* **3,** 124.

Schaller KL & Caldwell JH. (2000). Developmental and regional expression of sodium channel isoform NaCh6 in the rat central nervous system. *J Comp Neurol* **420,** 84-97.

Scheffer IE, Harkin LA, Grinton BE, Dibbens LM, Turner SJ, Zielinski MA, Xu R, Jackson G, Adams J, Connellan M, Petrou S, Wellard RM, Briellmann RS, Wallace RH, Mulley JC & Berkovic SF. (2007). Temporal lobe epilepsy and GEFS+ phenotypes associated with SCN1B mutations. *Brain* **130,** 100-109.

Schlaeger TM, Bartunkova S, Lawitts JA, Teichmann G, Risau W, Deutsch U & Sato TN. (1997). Uniform vascular-endothelial-cell-specific gene expression in both embryonic and adult transgenic mice. *Proc Natl Acad Sci U S A* **94,** 3058-3063.

Schlaepfer DD, Hanks SK, Hunter T & van der Geer P. (1994). Integrin-mediated signal transduction linked to Ras pathway by GRB2 binding to focal adhesion kinase. *Nature* **372,** 786-791.

Schlaepfer DD & Mitra SK. (2004). Multiple connections link FAK to cell motility and invasion. *Curr Opin Genet Dev* **14,** 92-101.

Schlichtholz B, Bouchind'homme B, Pages S, Martin E, Liva S, Magdelenat H, Sastre-Garau X, Stoppa-Lyonnet D & Soussi T. (1998). p53 mutations in BRCA1-associated familial breast cancer. *Lancet* **352,** 622.

Schmidt J, Rossie S & Catterall WA. (1985). A large intracellular pool of inactive Na channel alpha subunits in developing rat brain. *Proc Natl Acad Sci U S A* **82,** 4847-4851.

Schmidt JW & Catterall WA. (1986). Biosynthesis and processing of the alpha subunit of the voltage-sensitive sodium channel in rat brain neurons. *Cell* **46,** 437-444.

Schreiber M & Salkoff L. (1997). A novel calcium-sensing domain in the BK channel. *Biophys J* **73,** 1355-1363.

Schreibmayer W, Dascal N, Lotan I, Wallner M & Weigl L. (1991). Molecular mechanism of protein kinase C modulation of sodium channel alpha-subunits expressed in Xenopus oocytes. *FEBS Lett* **291,** 341-344.

Schrey M, Codina C, Kraft R, Beetz C, Kalff R, Wolfl S & Patt S. (2002). Molecular characterization of voltage-gated sodium channels in human gliomas. *Neuroreport* **13,** 2493-2498.

Schuelert N & McDougall JJ. (2012). Involvement of Nav 1.8 sodium ion channels in the transduction of mechanical pain in a rodent model of osteoarthritis. *Arthritis Res Ther* **14,** R5.

Schwab A. (2001). Function and spatial distribution of ion channels and transporters in cell migration. *Am J Physiol Renal Physiol* **280,** F739-747.

Schwab A, Fabian A, Hanley PJ & Stock C. (2012). Role of ion channels and transporters in cell migration. *Physiol Rev* **92,** 1865-1913.

Schwab A, Nechyporuk-Zloy V, Fabian A & Stock C. (2007). Cells move when ions and water flow. *Pflugers Arch* **453,** 421-432.

Schwab A, Wojnowski L, Gabriel K & Oberleithner H. (1994). Oscillating activity of a Ca(2+)-sensitive K+ channel. A prerequisite for migration of transformed Madin-Darby canine kidney focus cells. *J Clin Invest* **93,** 1631-1636.

Schwab A, Wulf A, Schulz C, Kessler W, Nechyporuk-Zloy V, Romer M, Reinhardt J, Weinhold D, Dieterich P, Stock C & Hebert SC. (2006). Subcellular distribution of calcium-sensitive potassium channels (IK1) in migrating cells. *J Cell Physiol* **206,** 86-94.

Scudamore CL. (2014). *A practical guide to the histology of the mouse*. John Wiley & Sons, Ltd.

Servitja JM, Marinissen MJ, Sodhi A, Bustelo XR & Gutkind JS. (2003). Rac1 function is required for Src-induced transformation. Evidence of a role for Tiam1 and Vav2 in Rac activation by Src. *J Biol Chem* **278,** 34339-34346.

Shah BS, Stevens EB, Pinnock RD, Dixon AK & Lee K. (2001). Developmental expression of the novel voltage-gated sodium channel auxiliary subunit beta3, in rat CNS. *J Physiol* **534,** 763-776.

Shattock MJ & Bers DM. (1989). Rat vs. rabbit ventricle: Ca flux and intracellular Na assessed by ion-selective microelectrodes. *Am J Physiol* **256,** C813-822.

Shaul YD & Seger R. (2007). The MEK/ERK cascade: from signaling specificity to diverse functions. *Biochim Biophys Acta* **1773,** 1213-1226.

Shimizu H, Watanabe E, Hiyama TY, Nagakura A, Fujikawa A, Okado H, Yanagawa Y, Obata K & Noda M. (2007). Glial Nax channels control lactate signaling to neurons for brain [Na+] sensing. *Neuron* **54,** 59-72.

Shrager P. (1989). Sodium channels in single demyelinated mammalian axons. *Brain Res* **483,** 149-154.

Sieg DJ, Hauck CR, Ilic D, Klingbeil CK, Schaefer E, Damsky CH & Schlaepfer DD. (2000). FAK integrates growth-factor and integrin signals to promote cell migration. *Nat Cell Biol* **2,** 249-256.

Sjostrom M, Stenstrom K, Eneling K, Zwiller J, Katz AI, Takemori H & Bertorello AM. (2007). SIK1 is part of a cell sodium-sensing network that regulates active sodium transport through a calcium-dependent process. *Proc Natl Acad Sci U S A* **104,** 16922-16927.

Small JV, Stradal T, Vignal E & Rottner K. (2002). The lamellipodium: where motility begins. *Trends Cell Biol* **12,** 112-120.

Smith MR, Smith RD, Plummer NW, Meisler MH & Goldin AL. (1998a). Functional analysis of the mouse Scn8a sodium channel. *J Neurosci* **18,** 6093-6102.

Smith NR, Sparks RL, Pool TB & Cameron IL. (1978). Differences in the intracellular concentration of elements in normal and cancerous liver cells as determined by X-ray microanalysis. *Cancer Res* **38,** 1952-1959.

Smith P, Rhodes NP, Shortland AP, Fraser SP, Djamgoz MB, Ke Y & Foster CS. (1998b). Sodium channel protein expression enhances the invasiveness of rat and human prostate cancer cells. *FEBS Lett* **423,** 19-24.

Smith PL, Baukrowitz T & Yellen G. (1996). The inward rectification mechanism of the HERG cardiac potassium channel. *Nature* **379,** 833-836.

Smith RD & Goldin AL. (1996). Phosphorylation of brain sodium channels in the I--II linker modulates channel function in Xenopus oocytes. *J Neurosci* **16,** 1965-1974.

Sokolov S, Scheuer T & Catterall WA. (2007). Gating pore current in an inherited ion channelopathy. *Nature* **446,** 76-78.

Sontheimer H. (2008). An unexpected role for ion channels in brain tumor metastasis. *Exp Biol Med (Maywood)* **233,** 779-791.

Sontheimer H, Fernandez-Marques E, Ullrich N, Pappas CA & Waxman SG. (1994). Astrocyte Na+ channels are required for maintenance of Na+/K(+)-ATPase activity. *J Neurosci* **14,** 2464-2475.

Sorlie T, Perou CM, Tibshirani R, Aas T, Geisler S, Johnsen H, Hastie T, Eisen MB, van de Rijn M, Jeffrey SS, Thorsen T, Quist H, Matese JC, Brown PO, Botstein D, Lonning PE & Borresen-Dale AL. (2001). Gene expression patterns of breast carcinomas distinguish tumor subclasses with clinical implications. *Proc Natl Acad Sci U S A* **98,** 10869-10874.

Soroceanu L, Manning TJ, Jr. & Sontheimer H. (1999). Modulation of glioma cell migration and invasion using Cl(-) and K(+) ion channel blockers. *J Neurosci* **19,** 5942-5954.

Sotiriou C, Neo SY, McShane LM, Korn EL, Long PM, Jazaeri A, Martiat P, Fox SB, Harris AL & Liu ET. (2003). Breast cancer classification and prognosis based on gene expression profiles from a population-based study. *Proc Natl Acad Sci U S A* **100,** 10393-10398.

Spampanato J, Escayg A, Meisler MH & Goldin AL. (2001). Functional effects of two voltage-gated sodium channel mutations that cause generalized epilepsy with febrile seizures plus type 2. *J Neurosci* **21,** 7481-7490.

Spampanato J, Kearney JA, de Haan G, McEwen DP, Escayg A, Aradi I, MacDonald BT, Levin SI, Soltesz I, Benna P, Montalenti E, Isom LL, Goldin AL & Meisler MH. (2004). A novel epilepsy mutation in the sodium channel SCN1A identifies a cytoplasmic domain for beta subunit interaction. *J Neurosci* **24,** 10022-10034.

Sparks RL, Pool TB, Smith NK & Cameron IL. (1983). Effects of amiloride on tumor growth and intracellular element content of tumor cells in vivo. *Cancer Res* **43,** 73-77.

Speyer CL, Smith JS, Banda M, DeVries JA, Mekani T & Gorski DH. (2012). Metabotropic glutamate receptor-1: a potential therapeutic target for the treatment of breast cancer. *Breast Cancer Res Treat* **132,** 565-573.

Srinivasan J, Schachner M & Catterall WA. (1998). Interaction of voltage-gated sodium channels with the extracellular matrix molecules tenascin-C and tenascin-R. *Proc Natl Acad Sci U S A* **95,** 15753-15757.

Stafstrom CE. (2011). A persistent little current with a big impact on epileptic firing. *Epilepsy Curr* **11,** 64-65.

Stafstrom CE, Schwindt PC, Chubb MC & Crill WE. (1985). Properties of persistent sodium conductance and calcium conductance of layer V neurons from cat sensorimotor cortex in vitro. *J Neurophysiol* **53,** 153-170.

Stefani E, Ottolia M, Noceti F, Olcese R, Wallner M, Latorre R & Toro L. (1997). Voltage-controlled gating in a large conductance Ca2+-sensitive K+channel (hslo). *Proc Natl Acad Sci U S A* **94,** 5427-5431.

Stevenson D, Binggeli R, Weinstein RC, Keck JG, Lai MC & Tong MJ. (1989). Relationship between cell membrane potential and natural killer cell cytolysis in human hepatocellular carcinoma cells. *Cancer Res* **49,** 4842-4845.

Stillwell EF, Cone CM & Cone CD, Jr. (1973). Stimulation of DNA synthesis in CNS neurones by sustained depolarisation. *Nat New Biol* **246,** 110-111.

Stock C & Schwab A. (2015). Ion channels and transporters in metastasis. *Biochim Biophys Acta* **1848,** 2638-2646.

Strobl JS, Wonderlin WF & Flynn DC. (1995). Mitogenic signal transduction in human breast cancer cells. *Gen Pharmacol* **26,** 1643-1649.

Sugawara T, Tsurubuchi Y, Agarwala KL, Ito M, Fukuma G, Mazaki-Miyazaki E, Nagafuji H, Noda M, Imoto K, Wada K, Mitsudome A, Kaneko S, Montal M, Nagata K, Hirose S & Yamakawa K. (2001). A missense mutation of the Na+ channel alpha

II subunit gene Na(v)1.2 in a patient with febrile and afebrile seizures causes channel dysfunction. *Proc Natl Acad Sci U S A* **98,** 6384-6389.

Sugimoto T, Yoshino M, Nagao M, Ishii S & Yabu H. (1996). Voltage-gated ionic channels in cultured rabbit articular chondrocytes. *Comp Biochem Physiol C Pharmacol Toxicol Endocrinol* **115,** 223-232.

Sundelacruz S, Levin M & Kaplan DL. (2008). Membrane potential controls adipogenic and osteogenic differentiation of mesenchymal stem cells. *PLoS One* **3,** e3737.

Sundelacruz S, Levin M & Kaplan DL. (2009). Role of membrane potential in the regulation of cell proliferation and differentiation. *Stem Cell Rev* **5,** 231-246.

Sundelacruz S, Levin M & Kaplan DLP. (2013). Depolarization alters phenotype, maintains plasticity of pre-differentiated mesenchymal stem cells. *Tissue Eng Part A.*

Surmeier DJ & Kitai ST. (1997). State-dependent regulation of neuronal excitability by dopamine. *Nihon Shinkei Seishin Yakurigaku Zasshi* **17,** 105-110.

Suy S, Hansen TP, Auto HD, Kallakury BV, Dailey V, Danner M, Macarthur L, Zhang Y, Miessau MJ, Collins SP & Brown ML. (2012). Expression of Voltage-Gated Sodium Channel Na1.8 in Human Prostate Cancer is Associated with High Histological Grade. *J Clin Exp Oncol* **1**.

Szaszi K, Sirokmany G, Di Ciano-Oliveira C, Rotstein OD & Kapus A. (2005). Depolarization induces Rho-Rho kinase-mediated myosin light chain phosphorylation in kidney tubular cells. *Am J Physiol Cell Physiol* **289,** C673-685.

Takahashi A, Camacho P, Lechleiter JD & Herman B. (1999). Measurement of intracellular calcium. *Physiol Rev* **79,** 1089-1125.

Takanami I, Inoue Y & Gika M. (2004). G-protein inwardly rectifying potassium channel 1 (GIRK 1) gene expression correlates with tumor progression in non-small cell lung cancer. *BMC Cancer* **4,** 79.

Tan HL, Kupershmidt S, Zhang R, Stepanovic S, Roden DM, Wilde AA, Anderson ME & Balser JR. (2002). A calcium sensor in the sodium channel modulates cardiac excitability. *Nature* **415,** 442-447.

Teramoto H, Coso OA, Miyata H, Igishi T, Miki T & Gutkind JS. (1996). Signaling from the small GTP-binding proteins Rac1 and Cdc42 to the c-Jun N-terminal kinase/stress-activated protein kinase pathway. A role for mixed lineage kinase 3/protein-tyrosine kinase 1, a novel member of the mixed lineage kinase family. *J Biol Chem* **271,** 27225-27228.

Terlau H, Heinemann SH, Stuhmer W, Pusch M, Conti F, Imoto K & Numa S. (1991). Mapping the site of block by tetrodotoxin and saxitoxin of sodium channel II. *FEBS Lett* **293,** 93-96.

Thompson EW, Paik S, Brunner N, Sommers CL, Zugmaier G, Clarke R, Shima TB, Torri J, Donahue S, Lippman ME & et al. (1992). Association of increased basement membrane invasiveness with absence of estrogen receptor and

expression of vimentin in human breast cancer cell lines. *J Cell Physiol* **150,** 534-544.

Tokuoka S & Morioka H. (1957). The membrane potential of the human cancer and related cells. I. *Gan* **48,** 353-354.

Tombes RM, Grant S, Westin EH & Krystal G. (1995). G1 cell cycle arrest and apoptosis are induced in NIH 3T3 cells by KN-93, an inhibitor of CaMK-II (the multifunctional Ca2+/CaM kinase). *Cell Growth Differ* **6,** 1063-1070.

Tong XP, Li XY, Zhou B, Shen W, Zhang ZJ, Xu TL & Duan S. (2009). Ca(2+) signaling evoked by activation of Na(+) channels and Na(+)/Ca(2+) exchangers is required for GABA-induced NG2 cell migration. *J Cell Biol* **186,** 113-128.

Torre LA, Bray F, Siegel RL, Ferlay J, Lortet-Tieulent J & Jemal A. (2015). Global cancer statistics, 2012. *CA Cancer J Clin* **65,** 87-108.

Trainer VL, Baden DG & Catterall WA. (1994). Identification of peptide components of the brevetoxin receptor site of rat brain sodium channels. *J Biol Chem* **269,** 19904-19909.

Traub O, Ishida T, Ishida M, Tupper JC & Berk BC. (1999). Shear stress-mediated extracellular signal-regulated kinase activation is regulated by sodium in endothelial cells. Potential role for a voltage-dependent sodium channel. *J Biol Chem* **274,** 20144-20150.

Trudeau MC, Warmke JW, Ganetzky B & Robertson GA. (1995). HERG, a human inward rectifier in the voltage-gated potassium channel family. *Science* **269,** 92-95.

Trudeau MM, Dalton JC, Day JW, Ranum LP & Meisler MH. (2006). Heterozygosity for a protein truncation mutation of sodium channel SCN8A in a patient with cerebellar atrophy, ataxia, and mental retardation. *J Med Genet* **43,** 527-530.

Tseng A & Levin M. (2013). Cracking the bioelectric code: Probing endogenous ionic controls of pattern formation. *Commun Integr Biol* **6,** e22595.

Tseng AS, Beane WS, Lemire JM, Masi A & Levin M. (2010). Induction of vertebrate regeneration by a transient sodium current. *J Neurosci* **30,** 13192-13200.

Tseng AS & Levin M. (2012). Transducing bioelectric signals into epigenetic pathways during tadpole tail regeneration. *Anat Rec (Hoboken)* **295,** 1541-1551.

Turner KL & Sontheimer H. (2014). Cl- and K+ channels and their role in primary brain tumour biology. *Philos Trans R Soc Lond B Biol Sci* **369,** 20130095.

Turner N, Tutt A & Ashworth A. (2004). Hallmarks of 'BRCAness' in sporadic cancers. *Nat Rev Cancer* **4,** 814-819.

Ulbricht W. (1969). The effect of veratridine on excitable membranes of nerve and muscle. *Ergeb Physiol* **61,** 18-71.

Ulbricht W. (1998). Effects of veratridine on sodium currents and fluxes. *Rev Physiol Biochem Pharmacol* **133,** 1-54.

Ullrich N, Bordey A, Gillespie GY & Sontheimer H. (1998). Expression of voltage-activated chloride currents in acute slices of human gliomas. *Neuroscience* **83,** 1161-1173.

Uysal-Onganer P & Djamgoz MB. (2007). Epidermal growth factor potentiates in vitro metastatic behaviour of human prostate cancer PC-3M cells: involvement of voltage-gated sodium channel. *Mol Cancer* **6,** 76.

van 't Veer LJ, Dai H, van de Vijver MJ, He YD, Hart AA, Mao M, Peterse HL, van der Kooy K, Marton MJ, Witteveen AT, Schreiber GJ, Kerkhoven RM, Roberts C, Linsley PS, Bernards R & Friend SH. (2002). Gene expression profiling predicts clinical outcome of breast cancer. *Nature* **415,** 530-536.

van Bemmelen MX, Rougier JS, Gavillet B, Apotheloz F, Daidie D, Tateyama M, Rivolta I, Thomas MA, Kass RS, Staub O & Abriel H. (2004). Cardiac voltage-gated sodium channel Nav1.5 is regulated by Nedd4-2 mediated ubiquitination. *Circ Res* **95,** 284-291.

van Gassen KL, de Wit M, van Kempen M, van der Hel WS, van Rijen PC, Jackson AP, Lindhout D & de Graan PN. (2009). Hippocampal Nabeta3 expression in patients with temporal lobe epilepsy. *Epilepsia* **50,** 957-962.

Van Petegem F, Lobo PA & Ahern CA. (2012). Seeing the forest through the trees: towards a unified view on physiological calcium regulation of voltage-gated sodium channels. *Biophys J* **103,** 2243-2251.

Vassilev P, Scheuer T & Catterall WA. (1989). Inhibition of inactivation of single sodium channels by a site-directed antibody. *Proc Natl Acad Sci U S A* **86,** 8147-8151.

Vassilev PM, Scheuer T & Catterall WA. (1988). Identification of an intracellular peptide segment involved in sodium channel inactivation. *Science* **241,** 1658-1661.

Vaughan Williams EM. (1975). Classification of antidysrhythmic drugs. *Pharmacol Ther B* **1,** 115-138.

Vaupel P, Kallinowski F & Okunieff P. (1989). Blood flow, oxygen and nutrient supply, and metabolic microenvironment of human tumors: a review. *Cancer Res* **49,** 6449-6465.

Vinciguerra M, Deschenes G, Hasler U, Mordasini D, Rousselot M, Doucet A, Vandewalle A, Martin PY & Feraille E. (2003). Intracellular Na+ controls cell surface expression of Na,K-ATPase via a cAMP-independent PKA pathway in mammalian kidney collecting duct cells. *Mol Biol Cell* **14,** 2677-2688.

Voloshyna I, Besana A, Castillo M, Matos T, Weinstein IB, Mansukhani M, Robinson RB, Cordon-Cardo C & Feinmark SJ. (2008). TREK-1 is a novel molecular target in prostate cancer. *Cancer Res* **68,** 1197-1203.

von Lintig FC, Dreilinger AD, Varki NM, Wallace AM, Casteel DE & Boss GR. (2000). Ras activation in human breast cancer. *Breast Cancer Res Treat* **62,** 51-62.

von Minckwitz G & Martin M. (2012). Neoadjuvant treatments for triple-negative breast cancer (TNBC). *Ann Oncol* **23 Suppl 6,** vi35-39.

Waechter CJ, Schmidt JW & Catterall WA. (1983). Glycosylation is required for maintenance of functional sodium channels in neuroblastoma cells. *J Biol Chem* **258,** 5117-5123.

Wagner V, Stadelmeyer E, Riederer M, Regitnig P, Gorischek A, Devaney T, Schmidt K, Tritthart HA, Hirschberg K, Bauernhofer T & Schreibmayer W. (2010). Cloning and characterisation of GIRK1 variants resulting from alternative RNA editing of the KCNJ3 gene transcript in a human breast cancer cell line. *J Cell Biochem* **110,** 598-608.

Waheed F, Speight P, Kawai G, Dan Q, Kapus A & Szaszi K. (2010). Extracellular signal-regulated kinase and GEF-H1 mediate depolarization-induced Rho activation and paracellular permeability increase. *Am J Physiol Cell Physiol* **298,** C1376-1387.

Wallace RH, Scheffer IE, Parasivam G, Barnett S, Wallace GB, Sutherland GR, Berkovic SF & Mulley JC. (2002). Generalized epilepsy with febrile seizures plus: mutation of the sodium channel subunit SCN1B. *Neurology* **58,** 1426-1429.

Wallace RH, Wang DW, Singh R, Scheffer IE, George AL, Jr., Phillips HA, Saar K, Reis A, Johnson EW, Sutherland GR, Berkovic SF & Mulley JC. (1998). Febrile seizures and generalized epilepsy associated with a mutation in the Na+-channel beta1 subunit gene SCN1B. *Nat Genet* **19,** 366-370.

Wang GK & Wang SY. (2003). Veratridine block of rat skeletal muscle Nav1.4 sodium channels in the inner vestibule. *J Physiol* **548,** 667-675.

Wang H, Zhang Y, Cao L, Han H, Wang J, Yang B, Nattel S & Wang Z. (2002). HERG K+ channel, a regulator of tumor cell apoptosis and proliferation. *Cancer Res* **62,** 4843-4848.

Wang JZ, Rojas CV, Zhou JH, Schwartz LS, Nicholas H & Hoffman EP. (1992a). Sequence and genomic structure of the human adult skeletal muscle sodium channel alpha subunit gene on 17q. *Biochem Biophys Res Commun* **182,** 794-801.

Wang Q, Shen J, Splawski I, Atkinson D, Li Z, Robinson JL, Moss AJ, Towbin JA & Keating MT. (1995). SCN5A mutations associated with an inherited cardiac arrhythmia, long QT syndrome. *Cell* **80,** 805-811.

Wang YF, Jia H, Walker AM & Cukierman S. (1992b). K-current mediation of prolactin-induced proliferation of malignant (Nb2) lymphocytes. *J Cell Physiol* **152,** 185-189.

Wang Z. (2004). Roles of K+ channels in regulating tumour cell proliferation and apoptosis. *Pflugers Arch* **448,** 274-286.

Watanabe H, Koopmann TT, Le Scouarnec S, Yang T, Ingram CR, Schott JJ, Demolombe S, Probst V, Anselme F, Escande D, Wiesfeld AC, Pfeufer A, Kaab

S, Wichmann HE, Hasdemir C, Aizawa Y, Wilde AA, Roden DM & Bezzina CR. (2008). Sodium channel beta1 subunit mutations associated with Brugada syndrome and cardiac conduction disease in humans. *J Clin Invest* **118,** 2260-2268.

Waxman SG. (2000). The neuron as a dynamic electrogenic machine: modulation of sodium-channel expression as a basis for functional plasticity in neurons. *Philos Trans R Soc Lond B Biol Sci* **355,** 199-213.

Waxman SG, Kocsis JD & Black JA. (1994). Type III sodium channel mRNA is expressed in embryonic but not adult spinal sensory neurons, and is reexpressed following axotomy. *J Neurophysiol* **72,** 466-470.

Weaver AK, Liu X & Sontheimer H. (2004). Role for calcium-activated potassium channels (BK) in growth control of human malignant glioma cells. *J Neurosci Res* **78,** 224-234.

Wei C, Wang X, Chen M, Ouyang K, Song LS & Cheng H. (2009). Calcium flickers steer cell migration. *Nature* **457,** 901-905.

Wei C, Wang X, Zheng M & Cheng H. (2012). Calcium gradients underlying cell migration. *Curr Opin Cell Biol* **24,** 254-261.

Weigelt B, Peterse JL & van 't Veer LJ. (2005). Breast cancer metastasis: markers and models. *Nat Rev Cancer* **5,** 591-602.

Weskamp M, Seidl W & Grissmer S. (2000). Characterization of the increase in [Ca(2+)](i) during hypotonic shock and the involvement of Ca(2+)-activated K(+) channels in the regulatory volume decrease in human osteoblast-like cells. *J Membr Biol* **178,** 11-20.

West JW, Numann R, Murphy BJ, Scheuer T & Catterall WA. (1991). A phosphorylation site in the Na+ channel required for modulation by protein kinase C. *Science* **254,** 866-868.

West JW, Patton DE, Scheuer T, Wang Y, Goldin AL & Catterall WA. (1992). A cluster of hydrophobic amino acid residues required for fast Na(+)-channel inactivation. *Proc Natl Acad Sci U S A* **89,** 10910-10914.

Westenbroek RE, Merrick DK & Catterall WA. (1989). Differential subcellular localization of the RI and RII Na+ channel subtypes in central neurons. *Neuron* **3,** 695-704.

Wicha MS, Liu S & Dontu G. (2006). Cancer stem cells: an old idea--a paradigm shift. *Cancer Res* **66,** 1883-1890; discussion 1895-1886.

Wilde AA & Brugada R. (2011). Phenotypical manifestations of mutations in the genes encoding subunits of the cardiac sodium channel. *Circ Res* **108,** 884-897.

Wilson GF & Chiu SY. (1993). Mitogenic factors regulate ion channels in Schwann cells cultured from newborn rat sciatic nerve. *J Physiol* **470,** 501-520.

Wingo TL, Shah VN, Anderson ME, Lybrand TP, Chazin WJ & Balser JR. (2004). An EF-hand in the sodium channel couples intracellular calcium to cardiac excitability. *Nat Struct Mol Biol* **11,** 219-225.

Winnicka K, Bielawski K, Bielawska A & Surazynski A. (2008). Antiproliferative activity of derivatives of ouabain, digoxin and proscillaridin A in human MCF-7 and MDA-MB-231 breast cancer cells. *Biol Pharm Bull* **31,** 1131-1140.

Wonderlin WF & Strobl JS. (1996). Potassium channels, proliferation and G1 progression. *J Membr Biol* **154,** 91-107.

Wonderlin WF, Woodfork KA & Strobl JS. (1995). Changes in membrane potential during the progression of MCF-7 human mammary tumor cells through the cell cycle. *J Cell Physiol* **165,** 177-185.

Wong HK, Sakurai T, Oyama F, Kaneko K, Wada K, Miyazaki H, Kurosawa M, De Strooper B, Saftig P & Nukina N. (2005). beta Subunits of voltage-gated sodium channels are novel substrates of beta-site amyloid precursor protein-cleaving enzyme (BACE1) and gamma-secretase. *J Biol Chem* **280,** 23009-23017.

Woodfork KA, Wonderlin WF, Peterson VA & Strobl JS. (1995). Inhibition of ATP-sensitive potassium channels causes reversible cell-cycle arrest of human breast cancer cells in tissue culture. *J Cell Physiol* **162,** 163-171.

Woodrough RE, Canti G & Watson BW. (1975). Electrical potential difference between basal cell carcinoma, benign inflammatory lesions and normal tissue. *Br J Dermatol* **92,** 1-7.

Workman P, Aboagye EO, Balkwill F, Balmain A, Bruder G, Chaplin DJ, Double JA, Everitt J, Farningham DA, Glennie MJ, Kelland LR, Robinson V, Stratford IJ, Tozer GM, Watson S, Wedge SR, Eccles SA & Committee of the National Cancer Research I. (2010). Guidelines for the welfare and use of animals in cancer research. *Br J Cancer* **102,** 1555-1577.

Wu L, Yong SL, Fan C, Ni Y, Yoo S, Zhang T, Zhang X, Obejero-Paz CA, Rho HJ, Ke T, Szafranski P, Jones SW, Chen Q & Wang QK. (2008). Identification of a new co-factor, MOG1, required for the full function of cardiac sodium channel Nav 1.5. *J Biol Chem* **283,** 6968-6978.

Wu YI, Frey D, Lungu OI, Jaehrig A, Schlichting I, Kuhlman B & Hahn KM. (2009). A genetically encoded photoactivatable Rac controls the motility of living cells. *Nature* **461,** 104-108.

Xia XM, Zeng X & Lingle CJ. (2002). Multiple regulatory sites in large-conductance calcium-activated potassium channels. *Nature* **418,** 880-884.

Xiao ZC, Ragsdale DS, Malhotra JD, Mattei LN, Braun PE, Schachner M & Isom LL. (1999). Tenascin-R is a functional modulator of sodium channel beta subunits. *J Biol Chem* **274,** 26511-26517.

Xing D, Wang J, Ou S, Wang Y, Qiu B, Ding D, Guo F & Gao Q. (2014). Expression of neonatal Nav1.5 in human brain astrocytoma and its effect on proliferation, invasion and apoptosis of astrocytoma cells. *Oncol Rep* **31,** 2692-2700.

Xing Z, Chen HC, Nowlen JK, Taylor SJ, Shalloway D & Guan JL. (1994). Direct interaction of v-Src with the focal adhesion kinase mediated by the Src SH2 domain. *Mol Biol Cell* **5,** 413-421.

Yamashita N, Hamada H, Tsuruo T & Ogata E. (1987). Enhancement of voltage-gated Na+ channel current associated with multidrug resistance in human leukemia cells. *Cancer Res* **47,** 3736-3741.

Yamazaki D, Kurisu S & Takenawa T. (2005). Regulation of cancer cell motility through actin reorganization. *Cancer Sci* **96,** 379-386.

Yang M & Brackenbury WJ. (2013). Membrane potential and cancer progression. *Front Physiol* **4,** 185.

Yang M, Kozminski DJ, Wold LA, Modak R, Calhoun JD, Isom LL & Brackenbury WJ. (2012). Therapeutic potential for phenytoin: targeting Na(v)1.5 sodium channels to reduce migration and invasion in metastatic breast cancer. *Breast Cancer Res Treat* **134,** 603-615.

Yang N, George AL, Jr. & Horn R. (1996). Molecular basis of charge movement in voltage-gated sodium channels. *Neuron* **16,** 113-122.

Yang N & Horn R. (1995). Evidence for voltage-dependent S4 movement in sodium channels. *Neuron* **15,** 213-218.

Yereddi NR, Cusdin FS, Namadurai S, Packman LC, Monie TP, Slavny P, Clare JJ, Powell AJ & Jackson AP. (2013). The immunoglobulin domain of the sodium channel beta3 subunit contains a surface-localized disulfide bond that is required for homophilic binding. *FASEB J* **27,** 568-580.

Yildirim S, Altun S, Gumushan H, Patel A & Djamgoz MB. (2012). Voltage-gated sodium channel activity promotes prostate cancer metastasis in vivo. *Cancer Lett* **323,** 58-61.

Yip D, Le MN, Chan JL, Lee JH, Mehnert JA, Yudd A, Kempf J, Shih WJ, Chen S & Goydos JS. (2009). A phase 0 trial of riluzole in patients with resectable stage III and IV melanoma. *Clin Cancer Res* **15,** 3896-3902.

York RD, Yao H, Dillon T, Ellig CL, Eckert SP, McCleskey EW & Stork PJ. (1998). Rap1 mediates sustained MAP kinase activation induced by nerve growth factor. *Nature* **392,** 622-626.

Young KA & Caldwell JH. (2005). Modulation of skeletal and cardiac voltage-gated sodium channels by calmodulin. *J Physiol* **565,** 349-370.

Yu FH, Westenbroek RE, Silos-Santiago I, McCormick KA, Lawson D, Ge P, Ferriera H, Lilly J, DiStefano PS, Catterall WA, Scheuer T & Curtis R. (2003). Sodium channel beta4, a new disulfide-linked auxiliary subunit with similarity to beta2. *J Neurosci* **23,** 7577-7585.

Yu Q & Stamenkovic I. (2000). Cell surface-localized matrix metalloproteinase-9 proteolytically activates TGF-beta and promotes tumor invasion and angiogenesis. *Genes Dev* **14,** 163-176.

Yu WH, Woessner JF, Jr., McNeish JD & Stamenkovic I. (2002). CD44 anchors the assembly of matrilysin/MMP-7 with heparin-binding epidermal growth factor precursor and ErbB4 and regulates female reproductive organ remodeling. *Genes Dev* **16,** 307-323.

Yuan P, Leonetti MD, Pico AR, Hsiung Y & MacKinnon R. (2010). Structure of the human BK channel Ca2+-activation apparatus at 3.0 A resolution. *Science* **329,** 182-186.

Zhai J, Lin H, Nie Z, Wu J, Canete-Soler R, Schlaepfer WW & Schlaepfer DD. (2003). Direct interaction of focal adhesion kinase with p190RhoGEF. *J Biol Chem* **278,** 24865-24873.

Zhang WM, Zhou J & Ye QJ. (2008). Endothelin-1 enhances proliferation of lung cancer cells by increasing intracellular free Ca2+. *Life Sci* **82,** 764-771.

Zhang X, Ren W, DeCaen P, Yan C, Tao X, Tang L, Wang J, Hasegawa K, Kumasaka T, He J, Wang J, Clapham DE & Yan N. (2012). Crystal structure of an orthologue of the NaChBac voltage-gated sodium channel. *Nature* **486,** 130-134.

Zhang XL, Peng XQ, Jing YL, Xie WR & Xie YK. (2003). Sialic acid contributes to generation of ectopic spontaneous discharges in rats with neuropathic pain. *Neurosci Lett* **346,** 65-68.

Zhang XY, Wen J, Yang W, Wang C, Gao L, Zheng LH, Wang T, Ran K, Li Y, Li X, Xu M, Luo J, Feng S, Ma X, Ma H, Chai Z, Zhou Z, Yao J, Zhang X & Liu JY. (2013). Gain-of-function mutations in SCN11A cause familial episodic pain. *Am J Hum Genet* **93,** 957-966.

Zhao P, Barr TP, Hou Q, Dib-Hajj SD, Black JA, Albrecht PJ, Petersen K, Eisenberg E, Wymer JP, Rice FL & Waxman SG. (2008). Voltage-gated sodium channel expression in rat and human epidermal keratinocytes: evidence for a role in pain. *Pain* **139,** 90-105.

Zheng YJ, Furukawa T, Ogura T, Tajimi K & Inagaki N. (2002). M phase-specific expression and phosphorylation-dependent ubiquitination of the ClC-2 channel. *J Biol Chem* **277,** 32268-32273.

Zhou Y, Morais-Cabral JH, Kaufman A & MacKinnon R. (2001). Chemistry of ion coordination and hydration revealed by a K+ channel-Fab complex at 2.0 A resolution. *Nature* **414,** 43-48.

Zhou Y, Wong CO, Cho KJ, van der Hoeven D, Liang H, Thakur DP, Luo J, Babic M, Zinsmaier KE, Zhu MX, Hu H, Venkatachalam K & Hancock JF. (2015). Membrane potential modulates plasma membrane phospholipid dynamics and K-Ras signaling. *Science* **349,** 873-876.

Ziechner U, Schonherr R, Born AK, Gavrilova-Ruch O, Glaser RW, Malesevic M, Kullertz G & Heinemann SH. (2006). Inhibition of human ether a go-go potassium

channels by Ca2+/calmodulin binding to the cytosolic N- and C-termini. *FEBS J* **273,** 1074-1086.